# AN INVESTIGATION INTO THE DRAINAGE CHARACTERISTICS AND BEHAVIOUR OF HYDRAULICALLY PLACED MINE BACKFILL AND PERMEABLE MINEFILL BARRICADES

**Thesis submitted by**

**Kirralee Jo RANKINE BEng(Hons)**

**in November 2005**

**for the degree of Doctor of Philosophy**
**in the School of Engineering**
**James Cook University**

## STATEMENT OF ACCESS

**I, the undersigned, the author of this thesis, understand that James Cook University will make it available for use within the University Library and, by microfilm or other means, allow access to users in other approved libraries.**

**All users consulting this thesis will have to sign the following statement:**

> **In consulting this thesis, I agree not to copy or closely paraphrase it in whole or in part without the written consent of the author; and to make proper public written acknowledgement for any assistance which I have obtained from it.**

**Beyond this, I do not wish to place any restriction on access to this thesis.**

Signature                                                            Date

## STATEMENT OF SOURCES

## DECLARATION

**I declare that this thesis is my own work and has not been submitted in any form for another degree or diploma at any university or other institution of tertiary education. Information derived from the published or unpublished work of others has been acknowledged in the text and a list of references is given.**

Signature Date

## DECLARATION – ELECTRONIC COPY

**I, the undersigned, the author of this work, declare that to the best of my knowledge, the electronic copy of this thesis submitted to the library at James Cook University is an accurate copy of the printed thesis submitted.**

Signature Date

# Acknowledgements

The author wishes to thank,

Mum, Dad and the family, – I would not have half the life I do, if I could not share the laughter, the tears, my frustrations and achievements with you all. Thank you so much. I appreciate every minute.

Dr. Nagaratnam Sivakugan – Siva, you have been a teacher, a mentor, but most of all a friend. I cannot thank you enough for everything you have opened my eyes to, and look forward to keeping our friendship for the rest of my life.

Rohini – Thank you for your friendship and for sharing Siva and so much of his time with me.

Richard Cowling – Your assistance has been greatly appreciated.

The Engineering Technical Staff (Warren O'Donnell, Stuart Petersen, Curt Arrowsmith and Don Braddick) – Thanks fellas.

I would also like to thank my examiners, Professor Braja Das, Professor Robert Holtz and Dr. Scott Fidler. Your comments and suggestions have been very helpful in the finalisation of this thesis.

***This work is dedicated to my wonderful family***

# Abstract

Hydraulic fills are quite popular as backfilling materials for underground voids created in the process of mining. For ease of transport through pipes, they are placed in the form of slurry and allowed to settle freely under self weight. Stopes can be approximated as rectangular prisms, and may extend as high as 200 metres. The horizontal access drives, used for transporting the ore, are blocked by porous barricade bricks before backfilling. Failures of barricades, and subsequent in-rush of wet hydraulic fill into the mines, have claimed several lives and contributed to severe economic loss world-wide.

The objective of this research is to carry out a thorough experimental study of the hydraulic fills and barricade bricks, with particular emphasis on load-deformation and drainage characteristics. Two separate numerical models were developed in FLAC and FLAC$^{3D}$, to simulate the backfilling process and to monitor the pore water pressure developments, fill and water heights and discharge rates. So far, the findings of the research were disseminated through four journal papers, a book chapter and seven papers in refereed international conferences. Overall, this study will improve the current state-of-the-art in hydraulic filling of mine stopes significantly.

More than 25 different hydraulic fills, from five different mines, were studied. All Australian hydraulic fills fall within a narrow band of grain size distribution and are classified as silty sands or sandy silts. Their specific gravity values range from 2.8 to 4.5. Constant head and falling head tests were carried out on reconstituted samples, produced from the hydraulic fill slurry, in a process that replicates the sedimentation process in the mine. The hydraulic fills settled to a porosity of 37%-48%, void ratio of 0.58-0.93, dry density (g/cm$^3$) of 0.58 times the specific gravity and relative density of 50%-80%. These values are in very good agreement with those measured in situ in Australia and U.S. The permeability values of the hydraulic fills, as determined in the laboratory, ranged from 10 mm/hr to 30 mm/hr, significantly less than the 100 mm/hr preferred for use in design by the mining industry. In situ, hydraulic fills with these permeabilities have performed satisfactorily with adequate drainage in the mine stope, implying that the 100 mm/hr limit may be excessively conservative when mine efficiency is considered.

Full barricade bricks, cylindrical samples cored from the bricks, and specially cast samples were tested for uniaxial strength, Young's modulus, failure strain and permeability. Uniaxial compression tests were performed on more than 50 cores in an attempt to carry out an extensive statistical analysis. Beta distributions were fitted to describe the strength, stiffness and failure strain. It is shown that wetting the bricks reduces the strength by about 25%. A unique permeameter was developed to simulate one-dimensional flow through the bricks and to measure the permeability. This was the first ever attempt to measure the permeability of barricade bricks, and it was shown that barricade bricks are 2-3 orders of magnitude more permeable than the hydraulic fill, thus justifying the assumption in the numerical models that the fill-barricade boundary is free draining.

A 2-dimensional numerical model was developed in *FLAC* that compared very well with Isaacs and Carter model, while having better features. The model simulates hydraulic filling process in the mines, and monitors the pore pressure developments throughout the stope, fill height and water height at all times. This model was extended to three dimensions using *FLAC*$^{3D}$.

# List of Publications

**BOOK CHAPTER**

Sivakugan, N., Rankine, K.J. and Rankine, R.M. (2005). Geotechnical Aspects of Hydraulic Filling of Underground Mine Stopes in Australia, Case Histories on Ground Improvement, Elsevier, Invited contribution.

**JOURNALS**

***“Emplaced Characteristics of Hydraulic Fills In a Number of Australian Mines"***
Rankine, K.J., Sivakugan, N. and Cowling, R. (2005). Journal of Geotechnical and Geological Engineering, Springer (In Press).

***“Permeabilities of Hydraulic Fills and Barricade Bricks”***
Sivakugan, N, Rankine, K.J. and Rankine, R. (2005). Journal of Geotechnical and Geological Engineering, Springer, (In Press)

***“Geotechnical Considerations in Mine Backfilling”***
Sivakugan, N, Rankine, R.M., Rankine, K.J. and Rankine, K.S. (2005). Journal of Cleaner Production, Elsevier (In Press).

***“Study of Drainage through Hydraulic Fill Stopes using method of Fragments”***
Sivakugan, N, Rankine, K.J. and Rankine K.S. (2005). Journal of Geotechnical and Geological Engineering, Springer (In Press).

**CONFERENCES**

“Geotechnical Characterization and Stability Analysis of BHP Cannington Paste Backfill”
Rankine, R.M., Rankine, K.J., Sivakugan, N., Karunasena, W., Bloss, M.L. (2001). XV$^{th}$ International Conference on Soil Mechanics and Geological Engineering, August, 2001, Istanbul, Turkey, 1241-1244.

"A Numerical Analysis of the Arching Mechanism in Pastefill throughout a Complete Mining Sequence"
Rankine, K.J., Rankine, R.M., Sivakugan, N., Karunasena, W. and Bloss, M. (2001). Proceedings of First Asian Pacific Congress on Computational Mechanics, Sydney, 461-466.

Geotechnical Characteristics of Cemented Mine Tailings”
Rankine, RM., Rankine, KJ., Sivakugan, N., Karunasena, W. and Bloss, M. (2001). Proceedings of The Third International Conference on Soft Soil Engineering (3rd ICSSE), Hong Kong, pp. 563-566.

**"*Three-Dimensional Drainage Modelling of Hydraulic Fill Mines*"**
Rankine, K.J., Rankine, K.S. and Sivakugan, N. (2003). Proceedings of the 12$^{th}$ Asian Regional Conference on Soil Mechanics and Geotechnical Engineering (12ARC), Singapore, pp. 937-940.

**"*Quantitative Validation of Scaled Modelling of Hydraulic Mine Drainage Using Numerical Modelling*"**
Rankine, K.J., Rankine, K.S. and Sivakugan, N. (2003). Proceedings of the International Congress on Modelling and Simulation, MODSIM 2003, Townsville, Ed. D.A. Post, pp. 2054-2059.

**"*Laboratory Tests for Mine Fills and Barricade Bricks*"**
Rankine, K.J., Sivakugan, N., Rankine, K.S. (2004). The 9$^{th}$ Australia New Zealand Conference on Geomechnics, Auckland, Vol. 1, pp. 225-231.

"Drainage Characteristics and Behaviour of Hydraulically Placed Mine Fill and Fill Barricades"
Rankine, K.J., Sivakugan, N. (2005). XVI$^{th}$ International Conference on Soil Mechanics and Geological Engineering, September, 2005, Osaka, Japan, 579-582.

# Contents

# List of Figures

# List of Tables

# List of Symbols

$A$ = cross-sectional area

$a$ = air content

$a_2$ = cross-sectional area of the standpipe in the falling head test

$C$ = Hazen's constant

$C_c$ = coefficient of curvature

$C_u$ = coefficient of uniformity

$C_v$ = viscosity coefficient

$D$ = constrained modulus

$D_r$ = relative density

$D_{10}$ = the grain size for which 10% of the particles are finer; effective grain size

$D_{30}$ = the grain size for which 30% of the particles are finer

$D_{50}$ = the grain size for which 50% of the particles are finer

$D_{60}$, = the grain size for which 60% of the particles are finer

$e$ = void ratio

$e_{min}$ = minimum void ratio

$e_{max}$ = maximum void ratio

$E$ = Young's modulus

$G_s$ = Specific gravity

$H$, $h$ = height

$h_L$ = head loss

$i$ = hydraulic gradient

$k$ = permeability

$k_e$ = effective permeability,

$k_{eq}$ = equivalent permeability for a layered system

$K_0$ = horizontal pressure coefficient (assumed to be 0.5),

$L$ = length

$M_a$ = mass of air

$M_s$ = mass of solids

$M_t$ = total mass

$M_w$ = mass of water

$n$ = porosity

$N_1$ = corrected blow count number

$Q$ = flow rate

$S$ = saturation

$S_v$ = grain surface per unit volume

$S_x$ = standard deviation

$t$ = the time taken for the water level to fall between the two electrodes

$u$ = pore water pressure

$V$, $V_t$ = total volume

$V_a$ = volume of air

$V_s$ = volume of solids

$V_v$ = volume of voids

$V_w$ =volume of water

$w$ = water content

$\bar{x}$ = mean

$\alpha$ = shape parameter for Beta distribution

$\beta$ = shape parameter for Beta distribution

$\beta_1$ = coefficient of skewness

$\beta_2$ = coefficient of kurtosis

$\varepsilon_f$ = failure strain

$\Phi$ = friction angle

$\gamma_w$ = unit weight of water

$\gamma'$ = effective unit weight of fill

$\nu$ = Poisson's ratio

$\rho_d$ = dry density

$\rho_w$ = density of water

$\sigma_h$ = barricade pressure

$\sigma_h'$ = effective horizontal pressure

$\sigma_v'$ = effective vertical pressure

# Chapter 1

# Introduction

## 1.1 General

The open stoping mining method is a mining technique used in the underground ore extraction process for very large ore bodies. Excavation initiates from the base of the ore body, and the roof and/or walls are progressively dug out, so the ore falls to the base of the stope[1]. Then the ore is crushed and transported via drives, to the surface for processing. The large voids, which may extend well over 100 m in height are generally backfilled using the by-products of the ore extraction and minerals processing.

The ore body is excavated through a very complex blasting pattern designed individually for the stopes. Access to the stopes for explosive placement is achieved via drives which are generally spaced at 20-40 m vertically up the wall of the stope (Fig. 1.1). Stopes will generally be designed with two to four drives at each access level.

To provide local and regional rock support for the subsequent removal of adjacent stopes, the voids are backfilled once ore extraction is complete. The fill material must have sufficient strength (often achieved through the addition of cement to the fill mix) to avoid instability when adjacent stopes are sequentially removed throughout the mining cycle.

To complete the extraction of an ore body, many stopes are required. These stopes are generally set out in a standard grid pattern, but specific details depend on the ore body

[1] An ore body is divided into individual volumetric units called "stopes", which are sequentially mined

geometry, the host rock and particular mine conditions. At any given stage of an underground mine operation, the excavation of several stopes will be under way at one time, and similarly several stopes will be in the backfilling stage. These individual stope operations are planned to allow sufficient distance between excavations to avoid stability problems.

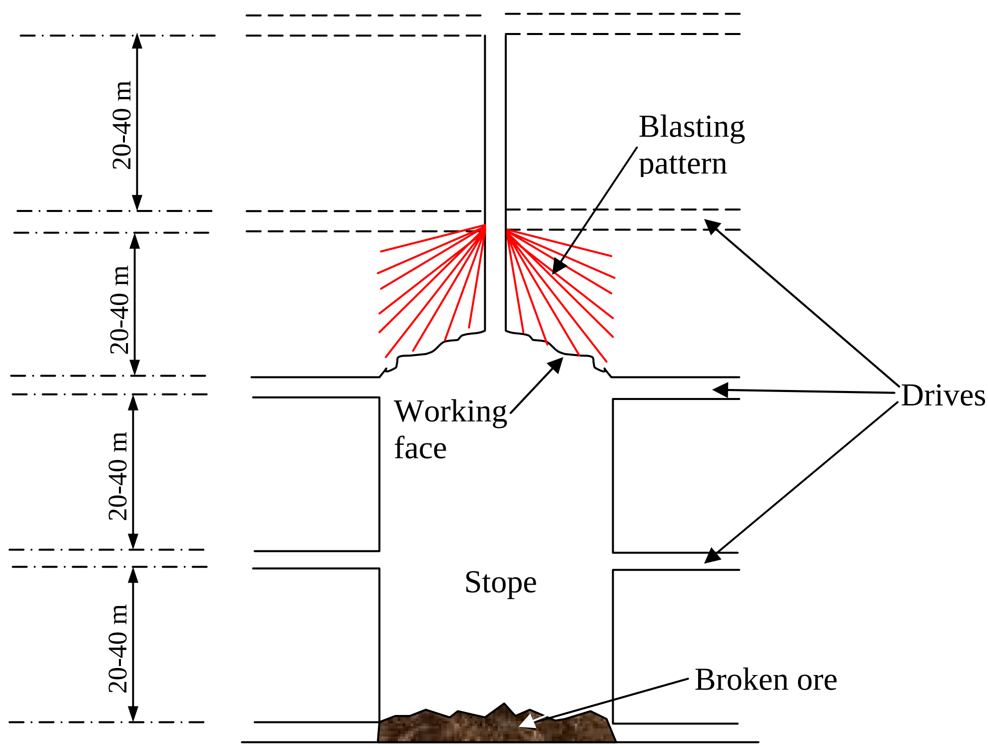


**FIG. 1.1 -Idealized schematic of stope during excavation**

This research will focus on the drainage characteristics and associated properties of a particular type of minefill material known as ‘hydraulic fill’, and some of the issues related to using this fill material in underground mining operations.

The manner in which the stope is backfilled depends on the type and characteristics of the fill, but the fill material is generally introduced to the highest point of the stope via either pipeline (for the case of paste or hydraulic fill) or by conveyor (in the case of aggregate or rock fill). When material enters the stope all drives to the stope must be completely sealed to prevent the fill from entering the drives. The fill is usually in a slurry form when placed in the stope, and without restraint, would easily flow into other parts of the mine. In hydraulic fill mining operations, permeable barricades are constructed within the drives to contain the fill slurry as it is being placed into the stope (Fig. 1.2).

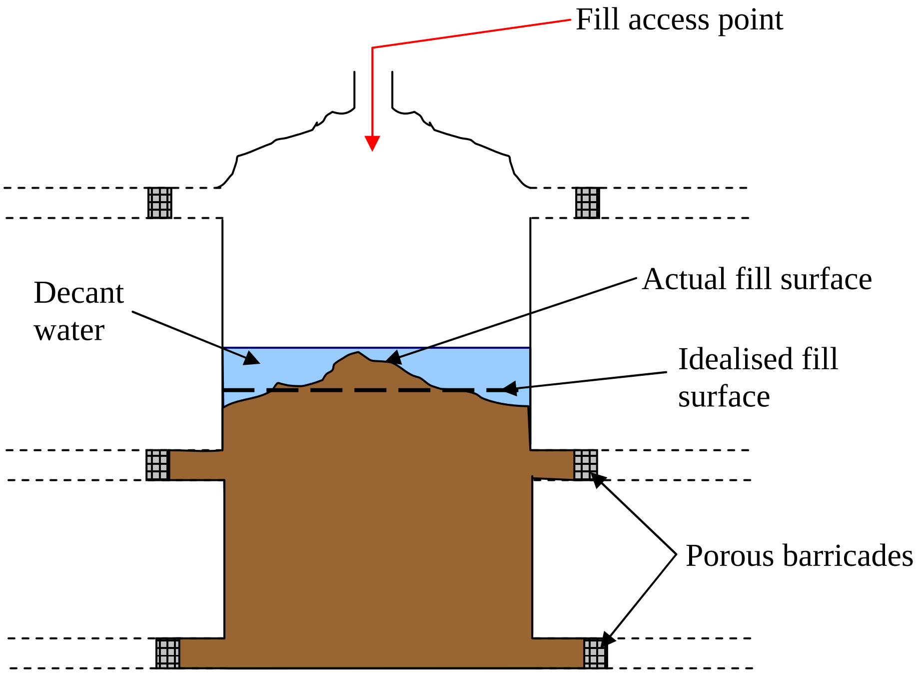


**FIG. 1.2 - Diagram of stope during filling**

Typically underground barricades take the form of walls constructed from specially designed permeable barricade bricks. The barricade construction may be fashioned as either flat, or curved convexly toward the fill material. In recent years, much attention has been directed to the use of shotcrete or pumped concrete for the containment of fill in underground mines. Unlike the permeable brick walls, these barricades are impervious and therefore to remove the water, they require drainage holes fitted with prefabricated drains in vertical, horizontal and inclined positions within the stope. It is suggested these drainage systems reduce the drainage paths and expedite the removal of water (Kuganathan 2001, Neindorf 1983). This relatively new method of containment barricade construction is still in its infancy, but with research, poses great potential for future use.

If the pressure build up behind the barricades (typically as a result of the pore pressure build-up, development of the lateral load from the hydraulic fill, and any dynamic loads) exceeds the strength of the barricade then failure occurs. As a consequence of barricade failure, hydraulic fill may surge from the stope into the mine, which is hazardous to mining operations, and has in recent cases resulted in tragedies. The objective of this thesis is to reduce this hazard by improving the current state-of-the-art for the filling and drainage operations of hydraulic fill mines, as well as the means by which the drainage of these mines is analysed.

## 1.2 Problem Statement

***Hydraulic fills are placed underground in the form of a slurry, which introduces substantial quantities of water into the stope. Underground failures have occured as a result of poor drainage of excess water from the stope during the backfilling stages of the operation. There has been great emphasis placed on developments in drainage analysis of hydraulically placed minefill and fill barricades from Australian mines, with a goal of improving safety.***

## 1.3 Relevance of the Research

The drainage performance of hydraulic fill and the permeable barricade needs to be adequately understood as it plays an important roll in the safety of underground hydraulic fill mining operations. Catastrophic fill barricade failures in underground hydraulic fill mines in Australia and overseas, have resulted in significant economic loss and loss of lives. Reliable knowledge of the drainage characteristics of underground hydraulic fill mines will improve mine safety and productivity through confidence in design and prediction.

Development of a functional 3-dimensional filling and drainage program, based on known geotechnical properties, will allow for the prediction of hydraulic fill drainage behaviour and associated stability throughout the mining cycle. This in turn, may lead to:

- increased safety in mine practices,
- increased productivity resulting from increased confidence with regard to filling rates and stope scheduling,
- the optimisation of hydraulic fill solids content and placement rates, and
- significant cost savings.

## 1.4 Thesis Overview

Chapter 1 introduced the research problem, objectives and the relevance of the research. An overview of the major issues associated with the drainage of hydraulic fill mines, and a brief description of the mining method have been presented. Chapter 2 briefly discusses the historical overview of hydraulic filling practices within Australia over the past decade, and presents the current practices and recent developments with regard to underground hydraulic fill mining and drainage analysis and prediction. The chapter discusses the purpose and requirements of backfill and specifically hydraulic fill.

Chapter 3 details the characterisation of typical Australian hydraulic fills. This chapter covers grain size distribution, specific gravity, permeability, water content, minimum and maximum dry densities, relative density, void ratio, friction angle and settlement properties for hydraulic fills, and describes unique laboratory testing techniques specifically developed for testing these materials.

The determination of drainage, strength and stiffness properties for the permeable barricade bricks used in underground hydraulic fill containment is described in Chapter 4. A statistical analysis is used to determine the reliability with which the laboratory determined strength and stiffness parameters may be used.

Chapter 5 describes the design, and verification of a 2-dimensional numerical model used to simulate the filling and drainage of a hydraulic fill stope. The 2-dimensional program is used to determine the relative influence of drainage input parameters on stope discharge and the development of pore water pressure, such that these may be prioritised for the extension of the 2-dimensional program into 3-dimensions. This extension and verification of the 3-dimensional program is detailed in Chapter 6. The 3-dimensional program is used to study the influence filling details and hydraulic fill material properties have on the water and fill heights and maximum pore water pressures throughout the filling and drainage of a stope. Three-dimensional numerical modelling is further used to study the geometrical influence multiple base drains and stope and drain size have on the discharge from the stope and the maximum pore water pressure predictions within typical underground stope geometries.

A summary of the findings from this research is presented in Chapter 7 and recommendations for future research will be put forth.

# Chapter 2

# Literature Review

## 2.1 General

The process in which recycled waste material from underground ore extraction is used to backfill the mine voids dates back for centuries. Originally, the backfilling process was based on very primitive mine filling systems, which consisted of predominantly waste material coupled with basic material transporting and processing. Today, the mining industry is the largest generator of solid wastes in Australia (Boger, 1998). Therefore, the backfilling of underground excavations created by ore removal with this process by-product is an integral part of the overall mining cycle because it provides an effective means of waste disposal, as well as ground support to allow for adjacent ore removal. Underground mining operations account for the creation of approximately 10 million cubic meters of void as a result of some 34 million tonnes of production, annually (Grice, 2001). The dry density of the settled backfills such as hydraulic fills is approximately 50% of the dry density of the parent rock (Cowling, 1998). Therefore, only about 50% of the excavated rock can be sent back in the form of hydraulic fill into the voids created. At Mount Isa Mines alone during the 1991/1992 financial year, approximately 4.2 $x10^6$ $m^3$ of void was filled underground with approximately 6.1 million tonnes of minefill material (Grice et al., 1993). With the industry under continual pressure as a result of the increased demand for minerals, as well as improved environmental awareness, the necessity for better understanding of the hydraulic fill behaviour and disposal techniques is of paramount importance to our society.

In mining, minefill refers to any waste material that is placed into the voids created by underground ore extraction. Minefill is predominantly placed underground for the purpose of either waste disposal, or to perform an engineering function. In a keynote presentation, Mr. Cowling succinctly quotes a description of the purpose of underground minefill given by Wilson (1979), as the material, or materials used:

> "*to fill the cavities created by mining so as to establish and retain safe working conditions economically*".

Materials used in minefill include one or more of the following: waste development rock, deslimed and whole mill tailings, quarried and crushed aggregate, sand and occasionally ice or salt. Very small quantities of binder material, normally Portland cement, or a blend of Portland cement with another pozzolan such as fly ash, gypsum or blast furnace slag may be added to the waste material to improve strength properties.

Most commonly, minefills are transported through pipes to the stope as a slurry. Typically, the point in which the slurry is discharged from the pipe into the stope is through the roof (which is referred to in the mining industry as the 'back') in the center or at the far end of the stope. These pipe systems are typically gravity driven, and the flow can range from laminar with low pressures (less than 1 MPa) through to turbulent with pressures exceeding 5 MPa within the pipes, depending on the minefill material (Grice, 1998 b).

An essential requirement in optimising mine efficiency is that the minefill being used is of lowest possible cost, without compromising the required engineering properties of the material. Typical minefill costs may range anywhere from $2 to $20 per cubic meter depending on the function for which it is being used (Grice 1998 b).

This Chapter aims to summarise the types, selection and purpose of minefill material and the mining methods that use minefills. The research undertaken for this dissertation has been done on a particular minefill material known as hydraulic fill. Current practices and published developments with regard to the properties and analysis of underground stopes using this material will be discussed and summarized both in this chapter and throughout the rest of the thesis.

The literature review is not only limited to this chapter. A more extensive coverage on hydraulic fills, barricade bricks and numerical modelling is given in Chapters 3, 4 and 5 respectively.

### 2.1.1 Mining Methods that Use Minefill

Underground mining methods may be divided into two distinct types: stable stope and caving, with a complete spectrum of methods available between these two extremes. The three stable stope methods which use minefill include open stoping, room and pillar, and cut and fill mining methods. Caving is a mining method whereby ore is allowed to collapse under its own weight through prolific natural fracturing and failures. In caving, the ore will fail where undermined and will continue to fail while there is a void and sufficient fracturing of the ore body. A comprehensive description of each of the mining methods is given by Hamrin (1982), Budavari (1983) and Brady and Brown (1985). This research will be based on the open stoping mining method in conjunction with hydraulic fill.

### 2.1.2 Purpose of Minefill

Minefill may be used for economic, environmental or engineering purposes. The purpose of minefill may be for any one or combination of the following:

- To reduce the need for large tailings dams.
- To provide higher rates of ore recovery.
- To lessen the environmental impact through effective waste disposal.
- To provide local and regional stability to the ore body.

The increased stability is not due to direct transfer of rock stresses into the minefill mass, the minefill is significantly softer than the surround intact rock. The increased stability is a result of reduced levels of relaxation in the rock, ensuring the integrity of the load carrying capacity of the rock (Barrett et al., 1978). Using the results of a finite element analysis, Yamaguchi and Yamatomi (1983), agree that the effect of minefill is to limit the deformation of the surrounding rock, and suggest that minefill restricts failure progression and as a consequence generates a slow and moderate “dilatant” failure in the rock mass around the void. Ultimately, these measures provide significant cost savings by optimising safe and economic mine functioning and the longevity of the mine.

A trend in Canadian mines has been described, where environmental legislations required the maximum quantity of mine waste to be returned to the underground workings (Nantel, 1998). The obvious limit of this mining direction was reached when the Australian Federal Government recommended approving an alternative for the proposed Jabiluka Mine (JMA) whereby all mill wastes were required to be placed underground. At first glance this seems very reasonable, and may be seen as a constructive requirement based on a desire to preserve environmental integrity. This however, as demonstrated by a study conducted in Queensland is not always the case, and such an approach may limit the financial viability of a significant number of mines (Grice, 1998 b). Grice showed that for one particular operation there was an excess mine volume of 46% which would have to be created to store all mill waste in the form of pastefill. The cost associated with mining this additional volume greatly exceeded the cost for surface disposal and subsequent rehabilitation.

There are three major criteria that any minefill must satisfy, as well as minimising environmental impact and optimising economic gain for the mine. These criteria include static stability, dynamic stability and drainage requirements. Each of these requirements are discussed briefly below.

<u>Static Stability Requirements</u>

The static requirements for placed minefill may include sufficient strength and stiffness to:

- be self supporting when vertical faces are exposed (in pastefill and cemented hydraulic fill) as a result of adjacent ore removal;
- support loading from equipment used in mucking (as a floor);
- permit mining underneath the fill by production blasting for undercut ore extraction;
- maintain local and regional stability by confining rock mass surrounding the stope; and
- permit development in the form of headings for access purposes or for use in mine ventilation.

In order to minimise loading on barricades, the minefill may also require high early strength in the case of pastefill and cemented fills (Grice, 2001).

Dynamic Stability Requirements

Close proximity blasting from production or development sized excavation is the main dynamic loading which the minefill must be capable of enduring. Although not common in Australia, the other type of dynamic loadings the fill material must be able to withstand are those associated with regional seismic events.

Drainage Requirements

Excess water within the minefill may come from either groundwater, service water or water used in the placement of minefill. Generally the majority of the water requiring drainage through the minefill mass comes from the water used to transport the fill to the site of deposition (i.e., the water used to suspend the particles as a hydraulic fill). Once placed, the solid particles settle, leaving some water on top of the solidified material as 'decant water' to percolate through the fill mass. To reduce the risks associated with large pore pressures, the water should be removed from the stope as quickly as practically possible. A rule-of-thumb design specification, established and used throughout the mining industry to ensure hydraulic fill permeabilities are of sufficient value to achieve this, is that the grain size distribution of the hydraulic fills should not have more than 10% less than 10 μm (Grice and Fountain, 1991; Grice et al., 1993; Bloss and Chen, 1998; Grice, 1998 a). A general range for the permeability of hydraulically placed backfills is between 20 mm/hr to 100 mm/hr, this is addressed further in Chapter 3. Pastefill, by definition, retains the water used for transportation purposes, and therefore this minefill type does not have drainage requirements.

The fill barricades that are constructed in the drives to contain the minefills as they are being placed underground, are also typically designed to allow for the drainage of water from stopes. The barricades must be constructed such that they do not restrict the flow of water from the stope and contribute to consequential pore pressure build up. Cowling (2002) suggests this is typically achieved by designing the barricades to be ten times more permeable than the fill mass.

### 2.1.3 Minefill Types and Selection

There are several types of minefill materials based on combinations of surface processing plant by-products called tailings, and development waste or quarried rock. These minefill materials include tailings-based products such as pastefill, hydraulic fill and cemented hydraulic fill, and sand fill, cemented sand fill, rock fill, cemented rock fill, aggregate fill and cemented aggregate fill (Bloss, 1992). The three major fill types used in Australia (Grice, 2001) and around the world are:

- *Hydraulic fill*: the coarser fraction of deslimed mill tailings slurries with a solids density[2] raised to over 70%. The fines that are removed from the tailings are disposed of in surface dams.
- *Pastefill*: total mill tailings, crushed to a grain size of less than 5 μm and thickened to around 80% solids density. Cement and water are added to the mix to achieve the required rheological and strength characteristics,
- *Rock fill*: crushed waste rock, from the surface or underground with an average aggregate size limit of 40 mm. Rockfill may be placed as is, or with cemented hydraulic fill or cemented water slurry.

The overall mine efficiency and viability is largely based on minefill selection and therefore minefill type is of paramount importance to the plan for the mining of an orebody. The plan for a mine must take into account the full lifecycle of the mine including shutdown and rehabilitation. The placement of tailings underground as minefill will reduce the environmental impacts of the mine as well as the costs associated with shutdown. By employing discounted cashflow techniques, the full operating and capital costs of the overall mine life can be assessed, taking into account the impact of expenditure on minefill compared with the saving in rehabilitation costs.

It has been suggested that minefill selection should be approached as an iterative process (Grice 1998 b). During the feasibility stage a number of mining methods should be identified, and factors such as mining rate, resource recovery and dilution

[2] The mining industry commonly refers to the 'solids density' or 'pulp density' of a minefill material. These terms refer to the percentage solids by weight of a minefill slurry.

levels considered. This information will provide the base set of options from which alternatives may be compared, addressing questions such as the following:

- What improvements to ground conditions can be expected?
- What is the increase in resource recovery rate?
- What is the impact on ventilation?
- Do the dilution rates increase or decrease?
- Will cement from fill dilution affect metallurgical recoveries?
- Is cyanide an issue?

Minefill material, regardless of type will be individual to a mine, and understanding as best as possible characteristics of the tailings such as grain size distribution, mineralogical composition and rheological properties is paramount when iterating through alternative minefill alternatives. Once a short list of two or three technically feasible systems that meet all of the operating and geotechnical needs of the mine is formulated, the systems are then assessed for economy over the entire predicted life of the operation, taking into consideration tangible environmental factors.

This research deals with the placement, containment and drainage of hydraulic fill, which has been considered the conventional mine filling practice, primarily due to the widespread use particularly in the 80's (Thomas and Holtham, 1989). Therefore hydraulic fill and the drainage and containment of hydraulic fill within underground stopes will be discussed further.

## 2.2 Hydraulic Fill

The introduction of hydraulically transported minefill in Australia was first reported at the South Mine of Broken Hill South Limited, Broken Hill, New South Wales in 1939 (Black, 1944). By 1944, all underground transportation of minefill within the South Mine was hydraulic (Black, 1944). During the 1940's and 1950's the use of hydraulic backfill systems became very common worldwide (Nantel, 1998). Today, hydraulic fill is used in at least nine different underground operations around Australia. These mines currently using hydraulic fill include two mines in Queensland, three mines located in New South Wales, two in Western Australia and two mines in Tasmania (Grice, 2001). Hydraulic fill is also used extensively in underground mines throughout the world, and consequently improvement in understanding the behaviour of underground hydraulic fill processes is obviously required.

The primary advantages of hydraulic fill over the other minefill alternatives include the simplicity and the low costs involved with production and delivery. The cost per cubic meter of placed hydraulic fill (uncemented) is approximately A$2 (Grice, 1998). Another advantage of hydraulic fill is that increasing strength is simply a matter of adding cement and increasing the quantity of cement as necessary. There are two significant disadvantages associated with the use of hydraulic fill in underground mines. The first is that permeable barricades must be constructed within the drives to retain the hydraulic fill as it is being placed in the stope, while permitting free drainage of excess water. The barricades are commonly constructed of specially made permeable concrete barricade bricks. The barricades are constructed between completion of ore excavation from a stope and commencement of filling and can take a two man crew between 2 to 3 shifts to build. The second major disadvantage is the high levels of water in the fill and the requirement to pump this water out of the mine.

### 2.2.1 Current Practices

Historically, the slurry typically had a pulp density of 65% to 75% solids by weight, but there has been a steady increase in pulp density over the past decade in an attempt to reduce the quantity of water required to be removed, and increase the proportion of solids placed in the underground voids. Rheological restrictions associated with the transportation of the slurry through pipes limits the solids content of the hydraulic fill, but current industry specifications suggest the density should exceed 70% solids by weight (Grice, 1998 a). It is suggested that the natural tendency for fill plant operators to add water to a fill line in an attempt to prevent blockages in the line, may have the opposite effect by allowing faster settling of the coarser fraction as a result of the leaner pulp (Thomas and Holtham, 1989). The stopes are filled at rates of approximately 150 t/hr to 300 t/hr of solids content, with various filling schedules (e.g. 12 hrs fill and 12 hrs rest until the stope is filled) to suit the processing plant and other constraints. The lines may be flushed with water from time to time.

Hydraulic fill is a heterogeneous slurry made from the by-product of ore which may be obtained from a wide range of geological conditions and mineralogical compositions. The desired minerals make up only a small percentage of the host rock mined and milled. The rest of the host rock mined is included in the waste product of the mill, and this affects the composition of the hydraulic fill. When excess water and fines are removed from the tailings the majority of clay minerals or micas that may be present in the ore or host rock are also removed. Hydroclones are by far the most widely used device for the preparation of hydraulic fill, with less conventional alternatives including mechanical classifiers and thickeners, with sieve bend, filtration, and flocculation systems also worthy of consideration perhaps in conjunction with other more conventional processes (Thomas and Holtham, 1989). Some of the advantages hydroclones have over alternative classifiers include:

- they are physically smaller then mechanical classifiers,
- simple, and
- low in capital and operating costs.

The hydroclones are however relatively inefficient in terms of preciseness of separation and they may be inflexible with regard to operation after they have been installed.

### 2.2.2 Geotechnical Considerations

Hydraulic fills produced from the tailings, are man-made, and are therefore much more uniform in their characteristics than are most natural deposits. Although as explained earlier in this chapter the tailings used to produce hydraulic fill may be sourced from a wide variety of ore and host rock mineralogical compositions and also processing techniques may vary slightly, many geotechnical properties of typical hydraulic fills may be characterised or described within a range or band. This section aims to detail some of the properties of hydraulic fills, commonly accepted within the mining industry.

#### Grain Size Distribution and Specific Gravity

Tailings may be easily separated with hydraulic cyclones, to produce almost any desired gradation in grain size distribution. It is widely accepted within the mining industry that the effective grain size (10% of the particles are finer than this) most suitably defines the ability of a hydraulic fill to percolate water and settle from a slurry, as well as the performance of the Portland cement additions in cemented hydraulic fill (Nicholson and Wayment, 1964; Thomas and Holtham, 1989). Current industry specification suggests that provided a hydraulic fill has less than 10% of the grain size distribution smaller than 10 μm, drainage requirements will be met (Grice and Fountain, 1991; Grice et al., 1993; Bloss and Chen, 1998; Grice, 1998 a).

The results of a comparative study of particle size analyses by hydrometer and laser diffraction methods, suggests that laser diffraction methods should be adopted as standard in geotechnical engineering and geoenvironmental engineering (Wen et al., 2002). It was found that hydrometer analysis underestimates the coarse silt and fine sand fractions which is the sizing that hydraulic fills fall within, and therefore this method may not be suitable or accurate (Wen et al., 2002). Nevertheless, all grain size distributions for the mining industry are done through laser sizing due to the importance placed on the accuracy of this parameter.

Unlike typical soils, the specific gravity values for hydraulic fills have a wide range as a result of the milling process and the vast range of ore and host rock compositions from which the tailings may be sourced. Soil grains in general have specific gravity of 2.6 to 2.8. In the case of hydraulic fill, due to the presence of other heavy minerals, the specific gravity values can be as high as 4.4.

Dry Density, Friction Angle, Porosity and Relative Density

A common belief within the mining industry is that hydraulic fill settles to a dry density ($g/cm^3$) of approximately half the specific gravity of the material (Cowling, 1998). As described in section 2.2.2.1, the specific gravity range for hydraulic fill is relatively wide and therefore, the range within which the dry density of a placed hydraulic fill may fall will also be reasonably wide.

As a result of the milling process, hydraulic fill particle shape is very sharp and angular, which would suggest relatively high friction angles. Several hydraulic fills have been reported with friction angles between 30º and 47º[3] Bloss (1992), and published triaxial test results on several hydraulic fill samples across the world also fall within this range (Pettibone and Kealy, 1971; Nicholson and Wayment, 1964).

[3] This was for a high density sample

Extensive in situ testing at various hydraulic fill operations around the world indicate hydraulic fills are typically placed at a medium-dense state, with a relative density of approximately 55% (Nicholson and Wayment, 1964; Pettibone and Kealy, 1971; Corson et al., 1981). The porosity of a free draining hydraulic fill is typically assumed to be approximately 50% (Grice, 1998 b), with published in situ values ranging from 30% to 50% (Nicholson and Wayment, 1964, Pettibone and Kealy, 1971). The values of these properties for several Australian hydraulic fills will be investigated as part of this research and compared to these values.

Permeability

The permeability of hydraulic fill is the property of primary interest because it is commonly used as the sole criteria in establishing the suitability of a tailings product for placement as hydraulic fill (Corson et al., 1981; Lamos, 1993). Approaches to both laboratory and field measurement of percolation rates through the hydraulic fill, are discussed in Herget and De Korompay (1978). They highlight that in many cases it has been found that there is little consistency between percolation rates observed in the laboratory and those existing in the field. Laboratory percolation rates, are referred to as 'absolute percolation rates (*k*)' and define the flow velocity for a fully saturated material at 20° Celcius under the influence of a hydraulic gradient of 1 unit of water head at 20° Celcius divided by the apparent flow path. Refer to Eqn. 2.1 for absolute percolation rate definition.

$$k = \frac{QLC_v}{AH} \qquad \text{Eqn. 2.1}$$

Here,
$k$ = absolute percolation rate (cm/s),
$Q$ = flow rate ($cm^3$/s),
$L$ = length of sample (cm),
$C_v$ = viscosity coefficient (the viscosity of water divided by the viscosity at 20ºC),
$A$ = cross sectional area of sample ($cm^2$), and
$H$ = height of water column (cm).

**FIG 2.1 - Three field permeameters (Herget and De Korompay, 1978)**

In situ effective percolation rate studies were undertaken in the field, using three different permeameters (Fig. 2.1) namely, tube permeameter, twin-rod permeameter and measuring electrode permeameter. Using the tube permeameter, the effective permeability was calculated as the height between the electrodes, divided by the time taken for the water level to fall between the electrodes (Eqn. 2.2)

$$k_e = \frac{H}{t} \qquad \text{Eqn. 2.2}$$

Here,
$k_e$ = effective permeability,
$H$ = height between the electrodes, and
$t$ = the time taken for the water level to fall between the two electrodes.

Both the twin-rod and measuring electrode methods illustrated above, employed similar falling head analysis to calculate the effective permeability with more accurate measurements. The results obtained from the three different permeameters compared well, but these in situ permeability values varied considerably from the absolute permeability values calculated in the laboratory. When factors for the parameters that affect drainage were applied to the absolute values, they related well to the effective values (Herget and De Korompay, 1978).

Hatanaka et al. (2001) studied permeability of undisturbed gravely samples obtained by freezing a gravel column. They found that Hazen’s equation greatly overestimated the permeability. Hatanaka et al. (2001) suggest that the permeability of gravel or sandy soils are not affected by the soil fabric. Therefore, they concluded that the in situ permeabilities can be estimated with a degree of confidence from the samples reconstituted in the laboratory.

A series of laboratory permeability tests were undertaken in 1981 as part of a research project by the United States Bureau of Mines, aimed at accurately defining the physical properties of hydraulic fill materials (Corson et al., 1981). The dependence of percolation rate on the void ratio of the material was identified, and as a consequence, a modified test that correlated the permeability of hydraulic fill to a range of densities was devised. This modified test is described in Wayment and Nicholson (1964), and the results may be used to estimate the flow of water through a fill material in a particular underground state. As will be discussed later, all hydraulic fills commonly settle under self weight in both laboratory tests and in situ conditions to relative densities and void ratios within a reasonably small band.

Research undertaken by Thomas was instrumental in establishing the rule-of-thumb percolation rate for hydraulic fill as 100 mm/hr, which has been standard across the industry since around the 1950's (Nantel, 1998; Cowling, 1998; Keren and Kainian, 1983). With improved understanding into fill drainage and placement practices this standard has come under debate, and the published permeability values of many hydraulic fills that are satisfactorily being used across Australia and worldwide fall well below this value (Brady and Brown, 2001; Herget and De Korompay, 1978; Pettibone and Kealy, 1971). It has even been proposed that a fill permeability of half of the standard value is acceptable (Keren and Kainian, 1983). This research will develop techniques suitable for quantifying the permeability of many Australian hydraulic fills and comparing them to the minimum permeability value specified by current rule-of-thumb practices.

Compressibility and Consolidation

"Consolidation" is the term used to describe volume change that occurs under constant load with the passage of time, which is different from "compression", which is the instantaneous volume change due to an increased load. Since deslimed hydraulic fills are granular with all clay fraction removed, they consolidate quickly and the excess pore water pressure is assumed to dissipate immediately upon placement.

Cohesionless materials, such as most hydraulic fills, are not generally brought to maximum density by dynamic or static loading, however, provided the material is free draining, vibrators may very quickly bring the material to a high density. Nicholson and Wayment (1964) propose the following benefits of increasing the initial density of hydraulic fills by vibratory compaction:

- A decrease in the amount of initial consolidation in the fill before giving effective support to the vein walls would be realized.
- The confined compressive strength of the fill material would be considerably increased.
- A decrease in the permeability of the material would be achieved, thereby reducing the scour of particles by better interlocking, which would decrease the possibility of piping.
- The surface bearing capacity of the fill would be increased so that it could be more effectively used for the bearing of hydraulic props and other temporary support systems and offer a denser surface for mucking on. This would reduce dilution of ore caused by digging into the fill in the cleanout phase of cut-and-fill mining.
- It would present a possible method of dewatering the slower percolating fills by increasing the exudation rate of void water to the surface, thus making it possible to use finer materials with less classification.
- It would offer a possible method of working material transported to a stope at a high slurry density but with insufficient water to distribute the material evenly about the stope.
- It would reduce the effects of shrinkage on fill surfaces in mines where capillary action (surfaces) tend to draw the fill away from the walls.

Results from Nicholson and Wayment (1964) suggest that air vibrators offer an effective means of compacting hydraulic fill.

Herget and De Korompay (1978) clearly show that based on the relationship between porosity ($n$), grain surface per unit volume ($S_v$) and permeability ($k$) developed by

Kozeny, 1933 (Eqn. 2.3) the change in percolation rate due to compaction will depend primarily on porosity. They expressed permeability as:

$$k = \frac{n^3}{5{S_v}^2(1-n)^2} \qquad \text{Eqn. 2.3}$$

Based on Eqn. 2.3, it can be shown for example, that a change in porosity from 0.37 to 0.47 would result in an increase in percolation rate by a factor of 2.8.

As shown above, if access for compaction equipment were feasible, compaction of hydraulic fill on placement may offer several benefits to the mine operation provided the decrease in void space does not completely restrict the flow of water. This research however, will primarily investigate the placement of fill under self weight (without compaction) which is the most common method of placement used in hydraulic fill mines in Australia.

Liquefaction

The primary hazard of slurry-based minefills is the potential for the materials to remobilise, or liquefy after placement. In a cohesionless granular fill mass, fill particles are kept in place by intergranular stresses. When cement is added, cohesion develops between particles. When loading is applied rapidly, pore pressure can build up until such time as the pore pressure equals or exceeds the total stress in the soil. This reduces the effective stress in the soil and thus the shear strength to zero and the soil liquefies. The soil particles are forced apart by the excess pore pressure, and become loosely suspended in a soil/water slurry, unable to be held in position by the forces applied by the surrounding particles. Fig. 2.2 shows the progression of a saturated cohesionless soil towards liquefaction, as the water pressure increases. The white arrows indicate the contact forces between the particles, with the magnitude of the forces being shown by the length. The column to the right hand side of each of the pictures shows the relative water pressure.

In uncemented hydraulic fills, the pore pressure is kept low by desliming the fine fractions and ensuring that the fill is relatively free draining (Grice, 1998 a). It has been shown that saturated hydraulic fill can still be remobilised through the “piping” phenomenon in fill masses (Bloss and Chen, 1998). Grice (1998 a) noted that in cemented hydraulic fills the quantity of fill that can be mobilised is typically limited to that material which has not yet undergone an initial set.

Weakly cemented sands with a range of cementation levels and unit weights were tested in a cyclic triaxial shear device by Clough et al. (1989). For the cemented sands under investigation an unconfined compressive strength (UCS) of 100 kPa was enough to prevent liquefaction under cyclic loads typical of a very large earthquake (M = 7.5). This level of cementation (i.e., UCS = 100 kPa) has been adopted worldwide to address the question of potential liquefaction of minefill masses. Additional levels of cement are sometimes added to account for any long-term decay of strength associated with sulphate attack or self-desiccation.

THESE IMAGES HAVE BEEN REMOVED DUE TO COPYRIGHT RESTRICTIONS

Soil grains in a soil deposit. The height of the blue column to the right represents the level of pore water pressure in the soil.

The length of the arrows represents the size of the contact forces between individual soil grains. The contact forces are large when the pore water pressure is low.

Observe how small the contact forces are reduced because of the high water pressure.

**FIG 2.2 - Behaviour of minefill under increasing pore water pressure (www.ce.washington.edu/~liquefaction/html/main.html)**

## 2.3 Discussion of Failure Mechanisms in Underground Mine Barricades

Several major barricade failures in the mid 1980’s at Mount Isa Mines prompted a large research program aimed at improving the understanding of drainage behaviours throughout the filling and draining of underground stopes (Bloss and Chen, 1988). The research involved monitoring water flows and pressures in stopes, and testing the limiting strengths of barricade. The development of numerical models to predict seepage behaviour of the hydraulic fills was concurrently being undertaken, and the data gained from monitoring used to verify these models through back analysis (Isaacs and Carter, 1983; Cowling et al., 1988; Traves, 1988; Grice, 1989; Cowling et al., 1989). The research concluded that provided the barricades were free draining, insufficient pressure was built up behind the barricades to cause failure. Observations made throughout this study lead to the development of the theory of piping within the hydraulic fill mass. For ‘piping’ defined in geotechnical engineering to occur, water has to flow upwards, thus reducing the effective stresses. A downward flow as suggested in Fig. 2.3 can only increase the effective stresses.

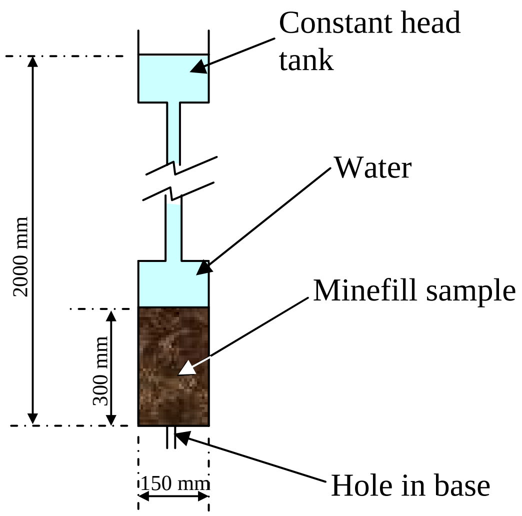


**FIG 2.3 - Test apparatus for observing the piping mechanism**

To improve the understanding of a pipe formation and propagation within hydraulic fill, a series of laboratory test simulations of the piping process were conducted. A constant head permeability apparatus (Fig. 2.3) was set up with a standard uncemented hydraulic fill sample of 300 mm depth. A two meter constant head of water was applied to the sample, and then a small hole at the base of the column was created to provide a discharge point for water and eroded fill.

Three key issues were raised from this research into ‘piping’:

1- The potential significance this piping mechanism has on barricade failures.
2- The ease with which this piping can be initiated and propagate within the hydraulic fill.
3- The limited knowledge that was available then in the area of piping in hydraulic fill.

The research results substantiate that to limit the possibility of a pipe of this type occurring in hydraulic fill stopes, slurry density should be maximised and quality control over the hydraulic fill product placed should be maintained. It is also suggested that paramount importance should be placed regular observation of each barricade, to ensure minefill does not leak through any of the barricades. Without a location for the minefill to discharge, the pipe will not generate.

Although piping has been depicted as the method of failure in this laboratory exercise and many of the hydraulic fill barricades in recent years (Grice, 1998 a; Brady and Brown, 2002), the sequence of events and soil mechanics leading to this mode of barricade failure is poorly understood in the mining industry. The experimental investigation into the development of an erosion tube in hydraulic fill by Bloss and Chen (1998) described above, refers to a “piping” mode of failure and correctly describe the processes as follows:

> *“Piping will commence at a fill boundary where there is a hole sufficiently large to discharge the eroded fill (for example a hole in a bulkhead or adjacent country rock). The pipe will propagate into the fill given that the flow rate is sufficient to erode particles of fill and the result pipe structure. Piping by itself cannot pressurise a bulkhead; however if the pipe intersects a body of water such as water ponding on top of the fill surface, then the energy contained in the water will not be dissipated in the low permeability fill medium. In this case, pressure will be transmitted along the pipe to the surface where piping initiated.”*

If the applied hydraulic pressure exceeds the strength of the barricade, then failure occurs. Bloss and Chen (1998) associate the failure behaviour depicted, with the piping mechanism described in geotechnical engineering by Terzaghi and Peck (1967), as a condition where the pore pressures exceed the vertical stresses therefore causing buoyancy of the soil particles (this is commonly referred to as liquefaction or quick-condition) which propagates in the form of a pipe. Other descriptions and explanations of piping are clearly provided in Holtz and Kovacs (1981), Reddi (2001) and Harr (1962). This geotechnical engineering definition of ‘piping’ is not the process that occurs when the erosion pipe develops as a result of leakage of hydraulic fill, and the two mechanisms should not be associated. To avoid confusion, this method of failure reported in hydraulic fill mining will be referred to as an ‘erosion tube’.

When leakage of fill is observed from a barricade, the failure would occur as detailed by Bloss and Chen (1998) with the development of the erosion tube initiating from the barricade. There are several cases recorded where the erosion tube is the believed method of failure, but a leakage point on the barricade has not been identified. Three explanation have been provided in literature, and they are discussed below,

1. The first cause of an erosion tube, is described as propagation of a tube “initiating from an unobserved leakage point at the barricade” (Grice, 1998). This is possible, but considering the emphasis the industry places on barricade safety, and the quantity of fill that must escape for the tube to reach the surface is considerable, it is unlikely that a barricade leak would go undetected.
2. It is also proposed that when complete tight filling has not been achieved behind a barricade, the tube may propagate as a result of fill discharge into this void shown in Fig. 2.4 (Bloss and Chen, 1998). Based on the rheological requirements of the hydraulic fill, the angle of repose is quite small (approx. 2 to 5 degrees, Grice, 2004), and even if the drive length were very large, only a small void would be created. Even so, if erosion were to initiate from the void, the overlying fill would continuously erode into the gap, until it had been filled, in the form of ‘slip’. For an erosion tube to develop, the soil must escape, which can occur after a barricade fails.

THIS IMAGE HAS BEEN REMOVED DUE TO COPYRIGHT RESTRICTIONS

**FIG 2.4 - Erosion tube initiating from void behind the barricade (reproduction of Figure 7, Bloss and Chen, 1998)**

3. The final, and most plausible explanation is that the leakage occurs into the country or host rock (Bloss and Chen, 1998). Although not covered in this particular research, arching[4] within underground stopes has been widely documented (Mitchell et al., 1975; Bloss, 1992; Rankine et al., 2001, Aubertin, 2003) and the degree of arching within a stope depends on geometry (Rankine, 2000; Belem et al., 2004) and location within the stope or drive (Rankine et al., 2004). Given the degree of arching that can occur particularly in areas such as the stope drives, the vertical stresses in these areas can be very low. If an erosion tube initiates from a region experiencing high degrees of arching, and thus with reduction in normal stresses, it is highly possible that the pore pressures imposed by the erosion tube reaching free surface water exceed the vertical stresses already reduced by arching. In this case liquefaction would occur and if this region of liquefaction extends to the barricade, the full hydrostatic head of the free water would be applied to the barricade. Therefore, if leakage into country or host rock occurs in regions where the vertical stresses have been reduced dramatically as a result of arching it is likely that liquefaction would occur. This is by far most likely to occur if the leakage initiates in the drives, where the vertical stresses remain very low. It is recommended that for mines dealing with highly fractured host rock, research should be directed into the value of sealing the entire drive using shotcrete so that leakage into the host rock in the drives cannot occur.

Although still under investigation, published accounts of the Bronzewing disaster which resulted in a triple fatality in the Normandy mine in Western Australia in 2000 detail that the "stock standard" barricade was inspected only an hour before the incident, and both visual inspection and inspection of installed monitoring devices indicated nothing appeared to be abnormal or unusual at the time (http://www.wsws.org/articles/2000/jul2000/mine-j01_prn.shtml). The reports specify that approximately 18 000 $m^3$ of sand-slurry surged up to 200 m down a decline ramp. These accounts are all consistent with failure resulting from erosion tube initiating

[4] Arching is a phenomenon in soil, in which stresses within the fill are redistributed froma weker soil mass into an adjacent stronger rock surrounding the fill.

from host rock, and liquefaction extending from the highly arched region within the drive, to the barricade.

Grain size distribution has been shown to be the most important parameter affecting the susceptibility of a cohesionless soil to the development of an erosion tube however, confining pressures, magnitude of hydraulic gradient and change in hydraulic gradient within the drive may all influence the likelihood of the erosion tube (Tomlinson and Vaid, 2000). Although the development and propagation of an erosion tube within hydraulic fill is not covered in this research, the findings of the experimental study undertaken by Tomlinson and Vaid, (2000) may prove valuable to further research in this direction. Similarly, the exact nature of the risk of liquefaction in underground hydraulic fill stopes, and methods to assess this risk are not fully understood within the industry, and it is suggested that further research be directed into liquefaction in hydraulic fill stopes.

Very limited literature exists on the analysis of hydraulic fill barricades. Kuganathan (2001), employed experimental and numerical modelling techniques to identify the general failure mechanism of hydraulic fill barricades. Two case studies of barricade failure incidents in Australia, were presented to identify key issues in barricade design and analysis. Kuganathan suggests that there are three main components which contribute to the drainage of a typical underground minefill and barricade system:

1- the minefill material,
2- the minefill in the access drive between the stope and the barricade, and
3- the barricade.

Kuganathan's suggestions for optimum safety in hydraulic fill mines focus on the design details of the access drives, stressing the importance of addressing the hydraulic gradient in the drive, the size of the drive and the effective permeability of the hydraulic fill/brick system.

Kuganathan describes the typical sequence of barricade failure to start with the high pore water pressure gradients in the access drive as a result of poor engineering design. This force on the barricade from the movement of the hydraulic fill in these high-pressure gradient zones exceeds the strength of the barricade, and tension cracks propagate in a 2-3m diameter circle until this central hole is punched out from the barricade. This barricade failure mechanism correlates with the most common failure mechanism observed by Mr. Richard Cowling (2002). The loose, saturated hydraulic fill conditions in the stope promote the development of an erosion tube and funnel flow mechanisms within the hydraulic fill mass. Kuganathan goes further to say that in some cases the whole hydraulic fill mass will flow out of the stope as a result of mass flow conditions developing due to liquefaction.

Four hydraulic fill barricade failures were reported between 1998 and 2001 in Australian mines, including the incident in Western Australia in 2000 where three miners lost their lives (Grice, 2001). Grice suggests that the failure observations tend to confirm the belief that saturation levels of the hydraulic fill determine the outcome of a barricade failure.

## 2.4 In Situ Monitoring of Hydraulic Fill Stopes

In situ monitoring of hydraulic fill stopes provide two major advantages that are critical to underground operations. The measurements included pore water pressures, flow rates and fill/water heights. The advantages are:

1- Identifies abnormalities in the filling process and during drainage.
2- Provides data for the evaluation of numerical modelling techniques and empirical developments as prediction tools.

The disadvantages associated with the monitoring of hydraulic fill and barricade pressures and drainage include:

1- Very high expenses associated with the purchase of measuring and monitoring equipment.
2- The measuring equipment is typically non-retrievable.

Although the financial costs associated with monitoring hydraulic fill stopes are very high, the advantages well outweigh those disadvantages and many operations have successfully monitored the discharge rates and pore pressures during the filling and drainage of stopes (Grice, 1998 a; Ouellet and Servant, 1998; Brady and Brown, 2002). It is common practice these days to install monitoring equipment in stopes prior to filling.

A good case of the use of in situ monitoring to study barricade pressures due to cemented hydraulic fill was presented by Mitchell et al. (1975). Instrumentation was placed in several heavily reinforced concrete barricades in a stope at Fox Mine in Northern Manitoba. The instrumentation included piezometers to measure the water pressures and pressure gradients, total pressure measurement devices which were incorporated in the barricade formwork, several 'mousetrap' drains and mid-level pressure gauges to compute if any water pressure was conveyed to the inner face of the barricade.

The barricade stresses measured by Mitchell et al. (1975) were substantially less than values predicted based using overburden weight (Eqn. 2.4).

$$\begin{aligned} \sigma_h &= \sigma_h' + u = K_o \sigma_v' + u \\ \sigma_h &= k_o \gamma' H + \gamma_w H = (K_o \gamma' + \gamma_w) H \end{aligned} \qquad \text{Eqn. 2.4}$$

Here,

$\sigma_h$ = barricade pressure,

$\sigma_h'$ = effective horizontal pressure,

$\sigma_v'$ = effective vertical pressure,

$u$ = pore water pressure,

$K_0$ = horizontal pressure coefficient (assumed to be 0.5),

$\gamma_w$ = unit weight of water (9810 N/m$^3$)

$\gamma'$ = effective unit weight of fill

$H$ = the height of the backfill above the barricade.

They suggested this was due to the strength gain in the cured minefill, and also due to the effects of arching (Barrett et al., 1978). The water balance study showed that the drainage characteristics of the hydraulic fill compared favourably to the predictions based on laboratory control specimens.

One of the largest in situ monitoring programs in the world has been at Mt Isa Mines, with the results being successfully used to verify several numerical modelling drainage tools and gain invaluable knowledge and understanding into the drainage behaviour of stopes (Cowling et al., 1988). Some of the comprehensive measurements taken during the filling of stopes at Mount Isa Mines alone, have included pore water pressures, earth pressures, fill and water heights within the stope, water volumes discharged from the stope and barricade loading and deformation.

## 2.5 Laboratory Modelling of Hydraulic Fill Stopes

Very limited scale modelling has been reported on hydraulic fill. To the author's knowledge there has been no reported scale modelling data published on the drainage of hydraulic fill stopes. Although scaled modelling provides a very attractive, and significantly more economically viable alternative to in situ monitoring, there are considerable limitations including:

- Modelling of cohesion. There are no reported instances of investigators being able to accurately model cohesive forces, as per those caused by cementation of a fill mass in static scale models. Mitchell and Wong (1982) assumed that the capillary attraction of a scale model approximated the cohesive forces of cement in the field. Nevertheless, in the case of hydraulic fill, there is no cohesion.
- Similitude of gravitational forces. Small, laboratory scale models of geotechnical structures, under gravity loads, lacks the proper similitude to generate the induced stresses within a fill mass, modelling the structures in an increased gravitational field through centrifuge testing has addressed this problem. Centrifuge testing has become more frequently used as a modelling tool over the past 50 years. Studies on the static stability of cemented fills as well as the effects of blast loading on minefill using centrifuge modelling have been reported in literature (Mitchell, 1998; Belem et al., 2004; Nnadi and Mitchell, 1991)

Neither of these limitations affect the study of flow through a non cohesive material that does not consolidate. These are approximations made for the study of drainage of hydraulic fill in this research.

## 2.6 Numerical Modelling of Hydraulic Fill Stopes

With the development of higher powered and more affordable computers, numerical methods have been increasingly utilised in minefill design to identify areas of potential instability.

Numerical simulation of hydraulic fill in mine stopes was initiated by a research contract between Mount Isa Mines (MIM) and L. Isaacs and J. Carter, which resulted in the development of a 2-dimensional model intended to provide a basic understanding of the concepts of the drainage of hydraulic fills in underground stopes (Isaacs and Carter, 1983). Through the use of this model, the developers were able to predict the drainage behaviour of hydraulic fill throughout the filling and drainage of an underground stope. The model requires limited parameter inputs, which were typical for sand of similar size grading as hydraulic fill, which were available at the time, and was restricted in its adaptability due to its fundamental geometric limitations. The barricades were assumed to be placed in flush with the stope, which is not very realistic. For safety reasons, barricades are always constructed at some distance from the stope. Work place health and safety requirements prohibit any access beyond the stope wall, into the unsupported empty stope. Therefore, barricades are always built at least a few meters away from the stope wall.

The model developed by Isaacs and Carter used an integrated finite difference solution method to determine the drainage configuration at each specified timestep. The model assumed the porous hydraulic fill material was homogeneous and isotropic and that Darcy's law for laminar flow was applicable. The top of the hydraulic fill and the phreatic surface was assumed to be horizontal, and when the phreatic surface fell below the full height of the tailings, the upper boundary used for the seepage analysis was the phreatic surface. The position of the phreatic surface was calculated based on the quantity of water in the stope. When new hydraulic fill and water was added, the fill was added directly to the existing hydraulic fill, and the water directly to the phreatic surface, therefore, the addition of each pour had an immediate effect on the flow from the drains at the base of the stope. This introduced minor error in the times and quantities for predicted drain flows.

The conclusions from the research conducted by Isaacs and Carter were that unless the pour rate was very low, the pore pressure developments within the stope were not significantly affected by the permeability of the hydraulic fill or the pour rate. They also concluded that the positioning of multiple drains had considerable impact on the pore pressure development within the system.

Although the research conducted by Isaacs and Carter has probably made the most significant contribution to date to the understanding of the drainage behaviour of hydraulic fill stopes, later research suggests that both pour rate and the hydraulic conductivity of the hydraulic fill does have a substantial effect on the pore pressure development within the system if the fill is not saturated. Considerable pore pressures may develop behind the wetting fronts in the hydraulic fill where the percolation rates have dropped significantly as a result of unsaturated flow (Wallace, 1975). The incorporation of saturated and unsaturated flow regimes would detect this effect.

The other major shortfall of the 2-dimensional model occurs in relating the output of the model to field measurements. The simplest method of in situ stope performance measurement is through outflow drainage rates from each of the barricades. The 2-dimensional model developed by Isaacs and Carter only indicates the overall quantities for individual levels (Cowling et al., 1988). Individual drain discharge approximation may be made by dividing the total discharge for each level by the number of drains on that level.

Work was conducted which extended the program through field experiments and parameter studies including minefill type, pulp density, pour and rest time, stope dimensions, blocked barricades and flushing time, to provide field data from which to back analyse the model parameters and verify the value of Isaacs and Carter's program as a stope drainage prediction tool.

Cowling et al. (1988) confirmed the validity of the seepage model developed by Isaacs and Carter through the back analysis of the field measurements. The work concluded that the coefficient of permeability values derived from this back analysis varied significantly from the laboratory values and that these values could only realistically be derived through the back analysis procedure. Cowling et al. (1988) determined that the influence the water content has on the effective porosity[5] is essential in the use of the model, and when accounted for provides close agreement with regard to pore pressure distribution as well as water balance within the system.

[5] Effective porosity accounts for the fraction of the voids that are active in conducting the water in the process of draining. It discounts the voids occupied by the residual water, which does not drain in engineering time.

The 2-dimensional finite difference model developed by Isaacs and Carter was further extended by Warren Traves for his Masters thesis in 1988 (Traves, 1988). The model was advanced into a 3-dimensional program, which incorporated several features allowing it to be more applicable to field conditions. The 3-dimensional model was capable of simulating the filling and drainage of irregular stope geometries, with heterogeneous hydraulic fill, and provided predictions of pore pressures and flows at specific positions within the stope.

Traves utilized a cells-based approach to simulate the geometry of the stope and the moisture flow through the hydraulic fill. The seepage simulation incorporated both saturated and partially unsaturated flow regimes, allowing for the replication of the delays in time between the placement of a hydraulic fill pour, and the time in which the wetting front reached the phreatic surface. Traves' model was also able to permit spatial variability in hydraulic fill properties and provided output data, which was in an appropriate form for analysis and comparison to both the existing 2-dimensional model and field data.

The validity of the 3-dimensional model was verified through comparison with the established 2-dimensional model (Traves and Isaacs, 1991). Through this validation the potential value of the model as a prediction tool for drainage analysis on existing and proposed hydraulic fill stopes was demonstrated.

Ouellet and Servant (1998) presented the findings from a series of 2-dimensional finite element simulations for cemented hydraulic fill stopes. Ouellet and Servant hypothesised that the geometry of the drain system of a stope had a significant impact on the drainage of the stope and aimed their research on providing a better knowledge of the role the drain system has on the dewatering process of the stope. A cemented hydraulic fill stope was instrumented and daily records were taken during the entire filling process. These field observations and instrumentation data obtained confirmed findings previously reported by others. The 2-dimensional model developed by Ouellet and Servant was done in the commercially available finite element program SEEP/W, which was capable of modelling both saturated and unsaturated flow regimes. The results from the application of the model varied considerably from seepage simulation analysis reported from programs written by Traves and Isaacs and Carter, as well as others including Barrett and Cowling (1980) and Grice (1989 a). The simulation results could not be quantitatively verified against the field results as was done by the other researchers and a qualitative rationale whereby the movement of water in the vertical direction is less than the horizontal one due to layering effects was suggested by Ouellet and Servant to justify their findings.

The additional stope filling and drainage program developed for this research will have the following three major benefits to the mining industry:

- Because the program will be written in a commercially available package, access to the entire industry will be easily available.
- *FLAC* allows for the extension of the program into a 3-dimensional analysis. There is currently no 3-dimensional stope filling and drainage programs that have been verified and are available to the mining industry.
- The development of design charts through the use of the *FLAC$^{3D}$* program will allow for stope drainage prediction by mine operators without the use of numerical modelling.

## 2.7 Objectives

The aims of this research were divided into the following sections:

1. To determine the typical drainage properties and behaviour of Australian hydraulic fills.
2. To determine the drainage and strength properties and behaviour of the permeable barricade bricks used for the containment of hydraulic fill in underground mines.
3. To develop and verify 2-dimensional and 3-dimensional numerical models for simulating the filling and drainage of underground stopes, and to use these to better understand the drainage behaviour of hydraulic fill in underground stopes.

To determine the relative effect the fill and permeable brick properties have on the drainage of underground stopes, using the typical values determined through a series of laboratory tests.

# Chapter 3

# Hydraulic Fill Characterisation

## 3.1 Introduction

Hydraulic fills are simply sandy silts, or silty sands with negligible clay fraction as a result of fill being passed through hydroclones in a process known as desliming. This chapter characterises the typical geotechnical properties of Australian hydraulic fills.

Table 3.1 lists the hydraulic fill samples obtained from six different sources across Australia, the dates they arrived at James Cook University and, condition in which the samples were received.

Samples B1 and B2, obtained in larger quantities were the first hydraulic fill samples studied in this research. In addition they were used in the preliminary studies that led to our unique sample preparation technique and permeability tests that are widely adopted by the mines in Australia (sections 3.4.2 – 3.4.4). Therefore, these are discussed in considerable length. Samples B2, B4 and B5 were sourced during a period in which mine B was not using a typical hydraulic fill and the grain size is finer than standard Australian hydraulic fills. These three samples are not considered representative of Australian fills, but grain size distribution, specific gravity and permeability tests were still performed to identify the effect of this aberration.

Wherever possible, tests were carried out as per the standard procedures specified in the Australian Standards and Lambe (1951). Procedures for some tests, not specified in the Australian Standards, were developed internally at James Cook University and are described in this thesis.

**TABLE 3.1 - Arrival dates and conditions for hydraulic fills tested**

| Mine | Sample | Arrival Date | Arrival Condition |
|---|---|---|---|
| **Mine A** | **A 1** | 5/07/2001 | 3 plastic buckets with the same wet tailings |
| | **A 2** | 22/03/2002 | 20 litre bucket of fill |
| **Mine B** | **B 1** | 18/06/2001 | 205 litre drum of *dry* fill, slightly contaminated by aggregates as large as 75 mm |
| | **B 2** | 18/06/2001 | 205 litre drum of *wet* fill, slightly contaminated by aggregates as large as 75 mm |
| | **B 3** | 22/03/2002 | Container of dry fill, not contaminated |
| | **B 4** | 22/03/2002 | Very small quantity of fill in container |
| | **B 5** | 22/03/2002 | Container of wet fill, not contaminated |
| **Mine C** | **C 1** | 5/07/2002 | Four 10 litre buckets |
| | **C 2** | 2/08/2002 | Four 10 litre buckets |
| | **C 3** | 1/03/2004 | Four 22 litre buckets |
| | **C 4** | 16/03/2004 | Four 22 litre buckets |
| **Mine D** | **D 1** | 13/03/2002 | Two 20 litre buckets of fill |
| | **D 2** | 13/03/2002 | Two 20 litre buckets of fill |
| | **D 3** | 13/03/2002 | Four 20 litre buckets of fill |
| | **D 4** | 13/03/2002 | Four 20 litre buckets of fill |
| | **D 5** | 23/03/2002 | Two 20 litre buckets of fill |
| | **D 6** | 24/03/2002 | Two 20 litre buckets of fill |
| | **D 7** | 25/03/2002 | Two 20 litre buckets of fill |
| | **D 8** | 26/03/2002 | Two 20 litre buckets of fill |
| | **D 9** | 27/03/2002 | Two 20 litre buckets of fill |
| **Mine E** | **E 1** | 24/07/2001 | Small packet of dry fill |
| | **E 2** | 25/07/2001 | Small packet of dry fill |
| | **E 3** | 26/07/2001 | Small packet of dry fill |
| | **E 4** | 27/07/2001 | Small packet of dry fill |
| **Mine F** | **F 1** | 13/07/2001 | 20 litre bucket of wet fill in a plastic bag |

## 3.2 Grain Shape

Scanning electron micrographs were taken to determine the grain shape of the hydraulic fill samples. Figs. 3.1 and 3.2 show electromicrographs taken of fills from mines A, C and D. Typically, hydraulic fills have been reported to have a highly angular grain shape (Nicholson and Wayment, 1964, Pettibone and Kealy, 1971). This angularity can be attributed to the crushing of the waste rock.

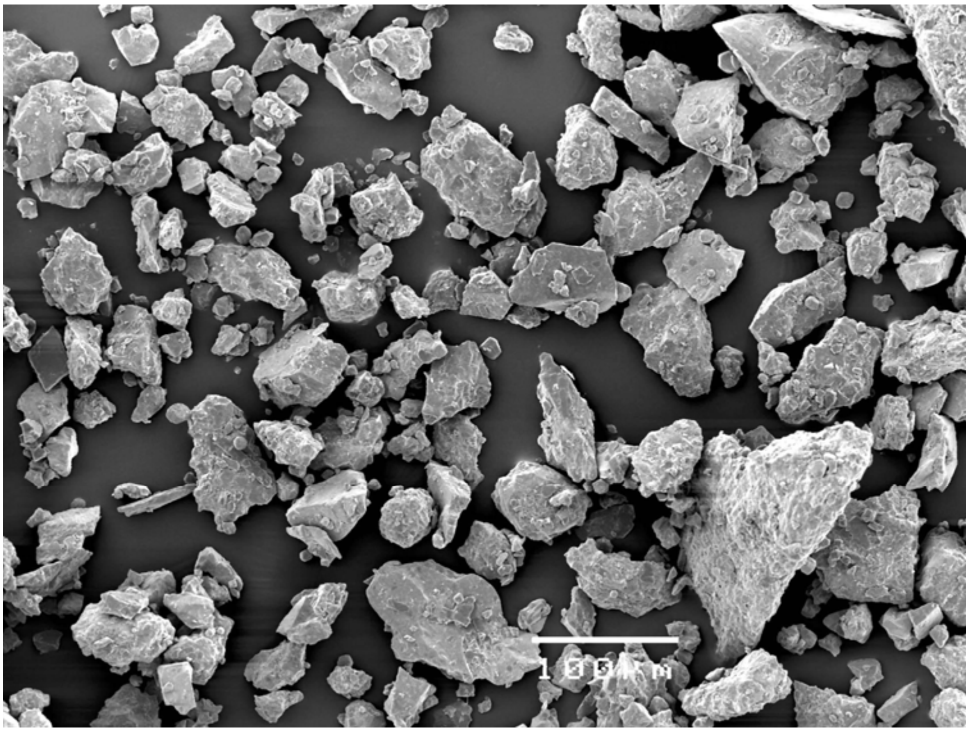


**FIG. 3.1 - Electromicrograph of hydraulic fill A2**

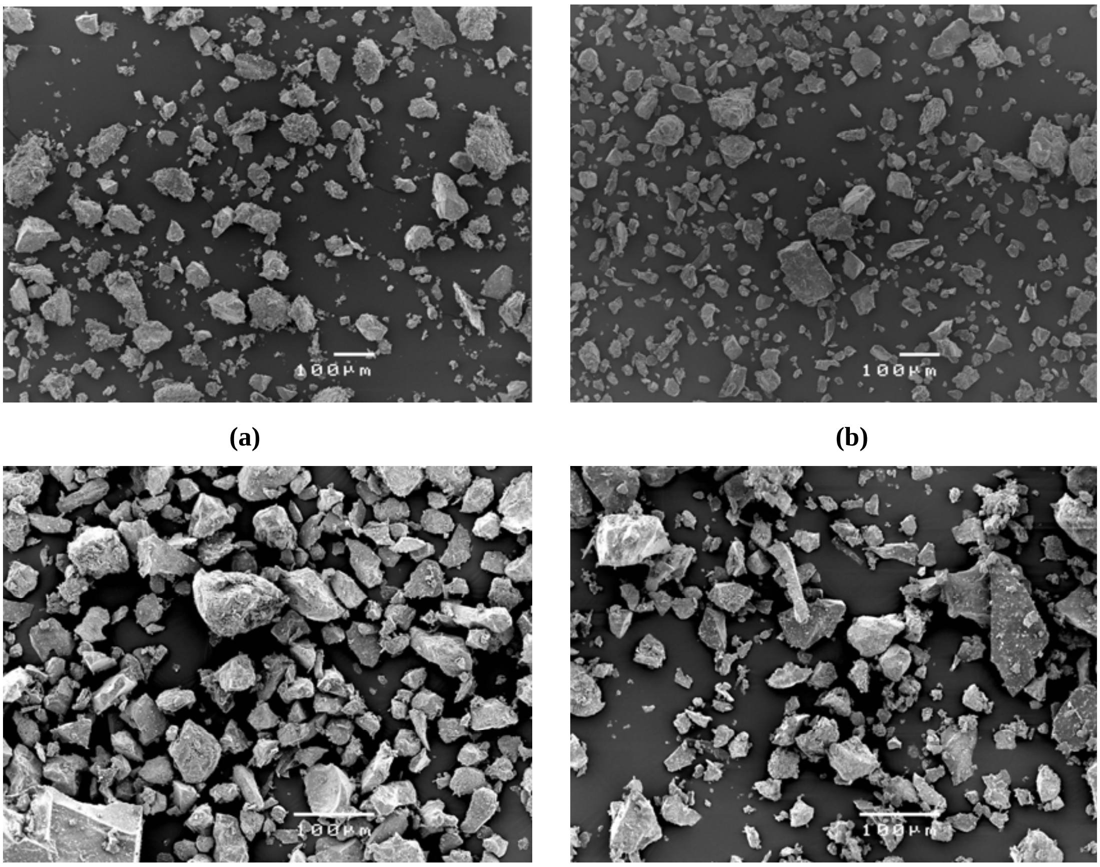


**(a)** **(b)**

**(c)** **(d)**

**FIG. 3.2 - Electromicrographs of hydraulic fills (a) C1 (b) C2 (c) C3 and (d) D6**

The grains in all electromicrographs are quite angular, suggesting the materials will have a relatively high friction angle, which is confirmed in section 3.7

## 3.3 Grain Size Distribution and Specific Gravity

Grain size distribution is considered an important factor in regulating the flow through granular soils (Budhu, 2000). Grain size distribution tests were carried out on all 25 fill samples, and the results are plotted in Fig. 3.3.

Both samples B1 and B2 were contaminated with aggregates as large as 75 mm. A grain size analysis on uncontaminated fill from mine B (B3, B4 and B5) indicated the largest grain size was 600 μm. Therefore, B1 and B2 were sieved to remove the coarser contaminants (grains larger than 600 μm) prior to performing the grain size distribution.

The Malvern MasterSizer-X laser particle sizer (Fig. 3.4) was used to provide a grain size distribution of the fill samples. The Malvern MasterSizer-X laser particle sizer works on the principle of laser ensemble light scattering, and consists of an optical measuring unit that forms the basic grain size sensor, and a computer that directs the measurement and performs information analysis and presentation of results. This method of grain sizing was selected over the use of hydrometer and sieve analysis because of the following advantages that arise from the use of this technique:

1. It is precise, providing high resolution size discrimination,
2. It is fast, typically requiring less than a minute to take a measurement,
3. A wide range of grain sizes can be selected for analysis, and
4. It is simple to use and sample preparation is straightforward.

Three separate tests were carried on each of the samples, to determine the grain size distribution, and the average results are plotted in Fig. 3.3. As indicated in Fig. 3.3, samples B2, B4 and B5 are not representative of typical Australian hydraulic fill samples and the curves show clearly a higher proportion of finer particles in these samples. The other hydraulic fill samples tested typically have $D_{10}$ values between approximately 7 μm and 40 μm.

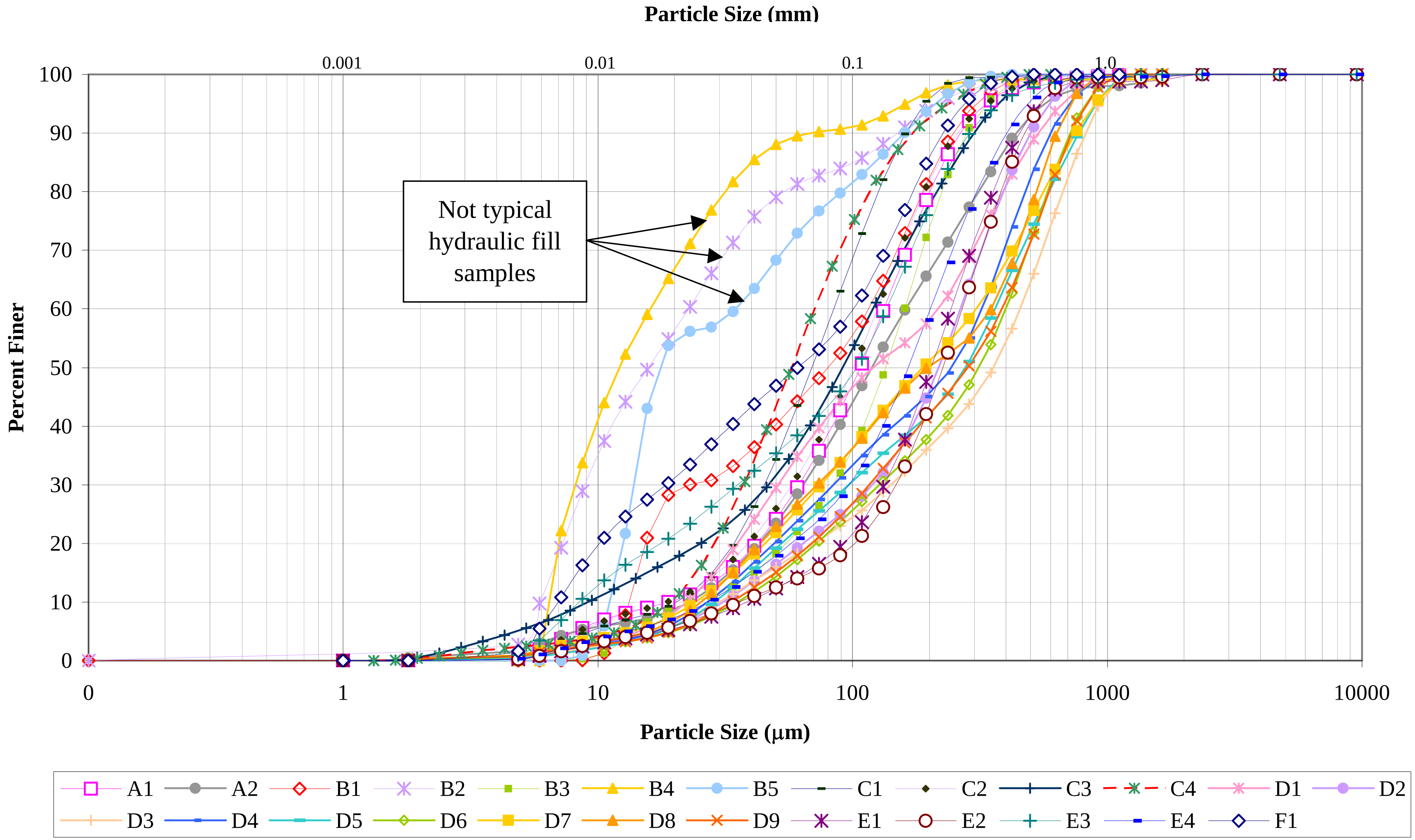


**FIG. 3.3 - Grain size distributions on all hydraulic fills**

**FIG. 3.4 - Malvern MasterSizer-X laser particle sizer**

3.3.1 Sample Preparation

All drums and buckets containing the fills from different locations had segregated during transport and storage. Therefore, they had to be remixed to achieve a homogeneous mix, giving good representative samples for the grain size analysis and further tests. Wherever necessary, they were stored in smaller containers for the ease of remixing.

Preparation of Fill from Mine B

Because some of the fill samples obtained from mine B were contaminated and required different preparation to the other fill samples, the preparation techniques are detailed below, for both the wet mine B sample, and the dry mine B sample.

*Dry Fill Sample (B1) from Mine B*

The entire contents of the 205 litre dry drum were divided into four approximately equal portions and transported to the rod mill (Fig. 3.5). One scoop from each of the four bins was placed into the barrel and this was repeated until a sufficient quantity was contained within the mixer. The sample was mixed for about five minutes to achieve a homogeneous mix, and then the mixed sample placed back into the empty

205 litre drum. The sample was sieved to 600 μm and the coarser fraction was removed.

**FIG. 3.5 - Rod mill**

*<u>Wet Fill Sample(B2) from Mine B</u>*

**(a)** **(b)**

**FIG. 3.6 - Unmixed (a) and homogenous (b) samples in the large pan mixer**

The surface water of the wet sample drum was removed and placed into smaller containers. The entire solids contents of the 205 litre drum were divided into five approximately equal portions and transported to the large pan mixer (Fig. 3.6). The quantity of water, initially removed from the drum, was divided into five portions of approximately equal volume. A fifth of the content from each of the solids containers was placed into the pan mixer, with one of the water portions (Fig. 3.6 a). The contents were mixed for approximately 10 minutes until a homogenous mix was achieved (Fig. 3.6 b). This procedure was repeated five times, until the entire contents had been mixed. The 60 litre sealable drum was set aside as a representable sample for future testing. The sample was dried and sieved to the grain size determined by the Malvern laser sizing prior to testing.

Preparation of Fill from Mines A, C, D, E and F

The samples of the fill mix from the mine sites A, C, D, E and F were of very good quality with no trace of any contaminants. These were separately mixed using the Creteangle Multi-Flow Mixer (Fig. 3.7) and grain size distributions were determined.

**FIG. 3.7 - Creteangle multi-flow mixer**

### 3.3.2 Grain Size Distribution

Malvern MasterSizer-X laser particle sizer was used for the grain size analysis of the fines for the reasons discussed before. For each of the fills, the grain size distribution was determined on three different samples. The results were quite consistent. The average grain size distributions for each of the 25 fill samples are presented in Fig. 3.3, and individual sample grain size curves for samples from mines A, B, C, D, E and F are plotted in Figs. A1.1, A1.2, A1.3, A1.4, A1.5 and A1.6 respectively, in Appendix 1. The values of $D_{10}$, $D_{30}$, $D_{50}$, $D_{60}$, $C_u$ and $C_c$ for all fill samples are summarised in Table 3.2.

**TABLE 3.2 – Grain size distribution data for hydraulic fill samples**

| | | $D_{60}$ μm | $D_{50}$ μm | $D_{30}$ μm | $D_{10}$ μm | $C_c$ | $C_u$ |
|---|---|---|---|---|---|---|---|
| **Mine A** | **A 1** | 132.91 | 106.44. | 61.51 | 19.06 | 1.49 | 6.97 |
| | **A 2** | 169.70 | 120.29 | 69.29 | 23.41 | 1.21 | 7.25 |
| **Mine B** | **B 1** | 112.86 | 79.18 | 25.75 | 13.34 | 0.44 | 8.46 |
| | **B 2** | 22.67 | 15.79 | 8.93 | 5.93 | 0.59 | 3.82 |
| | **B 3** | 159.85 | 135.03 | 83.84 | 23.39 | 1.88 | 6.83 |
| | **B 4** | 16.08 | 12.19 | 8.20 | 5.75 | 0.73 | 2.80 |
| | **B 5** | 34.71 | 17.74 | 13.90 | 11.13 | 0.50 | 3.12 |
| **Mine C** | **C 1** | 84.62 | 69.4 | 45.19 | 20.32 | 1.19 | 4.16 |
| | **C 2** | 125.53 | 101.39 | 57.87 | 18.59 | 1.44 | 6.75 |
| | **C 3** | 134.12 | 91.35 | 55.50 | 12.10 | 1.90 | 11.08 |
| | **C 4** | 71.16 | 57.3 | 37.34 | 19.22 | 1.02 | 3.70 |
| **Mine D** | **D 1** | 263.19 | 119.18 | 61.83 | 27.06 | 0.54 | 9.73 |
| | **D 2** | 323.09 | 218.42 | 145.51 | 37.71 | 1.74 | 8.57 |
| | **D 3** | 553.18 | 379.68 | 172.27 | 36.48 | 1.47 | 15.16 |
| | **D 4** | 390.72 | 257.73 | 102.32 | 32.80 | 0.82 | 11.91 |
| | **D 5** | 440.79 | 264.44 | 117.58 | 34.97 | 0.90 | 12.60 |
| | **D 6** | 485.65 | 317.27 | 154.79 | 42.93 | 1.15 | 11.31 |
| | **D 7** | 371.66 | 177.46 | 91.01 | 29.38 | 0.76 | 12.65 |
| | **D 8** | 424.55 | 211.07 | 88.31 | 30.90 | 0.59 | 13.74 |
| | **D 9** | 469.67 | 264.17 | 141.79 | 40.59 | 1.05 | 11.57 |
| **Mine E** | **E 1** | 244.51 | 179.60 | 133.18 | 38.64 | 1.88 | 6.33 |
| | **E 2** | 270.14 | 226.23 | 147.44 | 36.32 | 2.22 | 7.44 |
| | **E 3** | 136.33 | 103.59 | 36.64 | 8.48 | 1.16 | 16.08 |
| | **E 4** | 202.51 | 165.61 | 96.59 | 26.95 | 1.71 | 7.51 |
| **Mine F** | **F 1** | 100.41 | 61.06 | 18.52 | 6.97 | 0.49 | 14.41 |

$D_{10}$ is the grain size corresponding to 10% passing. i.e., 10% of the grains are finer than $D_{10}$. The effective grain size of a granular soil is generally given as $D_{10}$, which is a good representation of the size of the pore channels that allow the water to flow through. Hazen (1892, 1930) suggested that for clean (no fines) filter (uniformly graded) sands in loose state,

$$k \text{ (cm/s)} = CD_{10}^{2} \qquad \text{Eqn. 3.1}$$

where $C$ is a constant in the range of 0.01 to 0.015, and $D_{10}$ is in mm. $D_{50}$ is the median grain size, where 50% of the grains are less than this size. The general shape of a grain size distribution curve are commonly described using the coefficient of uniformity ($C_u$) and the coefficient of curvature ($C_c$), defined in Eqns. 3.2 and 3.3 respectively.

$$C_u = \frac{D_{60}}{D_{10}} \qquad \text{Eqn. 3.2}$$

$$C_c = \frac{D_{30}^2}{D_{60} D_{10}} \qquad \text{Eqn. 3.3}$$

The 25 fill samples, contained mainly silt-size (2-75 μm) and sand-size (> 75 μm) grains, with typically less than 1% clay fractions. The grain size distributions for samples B2, B4 and B5 were distinctly different to all other 22 samples. These samples contain a significantly higher fine silt content than the other hydraulic fills. It is widely understood within the mining industry that the fine grains have the most significant influence on permeability of the fill. Thomas and Holtham (1989) observed that 10 μm is generally selected as the arbitrary division between coarse and fine grains. Therefore, the rule-of-thumb adopted across Australia is to aim to have less than 10% particles passing 10 μm. Herget and De Korompay (1978), quote 35 μm as the typical $D_{10}$ value for hydraulic fills, and many other researchers with extensive experience have quoted hydraulic fill $D_{10}$ values in excess of 10 μm as typical (Kuganathan 2002; Cowling et al. 1988; Brady and Brown 2002; Bloss 1992). For this reason, samples B2, B4 and B5 were not considered as typical hydraulic fills in this research.

Excluding samples B2, B4 and B5, it can be seen in Fig. 3.3 that the grain size distribution curves for typical Australian hydraulic fills, fall within a very narrow band. The band is shown in Fig. 3.8. The coefficient of uniformity was quite low, ranging from 4 to 15 for the 25 Australian hydraulic fills studied (Table 3.2).

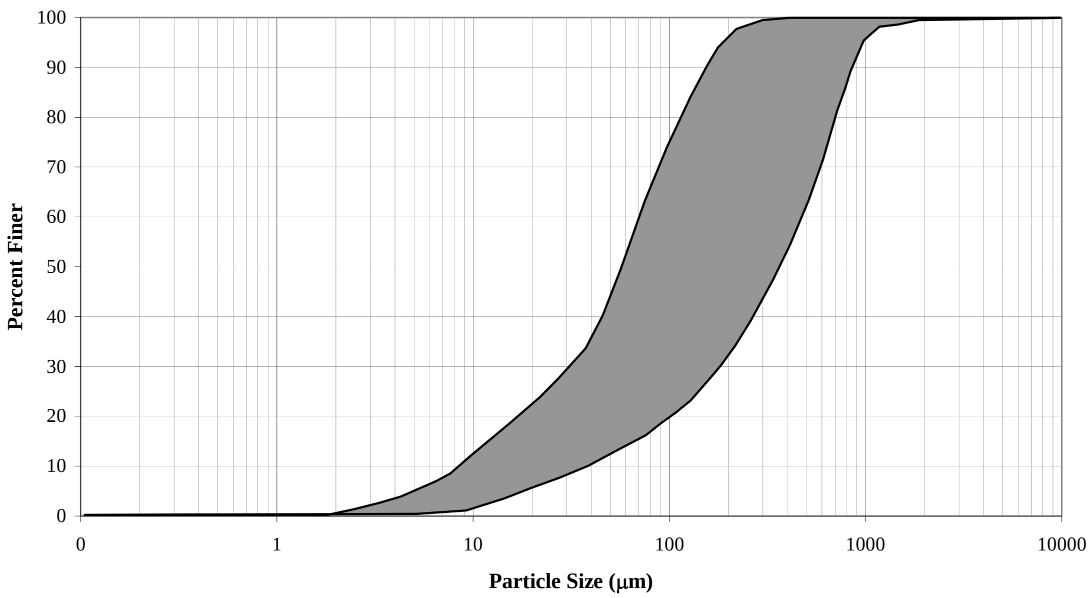


**FIG. 3.8 - Generalised grain size distribution for Australian hydraulic fills**

### 3.3.3 Specific Gravity

The specific gravity values were determined only for samples from mines A, B (excluding samples B3, B4 and B5), C and D. These were required in computing void ratios of the settled fill in the permeameter.

The specific gravity tests on the fills were carried out in 250 ml density bottles, as per AS1289.3.5.2-1995. The density bottles with hydraulic fill, half-full with water, were placed in a warm water bath for 30-45 minutes to remove entrapped air. This was later placed in a desiccator where a vacuum of 13 kPa (using KNF Neuberger vacuum pump, 0.12 kW, 1.7 Amp) was applied for about an hour to completely remove any remaining air within the sample. The water content of the original sample was determined as per AS1289.2.1.1-1992. The specific gravity values of all fills are summarised in Table 3.3. There is a wide range for fill specific gravity values ranging from approximately 2.79 to 4.35. It is common for fills to be pumped back underground as a certain percentage solids by weight (e.g., 72% solids). For this reason the specific gravity of the fill being placed will significantly influence the quantity of water that is also placed underground. At a specific solid content, larger values of specific gravity would imply larger mass of solids to fill in the stope and thus larger quantity of water in the slurry. For example, for two fills placed at 75% solid content, the first with $G_s$ = 2.77 and the second with $G_s$ = 4.35, the slurries will be 48% and 59% water by volume slurry respectively. This means that there would be a difference of 100 litres for every tonne of slurry pumped underground.

**TABLE 3.3 - Hydraulic fill specific gravity values**

| Mine | Sample | Specific gravity ($G_s$) |
|---|---|---|
| Mine A | A 1 | 2.79 |
| | A 2 | 2.80 |
| Mine B | B 1 | 2.88 |
| | B 2 | 2.77 |
| Mine C | C 1 | 4.35 |
| | C 2 | 3.45 |
| | C 3 | 3.69 |
| | C 4 | 3.02 |
| Mine D | D 1 | 3.42 |
| | D 2 | 3.71 |
| | D 3 | 3.53 |
| | D 4 | 3.50 |
| | D 5 | 3.50 |
| | D 6 | 3.53 |
| | D 7 | 3.32 |
| | D 8 | 3.12 |
| | D 9 | 3.42 |

## 3.4 Permeability of Hydraulic Fill

Permeability of soil is generally determined in the laboratory by constant head permeability tests or falling head permeability tests. Constant head permeability tests are suitable for coarse grained soils and falling head tests are suitable for fine grained soils. Hydraulic fills, which fall on the border between sand-size and silt-size grains, may be studied using either of the two tests. Both tests are based on Darcy’s law and assume laminar flow. Typical permeability values for fine sands and silts, which are similar to the hydraulic fills tested, vary in the range of $10^{-5}$ m/s to $10^{-7}$ m/s as shown in Table 3.4 (Terzaghi et al., 1996).

**TABLE 3.4 - Permeability and drainage characteristics of soils (Terzaghi et al. 1996)**

THIS TABLE HAS BEEN REMOVED DUE TO COPYRIGHT RESTRICTIONS

Several empirical relationships have been reported in the literature with regard to the permeability of soils. Some of the more common relationships are discussed in this section. In early to mid 1900s, several researchers attempted to develop relationships between porosity and hydraulic conductivity (Kozeny, 1927, 1933; Carman, 1956). However, these were mostly developed for clean filter sands (no fines and fairly uniform) in loose state (near $e_{max}$). $D_{10}$, also known as the effective grain size, is an important value in regulating the flow through granular soils, including hydraulic fills (Budhu, 2000). The following relationship (Eqn 3.1), developed by Hazen is commonly used to relate grain size to permeability in granular material,

$$k \text{ (cm/s)} = CD_{10}^2$$

where $C$ is a constant and $D_{10}$ is in mm (Hazen, 1930). The values for $C$ reported by Lambe & Whitman (1979) and presented in Table 3.5, show a wide spread for the constant C in Hazen's equation, far less than the suggested value of 1.0 when applied to a wide range of soils.

**TABLE 3.5 - Hazen's constant values reported by Lambe and Whitman (1979)**

THIS TABLE HAS BEEN REMOVED DUE TO COPYRIGHT RESTRICTIONS

Lambe and Whitman suggest a value of 1; Das (2002) suggests 1-1.5; Holtz and Kovacs (1981) suggest a value in the range of 0.4-1.2, with an average value of 1.0. The in situ measurements of coefficient of permeability of granular deposits in Mississippi River Valley, USA, as reported by Leonards (1962) are shown in Fig. 3.9 (vide Barnes, 2000) along with a band showing the values predicted by Hazen's equation. Here, it appears that Hazen's equation only forms a lower bound, with most in situ values being much greater than what is predicted by Hazen's equation.

THIS IMAGE HAS BEEN REMOVED DUE TO
COPYRIGHT RESTRICTIONS

**FIG. 3.9 - In situ permeability measurements of granular deposits in Mississippi River Valley, USA, as reported by Leonards (1962)**

Several relationships between void ratio and permeability have been published. Taylor (1948) showed that permeability of sand can be expressed as, $k = Ce^3/(1+e)$. For any clay, Taylor (1948) said that plotting $e$ in arithmetic scale and $k$ in log scale can be approximated by a straight line. This was questioned by Samarasinghe et al. (1982). They showed that permeability of sands and clays can be related to void ratio by $k = Ce^n/(1+e)$, where the constant $n$ depends on the soil, with values of 3.2 for crushed glass, 4 for kaolinite, and 5.2 for Liskeard clay. Carrier et al. (1983) showed that for slurried fine grained mineral wastes, including minefill and dredged materials, and remoulded clays, $k$ (m/s) = $Ce^n/(1+e)$ works very well over the range of void ratios (1-5) that is usually involved in this type of problems. They reported n values from 3.5 to 11 depending on the material. The permeability values of these materials ranged from $10^{-6}$ to $10^{-14}$ m/s. Casagrande (vide Das 2002) suggested that for fine or medium clean sands with bulky grain, $k = 1.4e^2k_{0.85}$ where $k_{0.85}$ is the permeability at $e$ = 0.85. As shown in Fig 3.10, for all soils e versus log $k$ is a straight line (Lambe and Whitman, 1979). All these developments suggest that $k$ is proportional to $e^n$ where $n$ is a real number, and plotting $e$ in arithmetic scale and $k$ in log scale is approximated by a straight line. Lambe & Whitman (1979) documented the wide range of permeability values of different soils, as measured in the laboratory (Fig. 3.10).



**FIG. 3.10 - Various laboratory measured soil permeabilities (Lambe and Whitman, 1979)**

The effect of consolidation pressure on the permeability of different soil types is shown in Fig. 3.11. It can be seen that the consolidation pressure does not reduce the permeability significantly in the case of coarse grained soils. Therefore, it is reasonable to assume a constant value of permeability at all depths within a hydraulic fill.

THIS IMAGE HAS BEEN REMOVED DUE TO
COPYRIGHT RESTRICTIONS

**FIG. 3.11 - Effect of consolidation pressure on permeability (Cedegren, 1967)**
**1 tsf = 95.76 kPa**

It can be seen in Figs. 3.3 and 3.8 that the grain size distributions for many Australian fills fall into a very narrow band. This research is focussed on drainage of hydraulic fill stopes, and therefore the permeability of these fills has been thoroughly analysed in this chapter, and the agreement to Hazen's empirical relationship (Eqn. 3.1) developed for clean sands has been reviewed.

### 3.4.1 Theoretical Developments

The theoretical developments for standard permeability testing of soils is divided into constant head test and falling head test, which are the two most commonly used soil permeability tests in the laboratory.

*Constant Head Test*

In a constant head test, water is allowed to flow through the sample under constant total head. The sample is held in a permeameter, and the water flows vertically. The flow is measured using a measuring cylinder. A schematic diagram is shown in Fig. 3.12 a. From the constant head loss ($h_L$), sample dimensions (cross-sectional area = $A$; length = $L$), and the flow rate ($Q$), permeability ($k$) can be computed using the following equation:

$$k = \frac{QL}{h_L At} \qquad \text{Eqn. 3.3}$$

Here, $Q$ is the quantity of water (cm$^3$) collected in time $t$ (seconds), $L$ and $h_L$ are in cm, $A$ in cm$^2$ and permeability $k$ is in cm/s.

*Falling Head Test*

In a falling head permeability test, the water in the standpipe is allowed to fall during a period of time $t$, where the head drops from $h_1$ to $h_2$ (Fig. 3.12 b). Applying Darcy's law, it can be shown that the permeability is given by:

$$k = \frac{a_2 L}{At} \ln \frac{h_1}{h_2} \qquad \text{Eqn. 3.4}$$

where $a_2$ and $A$ are the cross-sectional areas of the stand pipe and the sample, respectively, and $t$ is the time taken for height of water column $h$ to drop from $h_1$ to $h_2$ in the stand pipe. $L$ is the length of the sample.

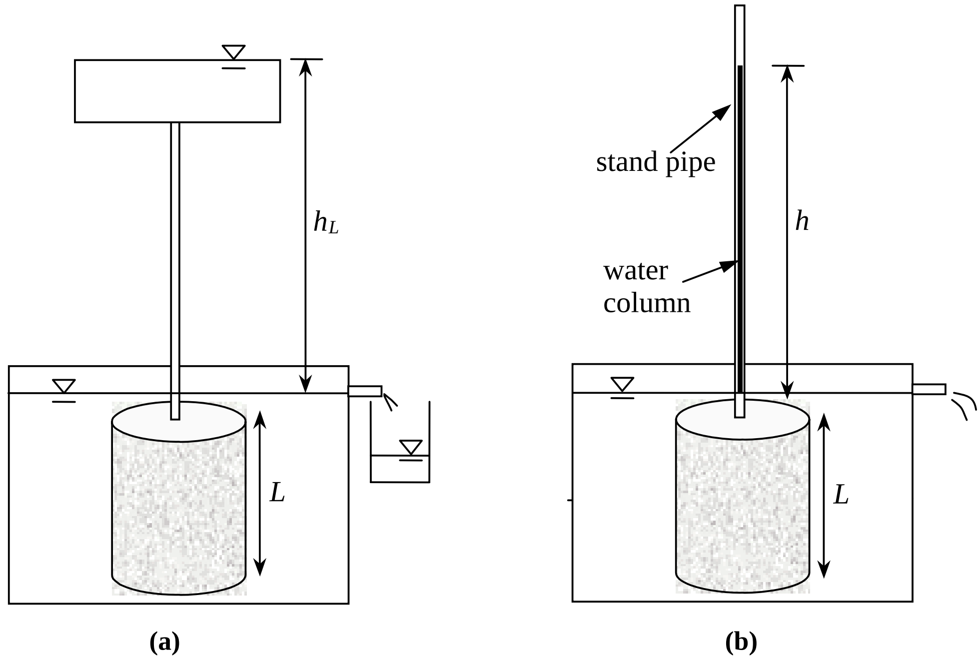


**FIG. 3.12 - Schematic diagram of (a) constant head and (b) falling head test apparatus**

3.4.2    Sample Preparation

The slurry samples were prepared to the water contents consistent with the in situ slurry that is placed in the mine. The fills consolidated under their own self weight, giving water contents and porosities and dry densities shown in Table 3.6.

B2 contained substantial fines (see Fig.3.3, and Table 3.2) and was quite different in grain size distribution from all other samples tested. When sample B2 was mixed at water content of 36.1% and placed in the permeameter, the resulting sample was of a consistency quite different from that obtained from all other samples, and typical slurry consistency. The fill mix was much more viscous and contained air pockets, which were difficult to remove through rodding, or vibrating techniques, or under the application of a vacuum for long durations of time. To overcome this problem, the fill was mixed at the higher water content of 55%, and was allowed to consolidate under the self weight as for the other samples. The water contents, void ratios and dry densities of the prepared and final samples are summarised in Table 3.6.

**TABLE 3.6 - State of permeability test samples**

| | | Specific gravity ($G_s$) | Slurry: % solids by weight | Settled fill in permeameter: Water content (%) | Porosity | Void ratio | Dry density (g/ml) |
|---|---|---|---|---|---|---|---|
| Mine A | A 1 | 2.79 | 73.6 | 23.0 | 0.40 | 0.67 | 1.70 |
| | A 2 | 2.80 | 73.7 | 24.4 | 0.41 | 0.69 | 1.66 |
| Mine B | B 1 | 2.88 | 74.2 | 23.2 | 0.40 | 0.67 | 1.72 |
| | B 2 | 2.77 | 64.5 | 33.4 | 0.48 | 0.93 | 1.44 |
| Mine C | C 1 | 4.33 | 77.3 | 18.4 | 0.44 | 0.78 | 2.42 |
| | C 2 | 3.45 | 77.8 | 19.1 | 0.38 | 0.62 | 2.13 |
| | C 3 | 3.69 | 75.2 | 17.1 | 0.39 | 0.63 | 2.26 |
| | C 4 | 3.02 | 75.2 | 19.4 | 0.37 | 0.59 | 1.90 |
| Mine D | D 1 | 3.42 | 77.3 | 18.4 | 0.37 | 0.58 | 2.16 |
| | D 2 | 3.71 | 77.3 | 17.5 | 0.40 | 0.66 | 2.23 |
| | D 3 | 3.53 | 77.3 | 20.1 | 0.41 | 0.70 | 2.08 |
| | D 4 | 3.50 | 77.3 | 20.1 | 0.42 | 0.72 | 2.04 |
| | D 5 | 3.50 | 77.3 | 20.0 | 0.41 | 0.70 | 2.06 |
| | D 6 | 3.53 | 77.3 | 18.8 | 0.40 | 0.66 | 2.13 |
| | D 7 | 3.32 | 77.3 | 20.1 | 0.40 | 0.68 | 2.98 |
| | D 8 | 3.12 | 77.3 | 23.7 | 0.42 | 0.72 | 1.81 |
| | D 9 | 3.42 | 77.3 | 20.8 | 0.42 | 0.72 | 1.98 |

Using the water content, the quantities of both water and dry fill required to fill the apparatus at this density were calculated. The fill mix was placed in the permeameter in five layers, and the quantity for two layers mixed at a time. The layer heights were marked on the inside of the permeameter, and the permeameter was placed within the permeability test overflow box shown in Fig. 3.13. Two pieces of Whatman No. 52 filter paper were cut to fit the inside diameter of the permeameter. One was saturated with distilled water and placed in the base of the apparatus.

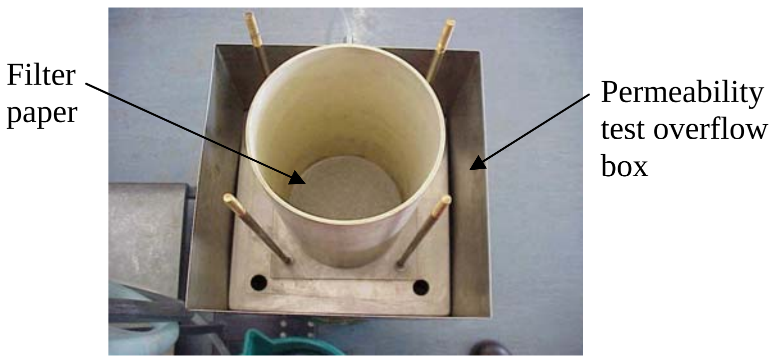


**FIG. 3.13 - Permeameter in test overflow box**

**(a)** **(b)**

**FIG. 3.14 - Decant water at surface of permeameter**

The fill slurry was mixed by hand until all grains were suspended and the mix behaved as a dense liquid. A 100 ml beaker was used to place the fill slurry into the permeameter in a circular motion ensuring even distribution of the fill across the area of the mould. At each one-fifth level marking, the solid that had not settled was stirred very gently by hand. The sample was then left for a period of approximately 10 to 30 minutes (depending on the fill being tested) until the build-up of decant water was apparent on the surface. The next layer of fill was then added using the same procedure. Once filled, the decant water was removed using a spoon (Fig. 3.14). The fill level within the permeameter was increased and decant water allowed to form before it was removed. This was repeated until the entire permeameter was filled with fill.

The second piece of filter paper was wet with distilled water and lowered onto the top of the fill sample ensuring no air voids were caught between the sample and the filter paper. The top of the permeameter was then fastened onto the apparatus, and the small void between the top of the apparatus and the filter paper completely filled with distilled water.

### 3.4.3 Constant Head Permeability Test

The constant head assembly was then attached to the top of the permeameter and secured tightly using a ring fastener. The connection was monitored very closely for leakage, and on any leakage Loctite 567 thread sealant was applied (Fig. 3.15).

**(a)** **(b)**

**FIG. 3.15 - Top of permeameter (a) without sealant, (b) with sealant**

The overflow tank surrounding the permeameter (Fig. 3.13) was filled with water to the level of the overflow pipe, and the apparatus was allowed to reach steady state over a period of approximately half an hour. The quantity of flow collected in a beaker placed under the overflow pipe over a period of time was measured. The duration of each collection period depended on the flow rate of the sample. Three consistent determinations of permeabilities were obtained for each of the three head values (106 cm, 126 cm and 153 cm). The consistency of the results was generally an indication of steady state, and the permeability was calculated using Eqn. 3.3. Usually the test was also performed over a long-term duration to ensure steady state flow had occurred prior to commencing the test. Fig. 3.16 a, shows a photograph of the constant head apparatus. After completion of the constant head test, a falling head permeability test was performed on the same sample prior to dismantling the apparatus and drying the sample in three equal portions to obtain water content values.

### 3.4.4    Falling Head Permeability Test

The same permeameter sample used in the constant head permeability test was also used in the falling head test (Fig. 3.16 b). The black water inflow pipe (Fig. 3.16 a) was removed from the constant head tank, and the permeameter with sample was attached to the falling head assembly. The 790 mm, 435.4 mm and 240 mm heights (above the tail water) were marked on the falling head stand pipe. These heights were calculated such that the theoretical time required for the head to fall between the first two marks was the same as that required for the second to third marks, where

$435.4 = \sqrt{(790)(240)}$ (Lambe, 1951). The water level in the stand pipe was started at the 790 mm level and the time required for the water level to fall to the two lower markings was measured and recorded. Generally, the 3.5 mm diameter stand pipe (the other option being 7.2 mm diameter) was used due to the relatively low permeability of the fill samples. This test was repeated a few times to ensure consistent values of permeability were determined using equation 3.6.

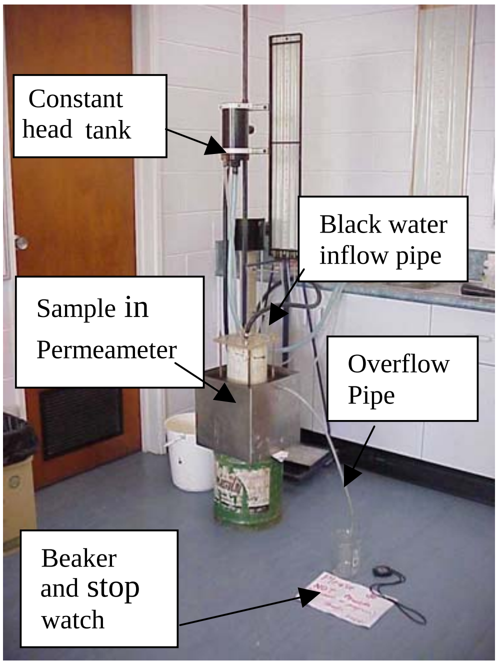


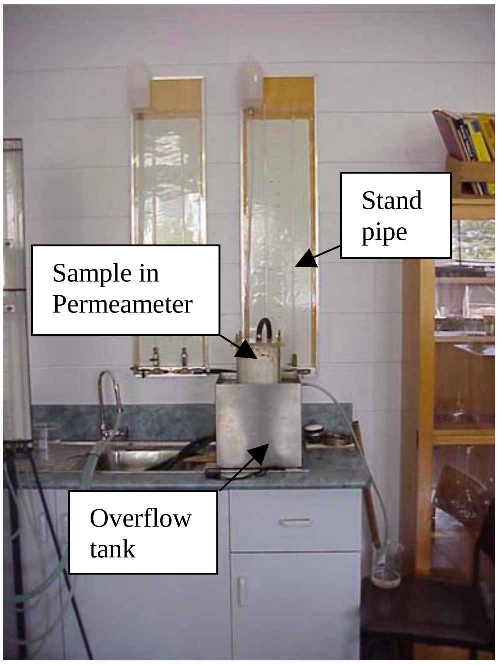


**FIG. 3.16 - Soil permeameter set-up (a) constant head (b) falling head**

On completion of the falling head permeability test, the permeameter was unfastened from the black water inflow pipe and removed from the overflow tank. The top of the permeameter was unscrewed, and excess water from above the top filter paper scooped from the container using a spoon. The height of the sample was measured and recorded and the filter paper discarded (Fig. 3.17 a). The permeameter cylinder was then lifted to leave the sample free standing (Fig. 3.17 b). The sample was divided into three approximately equal portions, and cut using a wire saw (Fig. 3.17 c). Wet weights were recorded prior to drying the sample for 24 - 48 hours and measuring dry weights. Using a mortar and pestle, the sample was crushed for reuse.

(a)

(b)

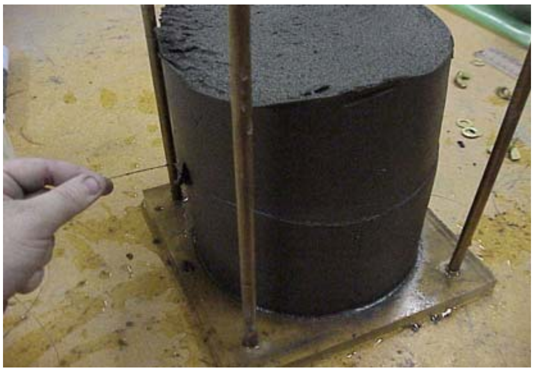

(c)

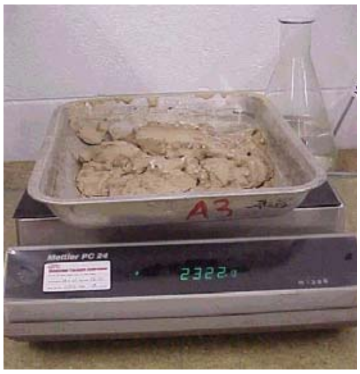


(d)

**FIG. 3.17 - Sample disassemble procedure (a) removal of excess water and filter paper (b) removal of apparatus cylinder (c) dividing the sample (d)weighing the sample**

A unique mobile fill permeability testing apparatus was designed and constructed so that these tests would be more easily performed on site. The apparatus was capable of performing both constant head and falling head tests without moving the permeameter, therefore reducing risk of error associated with sample disturbance. The apparatus is lightweight, portable and able to apply constant head values of up to 2.5 meters. The apparatus, which is constructed of stainless steel, is shown in Fig. 3.18. This setup is being used in Australian mines, which have also adopted the sample preparation techniques and test procedures described in 3.4.2 to 3.4.4.


**FIG.3.18 – JCU mobile constant and falling head permeability apparatus in a mine**

### 3.4.5 Hydraulic Fill Permeability Results

The constant and falling head permeability values, are shown in Table 3.7, showing very good agreement (Fig. 3.19).

**TABLE 3.7 - Fill permeability summary**

| | | Permeability (mm/hr) | | |
|---|---|---|---|---|
| | | **Constant head** | **Falling head** | **Average** |
| **Mine A** | **A 1** | 10.0 | 10.4 | 10.2 |
| | **A 2** | 18.7 | 19.4 | 19.1 |
| **Mine B** | **B 1** | 2.2 | 1.9 | 2.1 |
| | **B 2** | 0.5 | 0.6 | 0.6 |
| **Mine C** | **C 1** | 21.1 | 21.9 | 21.5 |
| | **C 2** | 18.0 | 17.9 | 17.9 |
| | **C 3** | 17.8 | --- | 17.8 |
| | **C 4** | 22.5 | --- | 22.5 |
| **Mine D** | **D 1** | 20.2 | 21.1 | 20.7 |
| | **D 2** | 23.8 | 24.3 | 24.0 |
| | **D 3** | 52.9 | 54.5 | 53.7 |
| | **D 4** | 20.2 | 20.7 | 20.4 |
| | **D 5** | 24.8 | 25.7 | 25.3 |
| | **D 6** | 30.6 | 31.0 | 30.8 |
| | **D 7** | 20.5 | 20.5 | 20.5 |
| | **D 8** | 31.1 | 31.9 | 31.5 |
| | **D 9** | 26.3 | 27.4 | 26.8 |

In the mining industry, mm/hr is the preferred unit for permeability (1cm/s = 36000 mm/hr).

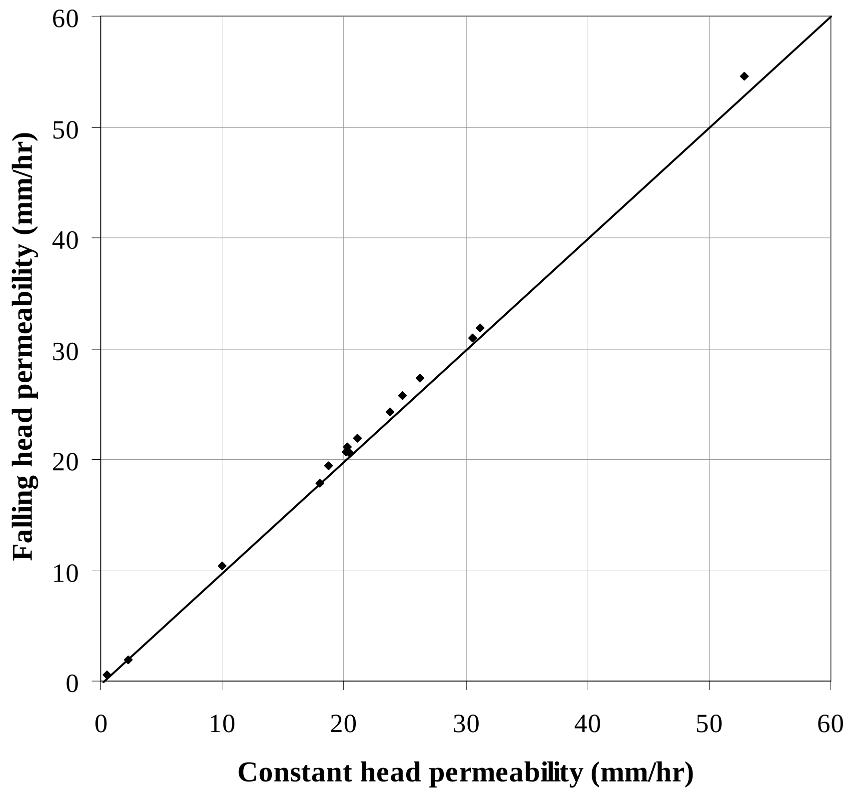


**FIG. 3.19 - Fill constant head and falling head permeability values**

The constant and falling head test results agreed well for all samples. Darcy's coefficient of permeability typically fell between 0.6 mm/hr and 53.7 mm/hr for all tests. The substantial difference in permeability values between the two mine B samples from the rest can be accounted for by the difference in grain size distribution (Table 3.2 and Fig. 3.3). B2 had permeability lower than fills tested from the other mines by an order of magnitude. The significantly larger proportion of relatively finer grain sizes in the B2 sample (the $D_{60}$ value for B2 is 22.7 μm and the $D_{60}$ value for B1 was 115.8 μm) reduces the permeability, which is indicated by the B1 sample being approximately 3.6 times more permeable than the B2. As seen in Table 3.2 and Fig 3.3, the $D_{30}$ value for B1 is significantly less than that of the other samples tested for permeability. This may be the reason B1 has a lower permeability than the other (disregarding B2) hydraulic fills tested.

### 3.4.6 Discussion of Hydraulic Fill Permeability Results

Mitchell et al. (1975) determined the permeability of the cemented hydraulic fill using 152 mm diameter and 305 mm high samples prepared in the laboratory. They found that the drainage characteristics in the mine stope agreed with the predictions based on the permeability values measured in the laboratory. The found that permeability decreased exponentially with curing time, from approximately 54 mm/hr measured between 10 and 20 days, to a minimum of approximately 25 mm/hr obtained at 150 days. The permeability values seemed to plateau after approximately 120 days of curing. The in situ permeability varied between 7.2 mm/hr and 23 mm/hr for the period of about 144 days which was the time taken to fill the stope. Limited tests done by the author on cemented hydraulic fills, in addition to the work for this research confirms that the permeability of cemented tailings decreases exponentially and plateaus to a minimum value after around 20 to 30 days.

Herget and De Korompay (1978) conducted permeability tests on 32 mm diameter and 300 mm high laboratory specimens of hydraulic fill and compared them with those obtained in the field using three field permeameters of different types. The limited data indicated that the field permeability values were slightly larger, but were of the same order as those obtained from the laboratory. Using the adjustment factors suggested in the paper to initially standardise both sets of permeabilities to indicate values representative for a sample at 20°C, and 100% saturation, and then a factor to make the laboratory permeabilities which were obtained at a porosity of 0.37 correspond to the more representative of the in situ porosity values of 0.47. The laboratory permeability of 10.1 cm/hr compared very well to the in situ measurements which ranged from 8.6 cm/hr to 9.7 cm/hr over two sites and three different measurement techniques for each site.

It can be seen from Figs. 3.3 and 3.8 that the grain size distribution for many Australian hydraulic fills fall into a very narrow band. According to USCS (The Unified Soil Classification System), they can be classified as silty sands with symbol of SM or sandy silts with symbol of ML. In Fig. 3.20 it is shown that the permeability values determined from constant head and falling head tests on the 153 mm diameter and 306 mm high laboratory samples are in good agreement with ones estimated from Hazen's (1930) empirical relationship given in Eqn. 3.1, with the constant *C* in the range of 0.03 – 0.05 when $D_{10}$ is in μm and *k* is in mm/hr. Hazen's equation can be used for preliminary estimates of the permeability of the settled hydraulic fill.

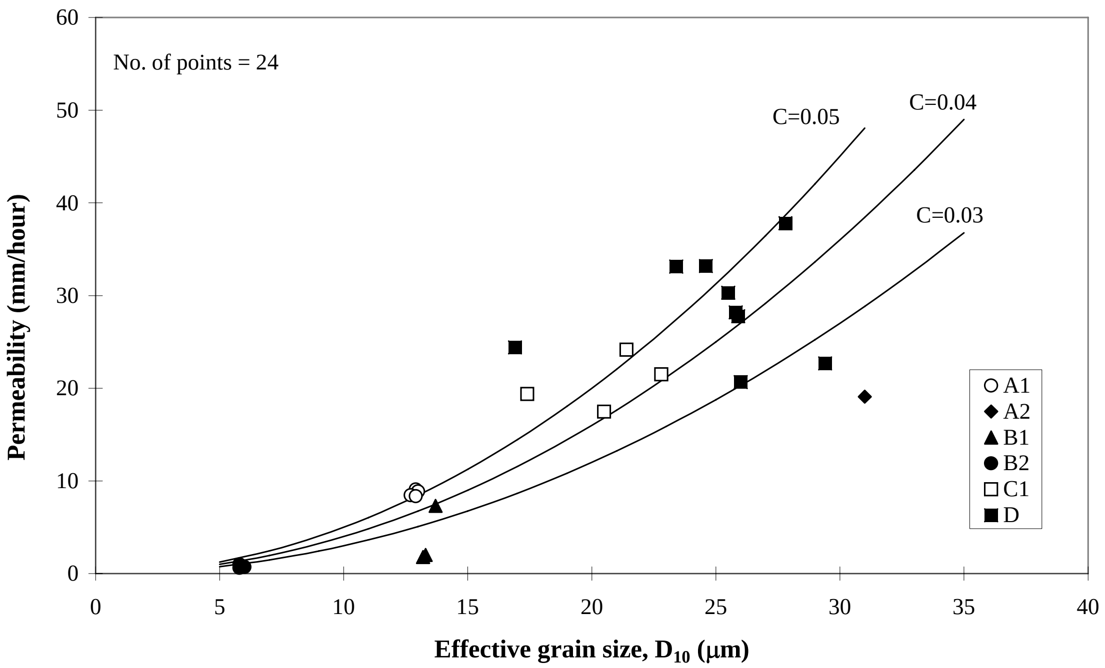


**FIG. 3.20 - Hazen's permeability – grain size relation for reconstituted laboratory samples**

## 3.5 Water content, Maximum and Minimum Dry Densities, Relative Density and Void Ratio

The void ratios, water contents and dry densities of the settled hydraulic fill are summarized in Table 3.6, and the available maximum void ratio ($e_{max}$), minimum void ratio ($e_{min}$) and relative density values are given in Table 3.8. The permeability test samples were prepared from slurries of the same water content as those used in the corresponding mines. The slurry sedimentation process within the permeameter mimics the hydraulic filling process in the mine and therefore the prepared hydraulic fill samples are a realistic representation of the hydraulic fill in situ. It is evident from Table 3.6, that the sample of Australian hydraulic fills tested for this research settle to porosity of about 37% to 48%, with water content of about 17% to 33%. The porosity field measurements of 45% and 48%, published by Herget and De Korompay (1978), closely matched the values obtained by the laboratory testing undertaken for this research.

**TABLE 3.8 - Relative densities of hydraulic fills**

| Mine | Sample | Void ratio, e | Minimum void ratio, $e_{min}$ | Maximum void ratio, $e_{max}$ | Relative density, $D_r$ (%) |
|---|---|---|---|---|---|
| Mine A | A 1 | 0.67 | 0.45 | 0.94 | 55.69 |
| | A 2 | 0.69 | 0.42 | 1.03 | 55.39 |
| Mine C | C 1 | 0.78 | 0.67 | 1.05 | 71.47 |
| | C 2 | 0.62 | 0.48 | 1.09 | 76.96 |
| | C 3 | 0.63 | 0.43 | 1.02 | 66.38 |
| | C 4 | 0.59 | 0.40 | 1.04 | 70.20 |
| Mine D | D 1 | 0.58 | 0.43 | 0.83 | 61.81 |
| | D 2 | 0.66 | 0.44 | 1.56 | 79.93 |
| | D 3 | 0.70 | 0.48 | 1.17 | 67.63 |
| | D 4 | 0.72 | 0.42 | 1.02 | 49.92 |
| | D 5 | 0.70 | 0.53 | 1.40 | 80.50 |
| | D 6 | 0.66 | 0.41 | 0.94 | 52.76 |
| | D 7 | 0.68 | 0.54 | 1.18 | 79.06 |
| | D 8 | 0.72 | 0.57 | 0.98 | 62.25 |
| | D 9 | 0.72 | 0.53 | 1.04 | 62.15 |

* Several tests were performed for each of the hydraulic fills tested to produce tables 3.6 and 3.8. The tabulated values are the average values, and therefore they may vary slightly between tables.

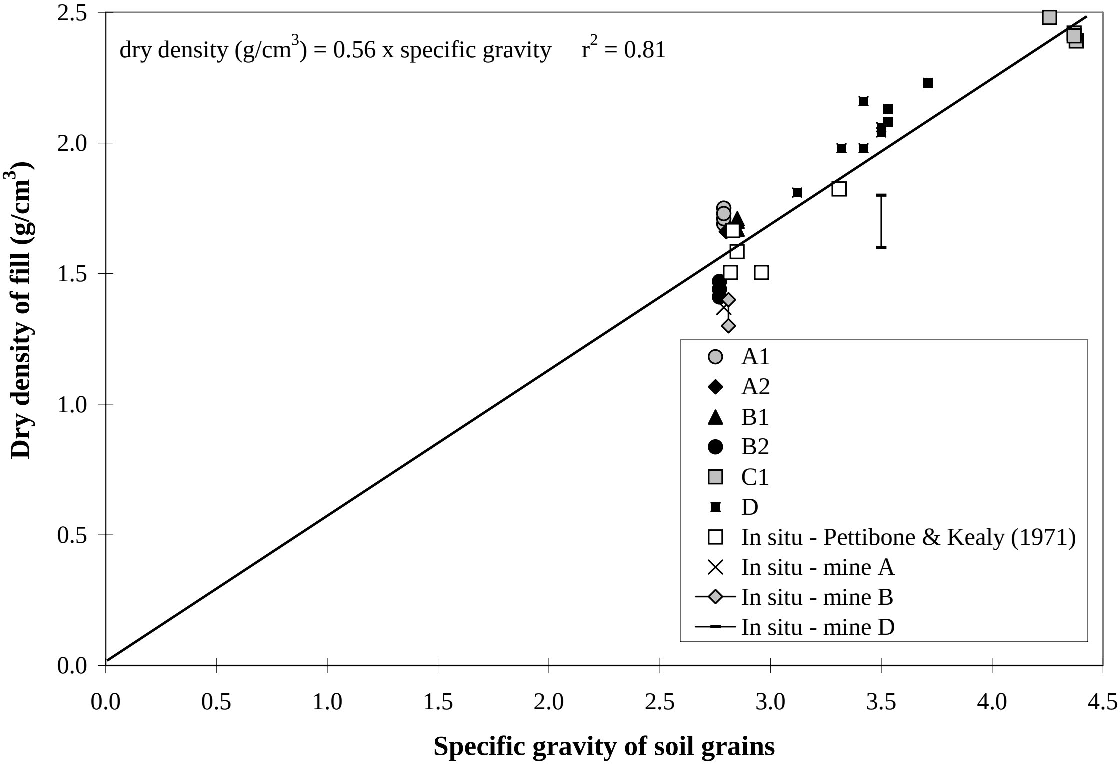


**FIG. 3.21 - Dry density – specific gravity relation**

Having all fills settle to porosity values in the range of approximately 37% to 48%, it may be expected that the dry density is proportional to the specific gravity of the soil grains. Variation of dry density of the settled fill against the specific gravity is shown in Fig. 3.21. Good agreement is shown between five in situ measurements by Pettibone and Kealy (1971) from mines in the United States, previously obtained in situ estimates from three Australian mines (Bloss, 1992; Brady and Brown, 2002; Cowling, 2003) and 24 laboratory values from six Australian hydraulic fills tested. It is quite clear that the dry density of the hydraulic fill is directly proportional to the specific gravity, and can be approximate by the following equation for all available data, Dry density (g/cm$^3$) = 0.56 x specific gravity Eqn. 3.5

The laboratory samples settled to a dry density of approximately 0.58 times the specific gravity, and the in situ dry density measurements obtained by Pettibone and Kealy (1971) averaged 0.51 times the specific gravity. On the basis of this, the entire numerical modelling work discussed in Chapters 5 and 6, was simplified by assuming the dry density of the fill was to be 0.5 times $G_s$ in t/m$^3$, implying void ratios of approximately 1 and porosity of 50%.

Maximum dry density and minimum dry density tests were carried out in an attempt to estimate the relative densities of the hydraulic fills. The values shown in Table 3.8 suggest that the hydraulic fills settle to a medium-dense to dense packing of grains according to AS 1276-1993 (Fig 3.22), giving relative densities in the range 50% to 80%. Pettibone and Kealy (1971) reported similar relative density values based on field measurements within some hydraulic fill stopes, and extensive in mine testing by the US Bureau of Mines indicated that hydraulic fill was typically placed at approximately 55% relative density (Corson et al., 1981).

It is interesting to note that the in situ hydraulic fill stopes were placed without any compaction and still attained medium dense to dense state.

The void ratio is plotted against the relative density for nine laboratory sedimented samples of hydraulic fills from Australian mines, and four in situ measurements in US mines, in Fig 3.22. All 13 points lie within the shaded area shown, suggesting approximately 45%-80% relative densities and void ratios of 0.6-0.8 for all hydraulic fills whether sedimented in the laboratory or placed in situ.

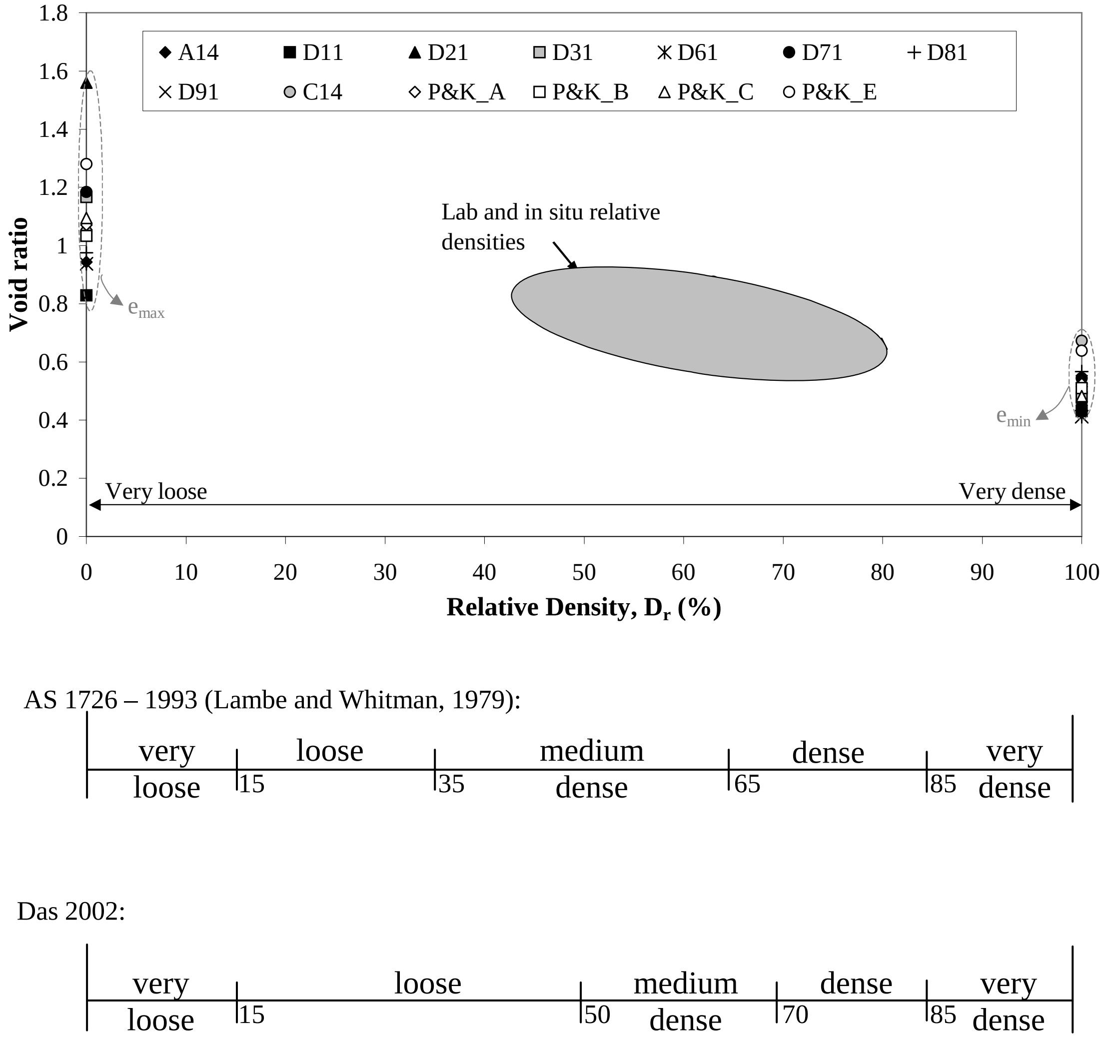


**FIG. 3.22 - Placement property data as relative density versus void ratio**

## 3.6 Placement Property Tests

The initial water content of hydraulic fill has significant influence on the in situ void ratio. Clarke (1988) suggested a procedure to study this through placing the hydraulic fills, mixed at different water contents, in a glass cylinder and vibrating for 5 mins before measuring the porosity. The bottom of the cylinder can be perforated to allow for drainage or sealed and undrained, depending on how rapid the drainage is expected in the mine. The main objective of the placement property test is to identify the optimum water content for the hydraulic fill that gives the minimum porosity (and thus the maximum dry density) on placement in the stope.

Phase relationships may be used to explain the placement property of a fill sample. The masses and volumes of the three phases are shown on the right hand and left hand sides respectively in the phase diagram in Fig. 3.23. Some of the standard geotechnical terms used in this report are defined below.

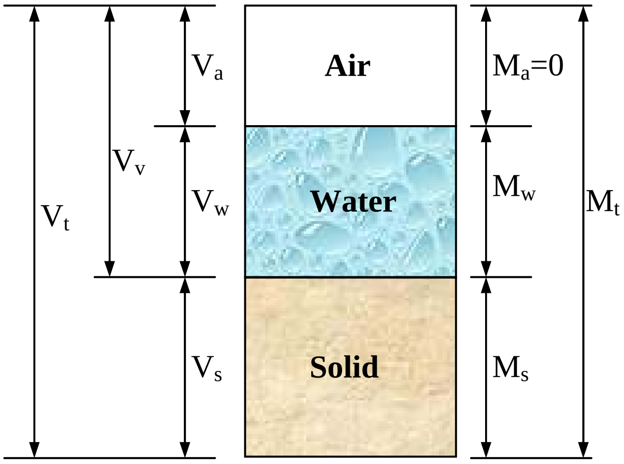


**FIG. 3.23 - Phase relationship for hydraulic fills**

*Water content* (*w*) is the water/solids ratio of a material, as defined in Clark (1988). Water content is generally expressed as a percentage, and is defined as follows,

$$w = \frac{M_w}{M_s} \times 100\,\% \qquad \text{Eqn. 3.6}$$

*Porosity* (*n*) is a measure of void space that includes air and water volumes, and is expressed as a percentage.

$$n = \frac{V_v}{V_t} \times 100\,\% \qquad \text{Eqn. 3.7}$$

*Air content* (*a*) is a measure of air volume and is also expressed as a percentage.

$$a = \frac{V_a}{V_t} \times 100 \qquad \text{Eqn. 3.8}$$

From simple phase relations, it can be shown that, at any time, *a*, *n*, *w* and $G_s$ are related by Eqn. 3.9.

$$n = \frac{a \;\; + wG_s}{1 + wG_s} \qquad \text{Eqn. 3.9}$$

Using this equation with $G_s$ = 3.53, Fig. 3.24 was developed for presenting the placement property data for hydraulic fill D6. This is similar to Fig. 4 of Clark's 1988 paper. The shaded region includes all possible situations where there is grain-to-grain contact. The region is bound by the maximum porosity line ($n$ = 48.4%) at the top and minimum porosity line ($n$ = 29.2%) at the bottom. At water contents greater than 27%, the porosity is greater than the maximum porosity achievable with grain-to-grain contact. In other words, the hydraulic fill is in the form of slurry at water contents greater than 27%. On the right side, the region is bound by the saturation line. The lowest porosity the fill can attain, still remaining saturated, is at 12% water content. Allowing for 1-3% air content, we expect to see a minimum porosity can be expected near 32% and optimum water content of 11% based on the above reasoning. A level of compaction may result from the relatively large fall distances that occur as the fill is being placed into the stope.

The effect of water on the placement of fill is described through Fig. 3.25. In the dry state (Fig. 3.25 a), the particles are paced at a certain density. When water is initially added in small quantities, it is absorbed by the surface texture of individual grains and this increases the porosity, by separating the grains slightly. Further addition of water fills the gaps between grains, in the form of water bridges (Fig. 3.25 b). The capillary tension between grains, caused by these water bridges, draws the grains more closely together, decreasing the porosity. As the proportion of water increases, the volume proportion of air decreases. The capillary forces increase toward a maximum at 100% water saturation, where the porosity is at a minimum (Fig. 3.25 c). Further addition of water (Fig. 3.25 d), causes the sample to form a slurry, and the porosity increases with increased water content while the sample remains saturated.

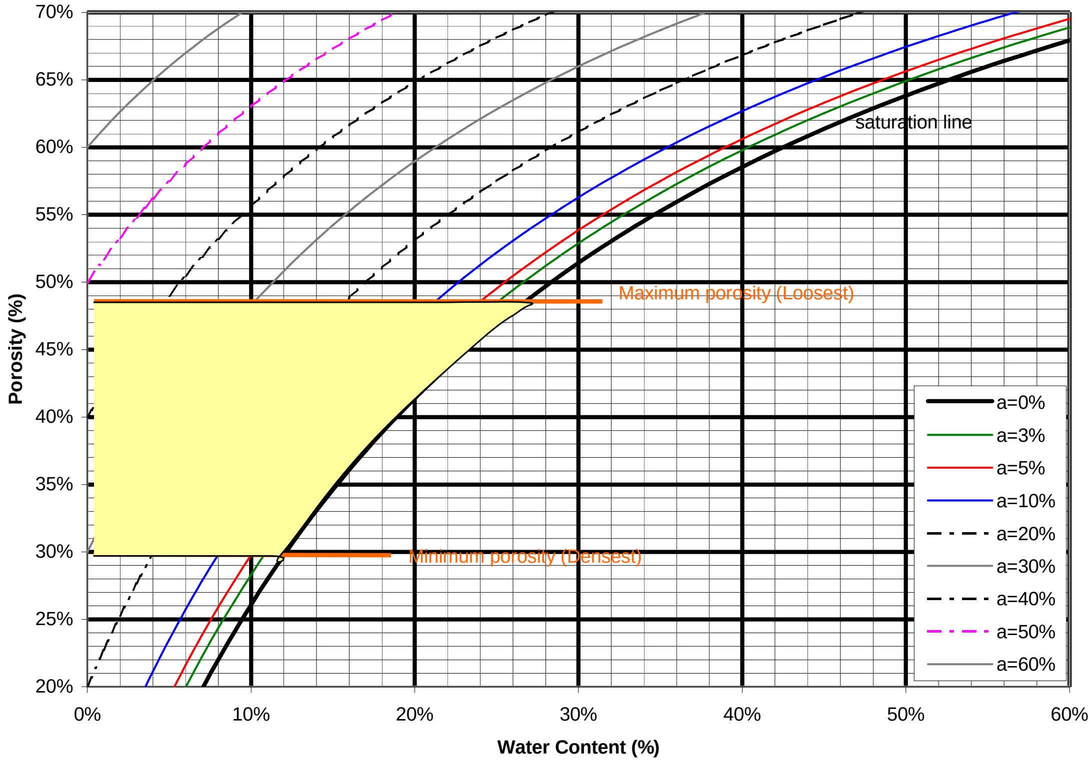


**FIG. 3.24 - Porosity – water content space for displaying placement properties**

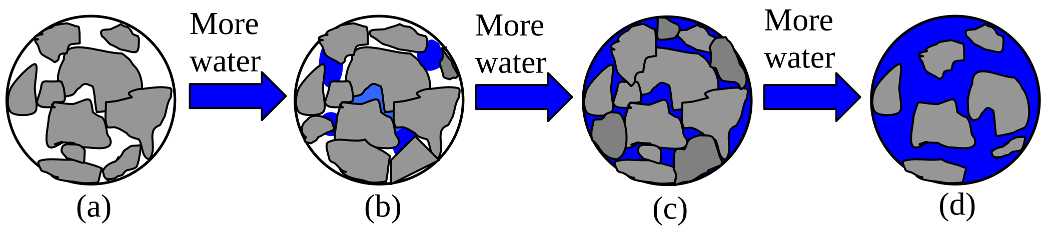


**FIG. 3.25 - Fill placement property variation with increased water**

The effect of water on the placement of fill described in Fig. 3.25 is most pronounced in uniformly graded samples, as a result of the narrow pore size distribution in these soils.

The dependence of grain packing on water content of a sample can be clearly described through the placement property curve, which plots the porosity of a sample against the water/solids ratio which is the water content (Fig. 3.26). The progression from (a) through to (d) illustrated in Fig. 3.25, is marked on the plot in Fig. 3.26. The limiting state of total saturation, (point (c) in both Figs. 3.25 and 3.26) defines both the optimum water content, and the minimum porosity. These are both functions of the particle distribution. The sample can only exist within the shaded region in Fig. 3.26.

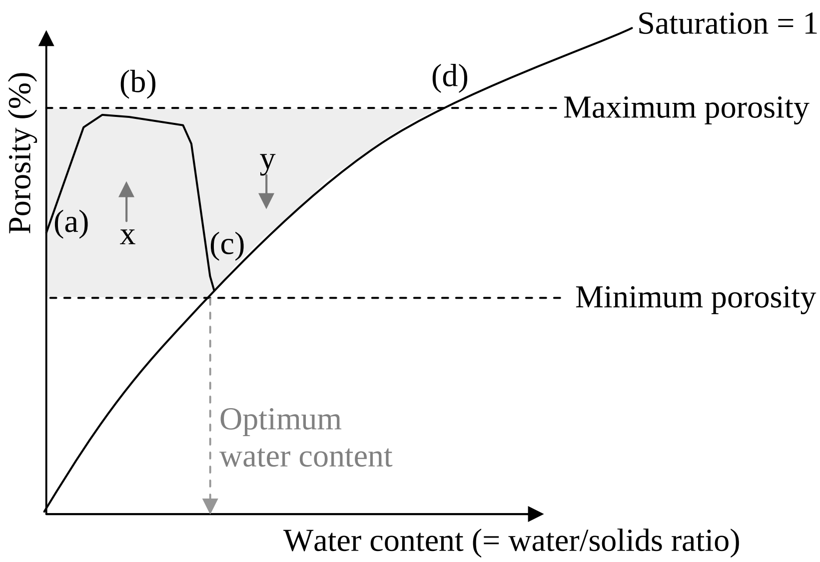


**FIG. 3.26 - Typical placement property curve**

There is also good value in the placement property curve where it can be used to assess whether the fill will contract or dilate when subjected to vibratory loading such as blasting. An element in the fill where the state is represented by x in Fig. 3.26, will expand on further vibratory loading whereas an element represented by y will contract. This was verified by some preliminary laboratory studies by Liston (2003).

### 3.6.1 Test Methodology

The hydraulic fill samples were prepared at various water contents ranging from 0 to 50%. The samples were placed in a 500 ml graduated cylinder and vibrated for 5 minutes and the resulting porosities and water contents were measured. More tests were carried out in the water content range of 0-16%, to define the placement property curve precisely, so that the optimum water content and minimum porosity can be found. Two tests were carried out with the initial water content of 40% and 50%, where the hydraulic fill was in the form of slurry. These were allowed to settle under their self-weight, without any vibration. Six tests were done with initial water contents of 20-50%, where little vibration (less than 5 minutes) was applied to see how they follow the saturation line.

It should be noted that all tests were carried out in a 500 ml measuring cylinder with no provision for drainage. If significant drainage is expected in the mines, it may be more meaningful to use a perforated base, thus allowing for drainage that mimics the conditions in situ.

### 3.6.2 Test Results

The placement property test carried out on one of the fills, D6, is shown in Fig. 3.27, where porosity is plotted against water content and Table 3.9. The same data is also presented as a plot of dry density against water content in Fig. 3.28. Placement property test is a form of compaction test, but the results are presented slightly differently. The 5-minute vibration suggested by Clark (1988) is the compactive effort in this exercise.

The shaded region, bounded by the horizontal maximum porosity (or minimum dry density) and minimum porosity (or maximum dry density) lines at the top and bottom, and the saturation line on the right, is where the fill can exist with inter-particle contact. The optimum water content for D6 is about 14%, which will give the minimum porosity and maximum dry density when placed. However, the fill materials are transported by pipes, and should have sufficient flow characteristics that require the hydraulic fill be transported and placed in the form of a slurry, with water content higher than the optimum water content. The intersection of the minimum porosity line and saturation curve give a first estimate of the optimum water content, which is 12% in the case of D6. Such estimate can be obtained simply from a Maximum Dry Density Test (ASTM D 4253-93), and does not require the placement property test described above.

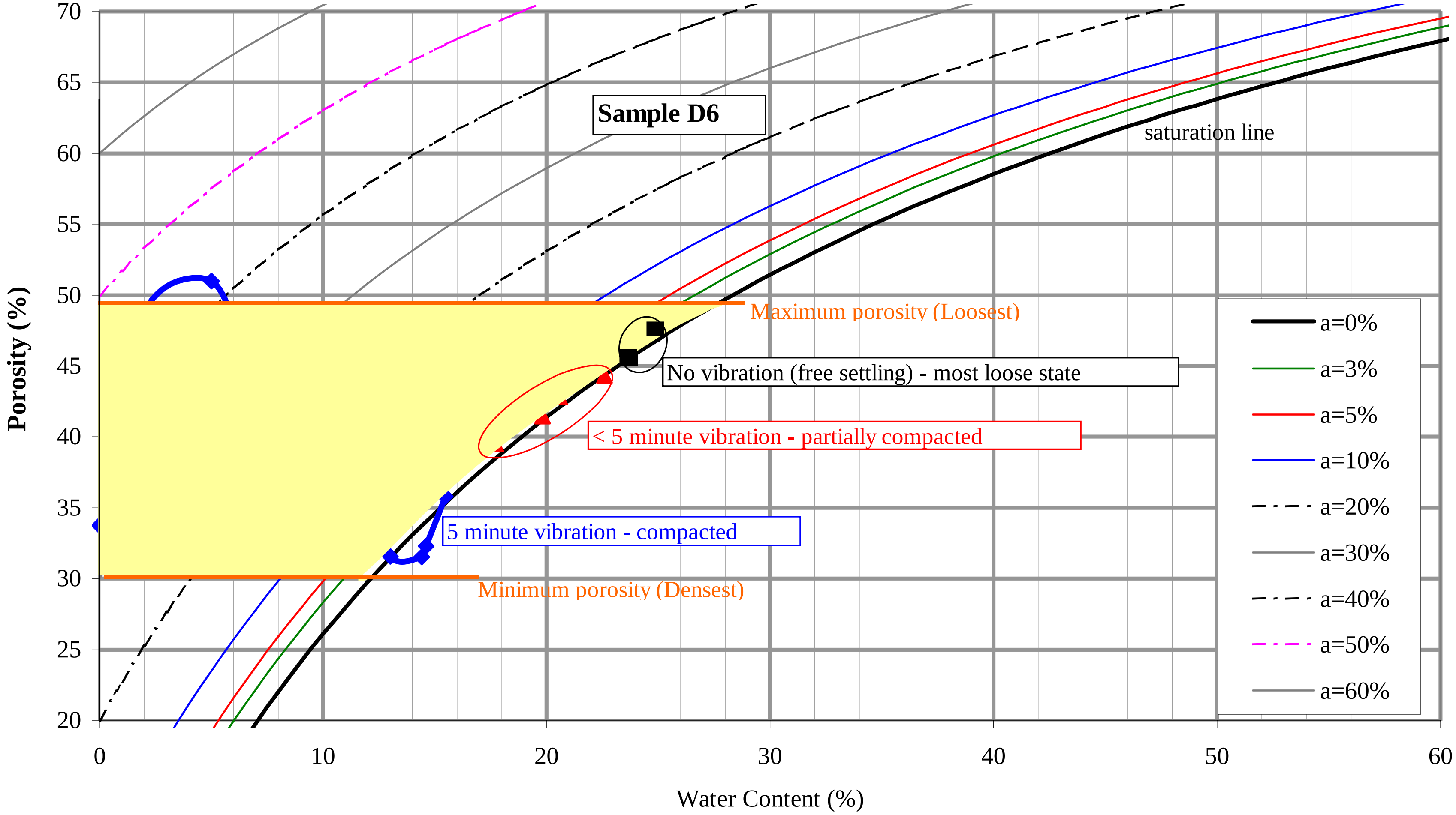


**FIG. 3.27 - Placement property curve for sample D6**

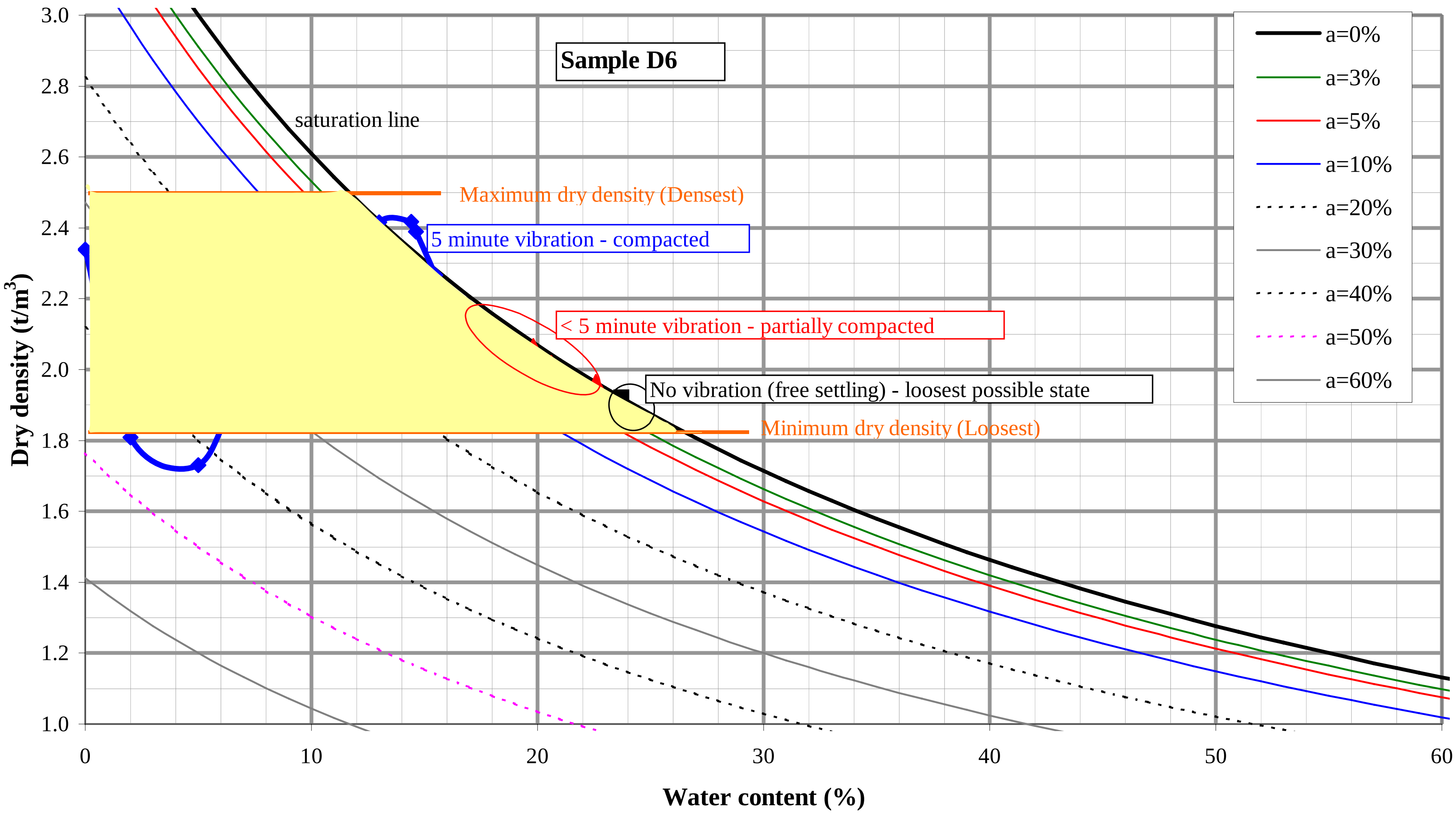


**FIG. 3.28 - Placement property curve for sample D6 as dry density versus water content**

When the initial water content is very high, in the order of 40% - 50%, the suspension followed the saturation line and settled to a porosity value slightly less than the maximum porosity. The two points are shown by the "■" symbol in Figs. 3.27 and 3.28. The higher the water content of the suspension, the closer the porosity is to the maximum porosity. The points shown by the "▲" symbol were obtained from slurries mixed at water contents ranging from 20% to 50%, but were vibrated for less than 5 minutes. They follow the saturation line in the shaded zone, and will move towards the optimum point with increased duration of vibration.

**TABLE 3.9 -Placement property test data**

| Before | After | | Remarks |
|---|---|---|---|
| w (%) | w (%) | n (%) | |
| 0 | 0.0 | 33.7 | 5 minute vibration. Sample not saturated |
| 2 | 2.0 | 48.8 | |
| 5 | 5.0 | 51.0 | |
| 7 | 7.0 | 44.6 | |
| 10 | 10.0 | 41.7 | |
| 11 | 11.0 | 36.4 | |
| 12 | 12.0 | 36.1 | |
| 13 | 13.0 | 31.6 | 5 min vibration; saturated; sample at densest state. |
| 15 | 14.4 | 31.5 | |
| 30 | 14.6 | 32.3 | 5 min vibration; settling from slurry; densest state. |
| 20 | 15.5 | 35.8 | 5 min vibration; w = 20 %. |
| 20 | 17.7 | 39.5 | < 5 min vibration; w = 20 %. |
| 20 | 18.4 | 41.7 | |
| 20 | 19.5 | 42.3 | |
| 30 | 19.8 | 41.5 | Slight compaction due to < 5 min vibration; settling from slurry. |
| 50 | 20.6 | 42.8 | |
| 40 | 22.6 | 44.3 | |
| 40 | 23.7 | 45.5 | Free settling from slurry under self weight to loosest possible state. |
| 50 | 24.9 | 47.6 | |

## 3.7 Direct Shear Tests

Friction angle is an important parameter in the static and dynamic stability analysis of hydraulic fill. Direct shear tests are carried out to determine the peak and residual friction angle of the hydraulic fill. Under-estimation of friction angle will result in under-estimation of the arching effect in hydraulic fills, and lead to a conservative evaluation of the overall stability of the material (Mitchell et al., 1975). Due to limited access and safety issues it is often difficult to carry out in situ tests within the stopes.

The tests are carried out on reconstituted fills representing the in situ grain packing in the stope, which can be at relative densities of 40% - 70% (section 3.5). Since there is no clay fraction, cohesion may be assumed zero.

From limited data it appears that the friction angles of the hydraulic fills, determined from direct shear tests are significantly higher than those determined for common granular soils. This can be attributed to the very angular grains that result from the crushing of the waste rock, which interlock more than the common granular soils. The high angularity of the grains can be seen in the scanning electron micrographs of the hydraulic fill samples are shown in Figs. 3.1 and 3.2.

Direct shear tests were performed in accordance with the Australian Standards (AS 1289.6.2.2 - 1998) on sample D6, over a range relative densities, to study the relevance of existing empirical relationships developed for clean granular materials.

Friction angle, relative density and *N*-value from standard penetration test are interrelated for granular soils. Meyerhof (1957) suggested that $N_1/D_r^2 \approx 41$ for clean sands. Skempton (1986) suggested that $N_1/D_r^2 \approx 60$ in sands for $D_r > 35\%$. Cuvrinovski and Ishihara (2001) showed that $N_1/D_r^2$ for granular soils can vary in the range of 10 to 100, depending on the void ratio range $e_{max} - e_{min}$. Therefore, it appears that the ratio $N_1/D_r^2$ should be quite different for uniformly graded hydraulic fills than what is observed for granular soils in general.

It is often not practicable to have the standard penetration or cone penetration test rigs into the underground mines, and therefore in the case of hydraulic fills, it is more useful to relate friction angle (which can easily be obtained in the laboratory by performing direct shear or triaxial tests on reconstituted samples) than the *N*-value to the relative density. The variation of peak friction angle with relative density for D6 is shown in Fig. 3.29, and Table 3.10. For relative density greater than 35%, the friction angle and relative density can be related for sample D6 by Eqn. 3.10.

$$\phi = 19D_r^{\ 2} + 33 \quad \text{for} \quad D_r > 35\% \qquad \text{Eqn. 3.10}$$

where $D_r$ is relative denstiy.

**TABLE 3.10 - Measured friction angle for hydraulic fill sample D6 with estimates based on empirical relations for granular soils**

| $D_r$ | Meyerhof (1957) | | Skempton (1986) | | Measured |
|---|---|---|---|---|---|
| (%) | $N_1$=41$D_r^2$ | $\phi$ (deg)* | $N_1$=60$D_r^2$ | $\phi$ (deg)* | $\phi$ (deg) |
| 51 | 10.6 | 30.0 | 15.6 | 32.0 | 38.2 |
| 75 | 23.1 | 34.2 | 33.8 | 37.0 | 43.6 |
| 93 | 35.5 | 37.5 | 51.9 | 41.2 | 49.2 |

* From $N_1$ - $\phi$ correlation after Peck et al. (1974)

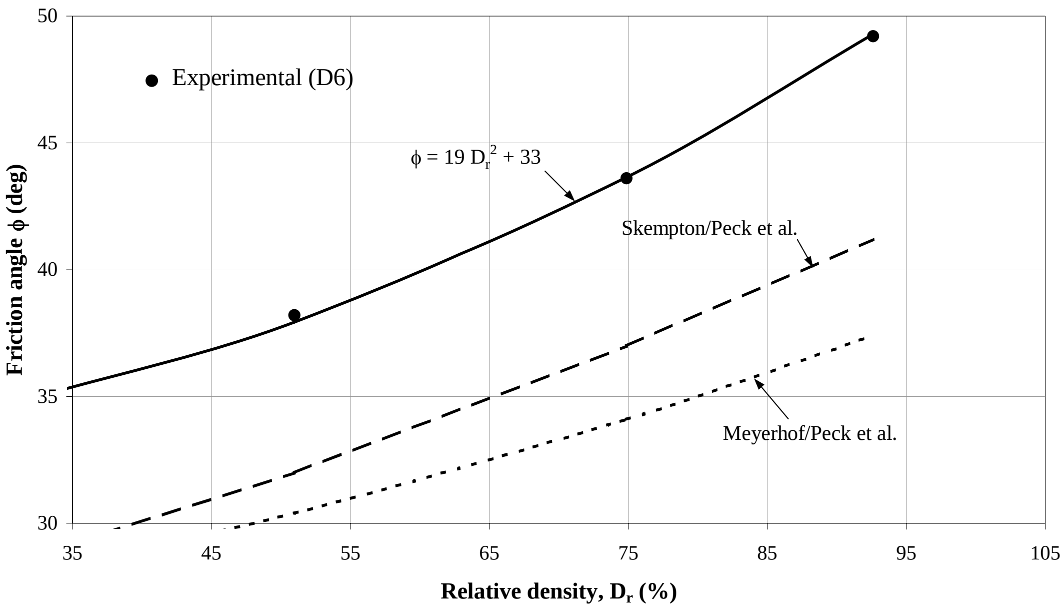


**FIG. 3.29 - Friction angle versus relative density for sample D6**

As shown in Table 3.10 and Fig. 3.29, the measured friction angles for sample D6 are substantially higher than what was estimated using Skempton's (1986), Meyerhof's (1957) and Peck et al. (1974) relations, for granular soils. It can be seen in Table 3.8 and Fig. 3.3, that most hydraulic fills used in Australian mines have an $e_{max} - e_{min}$ range of about 0.5, and they all have similar grain size distribution. Therefore, these hydraulic fills will have a unique $N_1/D_r^2$ ratio (Cubrinovski and Ishihara, 2001), and consequently a unique relationship between $\phi$ and $D_r$.

## 3.8 Oedometer Tests

Oedometer tests are carried out on the hydraulic fills to determine the constitutive modelling parameters for the Cam Clay model. The Cam Clay model is one of the constitutive models that can be adopted for the hydraulic fills when analysed using numerical modelling packages such as *FLAC*, *FLAC*$^{3D}$ or ABAQUS, but was not used in this research. In addition, oedometer tests are useful in determining the constrained modulus ($D$) from which the Young's modulus ($E$) can be estimated for an assumed value of Poisson's ratio ($\nu$) using the following equation,

$$E = \frac{(1-\upsilon)(1-2\upsilon)}{(1-\upsilon)} D \qquad \text{Eqn. 3.11}$$

Young's modulus is a crucial parameter in deformation calculations using most constitutive models. The oedometer tests on the hydraulic fills showed significant creep settlements that took place on the completion of consolidation settlements. This remains yet to be verified quantitatively and on full-scale stopes.

## 3.9 Chapter Summary

Unlike the typical granular soils, hydraulic fill materials have a wider range of specific gravity. From specific gravity tests conducted for this research, on over 15 different hydraulic fill samples from across Australia, the specific gravity values ranged from 2.8 through to 4.4. Hydraulic fills studied have shown similar and unique settling characteristics. When sedimented as a slurry with a typical solids content of between 65% and 75%, they all settle to a dry density (in t/m$^3$ or g/cm$^3$) of about 0.58 times the specific gravity in the laboratory, and the in situ data obtained by Pettibone and Kealy (1971) settled to a dry density of 0.51 times the specific gravity. The average of all settlement data gave a dry density of approximately 0.56 times the specific gravity.

Hazen's empirical equation, with $C$ = 0.03 – 0.05, can be used for first estimates of permeability values based on the grain size distribution of a granular material where $D_{10}$ is in μm and $k$ is in mm/hr. Extensive laboratory permeability testing of over 20 hydraulic fill samples, showed the permeability values were in the order of 10 to 30 mm/hr, and much less than the 100 mm/hr often desired by the mining industry.

Placement property tests show that when the hydraulic fill is sedimented from a very dilute suspension, the resulting fill will have porosity close to the maximum porosity, implying very low relative density. However, laboratory placement tests have demonstrated that when the hydraulic fill is mixed in the form of a slurry, with typical water content of 30% - 35%, the resulting hydraulic fill is rather dense, with relative densities of 55% - 80%, thus reducing the liquifaction potential.

As a result of the very angular grain geometry possessed by hydraulic fills, the friction angle of these materials is relatively high. From limited experimental data, it was shown that for hydraulic fills, the friction angle and relative density may be interrelated with a unique friction angle, relative density relationship. Further investigations into this relationship will have significant implications on the predictions of initial stresses and hence the liquifaction potential of the hydraulic fill material.

# Chapter 4

# Permeable Barricade Bricks

## 4.1 Introduction

When the mine is being filled, the horizontal drives at various sublevels are blocked by a retaining wall like structure, known as barricade or bulkhead. These are made of specially made permeable barricade bricks (Figs. 4.1 to 4.3). Barricade failure in underground mining operations is of major concern, because the potential for the outcome to be catastrophic or tragic is very high. Between 1980 and 1997, eleven barricade failures were recorded at Mount Isa Mines in both hydraulic and cemented hydraulic fills (Kuganathan, 2001). In 2000 a barricade failure in a Bronzewing Mine in Western Australia resulted in a triple fatality, and two permeable brick failures were reported later that same year, in relation to hydraulic fill containment, in Osborne Mine in Queensland (Grice, 2002).

The occurrences of many failures of these permeable barricade bricks throughout Australian underground hydraulic fill mines, are an indication of incomplete comprehension of the barricade material properties, the strength achieved through design and construction, and the stresses that the barricade will be exposed to. This section covers a thorough experimental study of strength, stiffness and permeability of permeable barricade bricks commonly used in hydraulic fill mines across Australia. Chapters 5 and 6 deal with the stress development within the fill of a hydraulic fill stope, and Chapter 3 deals with the properties of hydraulic fills from several Australian mines. Design and construction practices for underground barricades were not researched as part of this thesis. A brief description of porous brick barricade construction methods is given in section 4.1.2.

### 4.1.1 Underground Barricade History

The barricades in the early stages of minefill use were simply constructed of timber planks or poles with hessian (or burlap) to contain the sandfill (Bridges, 2003). These barricades were referred to as 'fill fences'. Throughout the 1970's and 1980's, as underground mining activity increased dramatically, with stopes becoming larger, the lack of field or numerical data on bulkhead pressures generally forced mines to over-design barricades which was often expensive, but was required in the absence of previous barricade pressure data. An example of this is demonstrated by Mitchell et al. (1975), with their monitoring barricade being designed as a 1 m thick heavily reinforced concrete bulkhead with interior 'mousetrap' drain pipes. The design strength of this barricade was well in excess of the measured horizontal pressures, and in this instance, the primitive timber fill fences designed for a working pressure of 100 kN/m$^2$ were found through historical success rate to be sufficient.


**FIG. 4.1 - Photograph of in place permeable brick barricade**

Gradually concrete, and even more commonly concrete blocks, replaced the use of timber for hydraulic fill containment in underground mines. Initially solid, impermeable bricks were used. The walls constructed from these impermeable bricks had to withstand full hydrostatic loading, then in the later stages these were replaced by permeable barricade bricks capable of relieving the hydraulic pressure build-up within the stope through drainage of excess water used in slurry placement.


**FIG. 4.2 - Construction of a curved barricade**


**FIG. 4.3 - Photograph of in place porous brick barricade**

On some mine sites, curved barricades, in the form of a horizontal arch have been used in place of the typical flat construction because they provide additional strength for an equivalent size and thickness of a flat brick wall (see Fig. 4.2). Also, in some mines such as Rand gold mine a sling type construction utilizing the tensile strength of steel ropes covered by cloth has been used (Bridges, 2003).

In recent years, much attention has been directed to the use of shotcrete or pumped concrete for the containment of fill in underground mines. These barricades may be fashioned in either a flat or curved construction and being impervious, drainage holes are fitted for fills such as hydraulic fill, requiring the removal of excess water. This relatively new method of containment barricade construction is still in its infancy, but with research, offers great potential for future use.

### 4.1.2 Barricade Construction

Due to the uncertainty associated with properties and geometry of barricade construction, there is no single standard technique for the design of permeable brick barricades. The three main methods of analysing barricade behaviour for design and construction purposes include:

1- Analytical methods,
2- Numerical modelling methods, and
3- Evaluation through field experience.

Analytical methods are a valuable means of obtaining a preliminary assessment of barricade performance, but the simplifications to the geometry, barricade/rock interface properties, and the properties of the barricade, limit the conviction with which these estimations may be applied to design. Some methods assume the barricade behaves in the same manner as a uniformly loaded slab with all sides restricted (Duffield, et al., 2003). The assumed failure pattern for this analysis is illustrated in Fig. 4.4 (a). More advanced analytical models incorporate the arching of the load across the barricade, but field observations have indicated the failure mechanism, is more aligned with ‘punching’ shear failure through the center of the barricade as shown in Fig. 4.4 (b) (Kuganathan, 2001; Cowling, 2003).

THESE IMAGES HAVE BEEN REMOVED DUE TO COPYRIGHT RESTRICTIONS

**(a)** **(b)**

**FIG. 4.4 - Barricade failure mechanisms (a) Theoretical (Duffield et al., 2003) (b) Observed (Kuganathan, 2001)**

Duffield et al. (2003), utilized an analytical approach developed by Park and Gamble (2000), to model reinforced and un-reinforced concrete slab floors restrained on all four sides with the supports capable of resisting arch thrust, to compare predicted barricade strengths to those obtained experimentally by full-scale testing of an underground brick barricade at Mount Isa Mines in collaboration with CSIRO (Beer, 1986 vide Duffield, 2000; and Grice, 1989). The model predicted a failure pressure of 427 kPa, which was well below the experimental failure pressure of 750 kPa for a 4 m x 4 m x 0.46 m thick barricade subjected to uniform loading (Duffield et al., 2003). This along with all other analytical methods of barricade performance contain too many simplifications which extensively limit the reality of the predictions.

A numerical model can simulate the barricade loading situation more realistically compared to the above. Reasonably realistic geometries and material and interface properties may be integrated into the solution. Despite the prediction more accurately mimicking reality, deficiencies still exist as a result of uncertainty surrounding the material properties and behaviours, which are often erratic.

The value of field experience is often not recognised for its worth as a tool in barricade performance analysis. Knowledge gained through practice and through barricade failures, provide a crucial insight into failure mechanisms, and validation to theoretical concepts. Unfortunately this information is not often available to the public, and therefore the sharing of knowledge within the industry is limited.

### 4.1.3 General Barricade Brick Properties

The barricade bricks used for the containment of hydraulic fill in underground mines are generally constructed of a mortar composed of a gravel, sand, cement and water mix in the approximate ratio of 40:40:5:1 respectively by weight[6]. Fig. 4.5 shows a photograph of typical barricade bricks (a), and an underground containment wall (b) constructed from the bricks. These individual bricks cost a mine approximately A$2.50.

It is known within the mining industry that the porous bricks used in underground barricade construction are prone to variability in strength (Kuganathan, 2001). Nevertheless, it is generally accepted that the manufacturer guarantees a minimum uniaxial compressive strength (UCS) of 10 MPa (Beer, 1986). Kuganathan (2001) and Duffield et al., (2003) suggest UCS values ranging from 5 MPa to 26 MPa, and the strength is quoted on the MIBW website as 8 MPa ± 2 MPa (www.mountisabrickworks.com.au). The compressive strength of general purpose concrete used in typical civil construction normally ranges between 20 and 30 MPa, and shotcrete mixes used in barricade construction are generally accepted to have a strength range of between 20 to 40 MPa.

**(a) – Typical barricade brick**


**(b) – Porous barricade brick wall**

**FIG. 4.5 - Photographs of porous barricade brick and wall construction**

[6] These ratios are based on rough estimates of mix proportions from one of the Australian barricade brick manufacturers used for this research.

The porous bricks are designed to be free draining, and therefore their permeability is believed to be at least in excess of 10 times that of hydraulic fill, which has a minimum acceptable permeability value of 10 mm/hr (Cowling, 2001). The barricade bricks have proven over time to satisfy the free-draining situation, and the reduction of permeability through migration of fines from the fill to the brick voids has not formally been recorded. Interestingly, as shown in Chapter 3, some of the hydraulic fills studied in this project have permeability constants less than 10 mm/hr, and the hydraulic fill systems in the mines have operated successfully.

## 4.2 Porosity of Barricade Bricks

The porosity of the mine barricade bricks is the volume of voids expressed as a percentage of the total volume. A rough approximation of the specific gravity, and thus porosity of the barricade bricks was found using Archimedes principle. Specific gravity tests were modified from soil testing procedures (AS1289.3.5.1 - 1995), to accommodate the barricade bricks. Porosity tests were undertaken on bricks from three separate mines, four bricks from mine A (A1_001 to A1_004), five bricks from mine D (A2_006 to A2_010), and four bricks from mine B (B_003 to B_005 and B_007) to obtain a representative value for both porosity and specific gravity of the barricade bricks. Bricks sourced from mines A and D were made by the same manufacturer, but were obtained at different times. Therefore, they are assigned labels of A1 and A2.

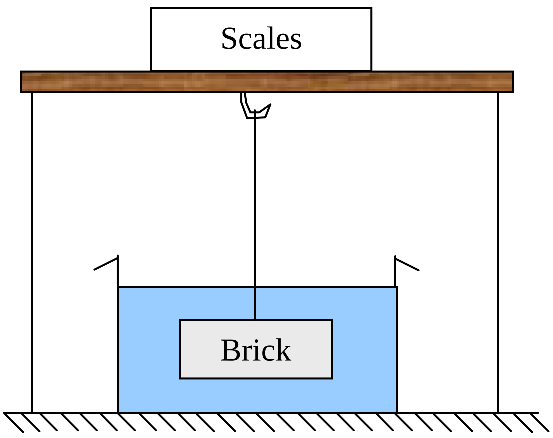


**FIG. 4.6 - Schematic diagram of brick porosity test**

A schematic diagram of the apparatus is shown in Fig. 4.6, and the methods of calculation of porosity *n*, and average specific gravity $G_s$, are detailed below. Table

4.1 summarises the results obtained from testing of the three varieties of barricade bricks.

If,

$V$ = Volume of the brick ($cm^3$)

$m_1$ = Dry weight, (g)

$m_2$ = Submerged weight, (g)

$\rho_w$ = Density of water = 1 $g/cm^3$

$$\Rightarrow V_v = \text{Volume of voids, } (\text{cm}^3) = V - \frac{(m_1 - m_2)}{\rho_w}$$

$$\text{Porosity, } n = \frac{V_v}{V}.100\%$$

$$\Rightarrow \text{Porosity, } n = \frac{\left(V - \dfrac{(m_1 - m_2)}{\rho_w}\right)}{V}.100\% = 1 - \frac{(m_1 - m_2)}{V.\rho_w}.100\%$$

$$\text{Average specific gravity } G_s = \frac{\text{mass of material}}{\text{mass of water}} = \frac{m_1}{m_2 - m_1}$$

### 4.2.1 Testing Methodology

**FIG. 4.7 - Brick suspended in water under scales in porosity test**

The general procedure used to test for brick porosity was as follows,

1. Dimensions and dry weights were measured for all brick samples,
2. Bricks were then immersed in water for no less than 24 hours,
3. Periodic tapping was done to remove air voids from within each brick,
4. Bricks were then individually suspended from a set of scales while being submerged in water (Fig. 4.7),
5. Submerged weights for each brick were recorded, and specific gravity and porosity values were calculated, and
6. Bricks were dried in preparation for testing permeability and infiltration behaviour under pressure.

This porosity test was performed on 4 A1 bricks, 5 A2 bricks and 4 B bricks.

### 4.2.2 Test Results

Table 4.1 summarizes the results obtained from the testing of barricade bricks from all three sources. These were computed using the mass of the bricks when dry and when saturated, as discussed in 4.2.1.

A1 bricks had specific gravity values that ranged between 2.37 and 2.41, and A2 bricks typically with a slightly lower value, fell within the range 2.31 to 2.38. Bricks from source B had the highest specific gravity values, and these values ranged from 2.53 to 2.56. The average specific gravity values for A1, A2 and B bricks were 2.39, 2.34 and 2.55 respectively. These values (shown in italics in Table 4.1) are considered to be a reasonable representation of the average specific gravity of each type of barricade brick. The average porosity values are 0.22, 0.15 and 0.20, for the A1, A2 and B bricks respectively. The range of permeability values (Table 4.4) obtained from the A2 set of bricks is relatively wide, and the average porosity value considerably lower than that of the other two variety of bricks, despite A2 being sourced from the same manufacturer as the A1 bricks. A full set brick dimensions, and results for all samples tested are provided in Table A4.1 in Appendix 4.

**TABLE 4.1 - Brick dimensions, porosity and specific gravity values**

| | Brick | Width (mm) | Depth (mm) | Length (mm) | Volume ($cm^3$) | Dry mass (kg) | Void volume $V_v$ ($cm^3$) | Porosity (%) | Specific gravity |
|---|---|---|---|---|---|---|---|---|---|
| **A1** | A1 _001 | 214 | 113 | 451 | 10875 | 19.71 | 2597 | 0.24 | 2.38 |
| | A1 _002 | 215 | 115 | 451 | 11126 | 21.63 | 1999 | 0.18 | 2.37 |
| | A1 _003 | 210 | 114 | 452 | 10822 | 20.60 | 2291 | 0.21 | 2.41 |
| | A1 _004 | 214 | 113 | 452 | 10913 | 19.85 | 2610 | 0.24 | 2.39 |
| | ***Average*** | ***213*** | ***114*** | ***452*** | ***10934*** | ***20.44*** | ***2374*** | ***0.22*** | ***2.39*** |
| **A2** | A2 _006 | 215 | 114 | 453 | 11062 | 23.28 | 974 | 0.09 | 2.31 |
| | A2 _007 | 214 | 114 | 452 | 11052 | 23.31 | 997 | 0.09 | 2.32 |
| | A2 _008 | 211 | 112 | 452 | 10689 | 20.58 | 1871 | 0.18 | 2.33 |
| | A2 _009 | 211 | 113 | 451 | 10810 | 20.35 | 2276 | 0.21 | 2.38 |
| | A2 _010 | 212 | 114 | 449 | 10828 | 20.59 | 2172 | 0.20 | 2.38 |
| | ***Average*** | ***213*** | ***113*** | ***451*** | ***10888*** | ***21.62*** | ***1658*** | ***0.15*** | ***2.34*** |
| **B** | B _003 | 189 | 91 | 394 | 6783 | 13.69 | 1432 | 0.21 | 2.56 |
| | B _004 | 189 | 92 | 393 | 6842 | 14.13 | 1257 | 0.18 | 2.53 |
| | B _005 | 189 | 91 | 395 | 6817 | 14.11 | 1278 | 0.19 | 2.55 |
| | B _007 | 189 | 91 | 393 | 6784 | 13.85 | 1377 | 0.20 | 2.56 |
| | ***Average*** | ***189*** | ***91*** | ***394*** | ***6806*** | ***13.95*** | ***1336*** | ***0.20*** | ***2.55*** |

## 4.3 Permeability of Barricade Bricks

Constant and falling head permeability tests were conducted to obtain permeability values for the bricks, and the variation in flow rates with applied pressures were also tested to obtain an understanding of brick behaviour under high pressures which may be experienced during situation such as when liquefaction occurs behind the barricade, or in the case where an erosion pipe connects the surface decant water to the barricade. It is a common misconception within the mining industry, that water pressures are very high in the fill directly adjacent to the barricades. The pressure gradient within the drive may be very high, but provided the permeable barricade bricks are free draining, the pore pressures at the barricade must be equal to zero.

Where possible, tests were carried out in accordance or as closely as possible to the appropriate Australian Standards, as given in Table 4.2. There are no standards available to test permeability of bricks. The standard testing procedures had to be modified from the soil testing standards to accommodate permeable barricade bricks. The permeability tests were carried out using a special pressure chamber, developed for this research, to study the infiltration characteristics of low-permeability materials such as concrete and mortar cores, and more permeable barricade bricks under water pressures as high as 350 kPa. A dimensioned schematic of the pressure testing chamber is given in Appendix 2 (Fig. A2.1).

**TABLE 4.2 - Procedures used for the permeability tests on barricade bricks**

| Test Procedure | Standard |
|---|---|
| Falling Head Permeability Test | AS 1289.6.7.2-2001 |
| Constant Head Permeability Tests | AS 1289.6.7.3-2001 |

Table 4.3 summarizes the bricks used in the brick permeability analysis, and the tests undertaken on them. In total, 17 constant head permeability tests, 12 falling head permeability tests and 12 flow-under-pressure tests were performed on bricks obtained from three Australian mines. All 12 falling head and flow-under-pressure tests were done on the same bricks that were subjected to constant head tests.

**TABLE 4.3 - Summary of brick permeability testing**

| | Sample | Constant head permeability test | Falling head permeability test | Flow-under-pressure test |
|---|---|---|---|---|
| **A1** | A1_001 | ✓ | ✓ | ✓ |
| | A1_002 | ✓ | ✓ | ✓ |
| | A1_003 | ✓ | ✓ | ✓ |
| | A1_004 | ✓ | ✓ | ✓ |
| **A2** | A2_004 | ✓ | × | × |
| | A2_005 | ✓ | × | × |
| | A2_012 | ✓ | × | × |
| | A2_013 | ✓ | × | × |
| | A2_014 | ✓ | ✓ | ✓ |
| | A2_016 | ✓ | × | × |
| | A2_017 | ✓ | ✓ | ✓ |
| **B** | B_003 | ✓ | ✓ | ✓ |
| | B_004 | ✓ | ✓ | ✓ |
| | B_005 | ✓ | ✓ | ✓ |
| | B_006 | ✓ | ✓ | ✓ |
| | B_007 | ✓ | ✓ | ✓ |
| | B_008 | ✓ | ✓ | ✓ |

### 4.3.1 Test Methodology

The following section details the apparatus, sample preparation and methodology required for constant head, falling head and pressure testing of permeable barricade bricks used in underground fill containment.

#### Brick Permeability Testing Apparatus

The cylindrical pressure chamber (Figs. 4.8 and 4.9) was constructed at James Cook University, to undertake constant and falling head permeability tests and flow variation with pressure tests on permeable barricade bricks. The pressure chamber provides an innovative and effective means by which the permeability of various materials may be obtained through three different permeability testing methods, and also allows for the analysis of the flow behaviour under applied pressure. The assembled pressure chamber is shown in Fig. 4.8 (a). The schematic diagram Fig. 4.8 (b), shows the positioning of the brick within the cell when fully assembled.

**(a) Photograph of apparatus**

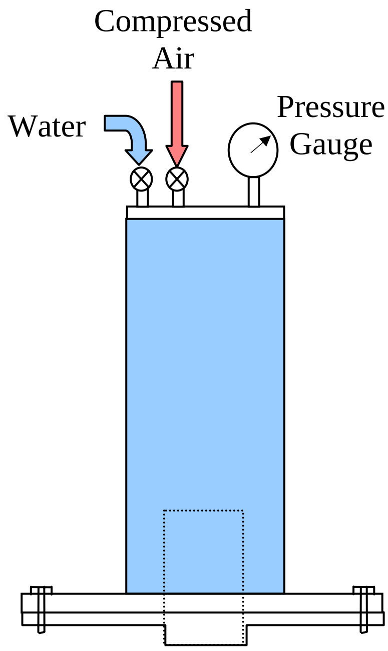


**(b) Schematic diagram of apparatus**

**FIG. 4.8 - Pressure testing chamber**

The cell was constructed in two parts – a pressure chamber (Fig. 4.9 a) and base plate (Fig. 4.9 b). Separate base plates were made to accommodate the different dimensions of the A1 and B bricks. Fig. 4.9 (b) shows a baseplate with the recess cut into the base, ready for the mounting of the brick. The rubber gasket placed between the baseplate and pressure chamber can also be seen in Fig. 4.9 (b). The top of the pressure chamber was constructed with a water inflow valve, a pressurised air inflow valve, an emergency pressure release valve, a pressure gauge, and a carrying hook and a sight glass was attached to the side of the chamber so the water level within the cell could be detected. The base plate and a water confinement chamber were connected using 8, 12 mm diameter high tensile bolts.

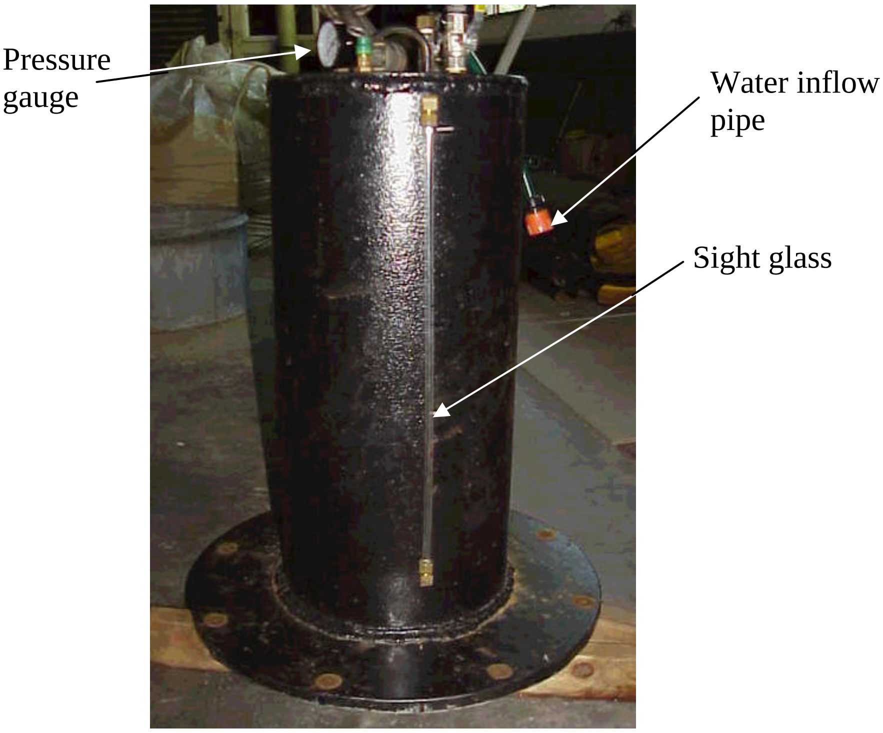


(a)

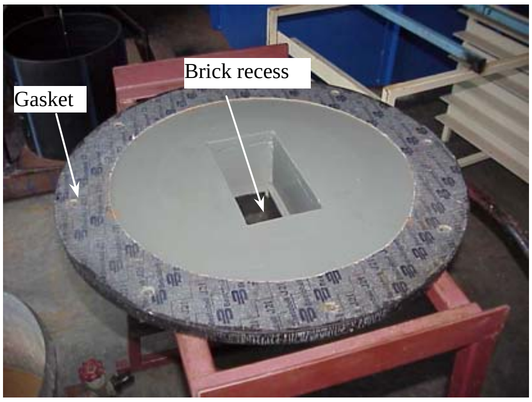


(b)

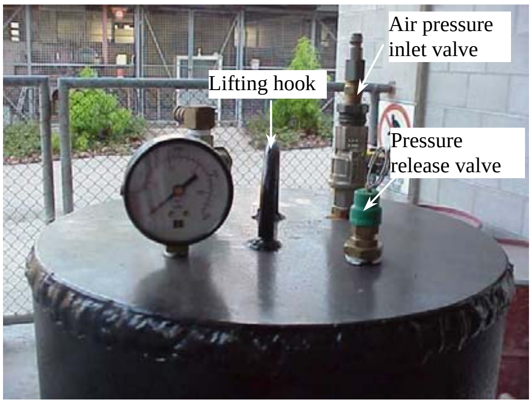


(c)

**FIG. 4.9 - Pressure testing cell (a) sight glass on side of the pressure chamber, (b) B base (c) top of confinement chamber**

The cell was initially tested for leaks to a maximum pressure of approximately 500 kPa prior to commencing any tests on bricks. The base of the pressure chamber was positioned on a stand to allow water to be easily collected from under the brick recess. The air pressure was applied via a 7.1 $m^3$ compressed air cylinder filled to 15 MPa, and air flow was fixed using a medical grade BOC Gases regulator with a pressure range from 0 to 100 kPa or a Veriflo regulator with a pressure range between 0 and 100 Psi (0 - 689.5 kPa). The BOC regulator was used to apply pressures between 0 and 100 kPa and the Veriflo regulator was used for pressures of 100 kPa and greater.

Specimen Preparation


**FIG. 4.10 - A1 porous bricks being sealed for testing**

Preparation of the bricks for constant and falling head permeability tests and pressure flow testing was undertaken in the same manner. To simulate an in situ drainage condition and determine the permeability using Darcy's law, it was necessary to ensure that the flow through the specimen was one-dimensional and was along the longitudinal direction as in the mine (see Fig. 4.2). The bricks were coated with a bitumen-based paint[7] along the length of the brick leaving the top and bottom ends exposed. Once set, a thick bituminous putty[8] was then applied over the paint. The

[7] Ormonoid Brushable Waterproofer – Heavy duty brush on bitumen coating
[8] Ormonoid Duraseal Bitumen based waterproofing putty

bricks were then placed in the seat and rapid setting foam[9] placed around the base to fill the gap between the brick and the wall of the recess. After curing was completed (over approximately 7 days), a silicone sealant[10] was generously applied to the brick to ensure that the foam was fully sealed, as were any additional gaps/holes in the bitumen coating. The sealant was then left to dry for a period of not less than 24 hours. Fig. 4.10 shows the bitumen sealing of A1 bricks. Fig. 4.11 shows a mine B brick, completely sealed, ready for testing.

**FIG. 4.11 - B brick completely sealed in base of pressure testing cell**

To verify the sample was completely sealed on all vertical walls, and also around the seal between the brick and the base plate, the following procedure was followed:

1. The pressure chamber was fixed to the base plate and then filled with water.
2. When full, the water inflow valve was closed and the pressure inflow valve opened to atmosphere. The water was allowed to flow under atmospheric pressure through the brick.
3. The height equivalent to the top of the brick when cast into the pressure chamber, was marked beside the sight glass (Fig. 4.9 a) using a permanent ink.
4. If the water level in the sight glass, fell below the top height of the brick within the cell, it was an indication that water was either permeating through walls of the brick (thus the flow was not limited to the vertical direction) or through the

[9] Selleys Space invader expanding filler, (300g can)
[10] Selleys Roof and gutter translucent silicone

base mould seal. If so, the pressure chamber was disassembled, and the sample re-sealed, and this verification process repeated until the sample was completely sealed within the pressure testing base mould. If the water level in the sight glass stopped at the top-height of the brick, it was concluded that there were no leaks through the walls of the brick and the sample was ready for testing.

5. The cell was then refilled, and water passed through the brick under maximum pressure of 350 kPa, and step 4 repeated to ensure the pressure loading did not cause the seal on the vertical walls and around the base of the brick to break.

Constant Head Permeability Test

The permeabilities of the barricade bricks (four A1, seven A2 and six B bricks, as detailed in Table 4.4) were found using the aforementioned pressure vessel, with modification to allow for a constant head setup, and an adaptation of the Australian Standard AS 1289.6.7.3-2001. A schematic representation of the constant head arrangement is shown in Fig. 4.12. All of the bricks were prepared in accordance with the procedure outlined in section 4.3.1.2.

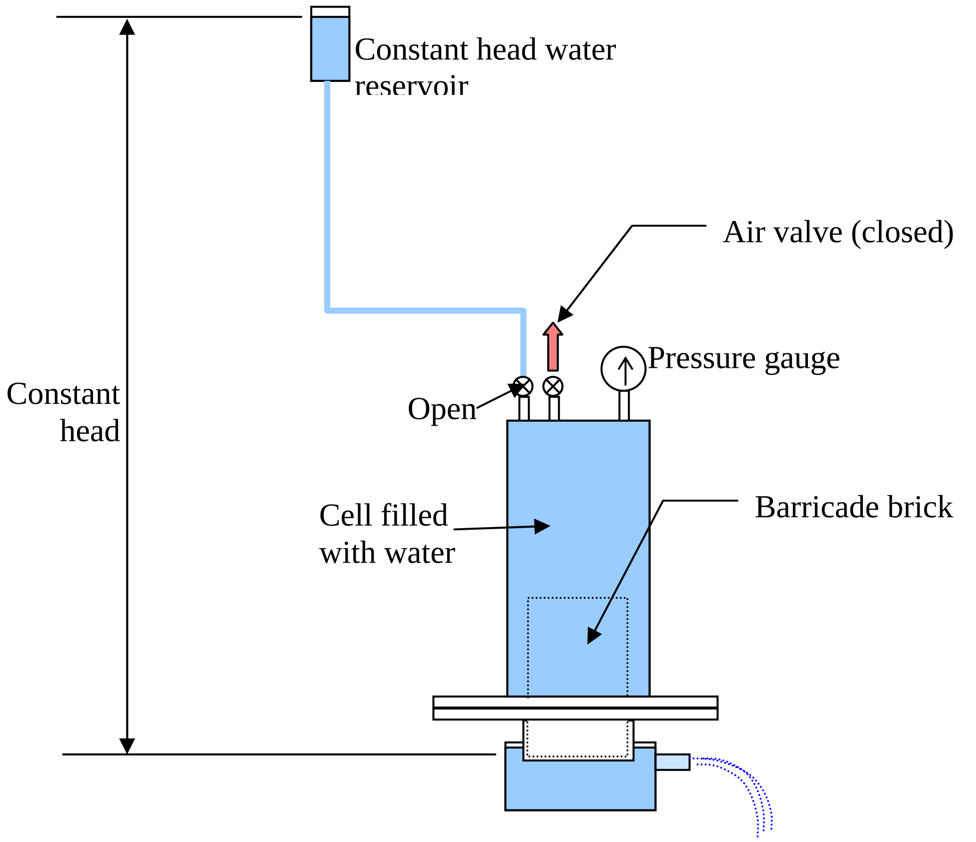


**FIG. 4.12 - Schematic representation of the constant head permeability test setup for the barricade bricks**

Water was allowed to flow through the brick for few minutes, to fill all the voids and to saturate the brick. Once steady state was achieved (i.e., when the flow per minute remained the same), the discharge over specific time was measured. Each brick was tested under three different heads. Three readings were taken at each head to ensure steady state was achieved and consistent results obtained.

Falling Head Permeability Test

The constant head permeability results obtain for four A1 bricks, two of the A2 bricks and six B bricks were verified using the falling head test. Tests were undertaken under a modified version of AS 1289.6.7.2-2001. The test apparatus is shown schematically in Figure 4.13.

Three markings were made on the standpipe, with the lowest marking slightly above the top height of the brick. The top mark identified the start of the falling head test (when the water level in the standpipe was even with the top mark). The middle mark was calculated as $h_2 = \sqrt{h_1 h_3}$ (Lambe, 1951). Theoretically, for 1-dimensional fluid flow, the time taken for the head to fall between $h_1$ and $h_2$ is equal to the time taken for the head to fall between $h_2$ and $h_3$. The permeability of the bricks was calculated using Eqn. 4.1.

$$k = 2.3 \frac{aL}{At} \log_{10} \frac{h_1}{h_2} \qquad \text{Eqn. 4.1}$$

Here,

$k$ = permeability (cm/s)

$a$ = cross-sectional area of the pressure chamber ($cm^2$)

$L$ = length of brick (cm)

$A$ = cross-sectional area of brick ($cm^2$)

$t$= time for standpipe head to decrease from $h_1$ to $h_2$ (s)

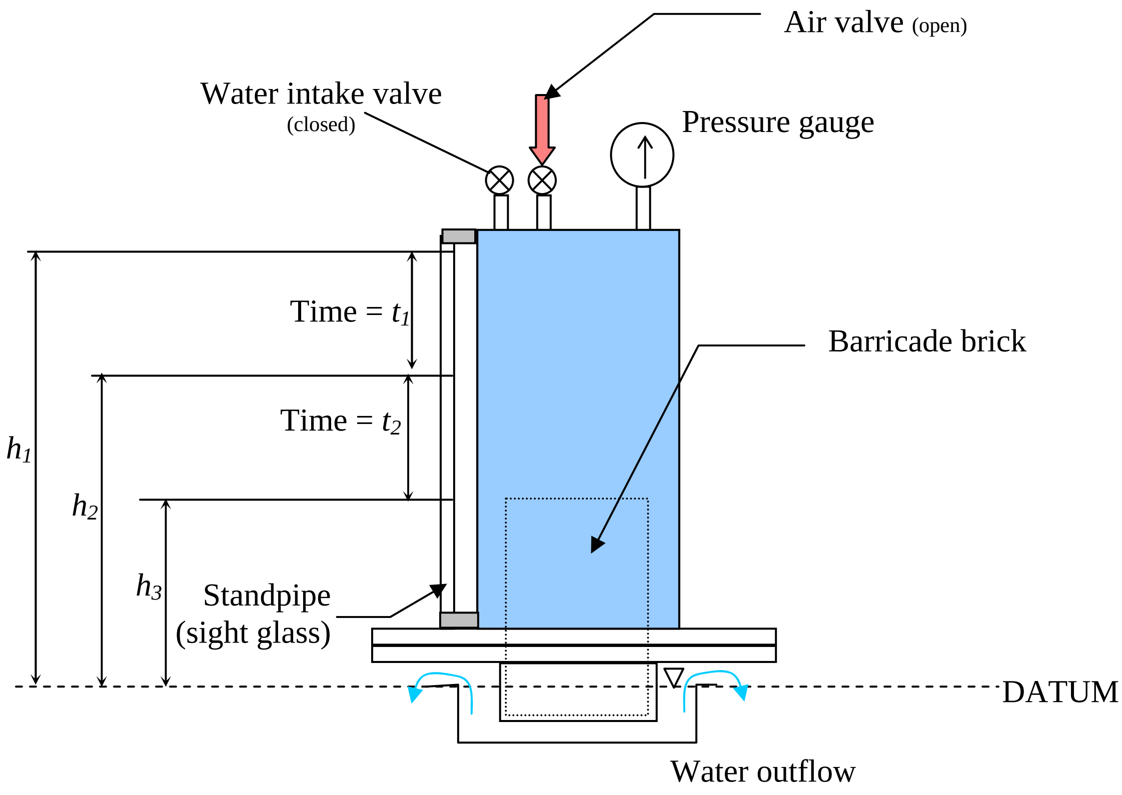


**FIG. 4.13 - Schematic representation of the falling head permeability test setup for the barricade bricks**

Flow-Under-Pressure Tests

Four A1 bricks, two A2 mine bricks and six bricks sourced from B mine, (refer to Table 4.3) were tested to define a set of curves showing the flow rate (l/min) versus applied pressure (kPa). The same bricks were subjected to constant and falling head permeability tests. Multiple bricks were used to define a range of values between which the flow rate could lie under a specific pressure. This was thought to be more representative way of defining the flow rates through bricks, which may have inherent variations during manufacture of the bricks.

To determine the flow rate for each pressure, the air pressure regulator was set to the desired level. For pressures below 100 kPa, the BOC Gases medical grade regulator was used and for pressures of 100 kPa and greater, the Veriflo regulator was used. Water was allowed to flow through the brick under pressure until the air voids were filled with water (i.e., the brick was saturated) and steady state achieved. The flow through the brick was collected and measured over a given period of time. The pressure chamber was refilled between each reading. For each brick, three comparable measurements were made to ensure consistency of flow. Fig. 4.14 shows a photograph of the flow-under-pressure test being undertaken on a brick.

**FIG. 4.14 - Photograph of brick being tested for flow rate under pressure**

4.3.2    Permeability Results for Barricade Bricks

The results for the constant head and falling head permeability tests and the flow-under-pressure tests on permeable barricade bricks are summarized below in Table 4.4. A complete set of test data is provided in Appendix 2.

Permeability of a porous medium is dependent on particle size, particle geometry, state of compaction and grading. In general, increasing particle size increases the permeability, and increasing the compaction reduces the permeability. A well graded sample will have a lower permeability than a poorly graded sample. This is because the grains pack more closely, as is the case for a material composed of more angular grains as opposed to the rounded particles. On inspection, an observer may easily see that the B bricks are composed of coarser aggregates, than that of theA1 and A2 bricks, which would suggest they would be inclined to possess a higher permeability. On the flip side, the B bricks tend to be composed of a more well graded range of materials. Therefore is it not possible based on visual inspection to predict which variety of brick would possess the higher permeability, and testing such as this is required to determine the relative permeabilities between the brick varieties.

Constant and Falling Head Permeability Constant

Although there was considerable scatter among individual brick type permeability results, as shown in Table 4.4, the results from both the constant and falling head brick permeability tests correlate very well.

**TABLE 4.4 - Constant and falling head barricade brick permeability summary**

| | Sample | Constant head permeability test (cm/s) | Falling head permeability test (cm/s) |
|---|---|---|---|
| **A1** | A1_001 | 0.16 | 0.30 |
| | A1_002 | 0.03 | 0.11 |
| | A1_003 | 0.07 | 0.08 |
| | A1_004 | 0.14 | 0.13 |
| | ***Average*** | ***0.10*** | ***0.15*** |
| **A2** | A2_004 | --- | 0.11 |
| | A2_005 | --- | 0.10 |
| | A2_012 | --- | 0.09 |
| | A2_013 | --- | 0.09 |
| | A2_014 | 0.07 | 0.05 |
| | A2_016 | 0.10 | 0.13 |
| | A2_017 | --- | 0.01 |
| | ***Average*** | ***0.08*** | ***0.08*** |
| **B** | B_003 | 0.31 | 0.24 |
| | B_004 | 0.21 | 0.15 |
| | B_005 | 0.13 | 0.10 |
| | B_006 | 0.13 | 0.10 |
| | B_007 | 0.14 | 0.12 |
| | B_008 | 0.24 | 0.24 |
| | ***Average*** | ***0.19*** | ***0.16*** |

The permeability values varied between 0.012 cm/s and 0.310 cm/s across all brick samples, and the spread of results for individual brick types covered a wide range. This permeability range is approximately that of clean sands. Both A1 and A2 bricks were typically less permeable than type B bricks, with A2 slightly less permeable than the A1 bricks. Table 4.4 and Fig. 4.15 show that the test results from the falling head permeability tests and the constant head permeability tests compare well. All permeability test results show that the permeable barricade bricks have permeabilities approximately three orders of magnitude larger than the permeabilities of typical Australian hydraulic fills (Table 3.7).

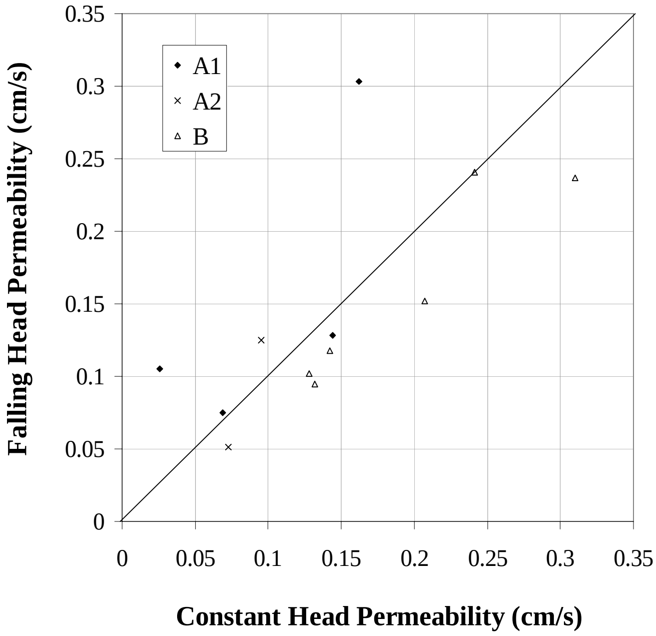


**FIG. 4.15 - Constant and falling head brick permeability comparison**

Flow-Under-Pressure

Fig. 4.16 shows the variation in discharge with pressure for the four A1, two A2 and six B barricade bricks, tested for flow rate under pressure. The expected trend of increased discharge with increased pressure is evident, but there is considerable spread between brick types, and even within individual bricks of the same type. As pressure applied approaches 350 kPa the discharge asymptopes between 20 to 60 l/min and 30 to 40 l/min for A1 and A2 bricks respectively, and 20 to 50 l/min for B bricks.

Flow rates under the maximum pressure tested (344 kPa) ranged from approximately 20 l/min to 60 l/min for the one (A1) brick variety. The implication of this substantial scatter for a these bricks which are produced under reasonably controlled conditions, is that had only one brick from the group been tested, the discharge potential for the other samples may have been incorrectly predicted by up to 300%. For this reason, and also to minimise lengthy and relatively exclusive testing requirements, the results have been manipulated in such a way that bricks only need to be tested at 300 kPa[11] rather than across the entire range of pressures saving substantial time and costs associated with the testing.

[11] 300 kPa was selected as the reference applied pressure because this value was more clearly marked on the dial guage therefore minimising error.

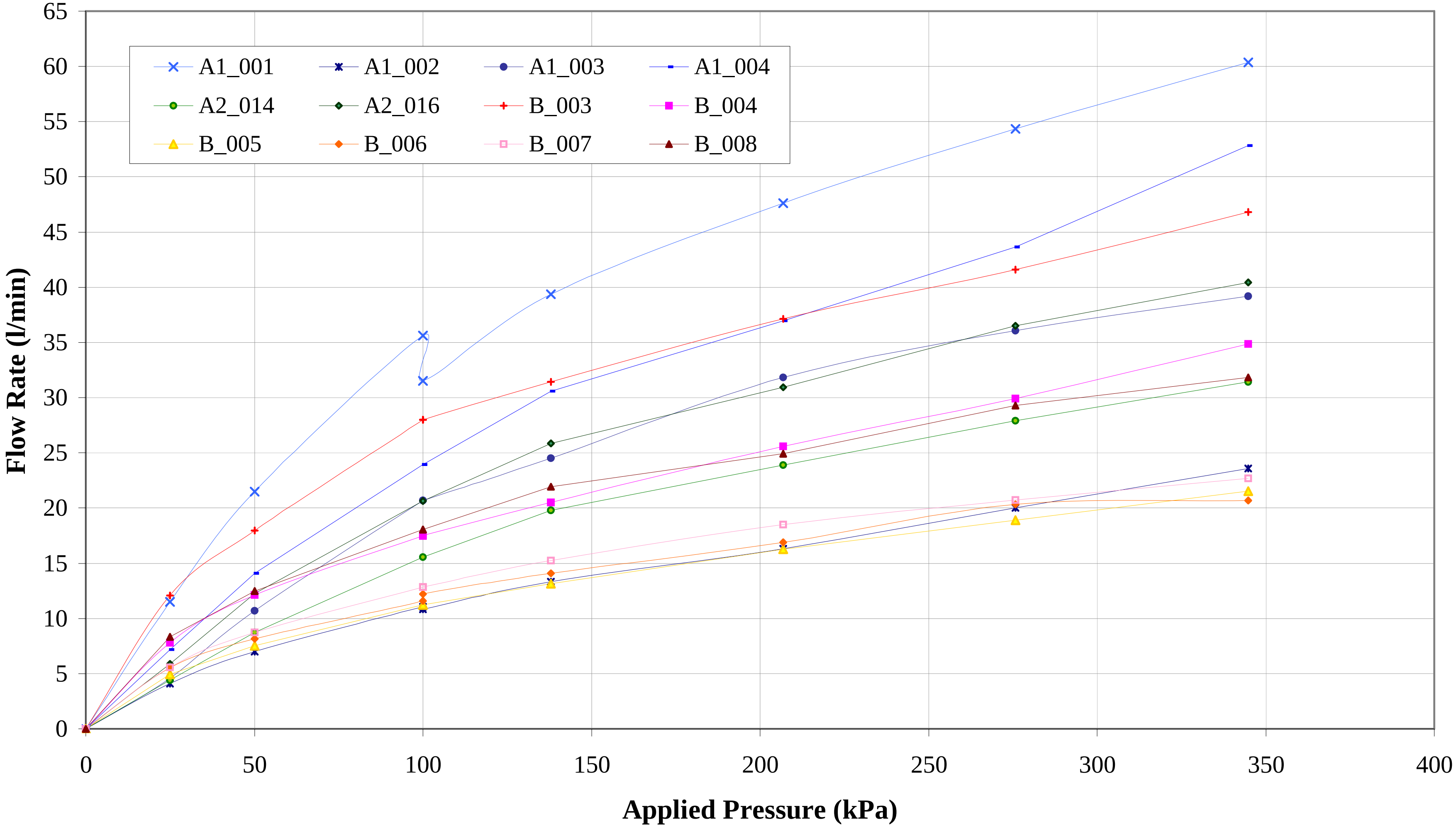


**FIG. 4.16 - Pressure versus flow plots for A1, A2 and B barricade bricks**

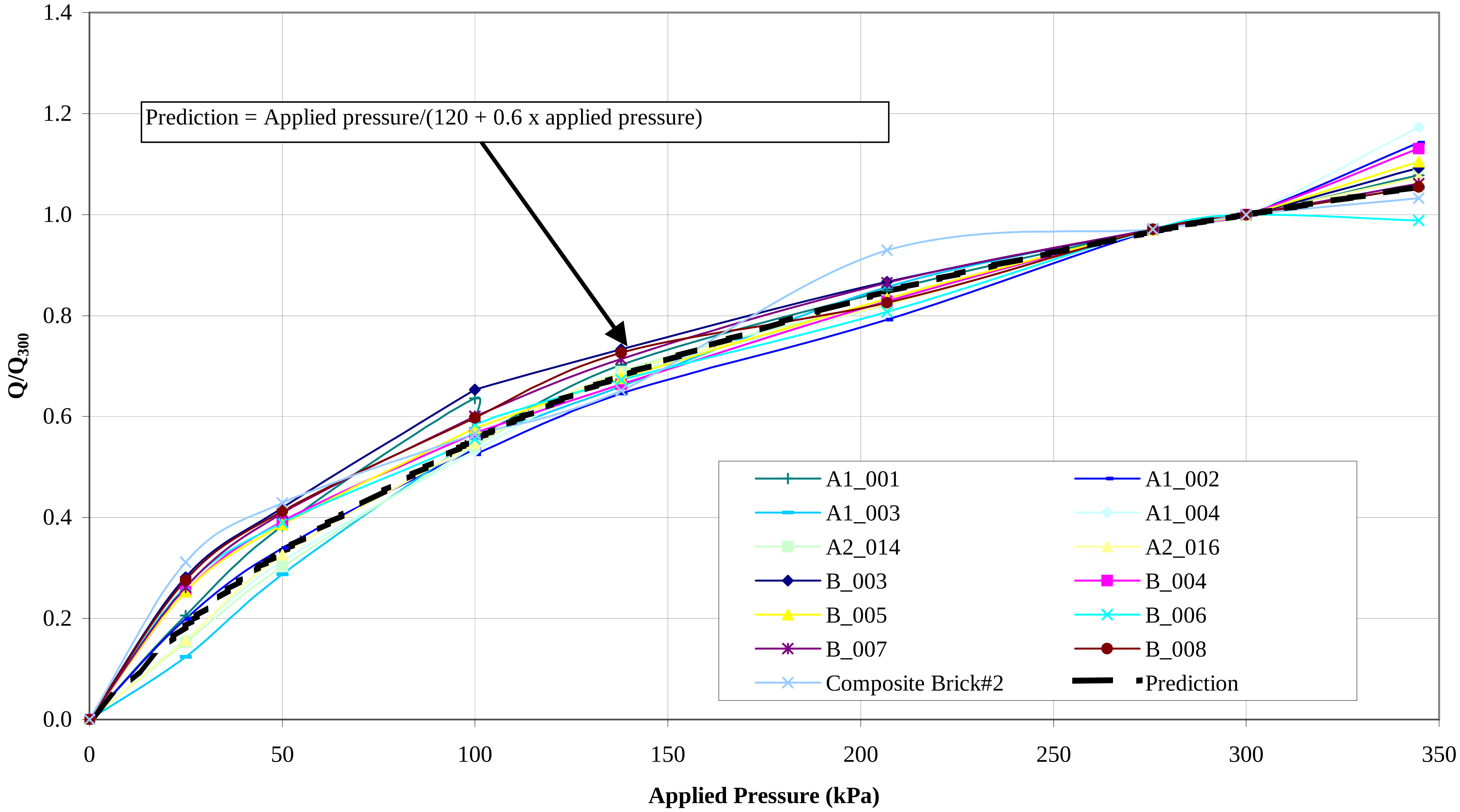


**FIG. 4.17 - $Q/Q_{300}$ for A1, A2 and B barricade bricks.**

By expressing the flow as a fraction of the flow obtained at 300 kPa, all pressure testing results (Fig. 4.17) collapse into a relatively narrow band for which an equation may be fitted to provide a good preliminary estimate to flow rates at any pressure (Fig. 4.17). This plot may be used as a simple tool to obtain an approximate flow rate under any pressure ranging up to approximately 300 kPa.

Darcy's law, which relates the permeability of a material to the hydraulic gradient[12] and the velocity of the flow, is only valid for laminar flow. At high pressures, the flow through the brick is turbulent, and therefore this law is invalid. By plotting the barricade brick pressure flow data as shown in Figs. 4.18 and 4.19, where the applied pressure is plotted against the velocity/hydraulic gradient ratio, which is permeability when the flow is laminar, trend lines can be extrapolated (dashed lines) to intersect the velocity/hydraulic gradient axis. At low pressures, flow through the barricade bricks is laminar, and therefore the intersection of the extrapolated trend lines with the x-axis in these plots (Figs. 4.18 and 4.19) provide an approximation for permeability value.

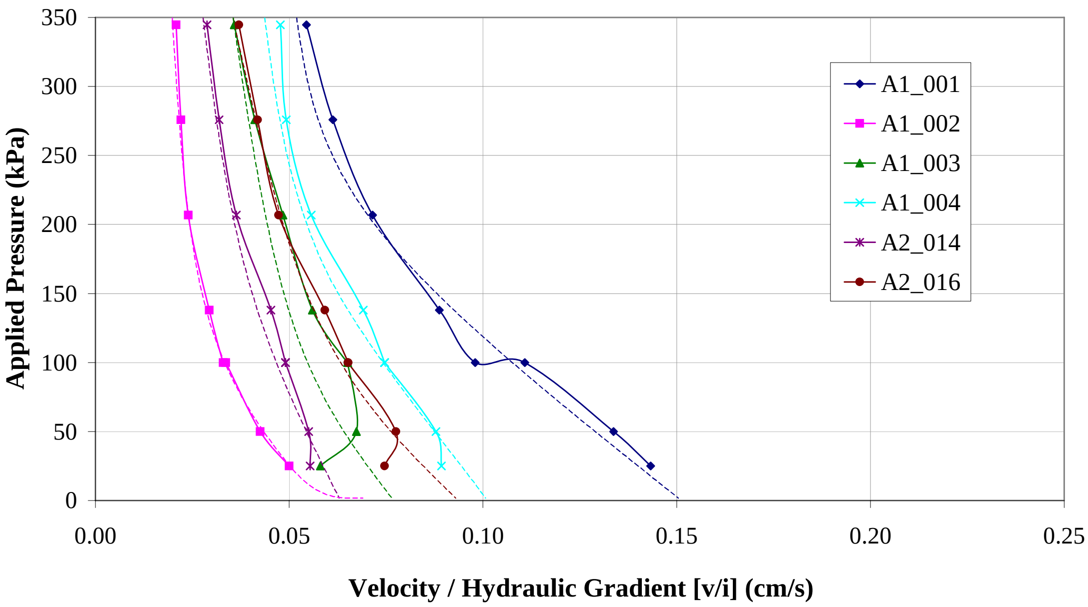


**FIG. 4.18 - Permeability estimation from pressure-flow curves for A1 and A2 barricade bricks**

[12] Hydraulic gradient i, is defined as the energy (or head) loss h, per unit length of material (l).

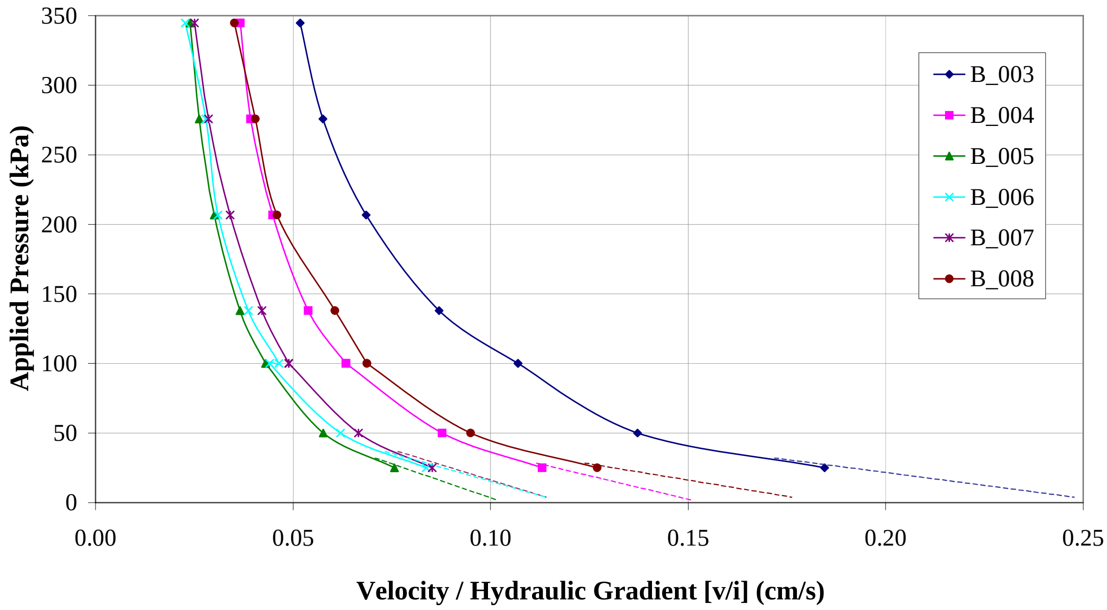


**FIG. 4.19 - Permeability estimation from pressure-flow curves for B barricade bricks.**

The predicted permeabilities for the B barricade bricks, estimated from the pressure-flow data ranges from approximately 0.10 cm/s to 0.25 cm/s, and the range for the A1 and A2 barricade bricks which are produced by the same manufacturer is slightly lower, and approximately falls between 0.07 cm/s and 0.15 cm/s. These predictions correlate very well with the constant and falling head test results, justifying the validity of this method of permeability prediction for barricade bricks. A complete table of the data relating to Figs. 4.18 and 4.19 is provided in tables A2.9 and A2.10 in Appendix 2.

Brick Permeability Summary

All bricks tested had significantly larger permeability than that of any of the hydraulic fill samples tested and reported in Chapter 3. Hydraulic fill permeability values average approximately 2 $\times 10^{-4}$ cm/s to 35 $\times 10^{-4}$ cm/s whereas the range for the permeable bricks used to contain the fill were tested to range between 1.2 $\times 10^{-2}$ cm/s and 3.1 $\times 10^{-1}$ cm/s, which generally places them 2-3 orders of magnitude more permeable than the fill. This has a significant impact on the understanding of the overall stope drainage system. This sizeable difference indicates that provided the barricades are built from the bricks in such a way that the construction does not impede the drainage performance, for modelling purposes it may be assumed that the barricade does not contribute to the pore pressure development within the fill, and hence the drainage of the system does not depend on the permeability of these bricks.

The flow-under-pressure testing for the bricks, used the pressure chamber described to study the 1-dimensional flow through porous bricks in the longitudinal direction, under the application of various pressures simulating the range of values representative of the underground barricade conditions. The results show, as expected, increase in discharge as a result of increased pressure applied, which reached a plateau after the peak value (approximately 350 kPa) was applied in this research.

The significant range of results obtained from both the permeability tests, and pressure tests confirms industry perception that manufacturing procedures for these porous bricks are not of an adequate standard to limit the variability, and to allow for confidence in barricade flow property predictions. Nevertheless, the permeability of the bricks is 2-3 orders of magnitude greater than that of the hydraulic fill. This justifies the assumption that the barricades are free draining.

Three methods of determining the permeability of underground permeable barricade bricks were described and the results were reproducible and compared very well among all three methods.

### 4.3.3 Composite Barricade Bricks

Underground hydraulic fill barricades are generally constructed as a vertical or curved wall, comprised of porous bricks which may be placed as a single layer, or several layers thick. Fig. 4.20 shows a photograph of a curved barricade constructed of one brick placed longitudinally and one perpendicularly to the flow of water, and offset by half a brick between bricks in the vertical direction.

A thin sand mortar layer, generally less than one centimeter in thickness is used between the bricks (Cowling, 2001). It has been shown in geotechnical engineering, that the equivalent coefficient of permeability of a stratified soil system calculated theoretically using existing equations, is substantially different to the directly measured values (Sridharan and Prakash, 2002). To investigate the validity of testing the permeability of layers brick systems, a testing methodology was developed and the results compared to the theoretical calculations.


**FIG. 4.20 – In situ barricade**

Two samples were prepared by cutting a standard porous brick in half and sandwiching a mortar layer, approximately 1 cm thick between the two halves. The mortar was mixed to cement:sand:water ratio of 0.5:1.0:0.92, The brick was cut such that the mortar would lie perpendicular to the flow of water when the water was passed in the longitudinal brick direction, (see Fig. 4.21). The sample was then placed in the humidity chamber, and allowed to cure at 100% humidity and room temperature (approximately 26°C) for a period of 28 days and brick permeability testing was undertaken as described in section 4.3.2 to determine the permeability of the cured mortar – brick composite, perpendicular to the bedding plane.

For a system with *n* layers, with heights $h_1$, $h_2 \ldots h_n$ with permeabilities of $k_1, k_2 \ldots k_n$ respectively, an equivalent permeability constant may be calculated (Das, 1997) as:

$$\frac{H}{k_{eq}} = \frac{h_1}{k_1} + \frac{h_2}{k_2} + \ldots \frac{h_n}{k_n} \qquad \text{Eqn. 4.2}$$

here,

$H$ = the total height of the system (= $h_1 + h_2 + h_3 \ldots h_n$)

$k_{eq}$ = an equivalent permeability constant for the entire system

Applying equation 4.2 for the composite brick system shown below, Eqn. 4.3 can be derived to calculate the equivalent permeability value for the composite brick.

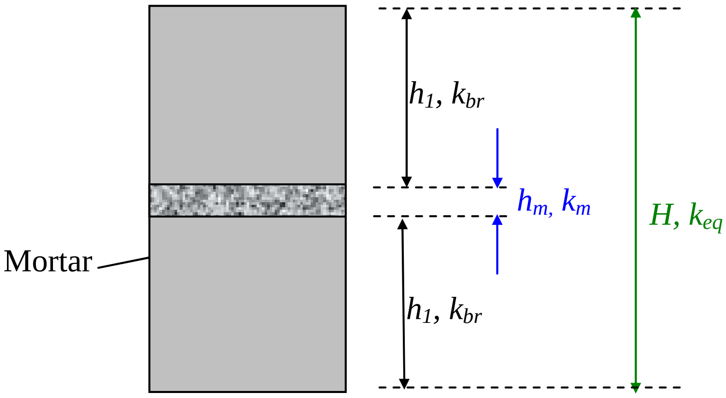


**FIG. 4.21 - Schematic diagram of composite brick**

$$\frac{H}{k_{eq}} = \frac{h_1}{k_{br}} + \frac{h_m}{k_m} + \frac{h_1}{k_{br}}$$

$$\frac{H}{k_{eq}} = \frac{2h_1}{k_{br}} + \frac{h_m}{k_m}$$

$$\frac{H}{k_{eq}} = \frac{2h_1 k_m + h_m k_{br}}{k_{br} k_m}$$

$2h_1$ is equal to the original length of the intact brick, $h_{br}$,

$$k_{eq} = \frac{H k_{br} k_m}{h_{br} k_m + h_m k_{br}} \qquad \text{Eqn. 4.3}$$

Here,

$k_{br}$ = permeability of the brick (cm/s)

$k_m$ = permeability of the mortar (cm/s)

Since $h_m k_{br} >>> h_{br} k_m$,

$$k_{eq} \approx \frac{H}{h_m} k_m \qquad \text{Eqn. 4.4}$$

Therefore, the permeability of the brick-mortar composite is mainly influenced by the permeability of the mortar, and then the relative thickness of the mortar.

Using the extreme range of possible brick and mortar permeability values (determined through separate laboratory tests undertaken on mortar alone) for theoretical calculations, it is shown in Table 4.5, that the results obtained from the laboratory testing did not agree well. In both falling and constant head tests, the results from laboratory testing were orders of magnitude higher than the theoretical values. This is probably due to cracking in the layer of mortar. Due to the less controlled environment with which the mortar is placed underground cracking within the mortar layers of an intact wall is considered likely. With the scale of the permeability values being considered, a small increase in flow, as would be experienced with water flowing through a crack, would produce a significant difference in the permeability. This testing methodology is not suitable for determining the equivalent permeability of a layered brick – mortar system. On the other hand, it is questionable whether the threshold estimates using Eqn. 4.3 will give reasonable estimates of $k_{eq}$ of in situ bricks.

**TABLE 4.5 - Comparison of theoretical and laboratory measured keq**

| | Theoretical $k_{eq}$ (cm/s) | | Laboratory determination of $k_{eq}$ (cm/s) | |
|---|---|---|---|---|
| **Brick ID** | **Lower bound** | **Upper bound** | **Constant head** | **Falling head** |
| Composite Brick #1 | 1.80 x$10^{-6}$ | 3.63 x$10^{-5}$ | 4.80 x $10^{-2}$ | 1.25 x $10^{-1}$ |
| Composite Brick #2 | 1.04 x$10^{-6}$ | 2.10 x$10^{-5}$ | 1.10 x $10^{-2}$ | 2.10 x $10^{-2}$ |

### 4.3.4 Barricade Brick Permeability Summary

- An innovative apparatus has been designed, constructed, verified and used effectively to perform three different permeability tests on permeable barricade bricks with consistent results.
- The pressure chamber designed for permeability testing may also be used to determine the flow variation with the application of pressure for separate permeable barricade bricks.

- Permeability results from modifications to standard constant and falling head tests and estimations extrapolated from pressure – flow tests agreed well, and a summary of the results for the various bricks tested is given in Table 4.6.
- 

**TABLE 4.6 – Constant head, falling head pressure-flow barricade brick permeability summary**

| | Sample | Constant head permeability test (cm/s) | Falling head permeability test (cm/s) | Pressure-flow test (cm/s) |
|---|---|---|---|---|
| **A1** | A1_001 | 0.162 | 0.303 | 0.150 |
| | A1_002 | 0.026 | 0.105 | 0.065 |
| | A1_003 | 0.069 | 0.075 | 0.075 |
| | A1_004 | 0.144 | 0.128 | 0.100 |
| | ***Average*** | ***0.100*** | ***0.153*** | ***0.098*** |
| **A2** | A2_004 | --- | 0.108 | --- |
| | A2_005 | --- | 0.102 | --- |
| | A2_012 | --- | 0.090 | --- |
| | A2_013 | --- | 0.089 | --- |
| | A2_014 | 0.073 | 0.051 | 0.065 |
| | A2_016 | 0.095 | 0.125 | 0.088 |
| | A2_017 | --- | 0.012 | --- |
| | ***Average*** | ***0.084*** | ***0.082*** | ***0.077*** |
| **B** | B_003 | 0.310 | 0.237 | 0.245 |
| | B_004 | 0.207 | 0.152 | 0.150 |
| | B_005 | 0.128 | 0.102 | 0.100 |
| | B_006 | 0.132 | 0.095 | 0.115 |
| | B_007 | 0.142 | 0.118 | 0.115 |
| | B_008 | 0.241 | 0.241 | 0.175 |
| | ***Average*** | ***0.193*** | ***0.158*** | ***0.150*** |

- The flow performance of individual bricks under pressure is considerably scattered, even between bricks obtained from the same manufacturer but produced in different batches. A time saving chart has been developed such that the flow performance of barricade bricks at various pressures is compared to the performance at 300 kPa, producing a very narrow band. The results can be plotted, and using this chart, rough flow estimates may be made for any brick at any pressure from only the results obtained for the brick at 300 kPa.
- The equivalent permeability of a layered barricade brick system could not be verified against theoretical developments due to cracking in the mortar layer.
- The permeability of permeable barricade bricks is two to three orders of magnitude greater than that of the hydraulic fill contained by the barricades and therefore the assumption that barricades are 'free-flowing' and do not

contribute to the pore pressure build up within the fill is justified provided construction specifications do not excessively inhibit flow.

## 4.4 Uniaxial Compression Tests

A very thorough testing schedule was staged over a period of approximately 1½ years, to obtain a comprehensive database of strength and stiffness properties of barricade bricks used in Australian hydraulic fill mines. This database was then used to assess the current industry perception on brick strength and deformation characteristics.

- The tests included 50 bricks from mine D (numbered 1 to 50), which were all cored (with the exception of brick 36 which was not supplied) across the lateral direction in such a way that two 86 mm diameter samples (labeled A and B) could be cut from each brick (Fig. 4.23). Eleven cores, (1B, 6B, 7B, 16B, 25B, 28B, 30B, 38B, 42B and 49B) were independently tested by Mr. Keith Clark at University of Queensland. This was used to ensure numerical integrity of results.

**FIG. 4.22 - Cored A2 bricks**

- Four B bricks (B_001, B_002, B_003 and B_004) and four A1 bricks (A1_001, A1_002, A1_003 and A1_004) were cored along the longitudinal axis for UCS testing. One 86 mm diameter cylindrical core was cut from each of the bricks except A1_002 which provided two samples from the one brick (A1_002 and A1_002A). The A2 (Table 4.7), 86 mm diameter cores were cut with aspect ratios of 2, and the B cores had an aspect ratio of 3. Traditionally, an aspect ratio of 2 is used for uniaxial tests on rock samples, and 3 for uniaxial tests on concrete samples. These aspect ratios were intentionally selected to observe the effect of varying the length on diameter ratio between 2 and 3.

**TABLE 4.7 - Unconfined compressive strength test barricade brick samples**

| Brick supplier | No. of samples | Label | Description | Sketch |
|---|---|---|---|---|
| A | 5 | A1_001 to A1_004 (with an additional sample (A1_002A) | Cores were cut in the longitudinal brick direction (86 mm diameter and lengths ranging from 245 mm to 258 mm) from each brick labelled with the same name. | 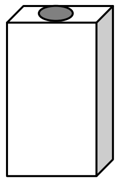 |
| A2 | 95 | A and B samples from 1 to 50 (except 36) | 86 mm diameter cores of approximately 172 mm in length were cut along the lateral direction of the bricks (2 cores cut from each brick). A was the first core. The cores were tested either dry, 7 days wet, or 90 days wetted. 11 samples were tested at an independent laboratory. | 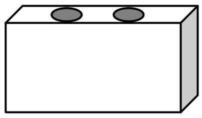 |
| A2 | 6 | A2_001, A2_002, A2_003, A2_004, A2_006 and A2_008 | Whole brick tested in the longitudinal direction. | 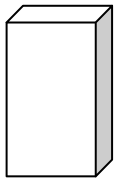 |
| B | 4 | B_001 to B_004 | Cores were cut in the longitudinal brick direction (86 mm diameter and lengths ranging from 245 mm to 258 mm) from each brick labelled with the same name. | 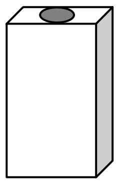 |
| Source A | 4 | Cylinder 1, Cylinder 2, Standard 1 and Standard 2 | Specially cast cylinders (153 mm diameter and approximate length of 300 mm), and two standard bricks cast from the same batch sulphur capped to give smooth ends. | 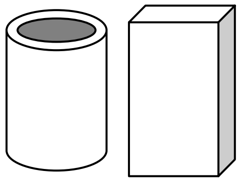 |

* A, A1 and A2 are from the same manufacturer

In addition to this, six whole A2 bricks were tested for strength and stiffness characteristics, and two cyclinders were specially cast by the same manufacturer that produced the A1 and A2 bricks (source A) and two standard bricks cast from the same batch of mortar. Table 4.7 summarises the samples tested for unconfined compressive strength.

The common practice for unconfined compressive strength tests on concrete is to carry out the tests on cores of length to diameter ratios of two, whereas in geotechnical applications, rock cores are usually tested with aspect ratios of three. Samples were all tested in accordance with AS 1289.6.4.1 - 1998. An aspect ratio of approximately three was used for the samples cored longitudinally, and two was used for the samples cored laterally, and the cylinders cast by source A. Table 4.8, details the dimensions, weights and densities for each of the A2 cores, and Table 4.9 summarises the average dimensions and aspect ratios for the samples tested for unconfined compressive strength.

### 4.4.1 Sample Preparation

Samples were prepared by coring full bricks using either a radial drill with a diamond tipped coring bit or a coring rig. The drill and coring rig are shown in Figs. 4.23 (a) and 4.23 (b), respectively. The cores were prepared with water as coolant on the coring bit. As a result the cores were wet on extrusion from the core barrel. Samples that were tested dry (All A1 and B cores, and A cores from A2 bricks, and core B’s obtained from A2 bricks, that were tested dry) were allowed to dry for a couple of days prior to testing. The A2 core B’s tested wet were immersed in water for a period of 7 days or 90 days. The dimensions of the prepared cores are shown in Table 4.8.

No further preparation was required for the whole A2 bricks and two Source A cast bricks tested for UCS. The ends of the Source A cylindrical samples were slightly uneven, therefore sulphur capping was required to make the surfaces smooth for the UCS tests (Fig. 4.24). The cylindrical bricks and standard bricks cast by source A for this research were made by mixing for 5 minutes 2000 kg of 16 mm gravel, 2000 kg of 4 mm river sand, 260 kg of cement and 50 litres of water, which was considered a typical barricade brick mix (www.mountisabrickworks.com.au).

**TABLE 4.8 - Dimensions and densities for A2 brick cores**

| Sample No. | Dia - 1 mm | Dia - 2 mm | Avg. Dia mm | Length1 mm | Length2 mm | Avg. length mm | Area $mm^2$ | Volume $cm^3$ | Weight kg | Density $g/cm^3$ |
|---|---|---|---|---|---|---|---|---|---|---|
| 1A | 87.6 | 87.6 | 87.6 | 171.8 | 172.1 | 172.0 | 6025.6 | 1036.10 | 1.92 | 1.85 |
| 1B | | | 87.3 | | | 172.3 | 5991.2 | 1031.99 | | |
| 2A | 87.6 | 87.4 | 87.5 | 172.0 | 172.0 | 172.0 | 6010.5 | 1033.68 | 1.88 | 1.82 |
| 2B | 87.7 | 88.0 | 87.8 | 171.7 | 171.3 | 171.5 | 6060.0 | 1039.26 | 1.88 | 1.81 |
| 3A | 87.5 | 87.4 | 87.5 | 172.4 | 172.3 | 172.3 | 6007.0 | 1035.04 | 1.92 | 1.86 |
| 3Bwet | 87.9 | 87.6 | 87.8 | 172.3 | 172.4 | 172.4 | 6049.7 | 1042.66 | 2.10 | 2.01 |
| 4A | 87.8 | 87.4 | 87.6 | 171.8 | 172.0 | 171.9 | 6028.3 | 1035.97 | 1.94 | 1.87 |
| 4Bwet | 87.8 | 87.8 | 87.8 | 172.3 | 172.4 | 172.4 | 6049.7 | 1042.66 | 1.98 | 1.90 |
| 5A | 87.9 | 87.9 | 87.9 | 172.4 | 171.8 | 172.1 | 6064.2 | 1043.52 | 1.94 | 1.86 |
| 5B | 87.9 | 87.9 | 87.9 | 172.0 | 171.9 | 171.9 | 6067.6 | 1043.27 | 1.96 | 1.88 |
| 6A | 87.9 | 87.9 | 87.9 | 171.5 | 172.2 | 171.9 | 6069.7 | 1043.17 | 1.96 | 1.88 |
| 6B | | | 87.9 | | | 172.3 | 6068.3 | 1045.81 | | |
| 7A | 88.0 | 87.9 | 87.9 | 172.0 | 171.7 | 171.8 | 6073.8 | 1043.76 | 1.94 | 1.86 |
| 7B | | | 87.9 | | | 171.6 | 6064.2 | 1040.49 | | |
| 8A | 88.0 | 88.0 | 88.0 | 171.2 | 171.9 | 171.5 | 6080.7 | 1043.12 | 1.94 | 1.86 |
| 8Bwet | 88.0 | 87.9 | 87.9 | 171.8 | 172.6 | 172.2 | 6074.5 | 1046.09 | 2.14 | 2.05 |
| 9A | 87.9 | 87.8 | 87.8 | 172.4 | 171.7 | 172.1 | 6059.3 | 1042.60 | 2.02 | 1.94 |
| 9Bwet | 87.9 | 87.9 | 87.9 | 172.1 | 171.5 | 171.8 | 6068.3 | 1042.66 | 2.00 | 1.92 |
| 10A | 87.9 | 88.0 | 87.9 | 172.0 | 172.0 | 172.0 | 6071.8 | 1044.25 | 2.00 | 1.92 |
| 10Bwet | 87.9 | 87.9 | 87.9 | 171.0 | 172.0 | 171.5 | 6066.2 | 1040.30 | 2.12 | 2.04 |
| 11A | 87.8 | 87.9 | 87.8 | 172.0 | 171.5 | 171.7 | 6060.0 | 1040.75 | 2.02 | 1.94 |
| 11Bwet | 87.8 | 87.8 | 87.8 | 171.3 | 171.7 | 171.5 | 6054.5 | 1038.41 | 2.04 | 1.96 |
| 12A | 87.8 | 87.9 | 87.8 | 172.0 | 171.1 | 171.5 | 6060.7 | 1039.62 | 1.92 | 1.85 |
| 12Bwet | 87.9 | 87.9 | 87.9 | 171.6 | 172.0 | 171.8 | 6064.9 | 1041.88 | 1.94 | 1.86 |
| 13A | 87.7 | 87.8 | 87.7 | 172.4 | 171.9 | 172.1 | 6042.8 | 1040.12 | 1.96 | 1.88 |
| 13Bwet | 87.5 | 87.6 | 87.6 | 171.9 | 172.5 | 172.2 | 6022.8 | 1037.25 | 2.00 | 1.93 |
| 14A | 88.0 | 87.8 | 87.9 | 171.6 | 171.4 | 171.5 | 6065.5 | 1040.36 | 2.00 | 1.92 |
| 14Bwet | 87.9 | 87.8 | 87.8 | 171.9 | 172.0 | 171.9 | 6060.7 | 1041.99 | 2.12 | 2.03 |
| 15A | 87.8 | 87.9 | 87.9 | 172.0 | 172.1 | 172.0 | 6062.1 | 1042.83 | 2.00 | 1.92 |
| 15B | 87.7 | 87.8 | 87.8 | 171.7 | 171.3 | 171.5 | 6049.7 | 1037.37 | 1.94 | 1.87 |
| 16A | 87.9 | 87.7 | 87.8 | 171.8 | 171.6 | 171.7 | 6052.4 | 1039.08 | 2.10 | 2.02 |
| 16B | | | 87.8 | | | 172.4 | 6051.7 | 1043.38 | | |
| 17A | 87.9 | 87.5 | 87.7 | 171.6 | 171.3 | 171.5 | 6044.2 | 1036.30 | 1.96 | 1.89 |
| 17Bwet | 87.9 | 87.6 | 87.7 | 172.1 | 172.3 | 172.2 | 6043.5 | 1040.60 | 2.09 | 2.01 |
| 18A | 87.9 | 87.7 | 87.8 | 171.9 | 171.5 | 171.7 | 6058.2 | 1040.14 | 1.96 | 1.88 |
| 18Bwet | 87.8 | 87.8 | 87.8 | 171.9 | 172.2 | 172.1 | 6058.0 | 1042.39 | 2.16 | 2.07 |
| 19A | 88.0 | 87.7 | 87.8 | 172.0 | 172.2 | 172.1 | 6056.6 | 1042.28 | 2.00 | 1.92 |
| 19Bwet | 87.9 | 87.7 | 87.8 | 171.7 | 172.0 | 171.8 | 6051.1 | 1039.81 | 2.05 | 1.97 |
| 20A | 88.0 | 87.8 | 87.9 | 171.9 | 171.8 | 171.9 | 6067.6 | 1042.87 | 1.96 | 1.88 |
| 20Bwet | 88.0 | 87.8 | 87.9 | 172.5 | 172.6 | 172.5 | 6064.2 | 1046.31 | 2.06 | 1.97 |
| 21A | 87.9 | 87.8 | 87.9 | 171.5 | 171.5 | 171.5 | 6066.2 | 1040.30 | 2.04 | 1.96 |
| 21Bwet | 88.0 | 87.7 | 87.8 | 171.4 | 171.1 | 171.3 | 6058.6 | 1037.57 | 2.12 | 2.04 |
| 22A | 87.9 | 87.6 | 87.7 | 170.8 | 170.9 | 170.8 | 6046.9 | 1033.06 | 2.04 | 1.97 |
| 22Bwet | 87.9 | 87.9 | 87.9 | 171.3 | 171.2 | 171.3 | 6066.2 | 1038.90 | 2.16 | 2.08 |
| 23A | 87.9 | 87.8 | 87.8 | 171.8 | 171.8 | 171.8 | 6060.7 | 1041.20 | 2.08 | 2.00 |
| 23Bwet | 88.0 | 87.8 | 87.9 | 171.9 | 171.5 | 171.7 | 6067.6 | 1041.78 | 2.20 | 2.11 |
| 24A | 88.0 | 87.8 | 87.9 | 171.7 | 171.3 | 171.5 | 6065.5 | 1040.33 | 2.04 | 1.96 |
| 24Bwet | 88.0 | 87.7 | 87.8 | 171.4 | 171.7 | 171.6 | 6058.0 | 1039.39 | 2.14 | 2.06 |
| 25A | 88.0 | 88.0 | 88.0 | 171.2 | 171.2 | 171.2 | 6078.0 | 1040.61 | 2.10 | 2.02 |
| 25B | | | 87.9 | | | 172.0 | 6068.3 | 1043.63 | | |
| 26A | 87.9 | 88.0 | 87.9 | 172.0 | 172.4 | 172.2 | 6073.1 | 1045.79 | 2.02 | 1.93 |
| 26B | 88.0 | 87.9 | 87.9 | 172.0 | 172.1 | 172.1 | 6071.1 | 1044.53 | 2.00 | 1.91 |
| 27A | 88.0 | 87.8 | 87.9 | 170.8 | 170.7 | 170.8 | 6069.0 | 1036.40 | 2.08 | 2.01 |
| 27Bwet | 87.9 | 87.9 | 87.9 | 172.3 | 171.7 | 172.0 | 6070.4 | 1044.23 | 2.12 | 2.03 |
| 28A | 87.9 | 87.9 | 87.9 | 171.3 | 171.8 | 171.6 | 6069.0 | 1041.20 | 2.08 | 2.00 |
| 28B | | | 87.8 | | | 172.1 | 6055.9 | 1041.92 | | |
| 29A | 88.0 | 87.8 | 87.9 | 171.7 | 171.7 | 171.7 | 6066.9 | 1041.78 | 2.00 | 1.92 |
| 29Bwet | 88.0 | 88.0 | 88.0 | 171.5 | 171.5 | 171.5 | 6080.7 | 1042.85 | 2.08 | 1.99 |
| 30A | 88.0 | 87.9 | 88.0 | 171.3 | 171.3 | 171.3 | 6075.2 | 1040.68 | 1.98 | 1.90 |
| 30B | | | 87.9 | | | 171.3 | 6061.4 | 1038.20 | | |
| 31A | 88.1 | 87.9 | 88.0 | 170.9 | 171.1 | 171.0 | 6078.0 | 1039.27 | 2.00 | 1.92 |
| 31Bwet | 88.0 | 87.9 | 87.9 | 170.7 | 170.4 | 170.5 | 6069.7 | 1035.03 | 2.12 | 2.05 |
| 32A | 88.0 | 87.9 | 87.9 | 171.3 | 171.5 | 171.4 | 6074.5 | 1041.39 | 2.06 | 1.98 |
| 32Bwet | 88.0 | 87.7 | 87.8 | 171.7 | 171.7 | 171.7 | 6059.3 | 1040.33 | 2.14 | 2.06 |
| 33A | 88.0 | 87.9 | 87.9 | 171.6 | 171.5 | 171.6 | 6071.1 | 1041.49 | 2.02 | 1.94 |
| 33B | | | 87.9 | | | 171.2 | 6068.3 | 1039.14 | | |
| 34A | 88.0 | 88.0 | 88.0 | 171.3 | 172.1 | 171.7 | 6083.5 | 1044.54 | 1.98 | 1.90 |
| 34Bwet | 88.0 | 88.0 | 88.0 | 171.7 | 171.4 | 171.5 | 6079.4 | 1042.76 | 2.16 | 2.07 |
| 35A | 88.0 | 87.9 | 87.9 | 171.6 | 172.2 | 171.9 | 6073.1 | 1043.97 | 2.00 | 1.92 |
| 35B | 87.9 | 88.0 | 88.0 | 171.5 | 171.8 | 171.6 | 6076.6 | 1042.90 | 2.02 | 1.94 |
| 36A | Brick not supplied | | | | | | | | | |
| 36B | Brick not supplied | | | | | | | | | |

**TABLE 4.8 (cont.) - Dimensions and densities for A2 brick cores**

| | | | | | | | | | | |
|---|---|---|---|---|---|---|---|---|---|---|
| 37A | 88.0 | 87.9 | 87.9 | 171.1 | 170.9 | 171.0 | 6074.5 | 1038.86 | 1.98 | 1.91 |
| 37Bwet | 87.9 | 88.0 | 87.9 | 171.4 | 171.4 | 171.4 | 6072.4 | 1040.88 | 2.00 | 1.92 |
| 38A | 88.0 | 87.9 | 87.9 | 170.7 | 171.3 | 171.0 | 6073.8 | 1038.47 | 2.06 | 1.98 |
| 38B | | | 87.8 | | | 172.2 | 6060.0 | 1043.66 | | |
| 39A | 88.0 | 87.9 | 88.0 | 171.1 | 171.6 | 171.4 | 6075.9 | 1041.11 | 2.08 | 2.00 |
| 39B | 87.9 | 88.0 | 87.9 | 171.4 | 171.5 | 171.4 | 6071.8 | 1040.79 | | 0.00 |
| 40A | 88.0 | 87.9 | 88.0 | 172.7 | 170.9 | 171.8 | 6080.0 | 1044.61 | 1.98 | 1.90 |
| 40Bwet | 88.1 | 87.9 | 88.0 | 172.7 | 171.6 | 172.2 | 6077.3 | 1046.27 | 2.16 | 2.06 |
| 41A | 88.0 | 87.8 | 87.9 | 171.0 | 171.1 | 171.1 | 6065.5 | 1037.51 | 2.02 | 1.95 |
| 41B | 87.9 | 87.9 | 87.9 | 171.6 | 171.7 | 171.7 | 6069.0 | 1041.90 | | 0.00 |
| 42A | 87.9 | 87.9 | 87.9 | 171.2 | 171.0 | 171.1 | 6069.0 | 1038.41 | 2.08 | 2.00 |
| 42B | | | 87.9 | | | 171.2 | 6072.4 | 1039.54 | | |
| 43A | 87.9 | 87.8 | 87.9 | 171.5 | 171.7 | 171.6 | 6064.2 | 1040.49 | 2.02 | 1.94 |
| 43B | 87.9 | 87.8 | 87.9 | 171.2 | 171.1 | 171.1 | 6066.2 | 1038.11 | | 0.00 |
| 44A | 88.0 | 88.0 | 88.0 | 170.9 | 171.5 | 171.2 | 6084.9 | 1041.52 | 2.10 | 2.02 |
| 44Bwet | 88.0 | 87.9 | 88.0 | 170.8 | 171.5 | 171.1 | 6078.0 | 1040.22 | 2.14 | 2.06 |
| 45A | 88.1 | 88.0 | 88.0 | 170.7 | 171.6 | 171.1 | 6087.0 | 1041.72 | 2.00 | 1.92 |
| 45Bwet | 88.0 | 87.8 | 87.9 | 172.2 | 171.8 | 172.0 | 6069.0 | 1043.72 | 2.12 | 2.03 |
| 46A | 88.0 | 88.0 | 88.0 | 170.8 | 170.4 | 170.6 | 6080.7 | 1037.31 | 2.02 | 1.95 |
| 46B | 88.0 | 87.8 | 87.9 | 171.8 | 171.7 | 171.8 | 6064.2 | 1041.58 | 2.08 | 2.00 |
| 47A | 88.0 | 87.9 | 88.0 | 170.8 | 171.0 | 170.9 | 6075.9 | 1038.16 | 2.00 | 1.93 |
| 47Bwet | 88.0 | 88.0 | 88.0 | 170.8 | 171.5 | 171.1 | 6078.0 | 1040.12 | 2.12 | 2.04 |
| 48A | 88.0 | 87.9 | 87.9 | 171.6 | 170.7 | 171.2 | 6071.1 | 1039.18 | 2.06 | 1.98 |
| 48Bwet | 88.0 | 88.0 | 88.0 | 171.8 | 171.2 | 171.5 | 6078.7 | 1042.37 | 2.20 | 2.11 |
| 49A | 88.0 | 88.0 | 88.0 | 171.2 | 171.3 | 171.2 | 6082.1 | 1041.50 | 2.08 | 2.00 |
| 49B | | | 88.0 | | | 171.5 | 6075.2 | 1041.78 | | |
| 50A | 88.0 | 88.0 | 88.0 | 170.4 | 169.5 | 169.9 | 6080.7 | 1033.30 | 2.06 | 1.99 |
| 50Bwet | 88.0 | 88.0 | 88.0 | 171.9 | 171.9 | 171.9 | 6079.4 | 1044.92 | 2.14 | 2.05 |

The additional JCU tests for research (JCU) - dry
The additional JCU tests for research (JCU) - soaked for a week
The additional JCU tests for research (JCU) - soaked for 90 days
90 days soaked (lost while crushing)
Cores tested at Uni of Qld by Keith Clark
Cores tested for Mine D (all A and 5B)
One missing brick

THESE IMAGES HAVE BEEN REMOVED DUE TO
COPYRIGHT RESTRICTIONS

**(a)** **(b)**

**FIG. 4.23 - Coring using the drill rig (a) Coring of the sample (b) Removal of cored sample**

**FIG. 4.24 - Sulphur capping to the ends of samples**

**TABLE 4.9 - Summary of UCS sample dimensions**

| Sample | Number Tested | Average Dimensions (mm) | Average Height (mm) | Average Aspect Ratio |
|---|---|---|---|---|
| A1 cores | 5 | 86 (diameter) | 253 | 2.95 |
| A2 cores | 95 | 86 (diameter) | 245 | 1.95 |
| A2 whole bricks | 6 | 114 x 213 | 255 | N/A |
| B cores | 4 | 86 (diameter) | 253 | 2.93 |
| A cylinders | 2 | 153 (diameter) | 303 | 1.98 |
| A standard bricks | 2 | 114 x 213 | 451 | N/A |

### 4.4.2 Test Methodology

The unconfined compressive strength tests were carried out as per the appropriate Australian Standards AS1289.6.4.1 – 1998, modified for concrete brick testing. The unconfined compressive strength (UCS) for each sample was found by crushing the sample using the 1000 kN MTS Universal Testing Machine (Serial No. 357) at James Cook University.

### 4.4.3 Statistical Analysis on Strength and Stiffness of A2 Cores

A thorough statistical analysis has been performed on the strength and stiffness of the standard autoclaved cured bricks from two separate and reputable Australian mine brick manufacturers, to determine a level of confidence with which the quoted strength values may be used in typical conditions to which the bricks would be exposed. The uniaxial compressive strength (UCS), Young's modulus (*E*) and the failure strain at maximum deviatoric stress ($\varepsilon_f$), of dry, 7 day wetted and 90 day wetted brick cores were studied. Unconfined compressive strength tests were performed on 95 A2 brick cores, 6 full A2 bricks, 5 longitudinal cores of A1 bricks, 4 longitudinal cores of B bricks, and 2 A1 bricks and 2 x 20 cm diameter brick cylinders cast from the same batch (refer to Table 4.9). The statistical study was undertaken on the 95 A2 cores, and the results were compared to the other barricade brick samples (Table 4.7) analysed in this research. The effect of coring was analysed by comparing core A's (the first samples cored from individual bricks) with core B's (the second sample cut), and the effects of wetting were studied by comparing dry core results with results obtained from cores that had been continuously submerged in a tank of water for either 7 days or 90 days duration.

Effects of Coring

A fraction of these cores were tested dry. Fig. 4.25 illustrates the comparison for uniaxial compressive strength (a), Young's modulus (b), and peak strain (c) results.

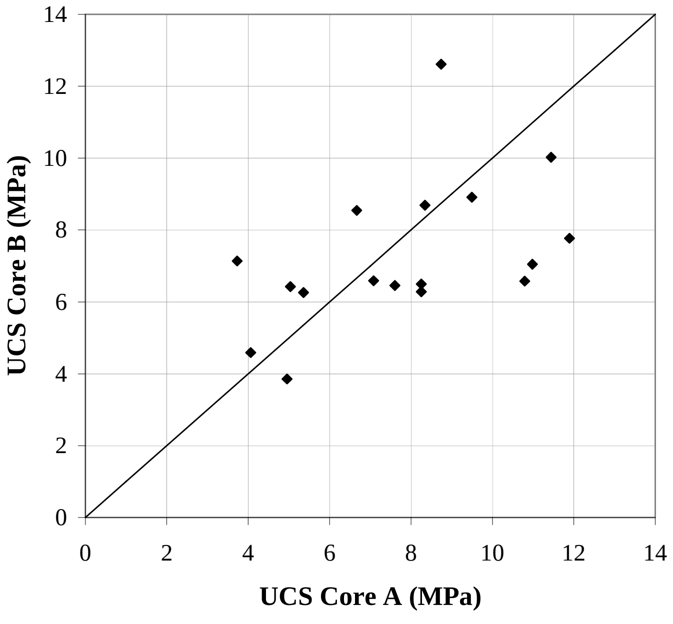


**(a) – UCS**

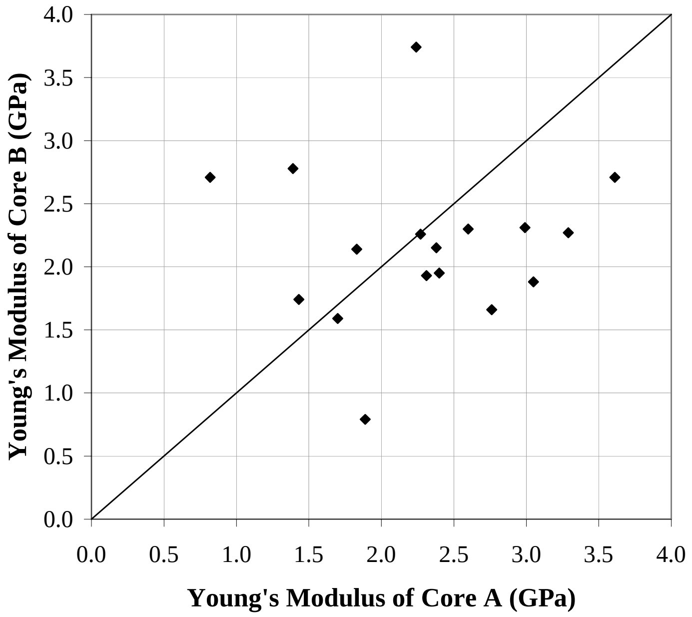


**(b) – Young's modulus**

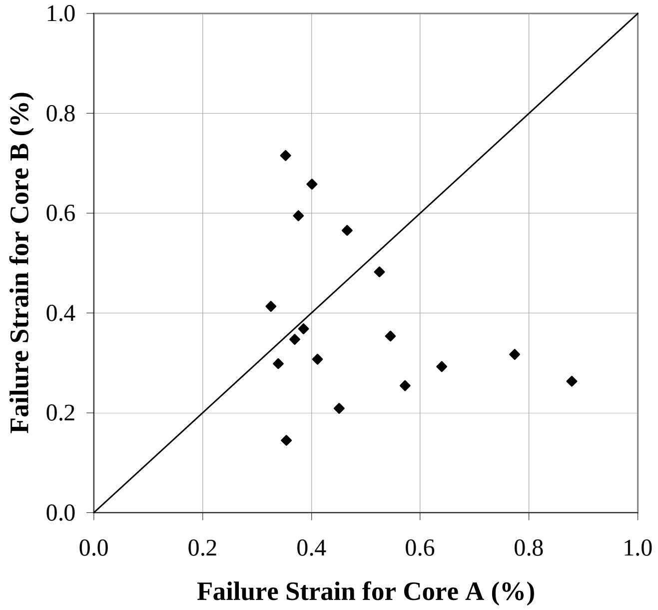


**(c) – Failure strain**

**FIG. 4.25 - Strength and stiffness comparison between dry core A and dry core B of A2 barricade bricks from Mine D**

Although there is considerable scatter in the UCS results, indicating substantial deviation in brick quality, the compressive strength of the samples is unaffected by coring process. The A cores indicate a slightly larger Young's modulus than that of B cores under the same testing conditions. This suggests that the coring process reduces

the stiffness of the bricks slightly which is likely the result of the wetting and vibration of the drill rig. Although a slight increase in brittleness is evident as a result of the coring (the peak strain of core A's is slightly larger than that of core B's), the scatter makes it difficult to conclude this. It is possible that the vibration and wetting used in the coring process removes some of the finer particles in the brick, thus reducing the ductility (i.e., increasing the brittleness) of the sample.

Effects of Wetting

By comparing the dry samples from a single brick (core A) with the second sample from the same brick (core B), which had been wet for either 7 days or 90 days, the effects of wetting could be analysed. Figure 4.27 shows the plots for UCS (a), Young's modulus (b) and failure strain (c) for the dry versus wet samples.

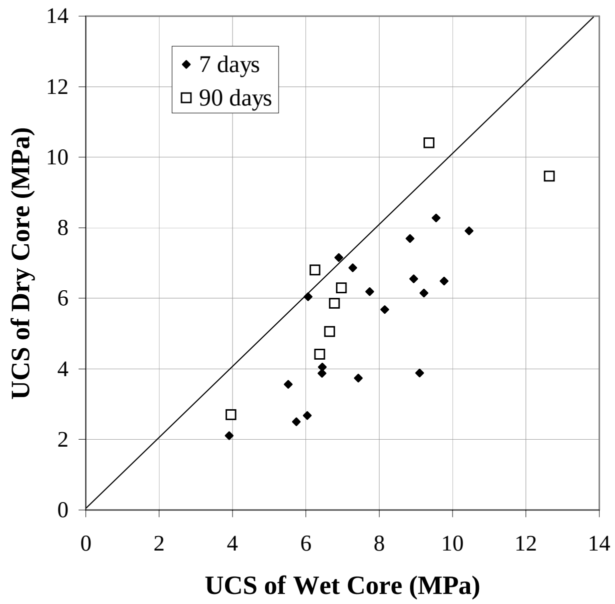


**(a) – UCS**

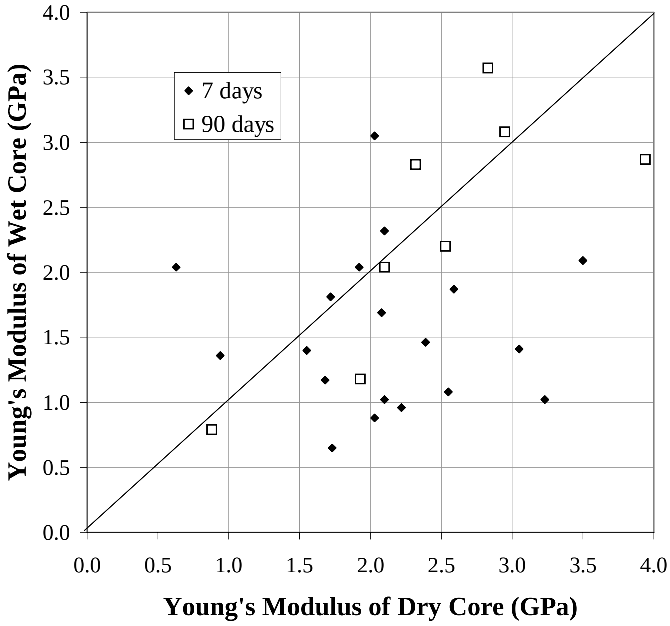


**(b) – Young’s modulus**

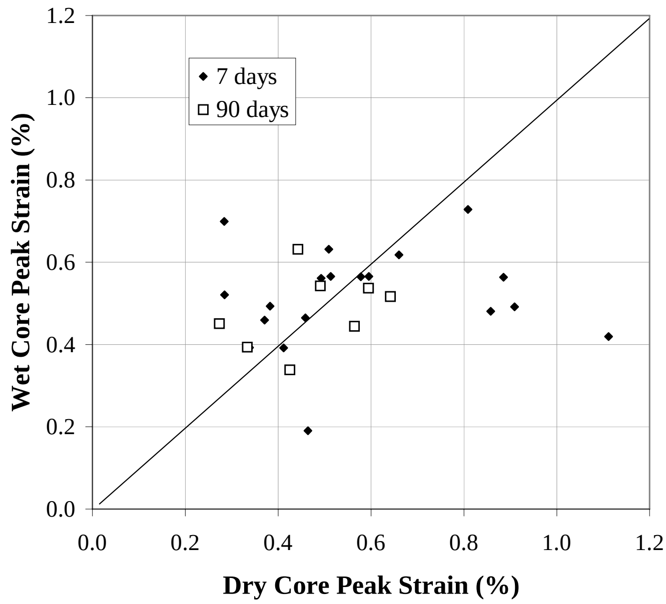


**(c) – Peak strain**

**FIG. 4.26 - Strength and stiffness comparison between wet and dry barricade brick core samples.**

There is a distinct loss of compressive strength as a result of wetting the brick. This loss appears to be in the order of approximately 25%, which is notable considering bricks are generally exposed to a saturated condition when placed underground, and manufacturer strength quotes are based on dry testing only. The wet core samples showed a lower stiffness than that of the dry cores, but this difference cannot be quantified because the variation is not significantly different to that found as a result of coring. No change in failure strain occurred as a result of wetting the samples. It is interesting to note that the loss in strength was not impacted by the length of time the bricks were saturated. In other words, the loss in strength is taking place once the brick is wetted. Remaining wet for an extended period does not reduce the strength further.

Strength and Stiffness Summary for A2 Cores

Across the series of uniaxial compressive strength tests undertaken on the 95 A2 core samples tested under various conditions, the following were observed.

1. There is substantial scatter in brick strength and stiffness.
2. The uniaxial compressive strength of the brick cores is unaffected by coring.
3. There is a slight reduction in sample stiffness resulting from coring.
4. The increase in brittleness evident as a result of coring cannot be justified as a trend due to the significant scatter among brick quality.
5. The compressive strength of the brick core samples is reduced by about 25% as a result of wetting, but the duration of wetting does not influence the strength loss.
6. No significant variation in the stiffness and peak strain of the samples was indicated as a direct result of wetting.

### 4.4.4 Probability Distribution Function for A2 Brick Core Strength and Stiffness

As with many sets of experimental data, probability distributions cannot be determined from a solely theoretical basis, and often the graphical representation (even when refined to removed anomalies and roughness) will not suffice as they lack the analytical advantage achieved through an equation. Harr (1977) succinctly presents an empirical method by which a systematic procedure may be employed to produce density functions for beta probability distributions.

An empirical distribution may be fitted to a set of data to provide both a prediction and a confidence with which the prediction may be made. Approximation by beta distribution is recommended for many data sets, such as material properties or parameters, whose measures must always be positive quantities and ranges are of reasonably limited extent. A beta-probability density function is defined over the range [*a*, *b*] as,

$$f(x) = \frac{1}{C}(x-a)^{\alpha}(b-x)^{\beta} \qquad \text{Eqn. 4.5}$$

where,

$$C = \frac{\alpha!\beta!(b-a)^{\alpha+\beta+1}}{(\alpha+\beta+1)!} \qquad \text{Eqn. 4.6}$$

And the shape parameters, $\alpha$ and $\beta$ can be obtained for data ranging from a to b, using the mean, variance, and coefficient of variation. Harr (1977) defines the terms,

$$\tilde{x} = \frac{\bar{x}-a}{b-a} \qquad \text{Eqn. 4.7}$$

and,

$$\tilde{V} = \left(\frac{S_x}{b-a}\right)^2 \qquad \text{Eqn. 4.8}$$

which are used to express $\alpha$ and $\beta$ as,

$$\alpha = \frac{\tilde{x}^2}{\tilde{V}}\left(1-\tilde{x}\right)-\left(1+\tilde{x}\right) \qquad \text{Eqn. 4.9}$$

$$\beta = \frac{\alpha+1}{\tilde{x}}-(\alpha+2) \qquad \text{Eqn. 4.10}$$

For clarity, the following definitions may be required to describe the charts developed from the brick core data.

- *The coefficient of skewness ($\beta_1$)* is defined as the degree to which the curve is off-centre from a perfect normal distribution curve.
- *The coefficient of kurtosis ($\beta_2$)* defines the degree of peakedness of the curve.

For a beta distribution, $\beta_1$ and $\beta_2$ are described by the following equations.

$$\sqrt{\beta_1} = \frac{2(\beta - \alpha)}{(\alpha + \beta + 4)}\sqrt{\frac{\alpha + \beta + 3}{(\alpha + 1)(\beta + 1)}} \qquad \text{Eqn. 4.11}$$

$$\beta_2 = \frac{3(\alpha + \beta + 3)\left(2(\alpha - \beta)^2 + (\alpha + 1)(\beta + 1)(\alpha + \beta + 4)\right)}{(\alpha + 1)(\beta + 1)(\alpha + \beta + 4)(\alpha + \beta + 5)} \qquad \text{Eqn. 4.12}$$

Beta distribution curves were fitted to the results obtained from the unconfined compressive strength tests undertaken on the 95 A2 barricade brick cores, with relative comparison drawn between dry core A's, dry core B's, 7 day wetted core B's and 90 day wetted core B's.

Unconfined Compressive Strength

A probability density function was fitted to the data obtained for each of the exposure conditions applied to the brick cores (dry, 7 days wetted and 90 days wetted). The limits a and b for the range of possible values, were determined using the mean and standard deviation for the entire (dry and wet) set of data. The UCS data for all cores tested (Appendix 2, Table A2.11) gave mean and standard deviation values of 6.57 MPa and 2.25 MPa respectively. The limits were bounded at three standard deviations either side of the mean, which provide a 99.73% confidence with which the predicted values would fall. A minimum value of zero MPa was set for a. Therefore, the a and b values were set as 0 MPa and 13.3 MPa for all probability density calculations undertaken on the UCS data.

Using these values for a and b, and the mean, and standard deviation for the particular exposure condition, the $\alpha$ and $\beta$ values for each were calculated using equations 4.7 to 4.10, detailed in section 4.4.4. An example of the method used to fit the beta probability density function to the data is described below for the dry USC data.

For the dry cores, the mean and standard deviation for the 27 cores tested were 7.5 MPa and 1.98 MPa respectively. Therefore substituting these values into equations 4.7 and 4.8 gives,

$$\tilde{x} = \frac{\bar{x} - a}{b - a}$$

$$\tilde{x} = \frac{7.5 - 0}{13.3 - 0}$$

$$\tilde{x} = 0.564$$

and,

$$\tilde{V} = \left(\frac{S_x}{b - a}\right)^2$$

$$\tilde{V} = \left(\frac{1.98}{13.3 - 0}\right)^2$$

$$\tilde{V} = 0.022$$

These values may then be used in Eqns. 4.9 and 4.10 to calculated the $\alpha$ and $\beta$ values as follows,

$$\alpha = \frac{\tilde{x}^2}{\tilde{V}}\left(1 - \tilde{x}\right) - \left(1 + \tilde{x}\right)$$

$$\alpha = \frac{0.564^2}{0.022}(1 - 0.564) - (1 + 0.564)$$

$$\alpha = 4.718$$

and,

$$\beta = \frac{\alpha + 1}{\tilde{x}} - (\alpha + 2)$$

$$\beta = \frac{4.718 + 1}{0.564} - (4.718 + 2)$$

$$\beta = 3.421$$

Using the designation for the beta function in Eqn. 4.5, the general equation for a beta distribution may be presented as follows,

$$f(x) = \frac{(b - a)^{-1-\alpha-\beta}}{\mathrm{B}(\alpha + 1, \beta + 1)}(x - a)^{\alpha}(b - x)^{\beta} \qquad \text{Eqn. 4.13}$$

where $a \leq x \leq b$, and $\beta > -1$, $\alpha > -1$, and $\mathrm{B}(\alpha+1, \beta+1)$ is obtained using Harr's gamma function table (Table A2.11, in Appendix 2) and the following relationship,

$$B(\alpha+1,\beta+1)=\frac{\Gamma(\alpha+1)\Gamma(\beta+1)}{\Gamma(\alpha+\beta+2)} \quad \text{Eqn. 4.14}$$

**TABLE 4.10 - UCS data for dry cores**

| Class limit | Interval | Frequency (F) | Relative frequency (F/N) | Mid-point |
|---|---|---|---|---|
| 0 – 0.999 | 0.999 | 0 | 0.000 | 0.4995 |
| 1 – 1.999 | 0.999 | 0 | 0.000 | 1.4995 |
| 2 – 2.999 | 0.999 | 0 | 0.000 | 2.4995 |
| 3 – 3.999 | 0.999 | 2 | 0.074 | 3.4995 |
| 4 – 4.999 | 0.999 | 0 | 0.000 | 4.4995 |
| 5 – 5.999 | 0.999 | 2 | 0.074 | 5.4995 |
| 6 – 6.999 | 0.999 | 10 | 0.370 | 5.4995 |
| 7 – 7.999 | 0.999 | 3 | 0.111 | 6.4995 |
| 8 – 8.999 | 0.999 | 3 | 0.111 | 7.4995 |
| 9 – 9.999 | 0.999 | 5 | 0.185 | 8.4995 |
| 10 – 10.999 | 0.999 | 1 | 0.037 | 9.4995 |
| 11 – 11.999 | 0.999 | 0 | 0.000 | 10.4995 |
| 12 – 12.999 | 0.999 | 1 | 0.037 | 11.4995 |
| | sum | 27 | 1 | |

Therefore, for the UCS dry core example,

$$B(\alpha+1,\beta+1)=\frac{(25.574)(36.731)}{(748324.884)}$$

$$B(\alpha+1,\beta+1)=0.0125526$$

and,

$$f(x)=(4.26205\times10^{-8})(x)^{4.718}(13.3-x)^{3.421}$$

The raw data, and the probability density function, fitted by approximation by beta distribution are shown on Fig. 4.28.

Beta distributions represent a wide range of probability distributions exhibiting skewed distributions and symmetrical bell-shaped curves, the uniform distribution, and U-shaped, J-shaped, and reverse J-shaped curves. Pearson defined the various distributions as types (Harr, 1977) and their shape is determined by the relative values of coefficient of skewness squared, $\beta_1^2$, and the coefficient of kurtosis, $\beta_2$, where the definitions of these parameters are given in Eqns. 4.11 and 4.12. A graphical representation of the relative $\beta_1^2$ and $\beta_2$ values, and their influence on beta distribution shape are detailed in Pearson's chart (Fig. A2.2) in Appendix 2.

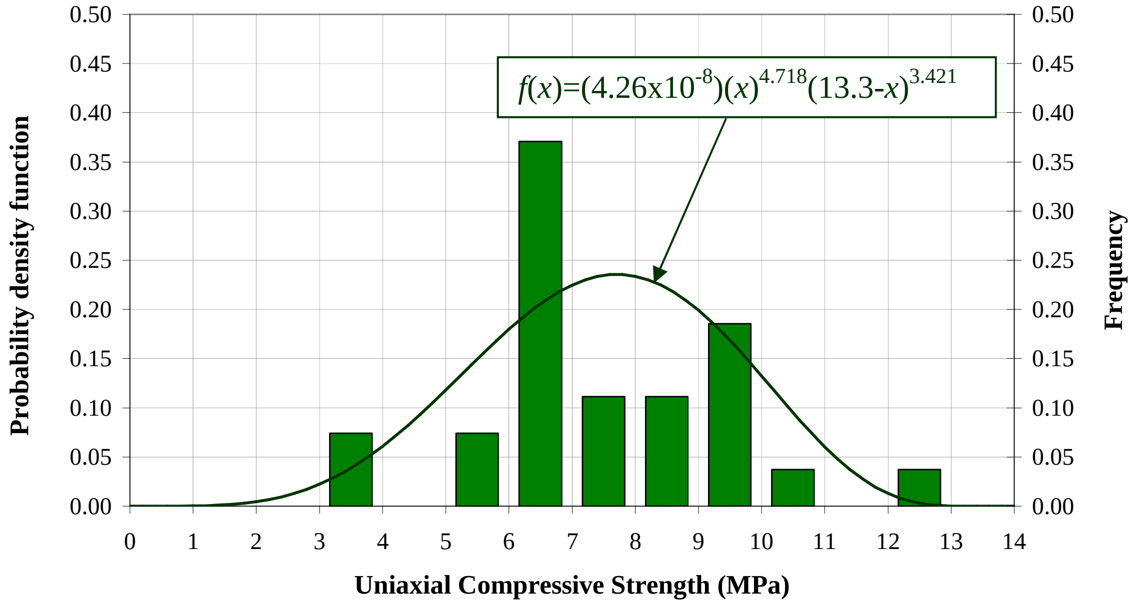


**FIG. 4.27 - Unconfined compressive strength frequency data for A2 barricade brick dry cores, with approximation by beta distribution**

The density function is described for the dry core UCS data (Fig. 4.27), is defined by Pearson's system as a type II curve. It is symmetrical, and bounded by a and b. The $\beta_1^2$ and $\beta_2$ values are 4.05 x $10^{-4}$ and 2.57 respectively. This plot clearly shows, that the beta prediction has a mean of between 7 and 8 MPa. The coefficient of kurtosis is very large quantifying the large scatter among the results.

Beta curves were fitted in this manner for the UCS data for the 7 days wetted and 90 days wetted cores. Individual plots of the raw data with the overlying distribution curve are printed in Appendix 2, as Figs. A2.3 to A2.5, and the distribution predictions for all three sets are compared below in Fig. 4.28. Fig. 4.28 shows a clear shift to the left for the wetted distributions, placing the average more than 2 MPa lower than the predicted average for the dry cores. The 90 days wetted prediction give a higher UCS average than the 7 days wetted, but fewer cores were tested at 90 days wet, and it is suggested that long-term wetting does not have a significant influence after the initial loss of strength caused by the original 7 days for which the cores were submerged.

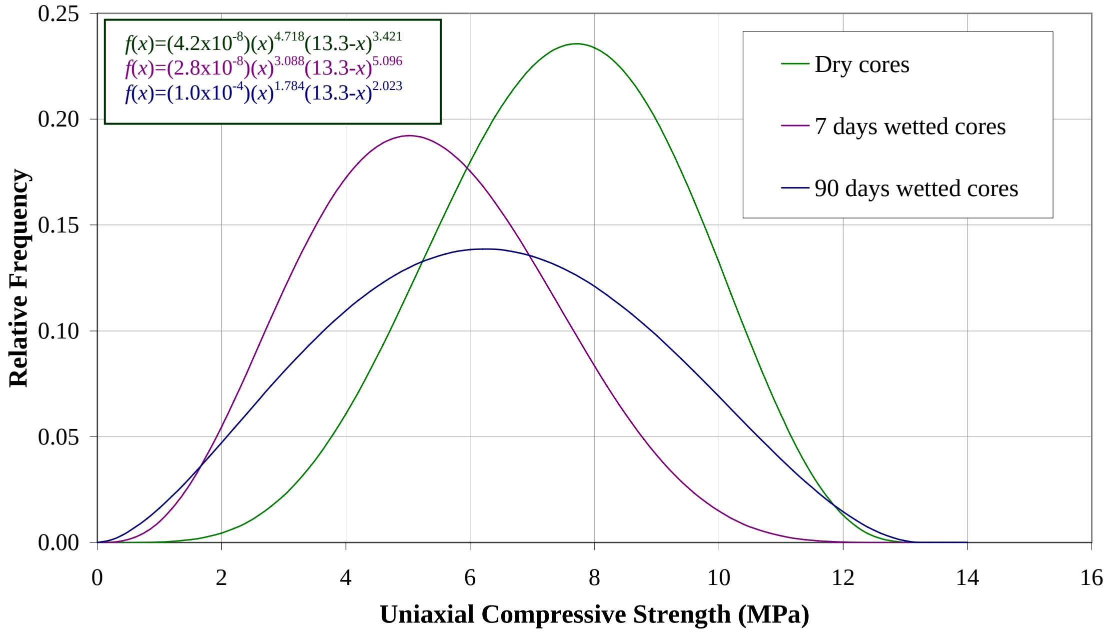


**FIG. 4.28 - Beta distributions for UCS core data**

The wetted relative frequency curves are also more spread for the wetted cores, indicating more scatter with regard to the data, and less reliability with which the mean strength could be used as a strength value.

Young's Modulus

Beta distribution curves were fitted in the same manner as described in section 4.4.4.1, using three standard deviations either side of the mean for all Young's modulus data, bounded by the value of zero as a minimum. The mean Young's modulus for all cores tested was 1.99 GPa and the standard deviation was 0.8. Therefore, a and b values of 0 GPa and 4.39 GPa were selected for all distribution curves. Like the UCS data, beta distribution equations were fitted to the dry, 7 days wetted and 90 days wetted data independently and plots of the raw data with the appropriate curve are included in Appendix 2, as Figs. A2.6 to A2.8 respectively. The beta distribution predictions for the Young's modulus data, are compared below in Fig. 4.29.

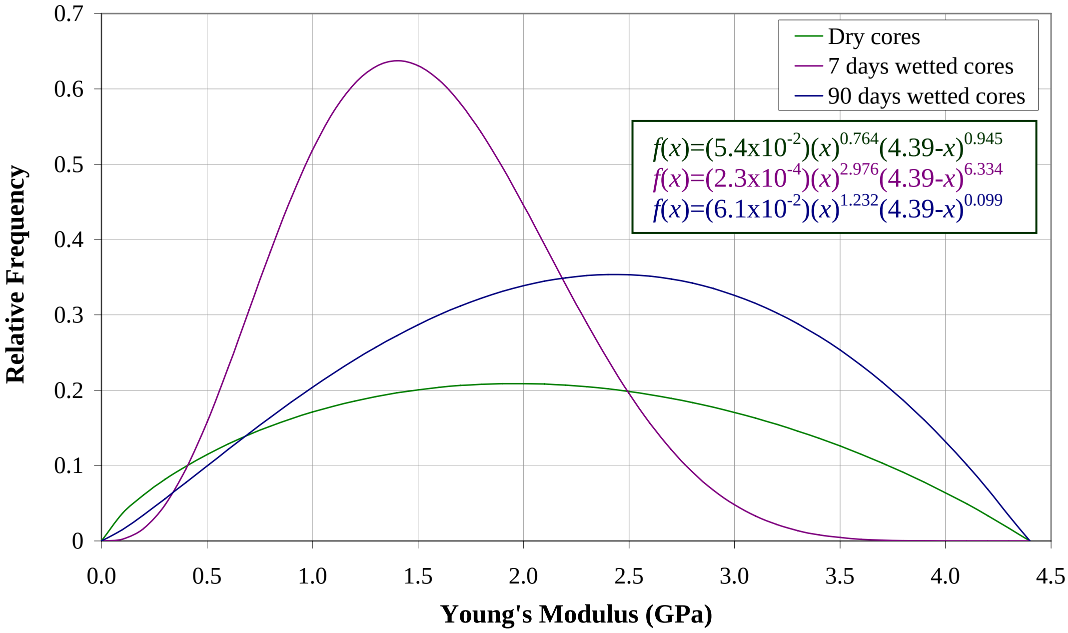


**FIG. 4.29 - Young's modulus data for A2 barricade brick cores, with beta distributions**

For the Young's modulus distributions, both the dry and 90 days wet curves indicate the data is very spread, and the flatness of the curve indicates larger coefficient of variation and the confidence with which the mean Young's modulus is predicted is quite low. The 7 day wetted curve is more peaked, but the Young's modulus average is quite low, and if more cores were tested, the geometry of the curve may resemble the other two curves more closely.

<u>Summary</u>

Statistical analysis techniques have been used to fit beta curves to the relative frequency data for both the UCS and the Young's modulus of the brick cores tested wet and dry. The raw data and predicted beta curves (with equations) for UCS and Young's modulus data on dry, 7 days wet and 90 days wetted cores are recorded in The Appendix. These curves present a graphical representation of the data, from which trends in behaviour may easily be established. For example, the loss of strength resulting from wetting the bricks is clearly shown in Fig. 4.28, by the distinct shift of the wetted curves to the left.

### 4.4.5 Effects of Sample Size and Shape

A brief analysis of the effects geometrical variation has on strength and stiffness was performed by comparing the two cylinders specially cast by source A with the standard bricks cast from the same batch of mortar mix. The results (Table 4.11) were compared to the results obtained from uniaxial compressive strength testing undertaken on full A2 brick samples which are manufactured by the same company.

As shown in Table 4.11, the strength and Young's modulus is relatively unchanged by geometrical differences between samples. As expected, the failure strain is slightly reduced with the increased aspect ratio of the standard brick samples from the specially cast cylinders, but this difference is not significant. The strength of the A2 bricks, which were manufactured in the same manner as the standard bricks was fairly consistent with the bricks and cylinders cast from a separate batch on request from the manufacturer, with brick A2_006 being the only anomaly with an excessively higher than average strength. The Young's modulus and peak strain values vary considerably between batches.

**TABLE 4.11 - Strength and stiffness summary for source A brick samples**

| Sample | Dimensions (mm) | UCS (MPa) | Young's Modulus (GPa) | Failure Strain (%) |
|---|---|---|---|---|
| A Cylinder 1 | 153 diam. x 303 | 6.2 | 3.2 | 0.4 |
| A Cylinder 2 | 153 diam. x 303 | 4.5 | 0.8 | 0.7 |
| ***Average*** | ***153 diam. x 303*** | ***5.3*** | ***2.0*** | ***0.6*** |
| A Standard 1 | 144 x 213 x 451 | 5.7 | 2.2 | 0.4 |
| A Standard 2 | 144 x 213 x 451 | 4.6 | 2.0 | 0.4 |
| ***Average*** | ***144 x 213 x 451*** | ***5.2*** | ***2.1*** | ***0.4*** |
| A2_001 | 114 x 206 x 452 | 6.4 | 0.75 | 1.5 |
| A2_002 | 113 x 209 x 453 | 5.4 | 0.5 | 1.2 |
| A2_003 | 113 x 210 x 454 | 4.8 | 0.6 | 1.1 |
| A2_004 | 112 x 211 x 451 | 5.9 | 0.7 | 1.1 |
| A2_006 | 114 x 215 x 453 | 14.7 | 1.1 | 2.2 |
| A2_008 | 112 x 211 x 452 | 5.4 | 0.6 | 1.2 |
| ***Average*** | ***113 x 210 x 453*** | ***7.1*** | ***0.7*** | ***1.4*** |

### 4.4.6 Uniaxial Compressive Strength Summary for Barricade Bricks

Firstly, it is important to note a fundamental misconception highlighted through this study. The average strength data obtained across all porous barricade brick samples tested regardless of exposure conditions or geometry, for uniaxial compressive strength (UCS)[13] was approximately 7.0 MPa, with a standard deviation of 2.8 MPa. Industry perception of brick strength varies considerably. Kuganathan (2001), suggests the strength of permeable bricks used in Mount Isa Mine is within the range 5 to 10 MPa, but other strength ranges quoted have been as high as 10 to 15 MPa (Duffield et al., 2003). Under in situ conditions, bricks are saturated. This research has shown the bricks have a distinct and significant (approximately 25%) loss of strength as a result of wetting, therefore reducing this average strength value further.

E/UCS values for soils, rocks and concrete may be used by engineers as a measure of relative strength and stiffness behaviours of these materials. By plotting the Young's modulus versus unconfined compressive strength values for the A2 cores as shown in Fig. 4.30, this value can easily be observed for the bricks exposed to both wet and dry conditions. Although the correlation between the data and the trend lines is reasonably poor, the gradients of all four exposure cases compare well, and therefore with such minor difference the E/UCS value for the bricks could be assumed to be unchanged by wetting or coring.

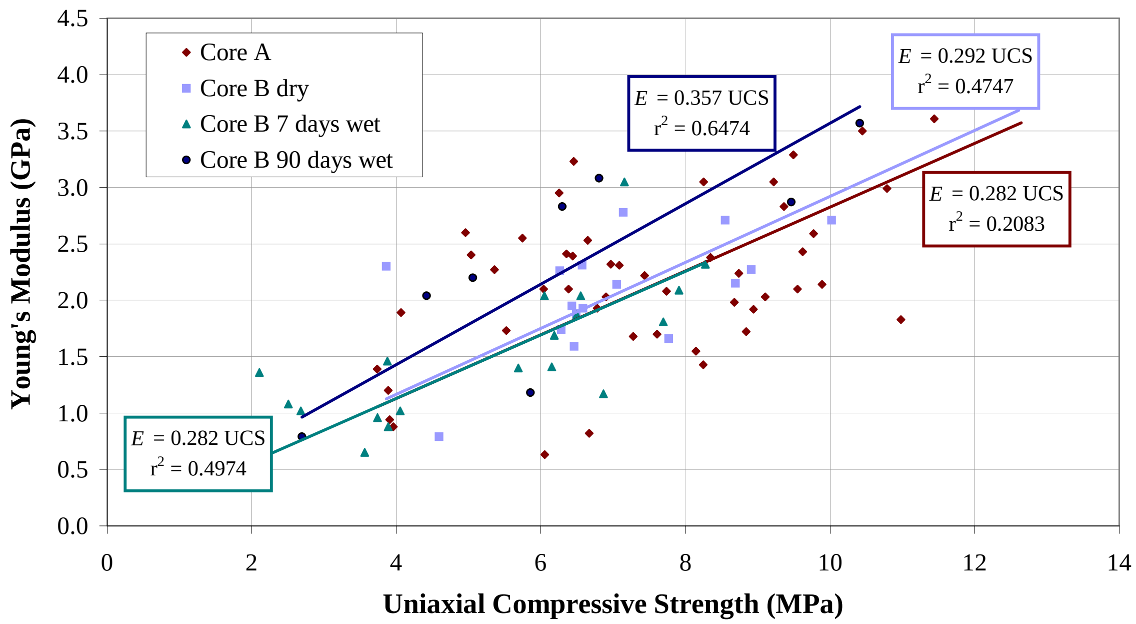


**FIG. 4.30 - Young's modulus versus uniaxial compressive strength for A2 barricade brick cores**

[13] Two independent laboratories were used to ensure validity of results, and there was no significant discrepancy between control samples.

A summary for the average uniaxial compressive strength, Young's modulus, failure strain and E/UCS ratio for the varieties of samples tested is shown in Table 4.12. Although there is a very significant scatter between the strength and stiffness results compared to other manufactured products such as steel, or even concrete (Table 4.13) this is expected due to the limited control the manufacturers have over the type and quality of product used in production.

**TABLE 4.12 - Uniaxial compressive strength test summary for barricade bricks and brick cores**

| Sample | UCS (MPa) | Young's modulus (GPa) | Failure strain (%) | E/UCS |
|---|---|---|---|---|
| A cylinders | 5.3 | 2.0 | 0.6 | 347 |
| A standard bricks | 5.2 | 2.1 | 0.4 | 410 |
| A2 Cores | 7.0 | 2.1 | 0.5 | 300 |
| A2 Bricks | 7.1 | 0.7 | 1.4 | 107 |
| B Cores | 14.3 | --- | --- | --- |
| A1 Cores | 3.3 | --- | --- | --- |
| ***Average*** | ***7.0*** | ***1.7*** | ***0.7*** | ***243*** |

The E/UCS ratio may be used to determine a relative behaviour of the porous bricks to other engineering materials. Clays are generally regarded to have an E/UCS value within the range 250 – 750 (Duncan and Buchignani, 1976), rocks typically within the range 300 – 1000, and concrete approximately 1000 (Table 4.13).

**TABLE 4.13 - Strength, stiffness and E/UCS summary for common engineering materials**

| Material | UCS (MPa) | Young's modulus (GPa) | E/UCS |
|---|---|---|---|
| Steel | 200-300 | 200 | 667 - 1000 |
| Concrete | 28 - 32 | 30 | 1000 |
| Clay | 0.025 – 0.5 | 0.002 – 0.25 | 250 – 750 |
| Barricade Bricks | 7.0 | 1.7 | 100 - 400 |

## 4.5 Chapter Summary

A series of laboratory studies were undertaken on typical Australian permeable bricks used for the construction of underground hydraulic fill barricades. The main objective was to study the drainage and strength characteristics of the barricade bricks, and their performance under pressures as high as 350 kPa. From this, a representative coefficient of permeability for the bricks and average strength and stiffness properties could be determined. Typical barricade bricks are composed of aggregate and cement, and were tested to show porosities between the values of 0.18 and 0.24, and a specific gravity range of 2.39 to 2.59.

There are no standards currently available to test permeability of bricks, and therefore Australian Standards AS 1289.6.7.2-2001 (falling head permeability test) and AS 1289.6.7.3-2001 (constant head permeability test) were modified from the standard soil testing procedures to accommodate the bricks. The permeability tests were carried out using a special pressure chamber, developed to study the one-dimensional flow characteristics of barricade bricks in the axial direction, under water pressures as high as 350 kPa. Three methods of determining the permeability of underground permeable barricade bricks were described and the results were reproducible and correlated very well among all three methods.

Although there was substantial deviation in permeability between bricks, the average permeability of the barricade bricks has been quantified as two to three orders of magnitude larger than the values obtained for the hydraulic fill. This has a significant impact on the understanding of the overall stope drainage system. The sizeable difference indicates that provided the barricades are built from the bricks in such a way that the construction or future migration of fines from the fill does not impede the drainage performance, for modelling purposes it may be assumed that the barricade does not contribute to the pore pressure development within the fill. Hence, the drainage of the system is not related to the permeability of these bricks.

The equivalent permeability of layered barricade brick systems, which are often used in underground containment wall construction could not be verified against theoretical developments due to cracking in the mortar layer.

Unconfined compressive strength tests were performed on 9 longitudinally cored bricks, 95 lateral brick cores, 8 intact bricks and two specially cast cylinders. The bricks were sourced from three separate mines and were obtained by those mines from two different Australian manufacturers. The average unconfined compressive strength for the samples regardless of exposure condition was approximately 7.0 MPa, with a standard deviation of 2.8 MPa. Under in situ conditions, the bricks are saturated. This research has shown the bricks have a distinct and significant (approx. 25%) loss of strength as a result of wetting.

A thorough statistical analysis has been performed on the strength and stiffness of the standard autoclaved cured bricks from two separate reputable Australian mine manufacturers, to determine a level of confidence with which the quoted strength values may be used in typical conditions to which the bricks would be exposed.

# Chapter 5

# Two-Dimensional Modelling of Underground Hydraulic Fill Stopes

## 5.1 Introduction

There is very limited material published specifically relating to the numerical modelling of the drainage of hydraulic fill stopes. The potential use of numerical modelling as a prediction tool in the drainage of underground cemented and uncemented hydraulic fill mines, could probably be attributed to the pioneering work undertaken for Mount Isa Mines Ltd. (MIM) by L.T. Isaacs and J.P. Carter (Isaacs and Carter, 1983). The work resulted in the development of a 2-dimensional model intended to provide a basic understanding of the concepts of the drainage of hydraulic fills in underground stopes, and produced many significant outcomes. The finite difference program, written in FORTRAN developed as a component of this work by Isaacs and Carter (1983), is still used as the predominant numerical model on which hydraulic fill drainage predictions are based within the Australian mining industry (Cowling, 2002). It is for this reason, along with availability of verification data, that the Isaacs and Carter program was utilized as the reference for the hydraulic fill drainage modelling undertaken in this research.

The program written by L.T. Isaacs and J.P. Carter in 1983 was originally implemented in the Department of Civil Engineering, University of Queensland. It is a 2-dimensional stope filling program capable of varying slurry composition, pour rates, fill/ rest cycle details, stope width and height sizes and mesh fineness. The implicit computation scheme utilized lends itself to very quick solution times. The program monitors the fill and water height, discharge rates and maximum pore water pressure values throughout the filling of the stope. Attention is drawn to some significant geometrical limitations of the program written by Isaacs and Carter. These include:

- the side walls of the stope must be vertical,
- the bottom of the stope must be horizontal, and
- the drains must be located flush with the stope wall.

### 5.1.1 *FLAC*

*FLAC* is an acronym for ***F***ast ***L***agrangian ***A***nalysis of ***C***ontinua, and represents the name for a 2-dimensional (plane strain, plane stress and axi-symmetric), explicit finite difference program, which was originally developed by the Itasca Consulting Group to primarily model soil and rock behaviour in geotechnical and mining engineering. The materials are represented by zones in a grid which may be moulded or adjusted to fit the geometry of the shape being modelled. The materials may yield and undergo plastic flow based on specified constitutive model behaviour, and in large-strain mode, the grid may deform and move with the material being modelled. The explicit, Lagrangian calculation scheme used in *FLAC*, combined with the mixed discretization zone allocation technique enables large deformations to be modelled accurately and because no large matrices are formed, large 2-dimensional calculations may be undertaken without excessive memory requirements. The simulations detailed in this Chapter, use *FLAC* Version 4.00, released in 2000.

*FLAC* contains a very powerful in-built programming language called *FISH*. *FISH* is embedded in *FLAC*, and enables the user to implement special programming requirements by defining new variables, functions and even constitutive models. For example, *FISH* permits user-prescribed property variations within the grid, custom-designed plotting and printing of user-defined variables, implementation of special grid generators, and specification of unusual boundary conditions, such as the changing boundary conditions required for the filling of a stope. Looping and conditional if-statements available in most programming languages (e.g., FORTRAN, BASIC) are also available through *FISH*. Without *FISH*, the capability of *FLAC* would be very limited. More than 50% of *FLAC* programmes used herein contain *FISH* routines.

The basic fluid-flow model in *FLAC* is capable of solving steady state or transient equation for flow in porous media, and may accommodate full saturated or partially saturated conditions. The capabilities in *FLAC* Version 4.00 are listed in the manual as follows (ITASCA, 2002):

1- *The fluid transport law corresponds to both isotropic and anisotropic permeability.*
2- *Different zones may have different fluid-flow properties.*
3- *Fluid pressure, flux, and impermeable boundary conditions may be prescribed.*
4- *Fluid sources (wells) may be inserted into the material as either point sources (interior discharge) or volume sources (interior well). These sources correspond to either a prescribed inflow or outflow of fluid and vary with time.*
5- *Both explicit and implicit fluid-flow solution algorithms are available.*
6- *Any of the mechanical models may be used with the fluid-flow models. In coupled problems, the compressibility of a saturated material is allowed.*

## 5.2 Verification Exercise: *FLAC* versus Isaacs and Carter (1983)

The verification exercise was undertaken to ensure the numerical integrity of the results obtained from the *FLAC* model. A series of drainage problems were designed and simulated for a simple stope geometry, using the *FLAC* program. The results were compared to Isaacs and Carter (1983) model that has previously been verified against in situ data.

### 5.2.1 Problem Definition

A fictitious stope drainage problem was designed based on typical input parameters for stope dimensions and fill properties, such that an identical data set could be used as input to provide a direct comparison between the 2-dimensional, finite difference flow-only code Isaacs and Carter, developed by L.T. Isaacs and J.P. Carter at the University of Queensland in 1983, and a similar simulation developed by the author in *FLAC*, for this dissertation. The verification exercise was designed to compare the water and tailings levels, and the discharge during a specific filling schedule. Maximum pore pressures compared later, matched the ones in Isaacs and Carter (1983). The *FLAC* code also incorporated capabilities to monitor these values throughout the drainage of the stope for the entire duration, since filling started and until the free water had completely drained from the stope, leaving the fill at residual water content.

The geometry of the stope used in the verification exercise is shown in Fig. 5.1. It is a 25 m wide, 150 m high stope with one drain located on right hand side of the base. The drain is one meter high in flush with the stope wall and because of the 2-dimensional simplification, if the stope were to be assumed 25 m in the z-direction, this models a 1 m by 25 m cross-sectional drain. As described in Chapter 4 drains are generally between 3 m and 6 m in width and height, which makes the drain typically between 9 $m^2$ and 36 $m^2$ in cross-sectional area. The equivalent cross-sectional area provided by this simulation falls within this typical range, despite the 2-dimensional simplification. The purpose of the verification exercise was to produce a model that mimicked that given by Isaacs and Carter (1983) as closely as possible. Once verified, this program could then be extended into three dimensions using *FLAC*$^{3D}$ so that more complicated geometries could be analysed.

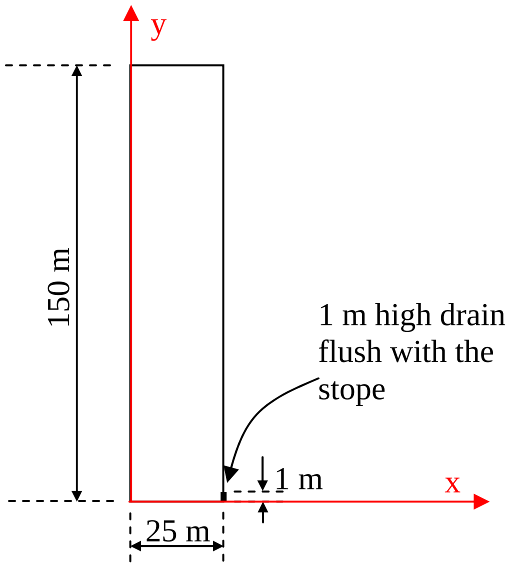


**FIG. 5.1 – Two-dimensional verification simulation geometry**

The simulation is based on a 12 hour filling followed by 12 hours resting schedule which is continued until the hydraulic fill reaches the height of the stope. The water is then continuously drained from the stope until the water height reaches the height of the drain. No discharge calculations are done until the hydraulic fill height passes the height of the drain while filling. The mesh is based on 1 m grid point spacing in both the x and y directions, and the grid origin is located in the bottom left hand corner of the stope as shown in Fig. 5.1, with gravity acting in the negative y-direction. It is found that 1 m x 1 m grid spacing in the stope and the drain gives the right balance between accuracy and solution time.

### 5.2.2 Input Parameters

The input parameters for the simulations are summarized in table 5.1.

**TABLE 5.1 - Input parameters for verification simulation**

| Input | Value |
|---|---|
| Coefficient of permeability, $k$ | 5.4 mm/hr |
| Specific gravity, $G_s$ | 2.9 |
| Dry density of fill, $\rho_d$ | 1.4 t/m$^3$ |
| Residual water content, $w$ | 25 % |
| Percent solids of slurry placed | 72 % |
| Steady state time step | 1 hour |
| Solids filling rate | 250 t/hr |
| Filling cycle | 12 hrs filling, 12 hrs resting |

Based on these input values, the following calculations were performed.

*FLAC* permeability (m$^2$/Pa.sec) = $\frac{Permeability(m/hr)}{60 \times 60} \div \gamma_w$ (9810 N/m$^3$)

Eqn. 5.1

Hydraulic fill porosity, $n = 1 - \frac{\rho_d}{G_s}$ Eqn. 5.2

Hydraulic fill void ratio, $e = \frac{n}{1-n}$ Eqn. 5.3

Saturated water content, $w_{sat} = \frac{e}{G_s}$ Eqn. 5.4

When the stope has fully drained, with all the free water removed, the water content is termed residual water content ($w_{res}$), which is less than the saturation water content ($w_{sat}$). The residual water is not removed in engineering time and remains within the stope, held in the voids.

It is the drainable free water that is of concern, and one of the objectives of the models is to see how quickly it can be removed. In a mine, this will determine the time requirements for adjacent mining works to occur.

While the saturation water content represents the entire void space, residual water content represents a fraction of the voids that are active in conducting the water in the process of draining. This fraction, defined as effective porosity, is given by:

$$n_{eff} = n - \frac{w_{res}.G_s}{1+e} \qquad \text{Eqn. 5.5}$$

### 5.2.3 Modelling Approach

Modelling undertaken for this exercise (as is generally the case with numerical modelling in geotechnical work) is not intended as an exact replication of the design problem, and should not be used to quantify numerical values of pore pressures or discharge rates within a stope. It is a simplification of reality, used as an intellectual means by which insight into the behaviours of the system may be gained. As testing procedures develop and the quality of input data improves so too will the accuracy of the modelling results – within the limitations of variation that occurs naturally within most geotechnical situations. The modelling approach utilized in the *FLAC* code presented in this chapter, enables the variability to be easily investigated for system sensitivity by simply varying the input parameters outlined in the initial stages of the code. The 2-dimensional program coded in *FLAC* was used as a preliminary step such that the program may be verified, and the overall problem investigated to determine the key objectives for which the 3-dimensional extension of the program (described in Chapter 6) would be used to investigate.

#### Program Design Methodology

The 2-dimensional program coded to simulate the filling and drainage of the underground hydraulic fill stope was done as a flow-only, steady state analysis in *FLAC*. The hydraulic fill does not contain any clay fraction and therefore a coupled analysis is not warranted. In the absence of clay fraction and with high permeability values, the consolidation process within the stope would almost be instantaneous. At the end of each hour of the filling cycle, the fill and water heights, boundary and initial conditions were computed based on the previous conditions, which simply involved mass balance and phase relations, and applied to the grid. The steady-state condition was solved to identify pore pressure distribution and flow values within the stope at each hour regardless of whether the stope was being filled or a rest period in which no additional fill entered the stope. This process was cycled through until the stope was completely filled. A separate subroutine was written to calculate the height of the free water surface (phreatic surface) every hour after the stope had been completely filled, until the stope had been completely emptied of free water leaving only the residual water in the stope.

*Grid Generation*

Initially, a grid of 25 zones in the x-direction and 150 zones in the y-direction (26 nodes in the x-direction and 151 nodes in the y-direction) was established, with nodes spaced at one meter for both directions. A sensitivity study, using different meshes showed that 1 m x 1 m grid struck the right balance between solution time and accuracy.

*Boundary and Initial Conditions*

Boundary conditions for a numerical model consist of quantities and locations of field variables, which are set or applied to the boundary nodes or faces of the model grid. For fluid flow models, the boundaries are impermeable by default, and the gridpoints (or nodes) are free to vary in pore pressure and saturation according to the inflow-outflow balance between neighbouring zones. Alternatively, a variable condition, or an explicit value may be set to the nodes.

For this particular modelling exercise, the nodes that form the boundary at the drain or discharge point of the stope, at the bottom right corner, were fixed with a pore pressure of zero and a fully saturated condition. As described in Chapter 4, the barricade bricks have a permeability often in excess of three orders of magnitude greater than the contained hydraulic fill. For this reason, the pore pressure at the interface between the fill and the barricade is assumed to be zero as was the assumption in previous stope drainage models by Isaacs and Carter (1983) and Traves (1988). Alternatively, it can be assumed that the pores within the barricade are fully saturated and therefore the pore pressure at the fill-barricade interface is linear varying from zero at the top to $\gamma_w D$, at the base, where $D$ is the drain height, (Sivakugan et al., 2005). Fig. 5.2 illustrates the two assumptions.

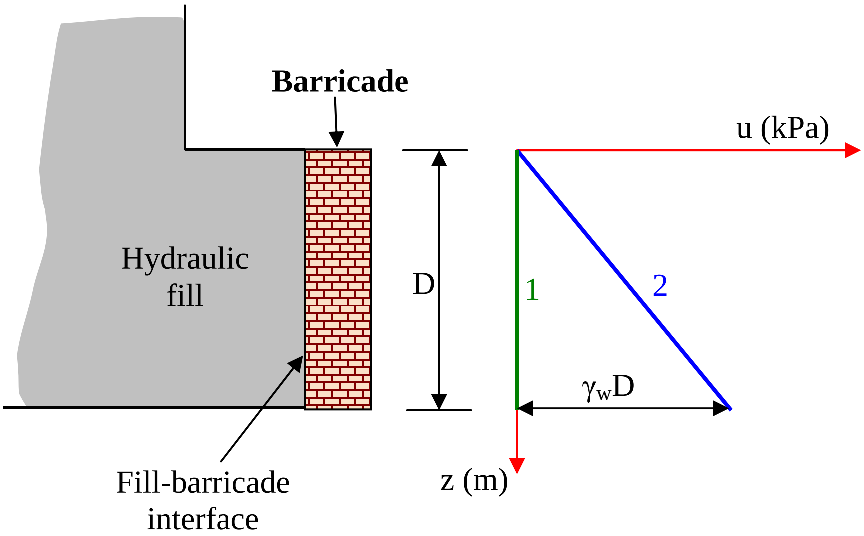


**FIG. 5.2 - Two pore water pressure distribution assumptions for fill-barricade interface**

Results published by Sivakugan et al., (2005) illustrate negligible difference in stope drainage and the maximum pore pressure between the two alternative barricade pore pressure boundary conditions. This is due to negligible drain height compared to the height and width of the stope. Therefore, for simplicity and consistency with the Isaacs and Carter model, alternative 1 was adopted for all modelling.

There were two cases considered for the boundary conditions applied to the top of the fill height. Case 1, was for the situation in which the water height was above the height of the fill, i.e., there was decant water (Fig. 5.3 a) and case 2, was for when the water height was below the height of the fill (Fig. 5.3 b).

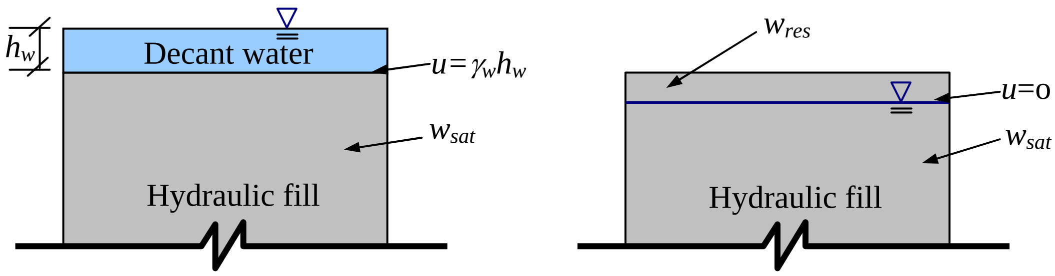


**(a) Case 1** **(b) Case 2**

**FIG. 5.3 - Boundary condition cases for surface of hydraulic fill**

For case 1, the nodes at the top of the hydraulic fill were fixed as saturated, and fixed to a pore pressure value equal to the overlying hydraulic head applied by the decant water. Case 2 had the nodes at the height of the water fixed as saturated, and the pore pressure at these nodes was fixed to zero. All the 2-dimensional *FLAC* simulations were undertaken as flow-only analysis and therefore no mechanical boundary conditions were required.

*Initial Conditions*

Prior to excavation, construction or the application of loading in any geotechnical or mining project, there is an in situ state of stresses that needs to be considered and applied to the *FLAC* grid to replicate this initial state. Initial conditions that pertain to mechanical calculation were not required, and only distributions of pore pressure, porosity, saturation, fluid modulus and tension limit were considered for the flow-only analysis. The pore pressure was initialized to the hydrostatic head values, which varied linearly from $\gamma_w H_w$ (where $H_w$, is the height of the water in the stope and $\gamma_w$ is the unit weight of water) at the base of the stope. Porosity, fluid modulus and tension limit were initialized uniformly across the model as the input value prescribed. All hydraulic fill under the height of the water was set at fully saturated.

*Sequential Filling Algorithm*

To simulate the sequential filling and drainage of an underground hydraulic fill stope, steady-state flow-only analysis solutions were carried out at hourly intervals and the results were used to determine input conditions for the subsequent hour.

The fill height at each stage of solution was based on the quantity of fill that had been placed into the stope at that given time. The filling schedule was a 12 hour filling period followed by a 12 hour rest period, cycled continuously until the fill height reached the height of the stope. During the filling hours, fill slurry entered the stope, and the fill height gradually increased by a height equal to the volume of dry hydraulic fill which would enter the stope for the input filling rate divided by the cross-sectional area of the stope. The volume of void within the fill matrix was calculated. The volume of water in the stope was determined as the total volume of water that had entered the stope minus the total volume that had exited the stope, and provided the volume of void within the fill matrix was larger than the volume of the water in the stope then the water level fell below the height of the fill (Fig. 5.3 b). If the volume of water remaining in the stope was larger than the void volume, then there was decant water above the fill (Fig. 5.3 a). With due consideration to these cases and the porosity of the fill, the water height was calculated for each hour and the system was solved for steady state conditions. The quantity of discharge over this hour was recorded and added to the total water discharged from the stope for the calculation of water height for the next hour.

Once the tailings height reached the height of the stope, then the model solved as a continuously draining stope under a steadily falling water with the same hourly steady-state calculations used for the resting periods in the filling stage of the simulation.

*Material properties and model selection*

The flow-only simulation was undertaken to determine the flow and pore pressure distribution within the system, independent of any mechanical effects. Initially, the grid was configured to enable the fluid analysis mode in *FLAC*. By default *FLAC* performs all flow analysis as fully coupled, therefore the mechanical calculation scheme was turned off. In *FLAC*, despite the solution being flow-only, dummy mechanical properties have to be assigned to prevent error messages. The mechanical properties assigned have no impact on the flow-only solution.

Fluid flow properties including permeability, porosity and fluid bulk modulus were assigned to zones for which the water height extended and pore pressure analysis was required. All zones above the height of the water were assigned the null material model, which defaults the zones to disengage fluid-flow. Correct values of permeability and porosity were assigned, but the fluid-bulk modulus was reduced to make the solution process quicker. This has no effect on the solution in the case of steady state flow-only analysis. The fill material was assumed to follow Mohr-Coulomb constitutive model, with specific parameters for bulk and shear moduli, density, cohesion, friction angle and tensile strength. Again, these have no effect on the solution in the case of a flow-only analysis.

Implicit Versus Explicit Solution

By default, *FLAC* utilizes an explicit solution scheme which is based on a relatively small timestep. When large changes in conditions are occurring, this is usually appropriate but because an implicit solution solves the whole system as a matrix which is iteratively solved, this may prove faster for slower changing conditions. An implicit solution scheme is available in *FLAC* for a fully saturated flow system. This was not covered in the scope of this thesis, and all solutions were solved explicitly.

### 5.2.4 Numerical Model Verification

L.T. Isaacs and J.P. Carter developed a computer program in FORTRAN as a research contract with Mount Isa Mines, for the analysis of the drainage of 2-dimensional stopes during hydraulic fill operation, in 1983. The formulation was implicit, and based on finite difference methods. The equations of pseudo steady state flow were solved and time marching proceeded with updating of time-dependent quantities at the end of each step. The results were verified against several case studies, and the program has since been used throughout Australia (Cowling, 2002). The logic behind the program written in *FLAC* for this research is essentially the same as that used by Isaacs and Carter.

Initially, to perform a preliminary check of program validity, a mass balance analysis was performed on both the Isaacs and Carter and the *FLAC* programs. The level of convergence of a system in *FLAC* may be examined by monitoring the unbalanced force ratio (or unbalanced force) between adjacent nodes throughout the model. This value may be prescribed using the 'sratio' command, such that the solution iterated to an unbalanced force ratio below this value. For a *FLAC* convergence criteria of sratio of 0.001, the average error in water mass balance was approximately 0.03% which compared very well to the Isaacs and Carter average of 0.07%. For the convergence criteria of sratio = 0.01, the error in the *FLAC* program is increased to approximately 3% which is still acceptable for this research considering how insignificant this small error in mass balance is to the overall system being analysed. Regardless of this, simulations were solved to the convergence criteria of sratio = 0.001, where time permitted.

The *FLAC* results for fill and water levels, and discharge rates throughout the filling of the verification simulation were compared to the results obtained from Isaacs and Carter for the identical simulation. As illustrated in Fig. 5.4, the water and fill heights compare very well between the two models.

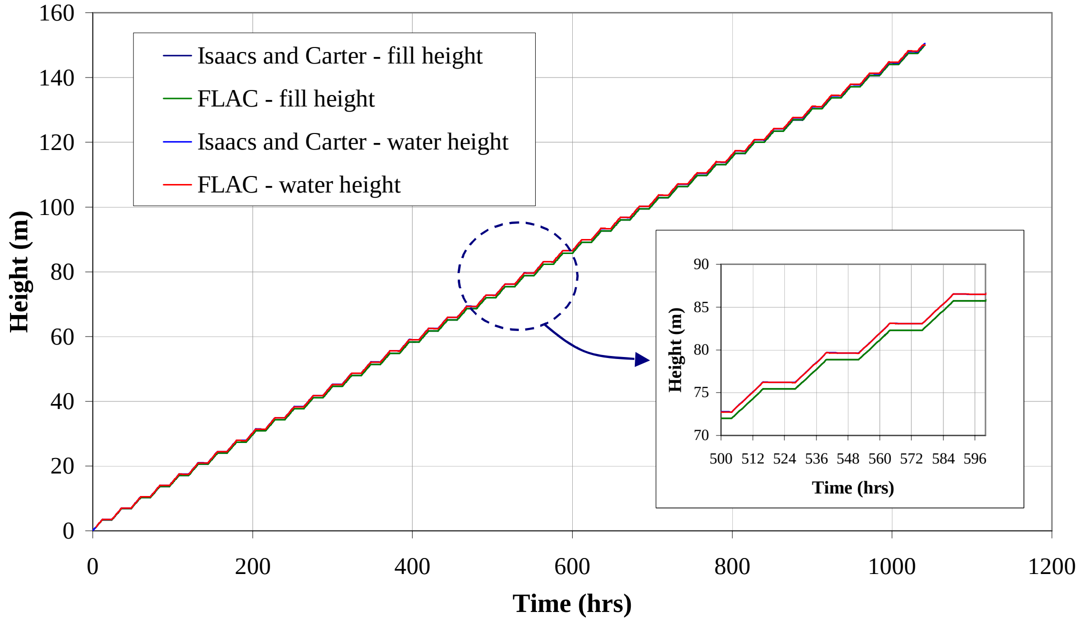


**FIG. 5.4 - Fill and water height comparison between Isaacs and Carter and *FLAC* for the verification simulation**

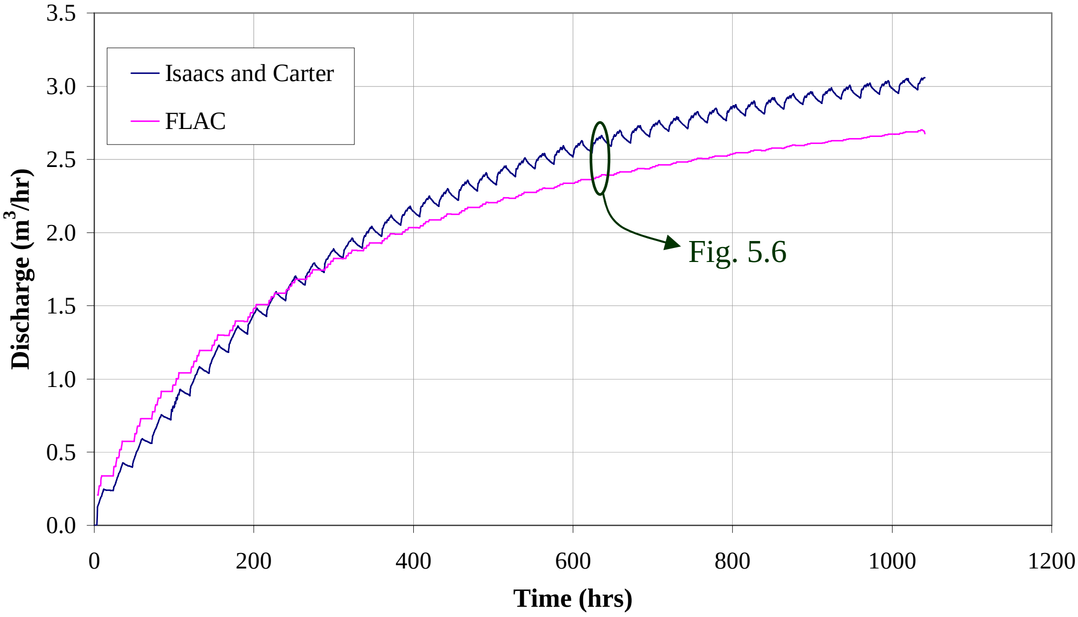


**FIG. 5.5 - Discharge rate comparison between Isaacs and Carter and *FLAC* for the verification simulation**

These results compare very well for this verification problem. This particular simulation had decant water throughout the entire filling of the stope (Case 1 in Fig. 5.3). Further verification was undertaken to ensure the two programs compared well for simulations in which the water level fell below the fill height (Case 2 in Fig 5.3), and these results are included in Section 5.4.8 which investigates the effects of filling schedules. The fill and water heights compare so closely between the two programs that the Isaacs and Carter results are basically directly under the FLAC results in Fig. 5.4.

To amplify the difference in results, the discharge rates throughout filling were observed. The discharge comparisons are plotted in Fig. 5.5. There is very good agreement in the early days of the filling schedule. At the end, however, there is a difference of up to about 15%.

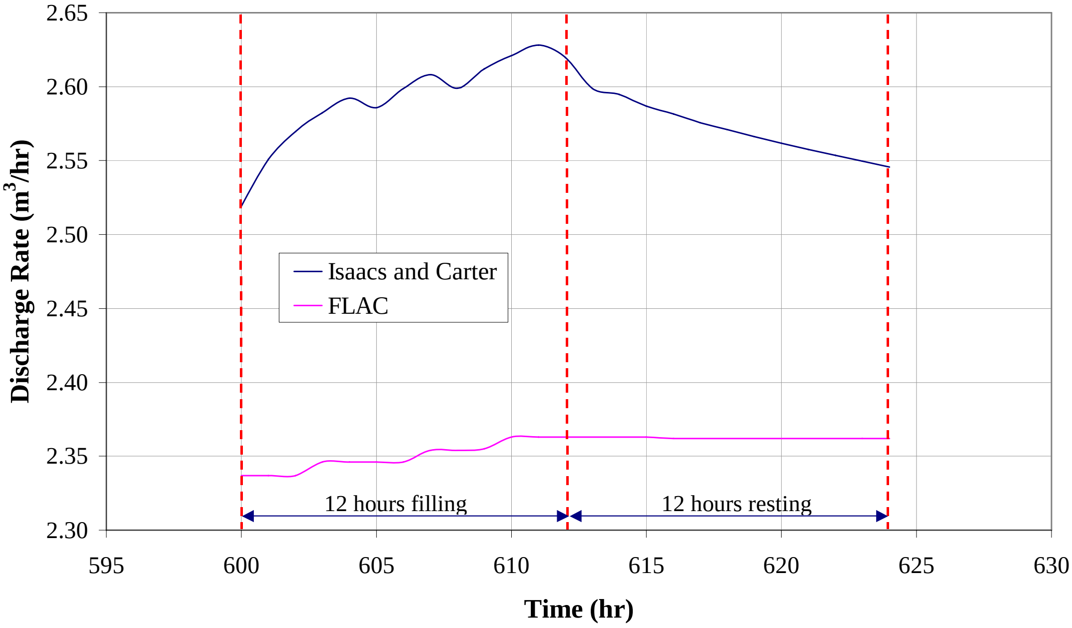


**FIG. 5.6 - Discharge results for Isaacs and Carter and *FLAC* for 24 hour period between hours 601 and 624**

It can be seen in Fig. 5.5 and 5.6 that there is an obvious difference in discharge behaviour over a single fill/rest 24 hour period between the two programs. Isaacs and Carter has a more pronounced ‘tooth-like’ behaviour over a single 24 hour period as shown in Fig. 5.6, which plots the discharge rates for both programs between hours 600 and 624. For this period, the water height remains above the fill height, and when the quantity of discharge is summed over the 12 hours filling and 12 hours draining the values shown in Table 5.2 are obtained. When these values are compared to the resultant changes in decant water height both programs give reasonable results (Table 5.2).

**TABLE 5.2 - The Isaacs and Carter and *FLAC* model output summaries between hours 600 and 624**

| | Time (hr) | Fill Height (m) | Water Height (m) | Decant height (m) | Change in Decant Height (m) | Discharge Rate ($m^3$/hr) | Sum of Discharge over 12 hours ($m^3$) | Change in decant as a result of discharge (m) |
|---|---|---|---|---|---|---|---|---|
| **Isaacs and Carter** | 600 | 85.72 | 86.47 | 0.75 | --- | 2.52 | --- | --- |
| | 612 | 89.14 | 89.95 | 0.81 | 0.06 | 2.62 | 33.69 | -0.05 |
| | 624 | 89.14 | 89.90 | 0.76 | -0.05 | 2.55 | 30.55 | -0.05 |
| ***FLAC*** | 600 | 85.71 | 86.48 | 0.77 | --- | 2.34 | --- | -- |
| | 612 | 89.14 | 89.96 | 0.82 | 0.05 | 2.36 | 33.46 | -0.05 |
| | 624 | 89.14 | 89.91 | 0.77 | -0.05 | 2.36 | 28.35 | -0.05 |

As is summarised in Table 5.2, the discharge over each 12 hour period (fill and then rest) results in a drop in decant height of approximately 5 cm. The Isaacs and Carter program illustrates that this reduction in decant water would produce a reduction in discharge rate of 0.07 $m^3$/hr, compared to the negligible change shown by the *FLAC* program (Fig. 5.6). Although this problem is 2-dimensional, a simple 1-dimensional analysis based on Darcy's law may be applied to the change in conditions of the 12 hour rest period (where the level of fill does not change) to provide a preliminary check of the discharge results. The 1-dimensional analysis will provide a much higher discharge rate than a 2-dimensional result, such as those calculated using the *FLAC* and Isaacs and Carter programs. A diagrammatic representation of the one-dimensional flow analysis is shown in Fig. 5.7.

Over the 12-hour rest period, the decant water height drops 5 cm for both the Isaacs and Carter and the *FLAC* simulations. Because the fill height does not change over this period of time, change in discharge rate may be presented as shown in Eqn. 5.6.

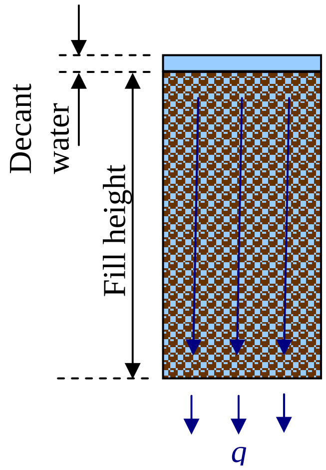


**FIG. 5.7 - One-dimensional approximation for flow analysis**

$$\Delta q = \frac{kA}{L}\left(\Delta \mathrm{h}_L\right) \qquad \text{Eqn. 5.6}$$

Here $\Delta q$ is the change in 1-dimensional discharge rate, $k$ is the permeability, $A$ is the cross-sectional area of the stope, $L$ is the fill height, and $\Delta h_L$ is the change in head loss and is equal to the change in decant height for the rest period. For the verification problem, where the permeability equals 5.4 mm/hr, the cross-sectional area is equal to 625 $m^2$ (25 m x 25 m), the fill height 89.14 m and the change in decant is -5 cm for both Isaacs and Carter and *FLAC* simulations, the change in 1-dimensional discharge rate is calculated as -0.0019 $m^3$/hr. The summary of results for this period of time provided in Table 5.2, shows that Isaacs and Carter, which is a 2-dimensional analysis and therefore should have a substantially smaller change in discharge rate, indicates the change to be in the order of -0.07 $m^3$/hr. *FLAC* shows no change in discharge rate over this rest period of time. This places significant doubt over the accuracy of the tooth-like pattern displayed in all the Isaacs and Carter discharge over time plots. By studying the flow net of the system at 600 hours (Fig. 5.8) this observation may be reiterated.

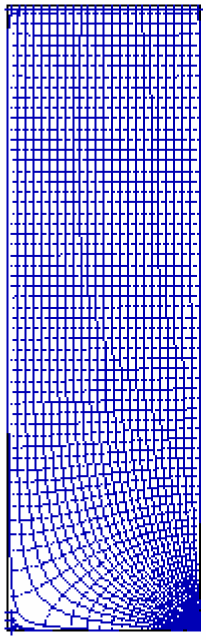

**FIG. 5.8 -Flow net at 600 hours**

The discharge at a specific time can be written as:

$$q = kh_L \frac{N_f}{N_d} \qquad \text{Eqn. 5.7}$$

where $N_f$ and $N_d$ are the number of flow channels and equipotential drops in the flow net. The flow net becomes coarser at the upper regions of the stope. Therefore, the 5 cm drop in $h_L$ can have insignificant influence on the flow net and the $N_f/N_d$ ratio. Therefore, from Eqn. 5.7:

$$\Delta q = k \frac{N_f}{N_d} \Delta h_L$$

The 5 cm drop in the original $h_L$ of 8600 cm can only change the discharge rate by $\frac{5}{8647} \times 100\% = 0.06\%$. In the Isaacs and Carter program the discharge rate is changed by 2.75%. In other words, the smoother discharge rate pattern seen for *FLAC* in Figs. 5.5 and 5.6 is more realistic.

Despite this discrepancy, as described in the introduction to this chapter, numerical modelling of this kind is ultimately used to obtain an appreciation of model behaviours and the inevitable intrinsic errors that result from material property and model geometry assumptions and simplifications, would outweigh this problem with Isaacs and Carter that has been magnified by observing the discharge over a single 24 hour period.

## 5.3 Sensitivity Analysis

A range of geotechnical parameters were used as input and a sensitivity analysis was undertaken to determine a qualitative appreciation for the behaviour of the system to this variation.

### 5.3.1 Sensitivity of Input Parameters

Laboratory testing on an extensive range of Australian hydraulic fill samples has shown that hydraulic fill slurry, with 65-75% solid content, generally settles under self-weight to a dry density (g/cm$^3$) of a little over half the specific gravity value of the fill (Cowling, 1998). This was demonstrated experimentally in section 3.5 of Chapter 3. For this reason, the dry density (g/cm$^3$) is fixed to half the specific gravity value and a sensitivity analysis was not done for this parameter.

Dry density can be written as:

$$\rho_d = \frac{G_s \rho_w}{1+e} \qquad \text{Eqn. 5.8}$$

Therefore, assuming dry density (g/cm$^3$) of $0.5G_s$ also implies that the void ratio is 1.0 and porosity is 50%. Thus, in all following simulations a hydraulic fill skeleton where 50% of the total volume is occupied by voids was assumed, irrespective of the other parameters.

Fluid flow-only analysis in *FLAC* uses the fluid input parameters of fluid bulk modulus and fluid density, permeability and porosity. Of these, it is assumed the fluid modulus and density do not vary, neglecting temperature effects. The fluid density is fixed to the value of 1000 kg/m$^3$ (the density of water). Although at room temperature, the fluid modulus is equal to 2 x $10^9$ Pa, this value is set to a very low number (e.g., 1 x $10^5$ Pa) because the simulation is steady state and not transient, therefore to speed convergence this value may be reduced consequently speeding diffusion calculation without affecting the output. This is clearly explained in the *FLAC* Fluid-Mechanical Interaction Manual. Therefore, parametric studies would only be required on the permeability, specific gravity, pumped slurry solids content and fill residual water content. A brief analysis was undertaken on the aforementioned parameters, to determine the sensitivity of these parameters in two-dimensions. This will be used to prioritise the sensitivity study and analysis performed by the 3-dimensional program described in Chapter 6.

Permeability

Constant head and falling head permeability tests carried out on various Australian hydraulic fill samples (see Chapter 3) generally give permeability values within the range 2 mm/hr to 35 mm/hr. The discharge rates, fill/water heights and maximum pore pressure results for a 25 m x 150 m stope with single drain flush with the stope wall, continuously filled at 250 t/hr, solved with permeability values of 2 mm/hr[14], 5.4 mm/hr 15 mm/hr and 35 mm/hr, are summarised in Figs 5.9 through 5.11. Other parameters are the same as in the verification exercise. The values of 2 mm/hr, 15 mm/hr and 35 mm/hr were selected to see the behaviour of the model across the range of permeability values obtained through laboratory testing, and 5.4 mm/hr was assumed in the verification exercise discussed before.

The discharge over time plot (Fig. 5.9) demonstrates a very pronounced difference in the water discharge rate from the stope for the typical range of fill permeability values obtained for Australian hydraulic fill samples. For this example, the discharge rate is almost 16 times greater for a fill with a permeability value of 35 mm/hr, compared to fill with a permeability of 2 mm/hr. It can be expected that for the same water height, with no decant, discharge rate is simply proportional to the permeability.

[14] 1mm/hr = 2.78 x $10^{-5}$ cm/s

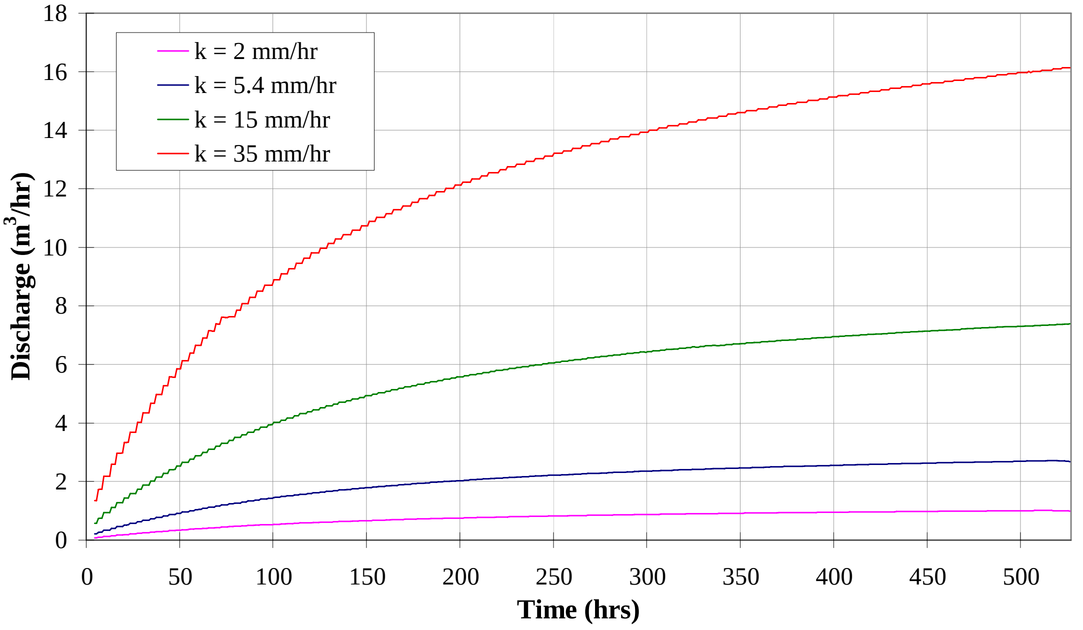


**FIG. 5.9 - Rate of discharge variation with permeability during filling**

One very important observation to note is the relative influence this significant difference has on the overall water heights within the stope, and thus the maximum pore pressure (Figs. 5.10 and 5.11 respectively). The total quantity of water discharged from the stope over the entire filling of the stope represents only a very small proportion of the water placed. In this example, the total discharge calculated from the highest permeability ($k$ = 35 mm/hr) simulation is merely 12.5% of the total water placed, and the discharge from the lowest permeability ($k$ = 2mm/hr) simulation accounts for less than 1% of the water placed into the stope over the filling duration. Nevertheless, the total drainable water that is drained in engineering time[15] is independent of the permeability; it depends only on the initial water content of the slurry, the porosity of the fill and residual water content.

In situ filling and drainage records from R454 stope at Mount Isa Mines Ltd. (Traves, 1988) substantiate this observation (Table A3.1 and Figs. A3.1 and A3.2). Stope R454 was filled between 31st August 1983 and 13th February 1984. In plan, the hydraulic fill stope is typically close to 45 m x 36 m, with a height of 75 m. There are three drains, located 0, 20 and 50 meters vertically from the base of the stope (stope plans and sections are included in the appendix). The sum of the water discharged from all three

[15] Engineering time is the measurable time for which the behaviour of a stope may have an influence on the operation of the mine.

drains during the entire filling period is less than 23% of the total water accounted for. This stope is discussed further in Section 5.4.3.2.

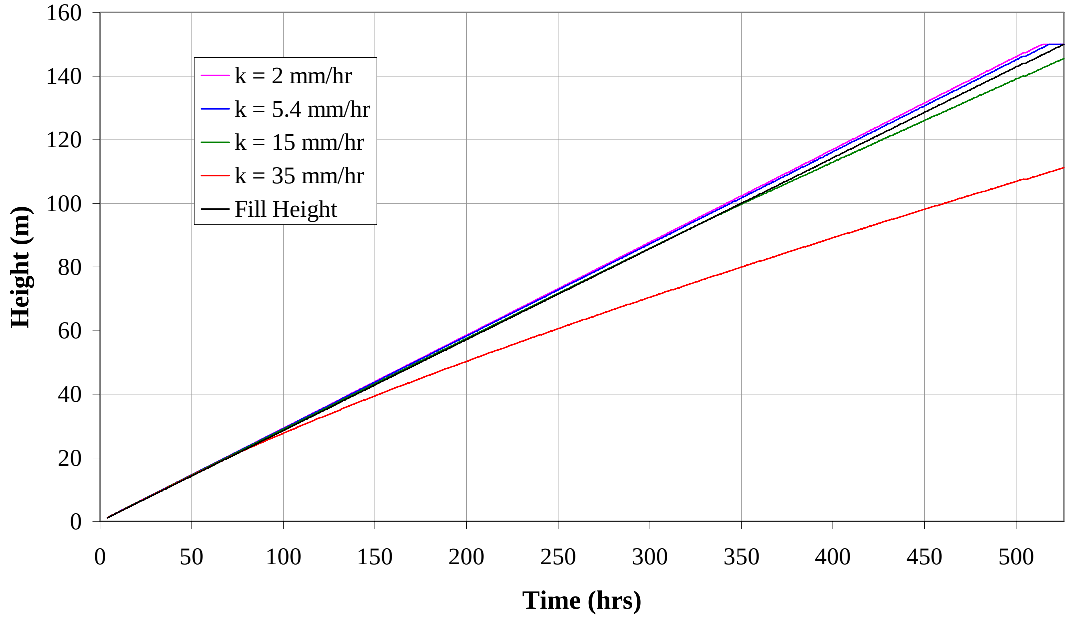


**FIG. 5.10 – Water height variation with permeability during filling**

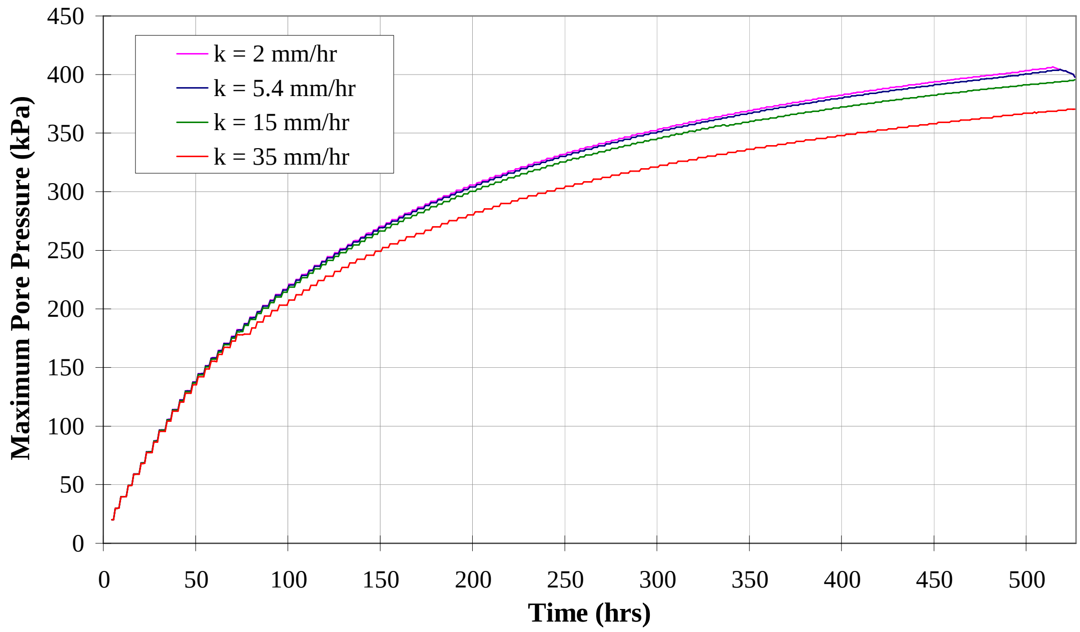


**FIG. 5.11 – Maximum pore pressure variation with permeability during filling**

It is fair to say that typically, the discharge water represents only a small proportion of the water placed into the stope, and thus the relative influence the drainage rate has on the water height may be very small, particularly if there is decant water. For $k$ = 2 mm/hr and $k$ = 5.4 mm/hr simulations, when there is decant, there is no significant difference in water height and maximum pore pressure, as seen in Figs. 5.10 and 5.11. For this reason, the pore pressure distribution within the stope does not vary significantly with the discharge rate (Figs. 5.9 and 5.11), especially when there is decant water.

Discharge rates however, do play an important roll in stope filling schedule. To optimise stope excavation and filling order, it is of benefit to know time requirements for the free water to be completely drained from the stope, so that adjacent works may commence. Discharge rate for a given geometry and fill and water height is a function of the hydraulic fill permeability and specific gravity of the fill grains[16]. This will be discussed further in subsequent sections. For modelling purposes, barricades are free draining and do not affect the discharge rate from a stope (Chapter 4). Therefore, although the permeability of the hydraulic fill does not dramatically affect the water heights or pore pressures achieved while filling a stope, it is vital for determining drainage times used in mine filling schedule.

Specific Gravity

Hydraulic fill slurry is generally pumped at specific solid (or water) contents. Therefore the quantity of water entering the stope is significantly influenced by specific gravity of the fill material. This is clearly shown when observing the difference in overall volume of water entering a 25 m x 25 m x 100 m stope for three different cases in which fills of different specific gravity values all pumped at 70% solids by weight. Table 5.3 summarizes the results, and the last column gives an indication of the quantity of free water that would be required to be drained if the residual water content was 25%.

As is shown in Table 5.3, the volume of water that enters the stope as well as the free water that has to drain increase with the specific gravity of the fill material for the same slurry density. For this example, there is a difference of about 8929 $m^3$ of water that needs to be drained from the stope across the range of specific gravity values in Table 5.3. This is sufficient water to significantly vary the water heights during any

[16] For placed hydraulic fill, dry density is approximately equal to half the specific gravity (Cowling, 1998) as described in Chapter 3, and page 145.

particular filling schedule and therefore a study of sensitivity to specific gravity must be performed to obtain a thorough understanding of hydraulic fill stope drainage behaviour. The drainage times will also be affected considerably. This will be covered later in the 3-dimensional sensitivity study described in Chapter 6.

**TABLE 5.3 - Water volume variation with fill specific gravity**

| **Case** | **Specific gravity, $G_s$** | **Stope volume ($m^3$)** | **Mass of solids (t)** | **Volume of water ($m^3$)** | **Volume of free water to drain ($m^3$) for $w_{res}$ of 25%** |
|---|---|---|---|---|---|
| 1 | 2.8* | 62500 | 875000 | 37500 | 15625 |
| 2 | 3.5* | 62500 | 109375 | 46875 | 19532 |
| 3 | 4.4* | 62500 | 137500 | 58929 | 24554 |

* Represent typical values from three large Australian mines backfilled by hydraulic fills

Residual Water content

The fill residual water content only has an effect on the simulation results when the water height is below the height of the fill material. When decant water is present, since the entire fill is saturated, residual water content will have no influence on the results. For this reason, the effect of residual water content is observed when the stope has been completely filled and the water and fill heights are at the full height of the stope. From this time, the water level drops and remains below the height of the fill, which stays constant at the height of the stope. Residual water content analysis is essential in determining the length of time required for a stope to completely drain such that adjacent works can be commenced. Free water drainage times for various residual water contents are investigated for the 3-dimensional stope, in Chapter 6. The lower the residual water content, the greater is the quantity of drainable water and thus greater is the time to fully drain the stope.

### 5.3.2 Mesh Sensitivity

The filling component of the program required even spacing of the nodes in the vertical (height) direction of the model for simplicity in computation. This allowed for ease of identification of node location for boundary and initial condition specification during the filling and drainage of the stope, where the phreatic and fill surfaces varied with time.

Three steady state, 2-dimensional scenarios were analysed to determine sensitivity of mesh size to the drainage and pore pressure measurements of the stope relative to the solution requirements.

Scenario 1

Scenario 1 utilized a uniformly spaced grid in both the x and y directions for a 20 m wide stope which was 80 m tall and had a 1 m x 1 m drain located in the bottom right hand corner of the model (Fig. 5.12 a). The node spacing was the same in both the x and y directions. Fig. 5.12 b shows the 1 m grid spacing consistent throughout the stope. All runs were solved to an sratio[17] of 0.001 on a Pentium IV 2.8 GHz computer. Three separate simulations were undertaken, and the mesh specifications and results are summarized in Table 5.4.

**TABLE 5.4 - Case 1 summary: Mesh size sensitivity**

| Details | Arrangement #1 | Arrangement #2 | Arrangement #3 |
|---|---|---|---|
| Mesh size | 1 m x 1 m | 0.5 m x 0.5 m | 0.333 m x 0.333 m |
| Flow Rate (*Q*) | 2.444 x$10^{-5}$ $m^2/s$ | 2.404 x$10^{-5}$ $m^2/s$ | 2.394 x$10^{-5}$ $m^2/s$ |
| Max Pore Pressure ($u_{max}$) | 358.8 kPa | 365.7 kPa | 368 kPa |

There is only about 2.1% difference in flow rate measurement, and 2.5% disparity in maximum pore pressure measurement. The influence of these very minor differences in discharge rates and pore pressure values becomes almost insignificant (refer to section 5.3.1.1) when considering the behaviour of the entire system during filling and drainage and therefore the smaller grid spacing cannot be justified for this research when bearing in mind the increased solution times required for the finer mesh. This is discussed further in Section 5.3.4, where it is shown that the arrangement 3 takes about 125 times longer to solve compared to arrangement 1.

[17] Sratio represents the unbalanced flow force ratio between two adjacent nodes, which is one of three default convergence criteria in *FLAC*.

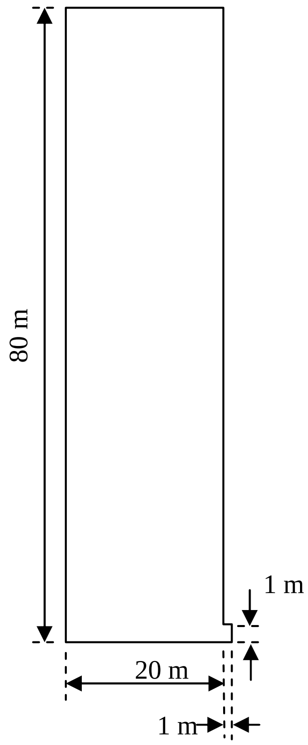


**(a) – Model Geometry**

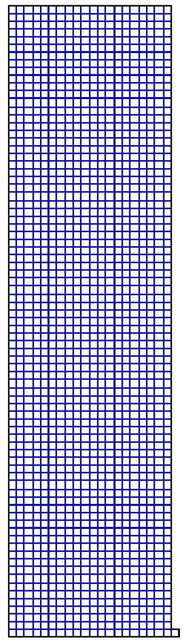

**(b) Mesh arrangement #1**

**FIG. 5.12 – Scenario 1 model to determine sensitivity of stope drainage to mesh size**

<u>Scenario 2</u>

The second scenario further analysed the mesh sizing efficiency, for a different stope arrangement. Four simulations were undertaken on a 50 m high, 20 m wide 2-dimensional stope with three 1 m x 1 m drains spaced 20 m apart. The geometry is shown in Fig. 5.12.

The first simulation had a 1 m square grid across the entire mode. The second had a uniform mesh of 0.5 m by 0.5 m, the third also uniform with a mesh spacing of 0.333 m x 0.333 m. The final simulation contained a finer mesh in the drains where the discharge measurements were recorded and a coarser mesh in the stope. This arrangement, had a 1 m x 1 m grid in the stope, and a 0.25 m x 0.25 m grid in the three drains. These arrangements, discharge values for each drain and maximum pore pressure measurements are summarized in Table 5.5.

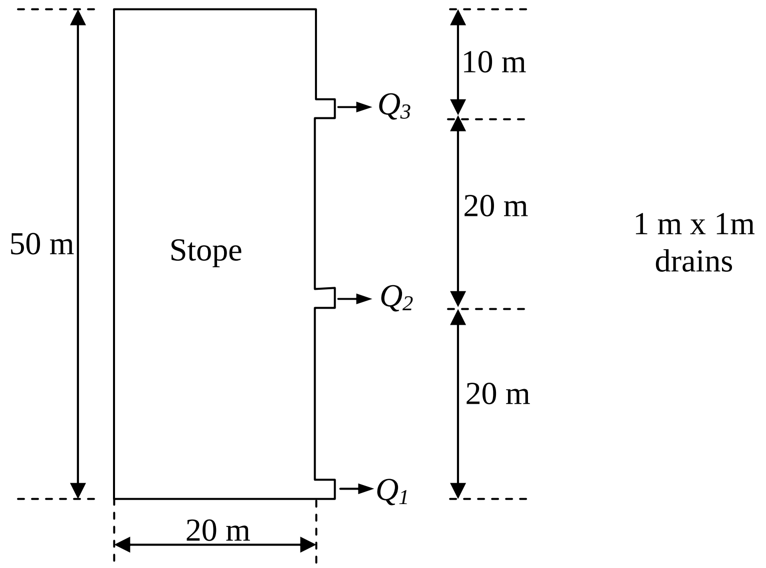


**FIG. 5.13 – Scenario 2: multiple drain mesh analysis geometry**

**TABLE 5.5 - Scenario 2 summary: Mesh arrangement sensitivity**

| Run | Mesh description | $Q_1$ (m$^2$/s) | $Q_2$ (m$^2$/s) | $Q_3$ (m$^2$/s) | $u_{max}$ kPa |
|---|---|---|---|---|---|
| 1 | 1 m square grid across entire model | 1.659 x10$^{-5}$ | 0.961 x10$^{-5}$ | 0.235 x10$^{-5}$ | 249.4 |
| 2 | 0.5 m square grid across entire model | 1.629 x10$^{-5}$ | 0.945 x10$^{-5}$ | 0.233 x10$^{-5}$ | 253.6 |
| 3 | 0.333 m square grid across entire model | 1.615 x10$^{-5}$ | 0.933 x10$^{-5}$ | 0.231 x10$^{-5}$ | 254.1 |
| 4 | 1 m square grid across stope, and 0.25 m square grid across drains | 1.649 x10$^{-5}$ | 0.961 x10$^{-5}$ | 0.234 x10$^{-5}$ | 249.6 |

As was demonstrated in Scenario 1, the variation in mesh sizing does not change the results significantly. Therefore it was assumed reasonable to sacrifice the slight accuracy for the computation time saved. The filling schedule simulated utilized a uniform grid so that boundary condition requirements could be met. It is demonstrated here that the refinement of mesh to tailor a grading between a finer grid in regions where monitoring or measurement were taken, and a coarser mesh in areas of the model further from these points would have very little impact on the results. There is hardly any difference between the discharge and pore pressure values observed for runs 1 and 4, where the main difference is a finer mesh within the drains for run 4.

Scenario 3

A further mesh sensitivity exercise was undertaken in two-dimensions to investigate the sensitivity of results to varying mesh sizing throughout a stope, and the implication this variation has on the solution time. A simple single drain stope arrangement was used, and three styles of mesh discretization were investigated. The three mesh styles included firstly a uniform mesh throughout the stope, secondly a finer mesh was used in the drain only, and then finally, a finer mesh was used in the base region of the stope reaching as high as the top of the drain (Fig. 5.14).

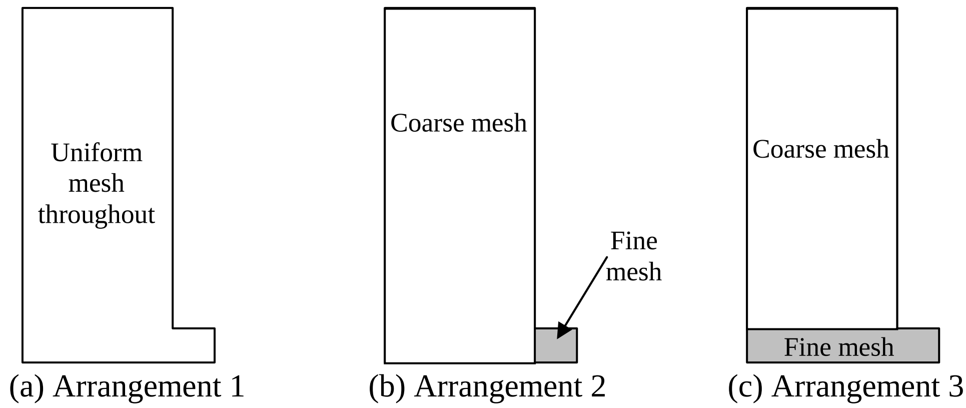


**FIG. 5.14 – Scenario 3: Mesh discretization arrangements**

Table 5.6 summarises the simulations undertaken for this investigation. The yellow rows are based on the uniform mesh (Fig. 5.14 a), the green rows for arrangement 2 (Fig. 5.14 b) and the orange rows for the third arrangement (Fig. 5.14 c). All simulations were solved on a Pentium IV 2.8 GHz PC, with 1 GB Ram, and all solved for sratio = $10^{-3}$, unless stopped early. The model was based on a 60 m high 2-dimensional stope of base width 20 m, and single 1 m high drain that was of 1 m depth.

**TABLE 5.6 – Relative runtime and output by different mesh arrangements**

| Mesh No. | Time step (s) | No. of steps | Flow time (s) | Actual running time | Flow rate (l/min per m) | max pp (kPa) | Hydgrad @ top | Mesh |
|---|---|---|---|---|---|---|---|---|
| 1 | 981 | 30170 | $2.96 \times 10^7$ | 13 s | 6.513 | 316 | 0.54 | 1m x 1m throughout |
| 2 | 245 | 131280 | $3.22 \times 10^7$ | 46 s | 6.501 | 316.5 | 0.54 | 1m x 1m in stope & 0.5m x 0.5m in drain |
| 3 | 61 | 418000 | $2.56 \times 10^7$ | 2 min 29 s | 6.485 | 316.3 | 0.54 | 1m x 1m in stope & 0.25m x 0.25m in drain |
| 4 | 245 | 127470 | $3.13 \times 10^7$ | 1min 2 s | 6.461 | 318.1 | 0.54 | 0.5m x 0.5m bottom 1m & 1m x 1m above |
| 5 | 61 | 411710 | $2.52 \times 10^7$ | 12 min 58 s | 6.418 | 319.1 | 0.54 | 0.25m x 0.25m bottom 1m & 1m x 1m above |
| 6 | 245 | 127450 | $3.12 \times 10^7$ | 7 min 33 s | 6.393 | 321.1 | 0.53 | 0.5m x 0.5m throughout |
| 7 | 61 | 420446 | $2.57 \times 10^7$ | 25 min 40 s | 6.374 | 321.1 | 0.53 | 0.5m x 0.5m in stope & 0.25m x 0.25m in drain |
| 8 | 109 | 282997 | $3.08 \times 10^7$ | 39 min 50 s | 6.357 | 322.6 | 0.53 | 0.33m x 0.33m throughout |
| 9 | 61 | 480000 | $2.94 \times 10^7$ | 2 hrs 1 min 10 s | 6.337 | 323.1 | 0.53 | 0.25m x 0.25m throughout |

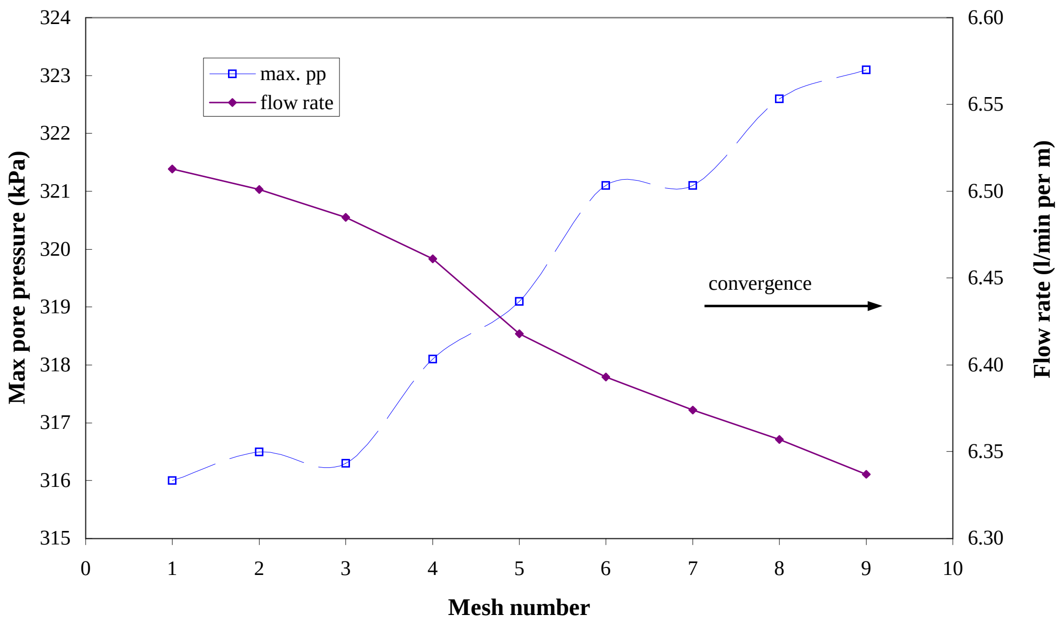


**FIG. 5.15 – Maximum pore pressure and flow rate variation with mesh arrangement**

Note: It can be seen that for all 9 runs the flow time (= No. of steps x time step) is approximately the same ($\approx 3.0 \times 10^7$ seconds). The time step is adjusted automatically to suit the mesh).

In Table 5.6 and Fig. 5.15, as the mesh number increases, the fineness of the mesh approximately increases, and therefore it can be assumed that as the mesh number increases the accuracy of the result increases too. By comparing the solution times recorded in Table 5.6 with the predicted pore pressures and flow rates in Fig. 5.15 some very interesting observations can be made with regard to the relative value in the various mesh arrangements. Firstly, is should be noted that the overall difference between all the results is only 2% for the maximum pore pressure measurements, and 3% for the flow rate predictions, and there is over 2 hours difference in solution time requirements.

By comparing the results from mesh 2 and 3, which are both arrangement 2 (Fig. 5.15), it is shown that by decreasing the zone size in the drain there is negligible change in maximum pore pressure prediction, but the accuracy with which the discharge is predicted increases slightly. For the 0.25% increase in accuracy in flow prediction, the solution time is more than tripled.

The solution time required for mesh 7 is about 3.4 times that required mesh 6, and yet as seen in Fig. 5.15, there is no increase in maximum pore pressure prediction and only very slight (approximately 0.3%) increased accuracy with which the discharge was predicted. Mesh 6 is based on arrangement 1, the uniform grid mesh, and mesh 7 is arrangement 2 with the finer mesh in only the drain section.

By comparing arrangement 2 with arrangement 3 for similar zone sizes in the coarse and fine mesh regions, it would be expected that the time increase would be fairly dramatic with little or no change to the flow measurement, and slight change in maximum pore pressure prediction because arrangement 3 includes a fine mesh in the point at the base of the stope furthest from the drain, where the maximum pore pressure is measured. This is not the case. From meshes 2 and 4 for example, it can be seen that the solution time for mesh 4 is only about 1.3 times more than that of mesh 2, and there is very little change (0.6% and 0.5% increase in accuracy for the discharge and pore pressure predictions respectively) in output.

### 5.3.3 Sensitivity of Solution Time

The *FLAC* manual publishes a set of solution times for an identical simulation undertaken on several different computers with various RAM and processor speed combinations. The table below reproduces some of the data from Table 5.1 in the

User's Guide of the *FLAC* Manual. It illustrates the runtime calculation rates (single precision *FLAC* version 4.0) for the computers listed, based on a 9684 zone model of Mohr-Coulomb material subjected to isotropic loading. The simulations are solved to 500 steps, and a *FISH* function was used to calculate the rate. Table 5.7 gives a gauge of comparative runtime calculation rates for typically available PC's.

**TABLE 5.7 - Relative runtime calculation rates for a specific problem solved by different computers**

| Computer | sec/gridpoint/1000 steps | Operating System |
|---|---|---|
| Intel Pentium II (Gateway 2000) 300 MHz | 0.0076 | Win 95 |
| Intel Pentium II (Gateway 2000) 400 MHz | 0.0050 | Win 95 |
| Intel Pentium III (Gateway 2000) 500 MHz | 0.0041 | Win 95 |
| AMD Athlon (Gateway Select)1.0 GHz | 0.0026 | Win 95 |

* Section 5.1 of the FLAC Version 4.0 User's Guide

**TABLE 5.8 - Case 1 summary: Mesh size sensitivity**

| Details | Arrangement #1 | Arrangement #2 | Arrangement #3 |
|---|---|---|---|
| Mesh size | 1 m x 1 m | 0.5 m x 0.5 m | 0.333 m x 0.333 m |
| Number of zones | 1601 | 6404 | 14409 |
| Number of nodes | 1703 | 6607 | 14701 |
| Convergence criteria (sratio) | 1 x$10^{-3}$ | 1 x$10^{-3}$ | 1 x$10^{-3}$ |
| Steps required | 47241 | 202204 | 500000 |
| Time step | 2.451 x $10^{-1}$ | 6.127 x $10^{-2}$ | 2.732 x $10^{-2}$ |
| Flow time | 1.158 x $10^{4}$ secs | 1.239 x $10^{4}$ secs | 1.362 x $10^{4}$ secs |
| Actual running time | 40 secs | 990 secs (16 mins 30 secs) | 5400 secs (1 hr 30 mins) |

The computer time required to solve a problem in *FLAC*, is mainly dependant on number of zones, convergence criteria, and specifications of the computer solving the program. A series of simulations were undertaken to demonstrate the machine solution time for firstly a steady state flow-only program solved to the same convergence criteria, on a Pentium IV 2.8 GHz machine using the Windows XP Professional operating system, with different mesh density. The problem is the same as the one shown in Fig. 5.12. Table 5.8 summarizes the solution times for the three arrangements.

As would be expected for a numerical model, the increase in numbers of zones and nodes increases the solution time. When the solution time for Arrangement No. 1 is compared to the solution time for Arrangement No. 2, it can be seen that by increasing the number of zones by four times, the solution time is increased by almost 25 times. Similarly, by comparing Arrangement No. 3 to Arrangement No. 1, increasing the zone number by 9 times increases the solution time by 135 times.

Next, to obtain an appreciation of the efficiency of various computer capabilities under different convergence criteria but for the same mesh, for the flow-only problem investigated in this research, a series of steady-state 2-dimensional simulations based on the verification model geometry (Section 5.2.1) were undertaken on three separate computers. A *FLAC* program was written to monitor the real time taken to solve the model to various convergence criteria. An example *FISH* program is documented in the Appendix (Program A3.1), and the results are summarised below in Table 5.9.

**TABLE 5.9 - Relative runtime for a steady-state stope problem solved by different computers**

| | **Computer Specifications** | **Convergence** | **$Q$ (m$^2$/s)** | **$u_{max}$ (kPa)** | **Sec/gridpoint** |
|---|---|---|---|---|---|
| 1 | Pentium IV 2.8 GHz 1.00 GB of RAM | Sratio = 1 x10$^{-3}$ | 0.1075 | 399.3 | 0.06179 |
| | | Sratio = 1 x10$^{-2}$ | 0.1075 | 399.3 | 0.06178 |
| | | Sratio = 1 x10$^{-1}$ | 0.1113 | 413.5 | 0.04437 |
| 2 | Pentium (R) IV 2.0 GHz 1.00 GB of RAM | Sratio = 1 x10$^{-3}$ | 0.1075 | 399.3 | 0.1403 |
| | | Sratio = 1 x10$^{-2}$ | 0.1075 | 399.3 | 0.1397 |
| | | Sratio = 1 x10$^{-1}$ | 0.1113 | 413.5 | 0.1004 |
| 3 | Pentium III 938 MHz 64 MB of RAM | Sratio = 1 x10$^{-3}$ | 0.1075 | 399.3 | 0.2160 |
| | | Sratio = 1 x10$^{-2}$ | 0.1075 | 399.3 | 0.2158 |
| | | Sratio = 1 x10$^{-1}$ | 0.1113 | 413.5 | 0.1560 |

As shown in Table 5.9, there is very little difference in runtime required between a solution with convergence criteria of sratio = 0.01 and that with sratio = 0.001. The solution time is distinctly faster for sratio = 0.1, but the system has not come to equilibrium, and therefore the computed values of discharge rate and pore pressure deviate slightly from the values for sratio of 0.001 and 0.01. This exercise indicates that clock speed has a greater influence over solution time than RAM. *FLAC* has an inbuilt function which limits the RAM used in solution to 8 MB unless otherwise specified.

### 5.3.4 Summary of Sensitivity Analysis for 2-dimensional *FLAC* Simulation

A 2-dimensional sensitivity analysis was undertaken on the input parameters, mesh grading and convergence criteria to determine the relative effect on the behaviour of the 2-dimensional system such that the parameters incorporated in the 3-dimensional sensitivity study could be prioritised.

This section has demonstrated that parametric studies are only required on the permeability, specific gravity, pumped slurry solids content and fill residual water content. All four parameters will be investigated in using the 3-dimensional program in Chapter 6.

The total drainable water, which is drained in engineering time from the stope, is independent of permeability; it depends only on the initial water content of the slurry, the specific gravity of the fill, and the residual water content.

The permeability of the fill determines the discharge rate for any given steady state condition. As demonstrated in section 5.3.1.1, the discharge volumes are relatively small compared to that of the free water within the stope, and therefore the relative influence the permeability has on water height and pore pressure within a stope may be very small, particularly if there is decant water.

Because the program assumes all fill below a single phreatic surface to be saturated, the residual water content only has an effect on water heights when the water level is below the height of the fill. Residual water content is essential in determining the engineering time required for a stope to drain of free water such that adjacent works may commence.

## 5.4 Two-dimensional Filling and Drainage Analysis for Hydraulic Fill Stopes

A series of simulations were undertaken using the 2-dimensional filling and drainage program written in *FLAC* to determine the relative behaviour of a stope with variation to filling schedule as well as geometric parameter variation. A series of simulations using programs similar to the example 2-dimensional filling program included in the Appendix (Program A3.2), were solved for various input parameters. Results from these simulations were used to determine the analysis to be undertaken in 3-dimensions in Chapter 6, as well as provide reference for which the 3-dimensional extension to the program may be valued upon.

### 5.4.1 Filling Schedule

Personal communications with several mine operators in Australia suggest that solids filling rate of 250 t/hr is the maximum achievable pour rate. This is also the maximum continuous filling pour rate used by Isaacs and Carter (1983). For this reason, this fill rate was selected to study the effect the filling schedule (e.g. 12 hr fill and 12 hr rest, 16 hr fill and 8 hr rest) has on the behaviour of the overall system during the filling cycle. The author appreciates that given an on-site scenario a consistent fill/rest cycle is very unlikely and many outside influences determine the fill and rest times of any given stope, but for research purposes, provided the extreme conditions are analysed it is reasonable to state that the actual circumstance will fall within that range of outcomes. Continuous filling, with no rest time for which the stope may drain without the addition of more water provides the worst-case filling schedule. This case will provide critical, or maximum possible water heights and pore pressures and is therefore used as the control for this research.

Despite the worst-case scenario being the primary focus of this research, an analysis of the degree of influence the filling schedule has on the behaviour of the system was undertaken. Fig. 5.16 shows the fill and water heights during filling for both the Isaacs and Carter and the *FLAC* programs for the filling of the verification stope geometry (Fig. 5.1) with different filling schedules. All runs assumed a fill rate of 250 t/hr of

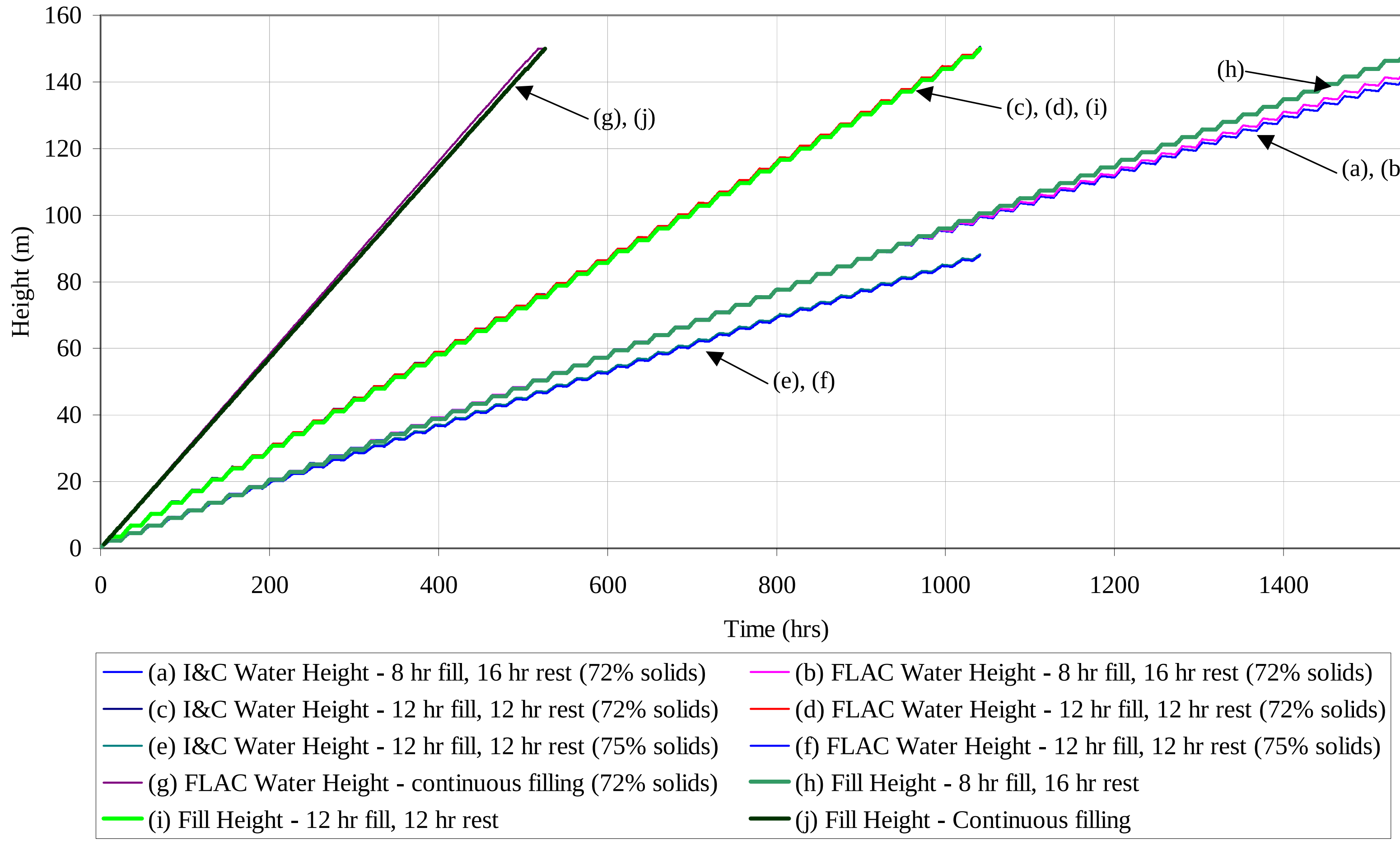


FIG. 5.16 - Fill and water heights during filling for various filling schedules

solids, as in section 5.2. Therefore regardless of the solid pulp density the slurry was poured at, the fill heights were identical for simulations with the same filling schedule.

As would be expected, the 12 hour fill, 12 hour rest cycle takes twice as long as the continuously filled case to complete fill the stope, and the 8 hour fill, 16 hour rest cycle takes three times as long as the continuously filled case. However, the relative heights of the water at any given fill height are not all that different. This is because, as described in Section 5.3.1 the quantity of water that is discharged over this period of time represents only a very small percentage of the water placed into the stope. Discharge rates and pore pressure distributions are calculated based on the fill and water heights for a given simulation. Therefore, with all other parameters remaining constant, the discharge rate and pore pressure distribution will be a function of the relative heights of fill and water.

By presenting the discharge rates for the various filling schedules as a function of water height (Fig. 5.17), the results collapse into a very narrow band. This is because, at a specific water height, discharge rates and maximum pore pressures are functions of the geometry. For both the Isaacs and Carter and the *FLAC* simulations, the discharge rates are slightly reduced with increased rest times. This is because the increased fill:rest ratio reduces the time available for water to drain from the stope. Therefore, for a point in time when the water reaches a particular height, the fill height will be lower, for the cases where there is not sufficient time for the water to drain at a rate equal to that of the water entering the stope. With reduced fill height under the same water height, the hydraulic gradient through the fill will be increased, resulting in increased pore pressures and discharge rates. This is not evident in the Isaacs and Carter simulations.

The very narrow band with which the results fall in Fig. 5.17, indicates that provided the quantity of water discharged from the stope represents only a small percentage of the overall water placed into the stope, the filling schedule has little effect on discharge rates or pore pressures, it merely changes the time in which these values are experienced.

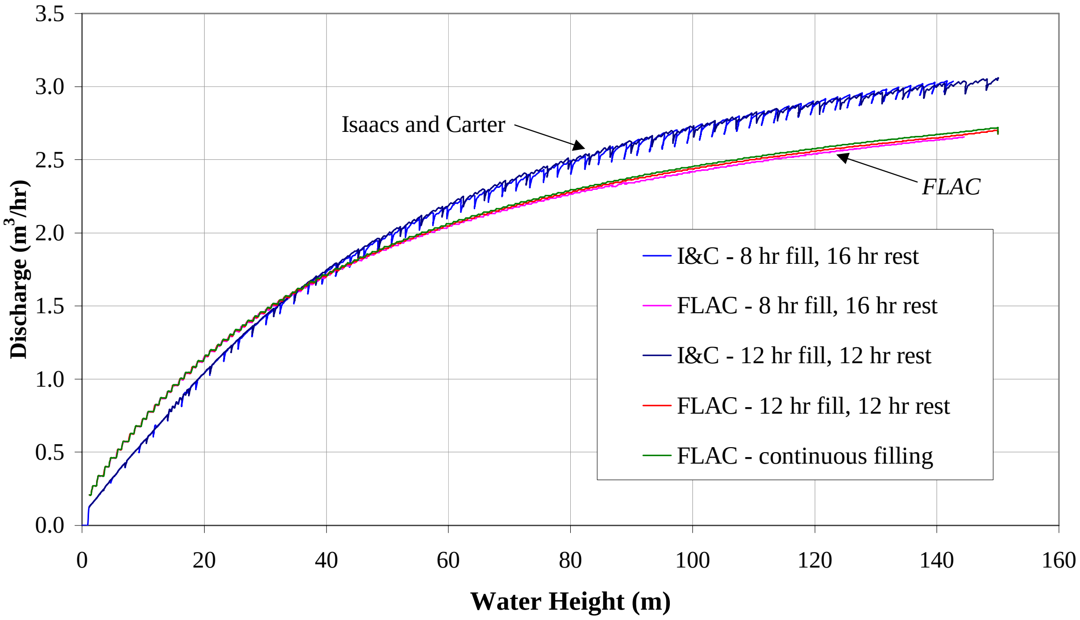


**FIG. 5.17 - Discharge rate vs. water height during filling for various filling schedules**

## 5.4.2 Filling Rate

As is the case with the filling schedule, the filling rate will influence the rate at which the fill and water levels raise, but have minimal effect on their heights relative to each other provided the discharge quantity represents only a small proportion of the total water placed in the stope. For typical stope simulations, where discharge rates from the stope remain very low, the rate at which the stope is filled will have almost no influence on the values of discharge and pore pressure at any given fill height – it will only influence the time in which these values are recorded (because the fill height increases more rapidly with increased filling rate). If time estimates were not required, the simulations could be performed at very high filling rates, and the output presented relative to either the fill or water height. Despite the computation time advantage that would be gained by increasing the filling rate to a value that would be unrealistic for any hydraulic fill operation, this option was not utilized in this research so that meaningful filling time requirements could be gained. A filling rate of 250 t/hr was used for all simulations in two and three dimensions.

### 5.4.3 Geometry

A brief analysis was undertaken to determine the relative effect variation in dimension, location and placement of drains, as well as stope dimension has on drainage and pore pressure distribution within a hydraulic fill stope. This was used to prioritise analysis required to be undertaken in the 3-dimensional study covered in Chapter 6.

#### Stope Dimensions

Stope geometry has a significant influence on the water drainage rates in hydraulic fill mines. The geometrical simplification required to model the 3-dimensional problem as 2-dimensional one does not allow for the investigation into the effects of various stope width to depth aspect ratios, inclined stopes, as well as the location, length and geometry of the drain. For this reason, this 2-dimensional program has been extended into three-dimensions using *FLAC*$^{3D}$, to more realistically represent the geometry. Although the influence some geometrical variation has on stope drainage behaviour, may be undertaken in using a 2-dimensional program such as Isaacs and Carter or the *FLAC* program presented in this chapter, this research involves extending the 2-dimensional program into three-dimensions (Chapter 6), and thus the geometrical analysis is primarily covered in that Chapter. Within the scope of this research, it was not possible to simulate every possible combination of hydraulic fill material property, stope and drain geometry and location and filling schedule, therefore limited case studies using the 2-dimensional program were performed to determine the relative influence of the various parameters on drainage so that the more critical parameter studies were undertaken and are presented in Chapter 6.

#### Multiple Drains

Due to ore removal requirements it is common practice for more than one access drive to be constructed for a single stope arrangement. These drives are often located on levels a vertical distance anywhere from 20 m to over 50 m apart, and several drives may access any particular level. Prior to refilling, the barricades are constructed across these drives and therefore, stope drain arrangements may vary considerably between stopes. Obviously, it is not possible to study all potential drain and stope geometrical arrangements, therefore, the relative effect geometrical variation has on drainage behaviour should be analysed.

*Drains at Various Sublevels*

Although this is a 2-dimensional modelling chapter, this 3-dimensional study of drains at various sublevels has been included in this Chapter because the 3-dimensionality of the problem is not being studied, purely the effect of additional drains at higher sublevels. It is quite obvious, that the number and location of drains within a given stope will dictate the drainage pattern for that stope. A very significant finding that arose from the work using the Isaacs and Carter program, undertaken for Mount Isa Mines Ltd. in the 1980's was with regard to modelling stopes with drains located at various levels within a single stope (Isaacs and Carter, 1983). This work highlighted that the majority of the water discharged from a stope, exits the drains at the base of the stope. These findings were reiterated by a 3-dimensional modelling case undertaken on a 15 m x 15 m x 60 m stope in *FLAC$^{3D}$* (Rankine et al. 2002). The study consisted of two 15 m$^2$ drains located along the vertical centre line of one of the stope faces. One of the drains was placed at the base of the stope, and three separate simulations were done for the placement of the second drain at 15 m, 30 m and 45 m up the face (Fig. 5.18 a). The stope was continuously filled. These simulations were compared to the case consisting of only the single base drain, (Fig. 5.18 b).

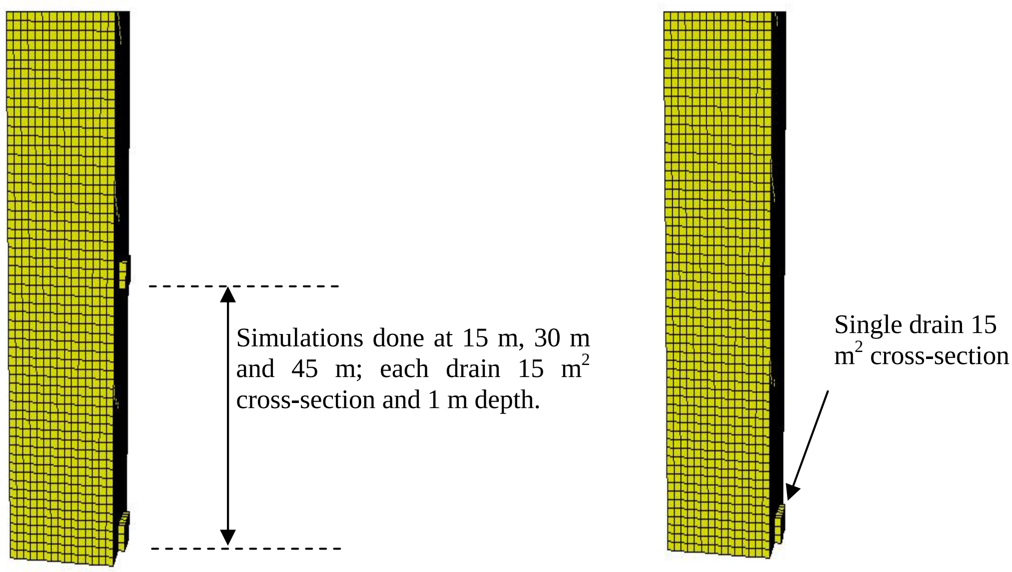


**(a)** **(b)**

**FIG. 5.18 - 3-dimensional model arrangement for (a) 2 drains located on levels either 15 m, 30 m or 45 m apart, and (b) single drain arrangement**

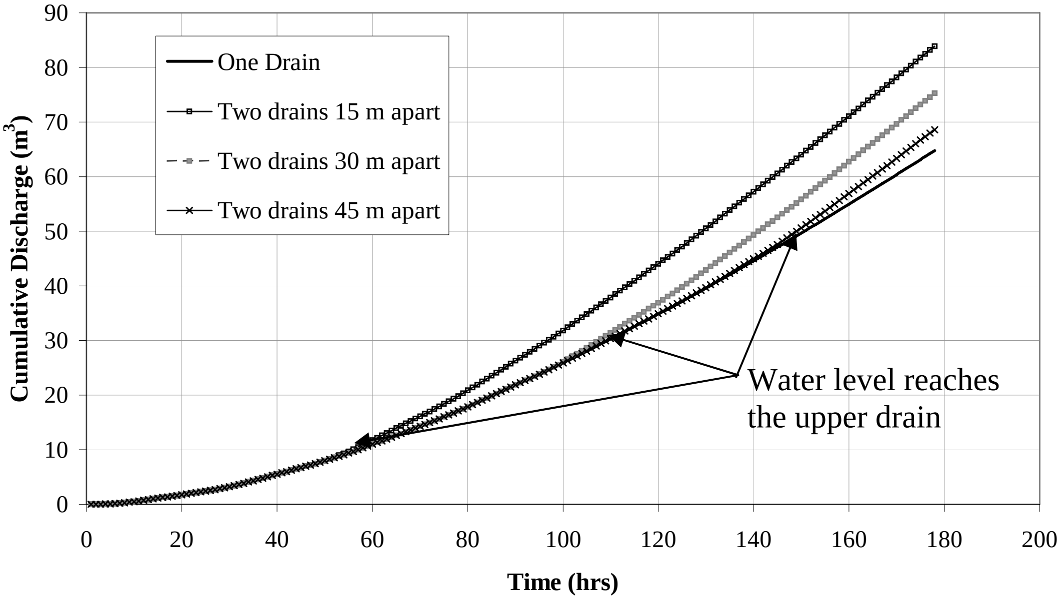


**FIG. 5.19 - Cumulative discharge for various drain arrangements**

Fig. 5.19 demonstrates the increased cumulative discharge from a stope as a result of additional outlet position. The plot clearly demonstrates the closer the second drain is located to the base of the stope, the more overall discharge that results from the stope. The rate of discharge from the second drain, with time after free water reaches the height of the drain is approximately equal for the 15 m, 30 m and 45 m drain locations. Obviously during the filling cycle, a drain located more closely to the base of the stope will commence draining earlier than that which is higher and the free water reaches at a later time. The plot shows that the additional drain does not have all that much effect on the overall discharge for the stope, and as the vertical distance between drains increases the influence is reduced further. This is further confirmed by in situ data (Traves, 1988).

Filling and drainage details from stope R454 at Mount Isa Mines Limited, filled between 31st August 1983 and 13th February 1984, may be used to provide an in situ verification to this behaviour (Traves, 1988). The R454 stope is approximately 45 m x 36 m in plan, and 75 m in height. Plans and sections of Stope R454, and a full set of the fill and drainage details are provided in the Appendix 3. This in situ example shows that the two drains, 18B and 18E, located a vertical distance of 20 m and 50 m respectively from the base drain (19E) carry an average of 6.8% for 18B and 2.6% for 18E of the total discharge from the stope. The remaining 90.6% exits the base drain. The stope is 75 m high which means the two additional drains are in the bottom third of the stope. Fig. 5.20 plots the percentage of total discharge each drain emits over the filling and drainage of the entire stope. The fill reaches the height of the stope at about day 57, and for all practical purposes the drainage ceased at approximately day 90.

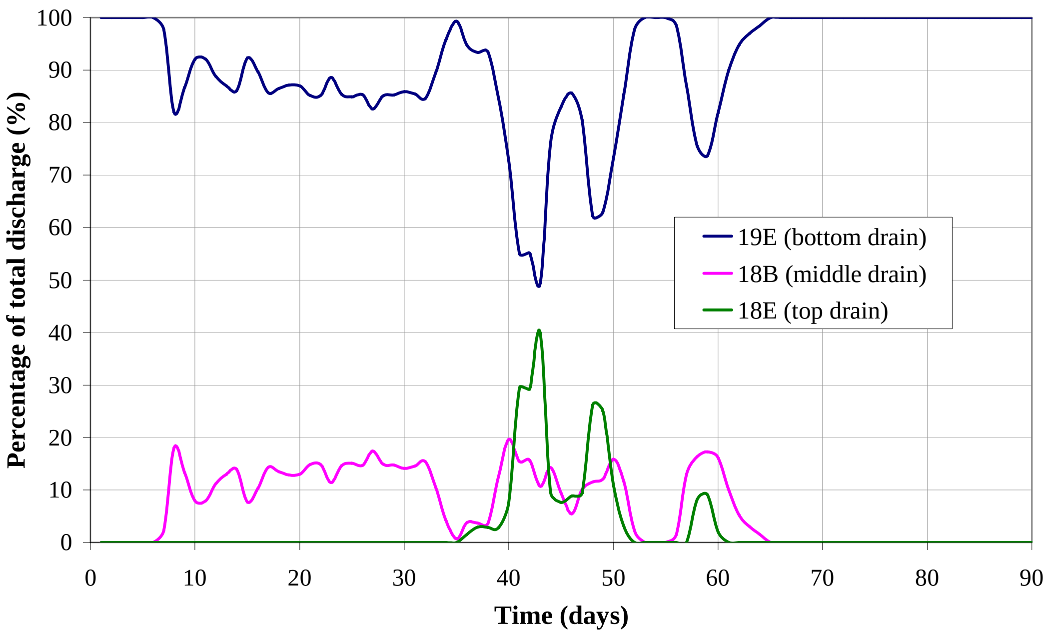


**FIG. 5.20 - Percentage of total discharge emitted by each drain during the filling and drainage of stope R454 at MIM**

There is limitless combinations of possible stope geometry, drain arrangement, fill material properties, proportions and pumping rates able to be investigated therefore, parameter studies must be optimised to study the parameters for which the drainage and pore pressure generation within the stope are most sensitive. As demonstrated in both the in situ example as well as the 3-dimensional case presented in the section, the base drain is the most critical in drainage of water from the stope. Therefore the 3-dimensional analysis discussed in Chapter 6 will only consider the drainage from barricades located at the base of the stope. Individual stope analysis should mimic the in situ condition as closely as possible, and therefore for case studies it is recommended that this simplification not be made, and the actual geometry and drain location be generated as directly as feasible based on modelling constraints.

*Multiple Drains on a Singular Level*

Due to geometrical simplification required for a 2-dimensional analysis, modelling multiple drains at the same level, on the same stope face is not possible using a 2-dimensional analysis. Two-dimensional analysis model the drain as if it were the length of the stope so if it were presented in 3-dimensions, it would appear as the pseudo 3-dimensional illustration in Fig. 5.21. The height of the drain is reduced so that the cross-sectional area of the drain exit is approximately that of the actual 3-dimensional drain. Drains located on the same levels, on opposite stope walls, may be simulated in two-dimensions, but because the analysis of two same-level, wall drains must be covered in the 3-dimensional analysis (Chapter 6), all simulations involving multiple drains at one level are only done in three-dimensions to reduce repetition and provide consistency.

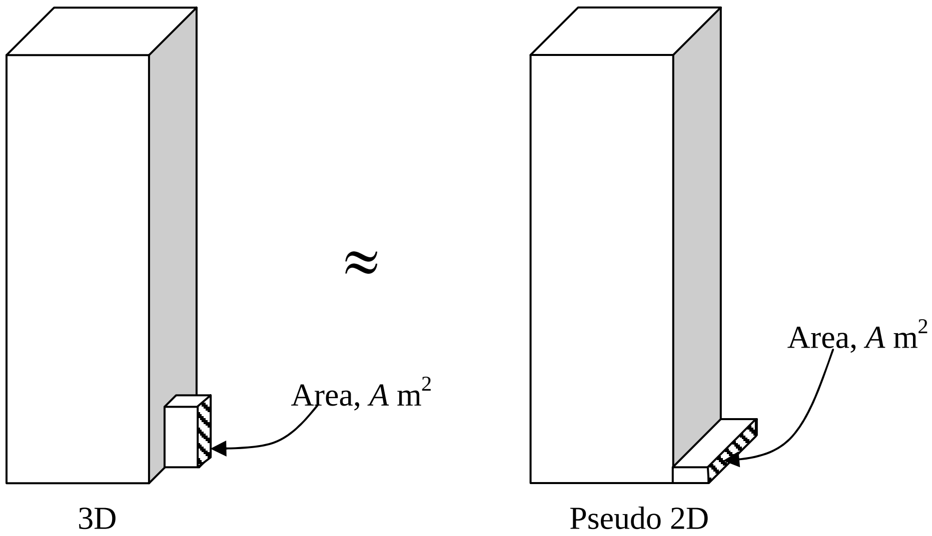


**FIG 5. 21 – A 3-dimensional and an equivalent pseudo 2-dimensional arrangement**

Drain Length

Drain length has a considerable influence on the pore pressure distribution, as well as the discharge rate from a stope. This can quite simply be observed by simulating the steady-state of the verification problem, detailed in Section 5.2 ($B$ = 25 m and $D$ = 1 m) for a case whereby the fill and water heights are equal to the stope height of 150 m, and the length of the drain is varied. To observe the relative effect of drain length on both discharge and maximum pore pressure within the stope, this simulation was undertaken with drain lengths of 0, 1, 2, 5, 10, 15 and 30 m. The results are recorded in Table 5.10.

**TABLE 5.10 - Variation in discharge and maximum pore pressure with drain length for the 2-dimensional verification stope**

| Drain Length (m) | Discharge ($m^3$/hr) | Maximum Pore Pressure (kPa) |
|---|---|---|
| 0 | 2.69 | 339.3 |
| 1 | 2.38 | 534.9 |
| 2 | 2.15 | 639.6 |
| 5 | 1.66 | 858.8 |
| 10 | 1.20 | 1060.0 |
| 15 | 0.94 | 1171.0 |
| 30 | 0.57 | 1325.0 |

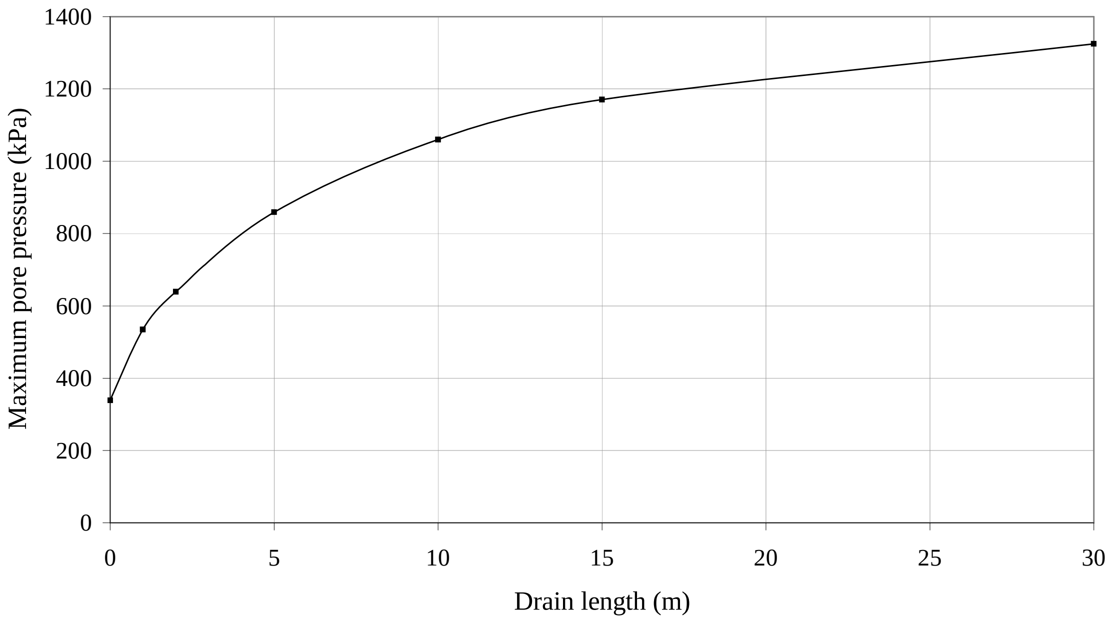


**FIG. 5.22 - Variation in maximum pore pressure with drain length**

By plotting the data in Table 5.10 it becomes clear that both the maximum pore pressure and the discharge rate within the stope will plateau to a maximum value at very large drain lengths (Figs. 5.22 and 5.23). As intuitively expected, the increase in drain length resulted in a reduction in drain discharge. As the barricade gets further from the stope, the flow path increases and the hydraulic gradient across the entire model decreases, resulting in reduced flow velocity, hence discharge.

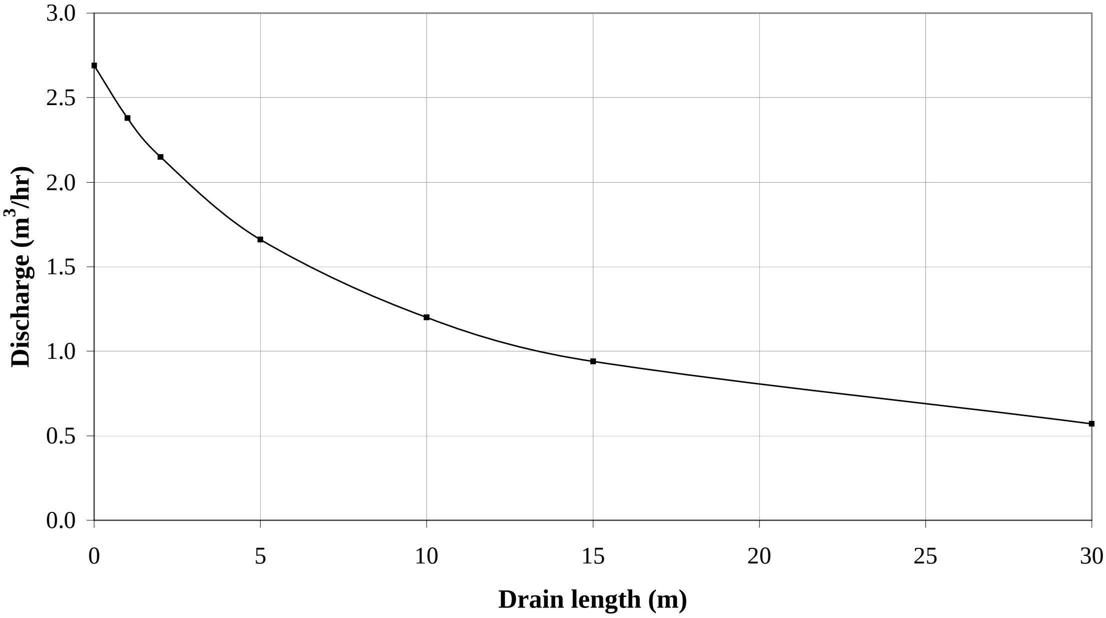


**FIG. 5.23 - Variation in discharge with drain length**

Fig. 5.24, shows the pore pressure contour plots for the drain section of the simulations with 15 m, 5 m and 0 m drains. As can be seen in Fig. 5.24, the maximum pore pressure values which in a 2-dimensional simulation occurs in the bottom stope corner furthest from the drain, varies considerably between the three simulations.

These contours also highlight the very large values of pore pressure that may be experienced within the drive of a hydraulic fill stope constructed with the barricade a large distance from the stope brow. There are very high pore pressure gradients illustrated within the drives of the stopes. In this example, with a single drain at the base of a 25 m x 25 m x150 m stope with both the water and fill heights equal to the stope height, pore pressure of up to 1171 kPa is predicted if the drive is 15 m in length. These very high pore pressure predictions can raise serious concerns regarding the potential for liquefaction within these regions.

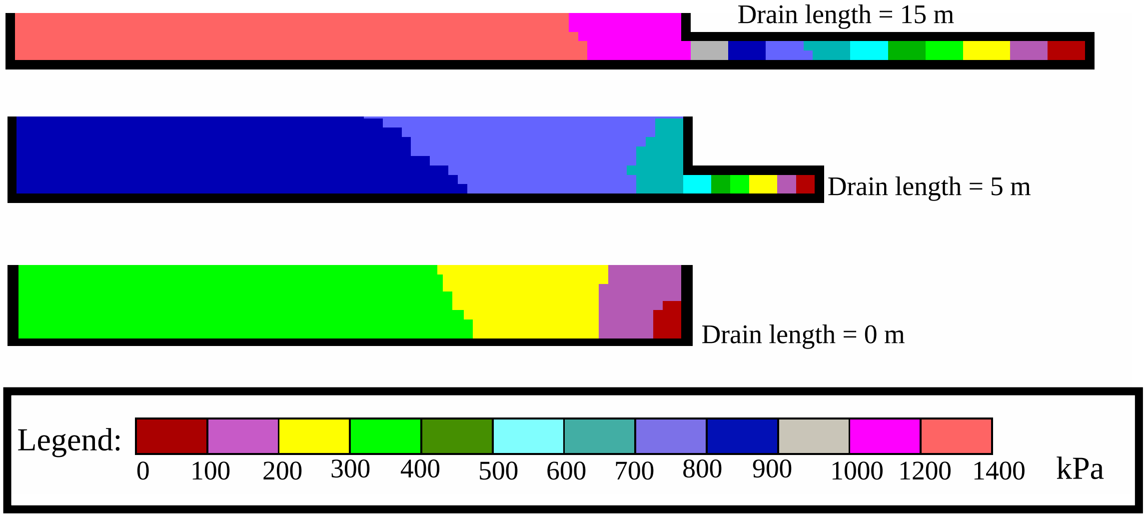


**FIG. 5.24 - Pore pressure contour plots in the bottom section of the 2-dimensional verification simulation with various drain lengths**

## 5.5 Chapter Summary

This chapter has been used to verify and evaluate the performance of a 2-dimensional replication of the program written by L. Isaacs and J. Carter in 1983 using the finite difference software *FLAC*. *FLAC* modelling has then been used to determine the critical parameters with which the 3-dimensional extension to the program will analyse in Chapter 6. Some major outcomes presented in this chapter, include:

- A 2-dimensional finite difference program which simulates the filling and drainage of a hydraulic fill stope was developed, using the geotechnical software package *FLAC*, manipulated through the in-built programming language *FISH*.
- The integrity of the *FLAC* 2-dimensional drainage model developed for this research is clearly verified through comparison with the commercially used, 2-dimensional finite difference program written by L. Isaacs and J. Carter for Mount Isa Mines Ltd. The Isaacs and Carter program has been verified previously against in situ data.
- The contrasts of the major advantages and disadvantages between the two models are discussed (i.e., solution times for the *FLAC* program are significantly larger than that for the Isaacs and Carter program as a result of the explicit solution scheme, but the flexibility of the program, monitoring facilities, the software availability and the ability to extend the program into

three-dimensions through the use of *FLAC$^{3D}$* greatly outweigh this increased solution time).

- A thorough sensitivity analysis was carried out with different mesh arrangements and mesh densities. It was shown that 1 m x 1 m uniform grid suits the best for the drainage studies modelled in this chapter. The slight increase in accuracy of the results does not justify the substantial increase in the computation time. On the basis of this finding, 1 m x 1 m x 1 m uniform mesh will be used for the 3-dimensional analysis in Chapter 6.
- The justification behind the inclusion of following list of parameters for analysis by the 3-dimensional program presented in Chapter 6 were discussed.
    - Permeability
    - Specific gravity
    - Solids content of slurry
    - Residual water content
    - Stope geometry
        - Drain length
        - Multiple drain position along the base of the stope
- It has been demonstrated through both in situ data, and numerical modelling techniques that from a stope with drains located on several vertical levels, the majority of discharge exits through the base drain. Because it is impractical to investigate all possible drain arrangements, the 3-dimensional analysis covered in Chapter 6 will only investigate the critical base drain positioning.
- The 2-dimensional drain length analysis indicates stope drainage and pore pressure distribution within a stope are significantly influenced by drain length. As the barricade gets further from the stope, the flow path increases and the hydraulic gradient across the entire model decreases, resulting in reduced flow velocity, hence discharge. Increasing the drain length increases the pore pressures within the stope. This behaviour will be accentuated by extending the problem into 3-dimensions and therefore drain length has been identified as an important parameter to investigate in the 3-dimensional analysis.

# Chapter 6

# Three-Dimensional Modelling of Underground Hydraulic Fill Stopes

## 6.1 Introduction

Underground stope arrangements are very much 3-dimensional in geometry, and although the 2-dimensional programs such as the one described in Chapter 5, provide a valuable tool for drainage prediction, the inherent approximations required substantially reduce the value of the model when dealing with complex 3-dimensional stopes. This chapter discusses the 3-dimensionality of the problem, describes the extension of the 2-dimensional program presented in Chapter 5 into a 3-dimensional model using *FLAC*$^{3D}$, and the implementation of the program to model the filling and drainage of a typical stope. The code for this program is included in Appendix 4. Steady state simulations are also used to analyse the relative effect particular parameters have on the drainage behaviour of a 3-dimensional stope.

### 6.1.1 Three-Dimensional Numerical Modelling in Underground Hydraulic Fill Stopes

As mentioned in Chapter 5, the implementation of monitoring equipment in underground stopes can be very difficult and expensive. Numerical modelling provides an effective means by which drainage behaviours may be analysed and the variation and sensitivity in drainage behaviour with geometry and fill properties may be easily and effectively studied. Three-dimensional numerical modelling, allows engineers to simulate geometries with fewer approximations than the 2-dimensional models, therefore making the predictions match the real behaviours better.

### 6.1.2 *FLAC$^{3D}$*

*FLAC$^{3D}$* is an extension to the well established 2-dimensional numerical modelling program *FLAC* developed by the Itasca Consulting Group, and used in Chapter 5. Like *FLAC*, *FLAC$^{3D}$* is an explicit finite difference program used in computational geomechanics. The numerical methods used in *FLAC$^{3D}$* are essentially the same as *FLAC* but the simulations model the 3-dimensional behaviour of structures built of soil, rock or other materials that undergo plastic flow when their yield criteria are reached. Both *FLAC* and *FLAC$^{3D}$* allow the user to implement subroutines written in *FISH*.

Like *FLAC*, the variables involved in the description of fluid-flow through a porous media are the pore pressure ($u$), saturation ($S$), and the three components of the specific discharge vector ($q_x$, $q_y$, $q_z$). These variables are related through Darcy's law (the transport law), the fluid mass-balance equation, the constitutive equation[18] and an equation of state for the unsaturated range which relates pore pressure to saturation. Assuming the volumetric strain rates are known, by substitution of the mass-balance equation into the constitutive relation, using Darcy's law, a differential equation in terms of pore pressure and saturation is formed. For a flow-only fully saturated analysis such as the programs developed in this research, where porous medium is assumed incompressible, the volumetric strain rates and equations for saturation are obviously not required. This differential equation may be solved for various geometries, properties, boundary and initial conditions.

The discretization and finite difference methods follow the general scheme presented in the Theory and Background of the Itasca *FLAC$^{3D}$* manuals. Each individual brick-shaped element is further discretized into tetrahedra in either of the ways shown in Fig. 6.1. The equations that describe pressures and saturation values are based on nodal or "gridpoints" calculations, and zone pressures and saturations are derived by simply averaging surrounding nodal values.

[18] The constitutive equation specifies the fluid response to changes in pore pressure, saturation, and volumetric strains.

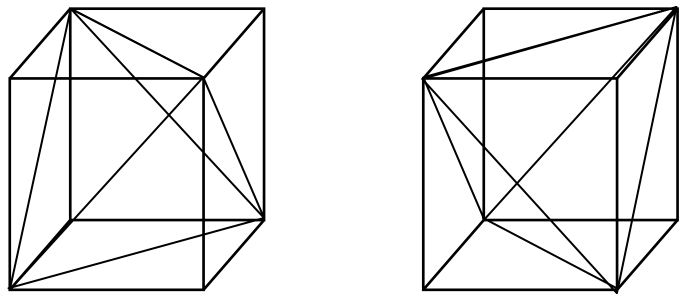

**FIG 6.1 - Mixed discretization method used in *FLAC$^{3D}$***

Attention is directed to two specifics of the numerical formulation:

1. All equations for both fluid analysis and boundary conditions in *FLAC* and *FLAC$^{3D}$* are expressed in terms of *pore water pressure* rather than *head*, both are conventionally used in soil mechanics.
2. *Permeability*, described in *FLAC* and *FLAC$^{3D}$* refers to the mobility coefficient, the coefficient of the pore pressure term in Darcy's law. It is defined as the ratio of intrinsic permeability to fluid dynamic viscosity, (see– *FLAC* 4.0 Manual – User's Guide, 2.8 System of Units).

   In traditional soil mechanics, $v = ki = k\dfrac{dh}{dx}$, but in *FLAC* computations $v = k\dfrac{du}{dx}$, therefore, it can be shown that if *du* has the units of Pa, and *v* has the SI units m/s, the *FLAC* permeability ($k_{FLAC}$) must have the units m$^2$/(Pa.s). The two permeabilities are related by:

   $$k_{FLAC} = \frac{k_{\text{soil mechanics}}}{\gamma_w} \qquad \text{Eqn. 6.1}$$

## 6.2 Using Flow Nets to Determine Scaling Factors

Flow nets are commonly used to provide solutions to a wide variety of 2-dimensional flow problems in geomechanics. A flow net is comprised of a system of flow lines (the direct path along which the fluid would pass) and equipotential lines (lines drawn through points of equal total head). The net is drawn in isotropic soil such that the flow lines and equipotential lines intersect at right angles (Fig. 6.2) thus, the flow is perpendicular to the equipotential lines. Although any orthogonal pattern can be used by engineers to determine flow rates, head and gradients, the simple square system is the most commonly adopted (Lambe and Whitman, 1979).

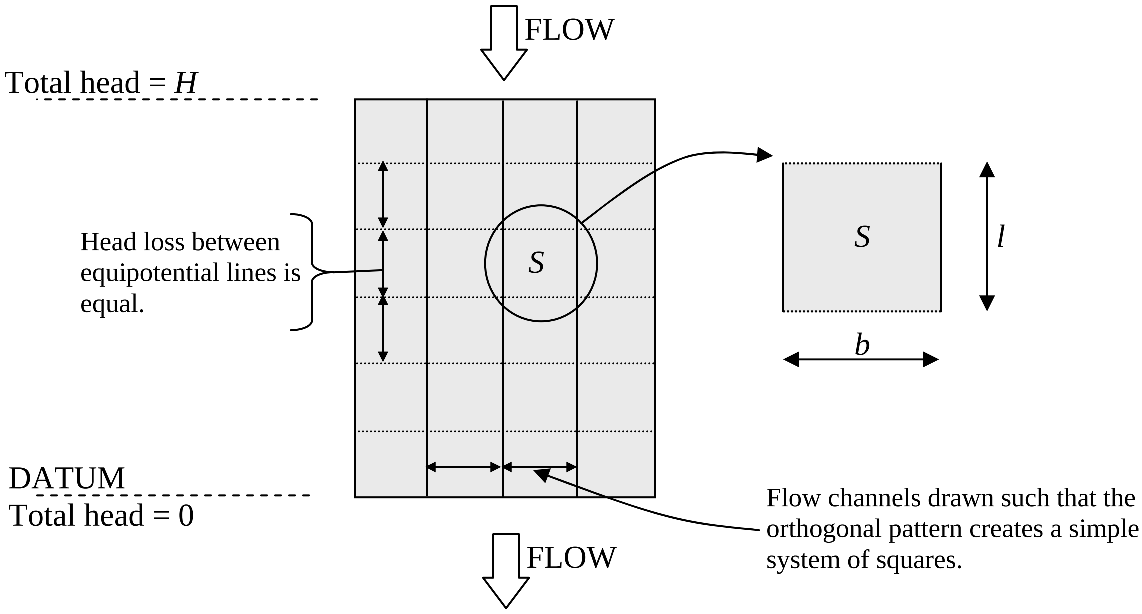


**FIG 6.2 - One-dimensional flow**

The total head lost per square of the net, is the total head loss across the system ($H_L$), divided by the number of head drops in the net, $n_d$. Therefore, the hydraulic gradient across each square, $i_S$ is equal to $\frac{H_L}{n_d l}$, where $l$ is the length of the square in the flow direction. If $a_S$ is the cross-sectional area of square, $S$ in plan view, the flow rate through a single square $S$, is equal to,

$$q_S = k i_S a_S \qquad \text{Eqn. 6.2}$$

The cross-sectional area, $a_S$ of square $S$ is equal to $b$ multiplied by the length perpendicular to the page, and because the net has been drawn as a square, $l$ is equal to $b$, it can be shown that the total flow across the system is equal to the flow for each of the flow channels, multiplied by the number of flow channels, $n_f$. Therefore,

$$\frac{Q}{L} = q_S n_f = k \frac{H_L}{n_d} n_f \qquad \text{Eqn. 6.3}$$

where $\frac{Q}{L}$ is the total flow per unit length of the system. $L$ is the length of the flow path for a water molecule. The ratio, $\frac{n_f}{n_d}$ is characteristic of the flow net and independent of both permeability ($k$), and the total head loss ($H_L$). It only depends on the geometry of the flow region. Harr (1962) refers to the reciprocal of the above ratio, $\frac{n_d}{n_f}$, as form factor of the flow region.

### 6.2.1 Flow Nets in 2-Dimensional Stopes

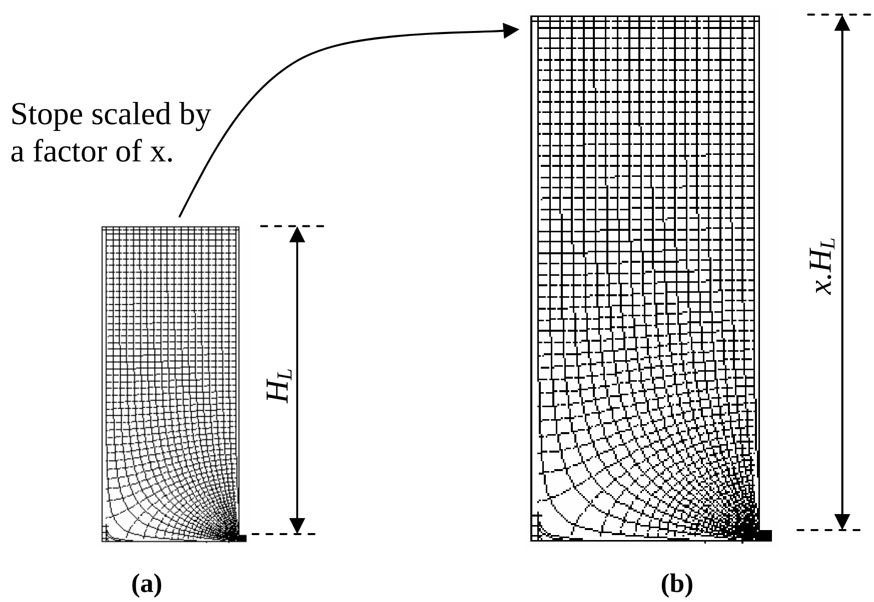


**FIG 6.3 – Scaling of a 2-dimensional stope and the flow nets**

These simple flow net principles may be used in an underground stope situation, to clearly explain the influence scaling has on pore pressure measurements as well as discharge from the stope. The 2-dimensional case is quite straight forward, and we will consider this first. Fig. 6.3 shows a typical 2-dimensional flow net for a stope with one single drain located at the base of the stope. This flow net was generated using *FLAC*.

If Fig. 6.3 (a) is scaled by a factor of x, it results in the geometry and associated flow net shown in Fig. 6.3 (b). The entire geometry has been scaled by a factor of x, therefore, the total head loss across the stope, and the head loss between each of the equipotential lines has been scaled by x, but the number of equipotential drops ($n_d$), the number of flow channels ($n_f$) and the permeability remain constant. Therefore $\frac{n_f}{n_d}$, (the ratio of the number of flow channels divided by the number of equipotential drops) remains constant regardless of the scaling factor. The discharge per unit length for (a) may be defined as, $Q_a = k_a H_{L_a} \frac{n_{f_a}}{n_{d_a}}$, and the discharge per unit length for (b) as $Q_b = k_b H_{L_b} \frac{n_{f_b}}{n_{d_b}}$, and the system is simply scaled by a factor of x. It can be shown that the amount the discharge from a scaled stope (b), relative to the original discharge (a) is equal to,

$$\frac{Q_b}{Q_a} = \frac{k_b H_{L_b} \frac{n_{f_b}}{n_{d_b}}}{k_a H_{L_a} \frac{n_{f_a}}{n_{d_a}}} \qquad \text{Eqn 6.4}$$

When the system is scaled by a factor of x, $k_a = k_b$; $\frac{n_{f_a}}{n_{d_a}} = \frac{n_{f_b}}{n_{d_b}}$; and $H_{La} = xH_{Lb}$. Thus,

$$\frac{Q_b}{Q_a} = x \qquad \text{Eqn. 6.5}$$

Similarly, the pore pressure measurements are scaled by a factor of x.

### 6.2.2 Flow Nets in 3-Dimensional Stopes

The 3-dimensional flow net is approached in much the same manner as the 2-dimensional net. Equipotential lines are now viewed as equipotential surfaces, and the flow channels incorporate the third dimension. The total head loss across the entire system is divided into a number of equipotential drops, $n_d$, which are defined by $n_d$+1 equipotential surfaces. The head loss across one cube of the flow net is $\Delta h = \frac{H_L}{n_d}$, (Fig. 6.4).

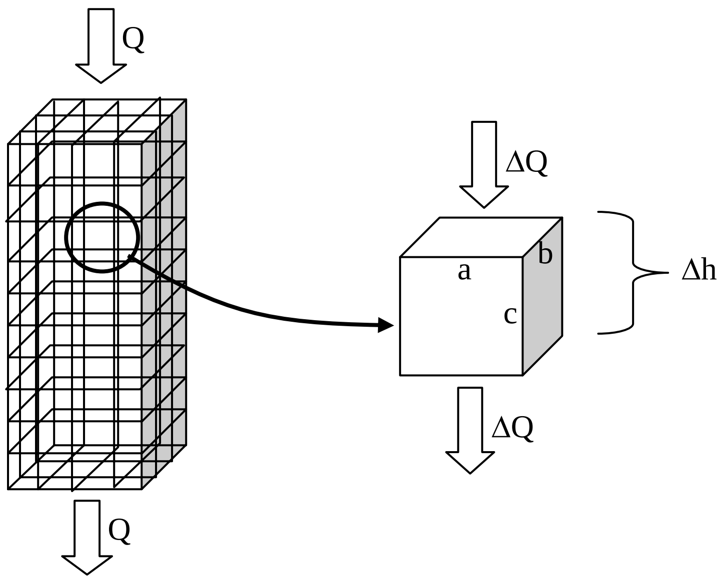


**FIG 6.4 - Three-dimensional flow net for 1-dimensional flow**

Between adjacent equipotential surfaces,

$$v = ki = k\frac{\Delta h}{c} \qquad \text{Eqn. 6.6}$$

and the flow through an individual flow channel is,

$$\Delta Q = vab = k\frac{\Delta h}{c}ab \qquad \text{Eqn. 6.7}$$

ΔQ, k, and Δh are constants between equipotential surfaces. $\frac{ab}{c}$ varies with flow net, but remains constant for a specific flow net. $\frac{n_f}{n_d}\frac{ab}{c}$ is constant for a problem and is independent of flow net.

The total flow calculated using a 3-dimensional flow net is,

$$Q = n_f \Delta Q = n_f k\Delta h\frac{ab}{c} \qquad \text{Eqn. 6.8}$$

and substituting $\frac{H_L}{n_d}$ for Δh, gives,

$$Q = kH_L\frac{n_f}{n_d}\frac{ab}{c} \qquad \text{Eqn. 6.9}$$

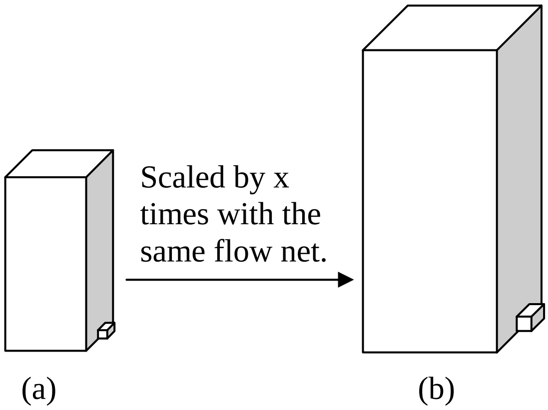


**FIG 6.5 - Three-dimensional scaling**

When a stope is scaled by a factor of x as shown in Fig. 6.5, all length dimensions of the stope are scaled by x. This results in the areas being scaled by a factor of $x^2$ and the volumes by $x^3$. Although the value of $\Delta h$ between each of the equipotential surfaces will be scaled by a factor of x, and each of the dimensions for the flow channel will be scaled by a factor of x, the number of flow channels and equipotential surfaces remains the same.

In Fig. 6.5,

$$Q_a = k_a H_{L_a} \frac{n_{f_a}}{n_{d_a}} \frac{a_a b_a}{c_a} \qquad \text{and} \qquad Q_b = k_b H_{L_b} \frac{n_{f_b}}{n_{d_b}} \frac{a_b b_b}{c_b}$$

It can be shown for a 3-dimensional case, that the amount of discharge from a scaled stope (b), relative to the original discharge (a) is equal to:

$$\frac{Q_b}{Q_a} = \frac{k_b H_{L_b} \frac{n_{f_b}}{n_{d_b}} \frac{a_b b_b}{c_b}}{k_a H_{L_a} \frac{n_{f_a}}{n_{d_a}} \frac{a_a b_a}{c_a}}$$

$$\frac{Q_b}{Q_a} = \frac{k_b}{k_a} \frac{H_{Lb}}{H_{La}} \frac{n_{fa}}{n_{fb}} \frac{n_{da}}{n_{db}} \frac{a_b}{a_a} \frac{b_b}{b_a} \frac{c_a}{c_b}$$

$$\frac{Q_b}{Q_a} = 1 \times x \times 1 \times 1 \times x \times x \times \frac{1}{x} = x^2$$

Thus,

$$Q_b = Q_a x^2 \qquad \text{Eqn. 6.10}$$

Therefore, by scaling a stope by three times, you increase the discharge from the drain by nine times, but the pore pressure measurements will only be scaled by a factor of 3.

A simple steady state scaling exercise has been undertaken in *FLAC*$^{3D}$ to numerically illustrate this. A stope with dimensions 10 m x 10 m x 20 m and a single drain located centrally along the base of one of the stope walls was scaled by 1.5 to give a 15 m x 15 m x 30 m stope, and then also scaled by a factor of 2 to give a stope of 20 m x 20 m x 40 m. All dimensions were scaled, therefore, the drain length and cross-sectional dimensions were also scaled by the appropriate factor. These dimensions are shown in Fig. 6.6. Table 6.1 shows that the discharge divided by the square of the factor by which the simulations were scaled is approximately the same for all simulations. Likewise, the maximum pore pressure divided by the appropriate scale factor is approximately equal between all three simulations.

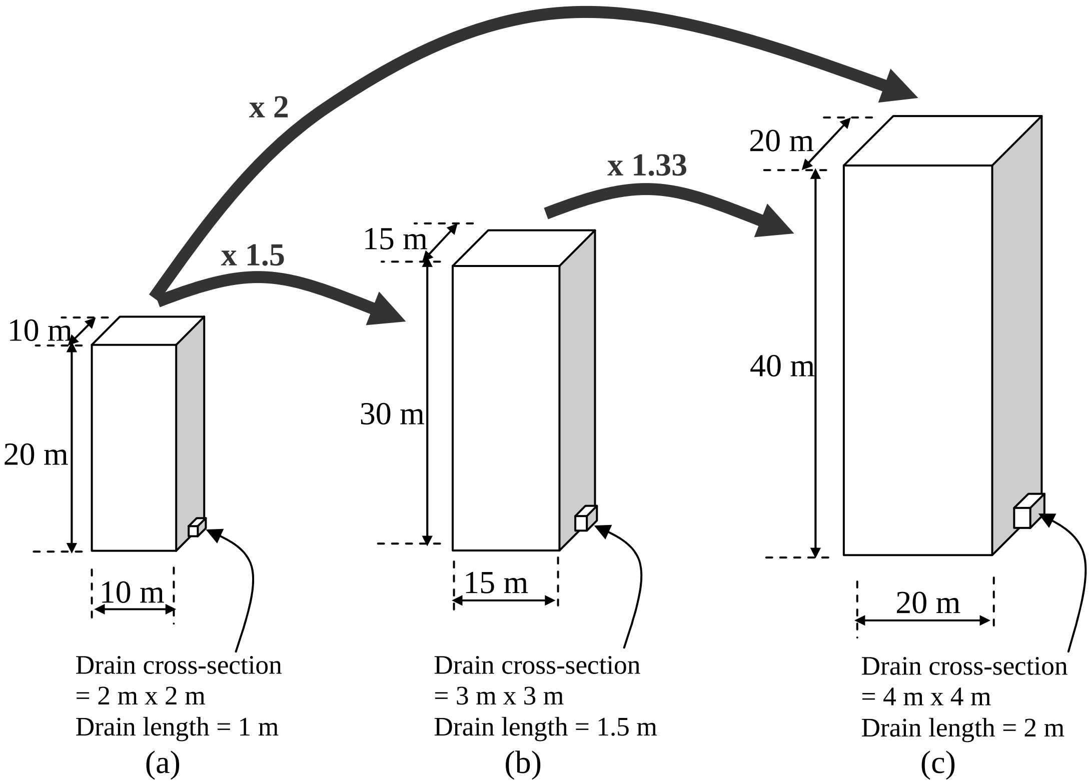


**FIG 6.6 - Three-dimensional modelling exercise to demonstrate stope scaling**

**TABLE 6.1 - Results for 3-dimensional scaling exercise in *FLAC*$^{3D}$**

| Dimensions (m) Stope | Dimensions (m) Drain | Scale Factor [SF] | $Q/(SF)^2$ ($m^3$/hr) | Maximum pore pressure (kPa)/(SF) |
|---|---|---|---|---|
| 10 x 20 | 1 x 2 | 1.0 | 0.155 | 152.7 |
| 15 x 30 | 1.5 x 3 | 1.5 | 0.153 | 153.3 |
| 20 x 40 | 2 x 4 | 2.0 | 0.152 | 153.5 |

This scaling exercise was repeated over a range of steady-state stope heights ($H_w$), and as shown in Fig. 6.7, the results show very good correlation. The flow rate is proportional to the square of the scale factor (Fig. 6.7).

This understanding of 3-dimensional scaling will be utilized throughout this chapter to determine equivalent discharge rates and pore pressure measurements for stopes that have the same geometry but are scaled. This is a useful tool in generating charts on stope behaviour based on geometry.

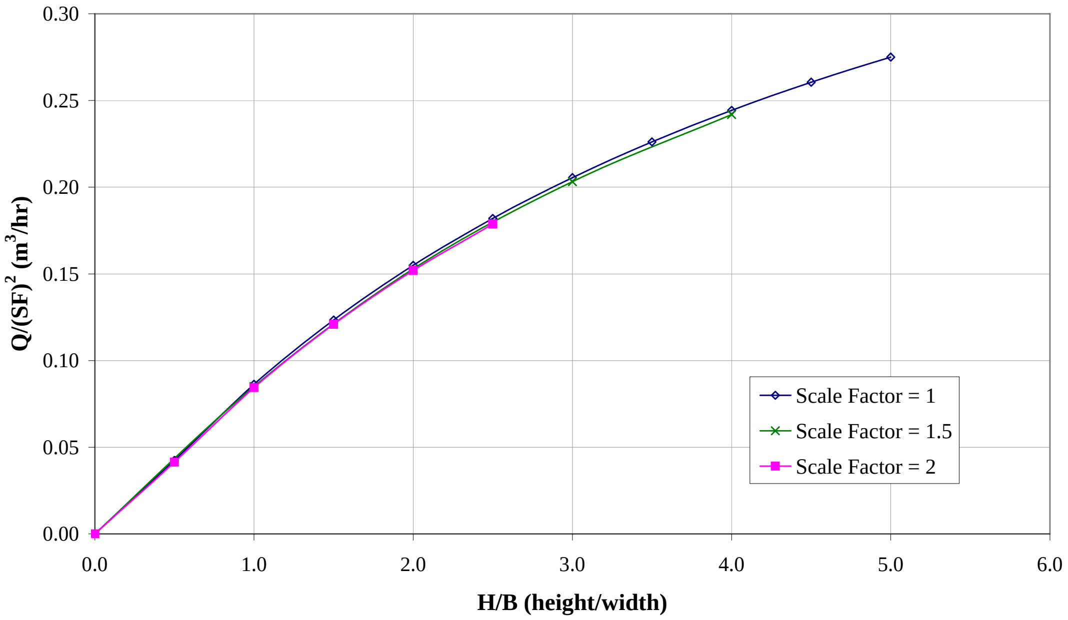


**FIG 6.7 - Three-dimensional scaling of discharge**

## 6.3 Three-Dimensional Stope Filling and Draining Program

Development of a 3-dimensional stope filling and draining program using *FLAC*$^{3D}$ forms a substantial component of this dissertation. The program simulates the complete filling and draining of the stopes and enables the user inputs such as filling schedule, slurry solids content, residual water content, etc. The numerical integrity of the program designed and coded in *FLAC*$^{3D}$ was verified using both the 2-dimensional *FLAC* program described in Chapter 5, as well as the program written by Isaacs and Carter. The verification exercise used a simple, single drain stope geometry, and results were compared between the three simulations.

### 6.3.1 Problem Definition

The stope drainage problem described in Section 5.2 was used to verify the 3-dimensional program. All material input parameters were identical to those used for the 2-dimensional simulations and these are summarized in Table 5.1. The boundary conditions, initial conditions and sequential filling algorithm matched the 2-dimensional program. The 2-dimensional simplification to the geometry was not required, and therefore the drain was modelled as a single drain of equivalent cross-sectional area (25 m$^2$) located centrally along the base of one of the stope walls (Fig. 6.8).

The geometry of the stope used in the verification exercise is shown in Fig. 6.8 b. It is a 25 m wide 25 m deep, 150 m high stope with one drain of cross-sectional dimensions 5 m x 5 m, located centrally along the base of one of the stope walls. The Isaacs and Carter program is not capable of modelling drain depth and therefore, the drain was placed flush with the stope wall for this verification exercise to maintain consistency between the 2-dimensional and 3-dimensional results.

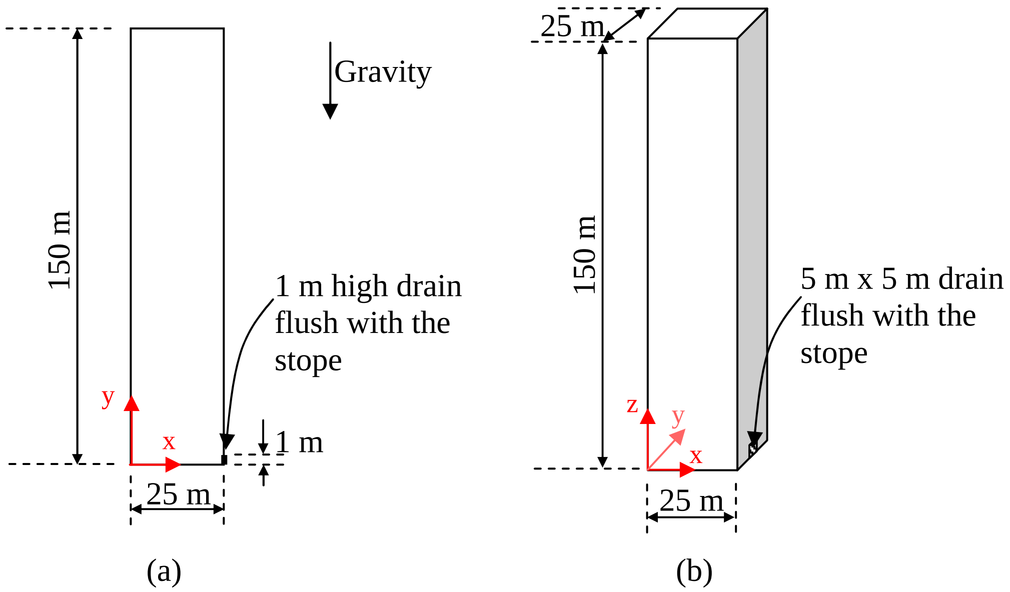


**FIG 6.8 - Verification geometry in (a) 2-dimensions, and (b) 3-dimensions**

As in the 2-dimensional simulation, this verification is based on a 12 hour filling followed by 12 hours resting schedule which is continued until the hydraulic fill reaches the height of the stope. No discharge calculations are done until the hydraulic fill height passes the height of the drain. Gravity is applied in the negative z-direction (Fig. 6.8 b).

Based on 3-dimensional scaling detailed in Section 6.2.3, the size of the model was reduced to speed solution time. The model was scaled down by 2.5 times and the grid mesh remained at 1 m spacing. An error is introduced by maintaining a 1 m grid spacing while scaling the stope, but it was found that adopting a finer mesh caused excessive solution times and therefore this error was considered acceptable. The 3-dimensional verification simulation was solved using the dimensions and input values detailed in Fig 6.9, and Table 6.2.

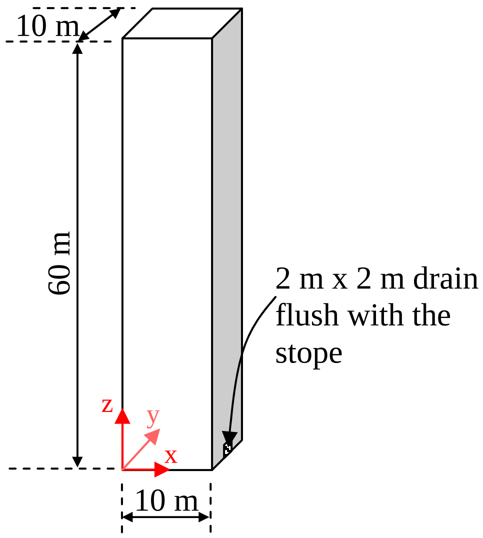


**FIG 6.9 - Scaled 3-dimensional stope geometry used in verification exercise**

**TABLE 6.2 - Input parameters for scaled verification simulation**

| Input | Value |
|---|---|
| Coefficient of permeability, $k$ | 0.0054 m/hr |
| Specific gravity, $G_s$ | 2.9 |
| Dry density of fill, $\rho_d$ | 1.4 t/m$^3$ |
| Residual water content, $w$ | 25 % |
| Percent solids of slurry placed | 72 % |
| Steady state time step | 1 hour |
| Solids filling rate | 16 t/hr |
| Filling cycle | 12 hrs filling, 12 hrs resting |

*Filling rate was scaled as $250/2.5^3$ = 16 t/hr

### 6.3.2 Numerical Model Verification

The *FLAC$^{3D}$* results for the fill and water levels, and discharge rates throughout the filling and resting (based on a 12 hour filling and 12 hour resting cycle) were compared to the results obtained from Isaacs and Carter and the *FLAC* program presented in Chapter 5, for the equivalent simulation. Computer solution time was significantly larger for the *FLAC$^{3D}$* analysis, and it took over a week to solve the verification exercise on an Intel Pentium(R) 4 2.0 GHz computer[19]. Although a 1 m grid spacing was adopted, due to the 2.5:1 scale used, this may be regarded as a 2.5 m grid spacing in all three directions for an unscaled full sized stope shown in Fig 6.8 b. The error introduced by this coarser mesh made an average difference of approximately 2% to the water mass balance over the entire 1041 hours of filling and resting, compared to the Isaacs and Carter and *FLAC* programs with 0.03% and 0.07% respectively. Due to the lengthy solution times otherwise, this error was considered acceptable.

The results compared very well for the verification exercise. The water and fill heights during the first 100 hours of filling and resting (Fig. 6.10), are so closely matched that even when zoomed over a 24 hour period (inset in Fig. 6.10) the individual results are unable to be distinguished between the Isaacs and Carter program, the *FLAC* program and the *FLAC$^{3D}$* program.

To amplify the difference in results between the programs, the discharge rates through filling were observed. The discharge comparisons for the first 100 hours of filling and resting are plotted in Fig. 6.11. There is a distinct difference in discharge rate behaviour between the Isaacs and Carter program and both the *FLAC* and *FLAC$^{3D}$* simulations during the resting stages of each 24 hour period. The Isaacs and Carter program shows a pronounced 'tooth-like' pattern, with a noticeable decrease in discharge rate during the resting stages of the filling cycle. This difference is discussed in section 5.2.4. Due to the geometrical simplification required to model a single drain located centrally along one wall as a 2-dimensional problem, the drain is modelled as the full depth of the stope with sufficient height to give an equivalent cross-sectional area. With the drain area located more closely to the base and stretching the full depth of the stope, it would be expected that the 2-dimensional simulations would produce

[19] Several other small programs (e.g. Email, MS Office), were running simultaneously which would have slowed solution time.

slightly higher discharge rates than the 3-dimensional simulation which is shown here (Fig. 6.11).

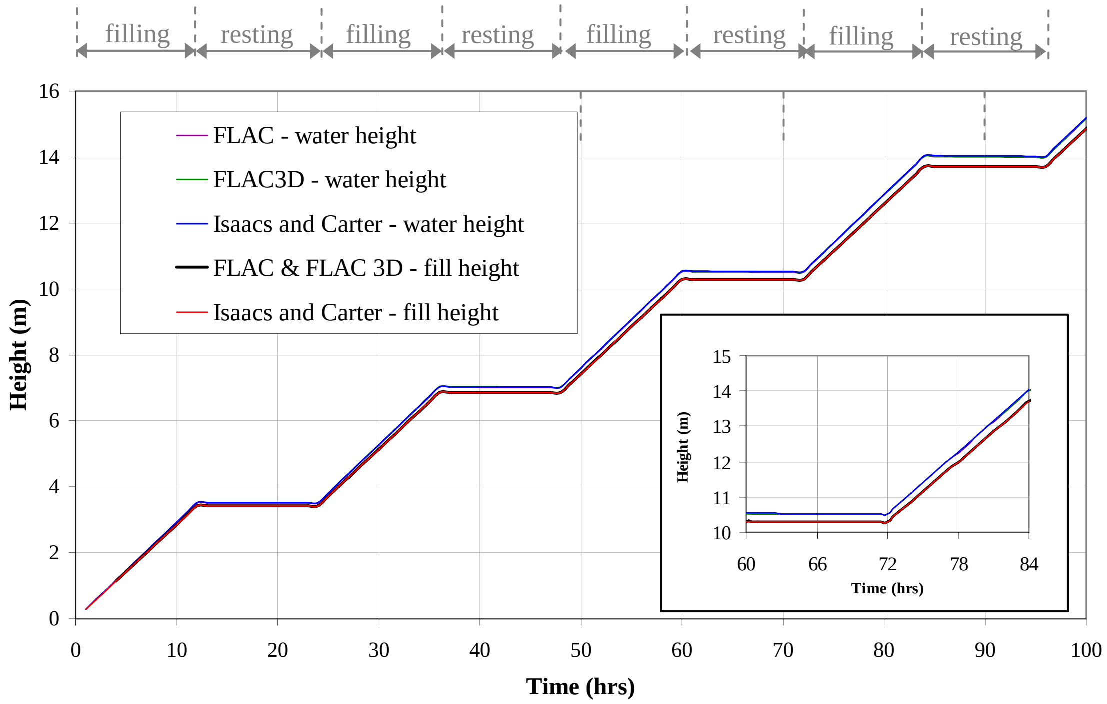


**FIG 6.10 - Fill and water height comparison between Isaacs and Carter, *FLAC* and *FLAC*$^{3D}$ for the verification simulation**

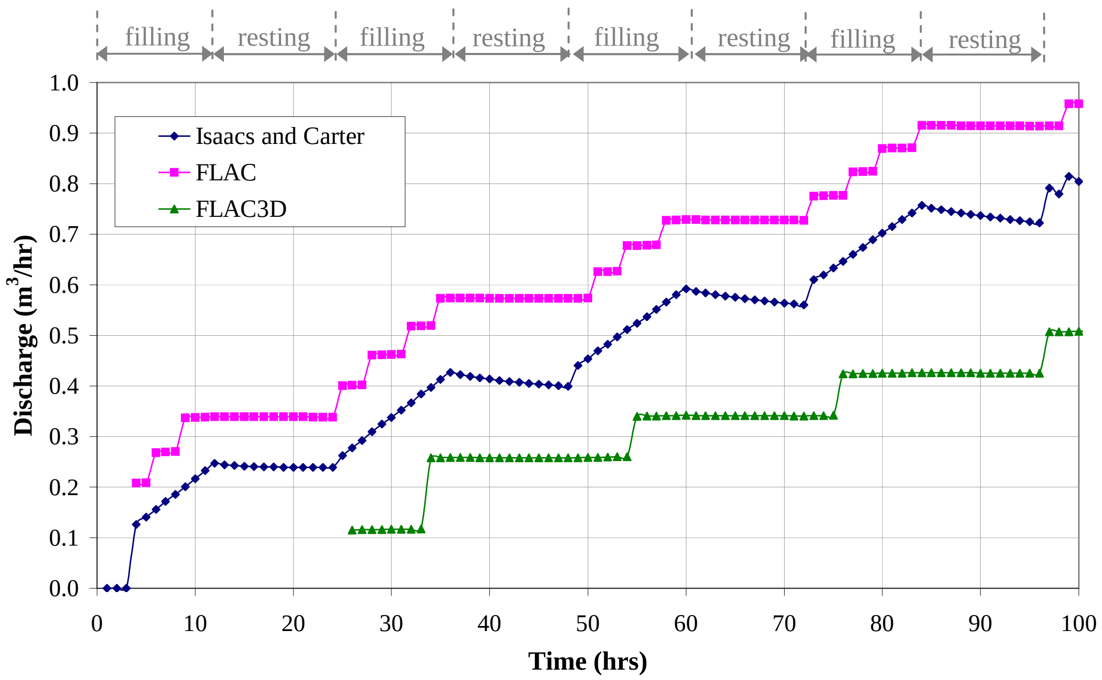


**FIG 6.11 - Discharge rate comparison between Isaacs and Carter, *FLAC* and *FLAC*$^{3D}$ for the verification simulation**

## 6.4 Three-Dimensional Filling and Drainage Analysis for Hydraulic Fill Stopes

Three-dimensional modelling using the *FLAC*$^{3D}$ stope filling program described and verified in section 6.3 has been used to investigate the effects of fill permeability, specific gravity, solids content and residual moisture content on the drainage of stopes. Due to extremely lengthy solution times and the large range of stope and drain dimensions, a steady-state *FLAC*$^{3D}$ analysis was used to analyse the effect of geometrical variation on drainage, and the results used to develop non-dimensionalized charts for drainage and maximum pore pressure within the stope over a range of typical stope geometries. The steady-state programs used to develop the charts modelled the water height at or less than the height of the fill (i.e., no decant water). Disregarding discharge, which often represents only a small proportion of the water being accounted for, simple phase relations can be used to determine the fill and water heights for a particular filling schedule, provided the material properties such as specific gravity, porosity of a settled fill and slurry water content are known.

### 6.4.1 Permeability

The permeability of hydraulic fill has a significant influence on the rate at which the excess water is removed from a stope (Lamos, 1993). There is a common rule-of-thumb specification accepted throughout the industry which states that the permeability of hydraulic fill must not be less than 100 mm/hr, to ensure effective drainage of a stope (Nantel, 1998; Cowling, 1998; Keren and Kainian, 1983). Through significant laboratory testing, for which the results are presented in Chapter 3, it has been found that the percolation rates for many Australian hydraulic fills fall well below this threshold value, and yet these operations have function satisfactorily for many years. Soil mechanics can, and has been used in the mining industry to quantify an lower limit for the permeability constant of a specific fill which may be used to ensure adequate stope drainage (www.mininglife.com). The following section discusses the current approach to determining this limiting permeability value (which assumes a hydraulic gradient of one across the entire stope, and further discusses the limitations of this assumption by approximating the actual hydraulic gradient values within the stope using numerical modelling techcniques.

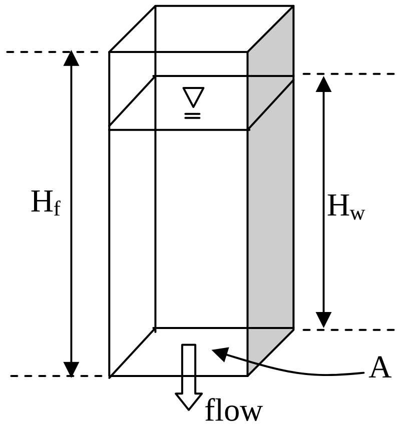


**FIG 6.12 - One-dimensional stope flow simplification**

By simplifying a stope into a 1-dimensional flow system with no decant water as shown in Fig. 6.12, where the cross-sectional area of the stope is $A$, the height of the fill is $H_f$ and the height of the water is $H_w$, the following relationships may be developed based on a fill porosity $n$, specific gravity $G_s$, fluid density $\rho_w$ and a slurry solids content, or pulp density of $C$ (in percentage).

Volume of fill ($V_f$) = $AH_f$

Volume of solids ($V_s$) = $AH_f(1-n)$

Mass of solids ($m_s$) = $AH_f(1-n)G_s\rho_w$

Water content of slurry ($w$) = $\dfrac{(1-C)}{C}\times 100\%$

Mass of water entering the stope ($m_w$) = $AH_f(1-n)G_s\rho_w\left(\dfrac{1-C}{C}\right)$

Volume of water entering the stope ($V_w$) = $AH_f(1-n)G_s\left(\dfrac{1-C}{C}\right) = H_w An$

Therefore, if there is no drainage:

$$\frac{H_w}{H_f} = \left(\frac{1-C}{C}\right)G_s\left(\frac{1-n}{n}\right) \qquad \text{Eqn 6.11}$$

Often, under typical filling conditions the discharge from a stope filled with a typical hydraulic fill material represents only a very small proportion of the average water being accounted for each hour (i.e., the water entering and exiting the stope during the hour). If this is the case, operators may disregard discharge and use equation Eqn. 6.11

to predict fill and water heights throughout the filling of a stope. The equation is not valid after the stope has been filled and the water is draining from the stope whilst no further fill is entering the stope. If the permeability values are very large, and the water level falls below the height of the fill these equations are not as reliable in fill and water height prediction.

Denoting the vertical height gain in fill as *F* (m/hr) and the mass of solids poured into the stope per hour as $W_s$ (t/hr),

The volume of solid poured per hour ($V_s$) */hr* = $\dfrac{W_s}{G_s \rho_w}$

Thus, the fill height increases at the rate of *F* given by,

$$F = \frac{W_s}{G_s \rho_w A(1-n)} \qquad \text{Eqn. 6.12}$$

To ensure no increase in water level within the stope, the quantity of water entering the stope, must equal or be less than the volume of water that is drained from the stope. Thus knowing, $v = ki_{entry}$, the quantity of water drained per hour is given by:

$$Q = vA = ki_{entry} A$$

Quantity of water entering the stope every hour is:

$$\frac{W_s}{\rho}\left(\frac{1-C}{C}\right) \qquad \text{Eqn. 6.13}$$

To ensure no increase in water level within the stope during filling,

$$kiA \geq \frac{W_s}{\rho_w}\left(\frac{1-C}{C}\right) \qquad \text{Eqn. 6.14}$$

In the past, a gravitational hydraulic gradient of 1 across the top of the stope has been assumed for underground hydraulic fill drainage analysis (www.mininglife.com). Substituting 1 for a hydraulic gradient at the top (entry) of the stope, and rearranging, Eqn. 6.14 becomes,

$$k \geq \frac{W_s}{A\rho_w}\left(\frac{1-C}{C}\right) \qquad \text{Eqn. 6.15}$$

This equation indicates that for certain stope, and fill conditions, a minimum permeability value may be specified such that effective drainage is maintained. For example, if a stope with cross-sectional dimensions of 50 m x 50 m, is filled at 200 t/hr with slurry of 75% solids content, the permeability must be greater than 26.7 mm/hr to ensure the water level does not rise.

For the 1-dimensional stope shown in Fig. 6.12, all streamlines are perfectly vertical and all equipotential lines are perfectly horizontal and therefore at all depths, the water velocity and the discharge are the same, and throughout the stope, the hydraulic gradient is 1. However, for both two and 3-dimensional analysis of stopes, where flow is constrained by the drain, the hydraulic gradient changes spacially, and therefore, Eqn. 6.15 is not valid.

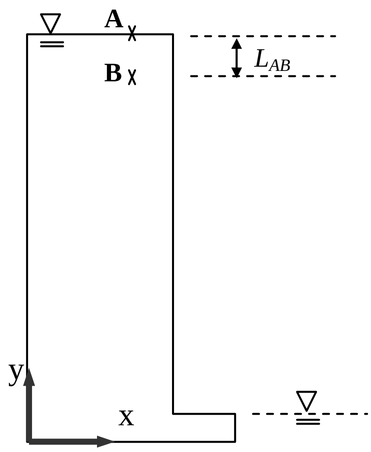


**FIG 6.13 – Two-dimensional stope**

The hydraulic gradient between points A and B (Fig. 6.13)is expressed as:

$$i_{AB} = \frac{TH_A - TH_B}{L_{AB}} = \frac{(EH_A + PH_A) - (EH_B + PH_B)}{L_{AB}}$$

$$i_{AB} = 1 + \frac{u_A - u_B}{\gamma_W L_{AB}}$$

where, *TH* denotes the total head which is the sum of the pressure head (*PH*) and the elevation head (*EH*), *u* is the pore pressure, $\gamma_w$ is the unit weight of water, and $L_{AB}$ is the length between points A and B. Therefore,

$$i_{AB} = 1 + \frac{1}{\gamma_w}\frac{\partial u}{\partial y} \qquad \text{Eqn. 6.16}$$

Because $\frac{\partial u}{\partial y}$ is negative, $i_{AB} \leq 1$.

The flow region within a 2-dimensional stope may be divided into three fragments, for which using method of fragments, form factors can be determined from the dimensions of the stope and drain (Sivakugan et al., 2005). The stope fragments are shown in Fig. 6.14. These fragments are bound by horizontal or vertical equipotential lines, shown by dashed lines in the figure. The assumption of equipotential line at the end of the drain being vertical implies that the pore water pressure distribution is linear, increasing from 0 at the top of the drain to $\gamma_w D$ at the bottom as in assumption 2, in Fig. 5.2. Where the stope and drain meet, the numerical simulations reveal that the equipotential lines are not strictly vertical, and that they are more closer to vertical a distance of 0.5$D$ or more away. The flow is approximately 1-dimensional within fragments 1 and 3, flowing vertically downward and horizontally respectively. Thus, the hydraulic gradients are constants within regions 1 and 3. For a typical hydraulic fill stope, the hydraulic gradient in fragment 1 will be considerably less than 1, and the hydraulic gradient in the drain will be much higher than 1. Using method of fragments calculations proposed by Sivakugan et al. (2005), for 2-dimensional stopes, the effect of stope and drain geometry on hydraulic gradient can be studied. Typical stope and drain geometry values and the respective hydraulic gradients for fragments 1 and 3 are recorded for 15 2-dimensional stopes in Table 6.3.

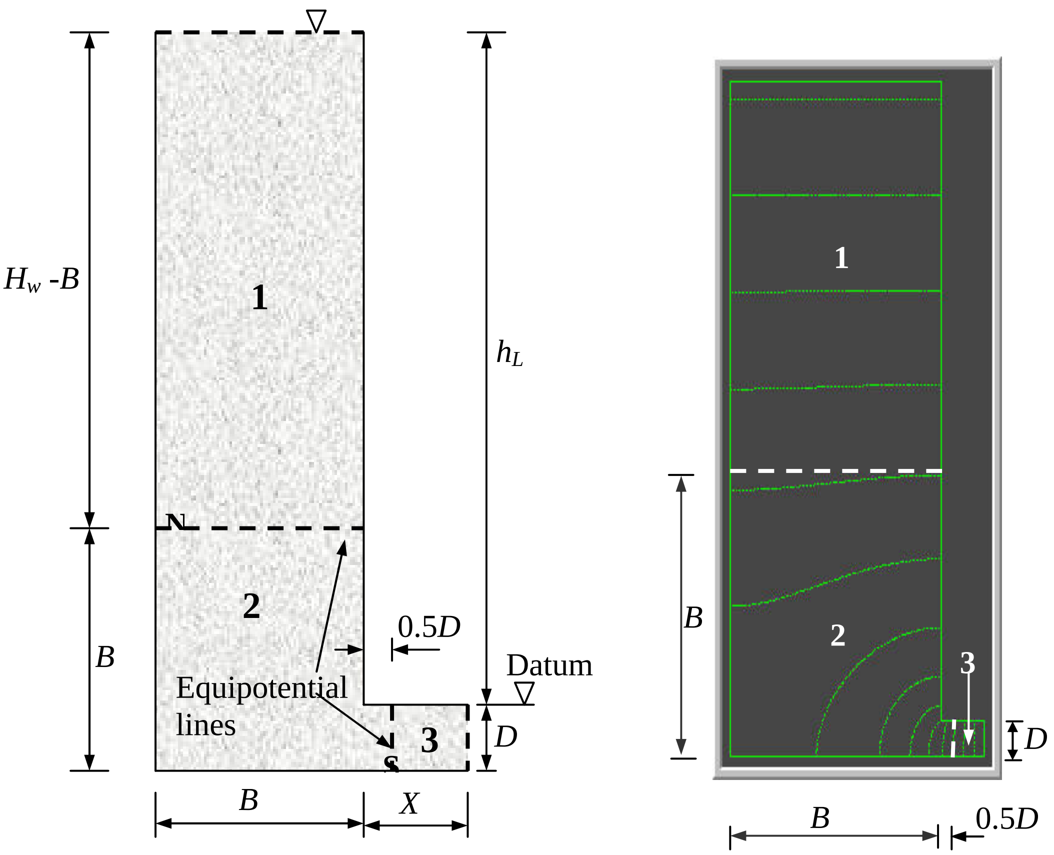


**FIG 6.14 - Equipotential lines and fragments for a typical 2-dimensional stope**

As shown for the 2-dimensional results presented in Table 6.3, the hydraulic gradient values within the upper region of the stope and within the drain vary considerably, depending on the dimensions. It can be shown that the hydraulic gradient at the top of the stope will always be less than one, and approaches one as the stope height approaches infinity. Quite obviously stope height is limited, and run #4 demonstrates that for some geometries even a 200 m high stope can have hydraulic gradient values at the top of the stope significantly less then one.

**TABLE 6.3 - Two-dimensional hydraulic gradient variation with stope geometry**

| **Run #** | ***B* (m)** | ***D* (m)** | ***X* (m)** | **$H_w$ (m)** | ***i* (top of stope)** | ***i* (at drain exit)** |
|---|---|---|---|---|---|---|
| 1 | 20 | 3 | 5 | 70 | 0.55 | 3.66 |
| 2 | 30 | 4 | 4 | 85 | 0.56 | 4.18 |
| 3 | 40 | 5 | 8 | 150 | 0.57 | 4.53 |
| 4 | 50 | 6 | 3 | 200 | 0.70 | 5.83 |
| 5 | 50 | 6 | 12 | 200 | 0.55 | 4.57 |
| 6 | 25 | 5 | 7 | 150 | 0.71 | 3.56 |
| 7 | 30 | 4 | 6 | 125 | 0.60 | 4.53 |
| 8 | 40 | 4 | 8 | 80 | 0.37 | 3.65 |
| 9 | 20 | 3 | 5 | 50 | 0.46 | 3.07 |
| 10 | 50 | 5 | 8 | 150 | 0.50 | 5.00 |
| 11 | 60 | 5 | 9 | 120 | 0.38 | 4.50 |
| 12 | 35 | 3 | 4 | 90 | 0.48 | 5.58 |
| 13 | 100 | 6 | 10 | 120 | 0.26 | 4.34 |
| 14 | 100 | 6 | 4 | 120 | 0.34 | 5.63 |
| 15 | 20 | 4 | 8 | 150 | 0.71 | 3.56 |

Because the hydraulic gradient is less than 1 at the top of the stope, Eqn. 6.15 will underestimate the permeability required to prevent increase in water height. Run No. 6 in Table 6.3 shows that even with a height of 6B which for engineering purposes is approaching the extreme height to width dimensions practically used in a mine, the hydraulic gradient for a 2-dimensional analysis is still only 0.71.

The hydraulic gradient at both the top of the stope, and at the drain exit may also be simply obtained for any steady state stope condition using 3-dimensional numerical modelling. Using these hydraulic gradient values obtained through 3-dimensional modelling in *FLAC*$^{3D}$ in equation 6.14, the individual stope permeability required to prevent increase in water height can be determined more realistically. The hydraulic gradient at the top of the stope and at the drain exit calculated using the *FLAC*$^{3D}$ model are shown in Table 6.4, and an example of the design charts developed using Eqn. 6.14 is given in Fig. 6.15 for stope with base dimensions of 20 m x 20 m, and a 4 m long drain of cross-sectional dimensions 4 m x 4 m located centrally along the base of one of the stope walls. The plot provides minimum fill permeability values required for the water level to cease raising, based on the solids content of the slurry being placed at 200 t/hr solids.

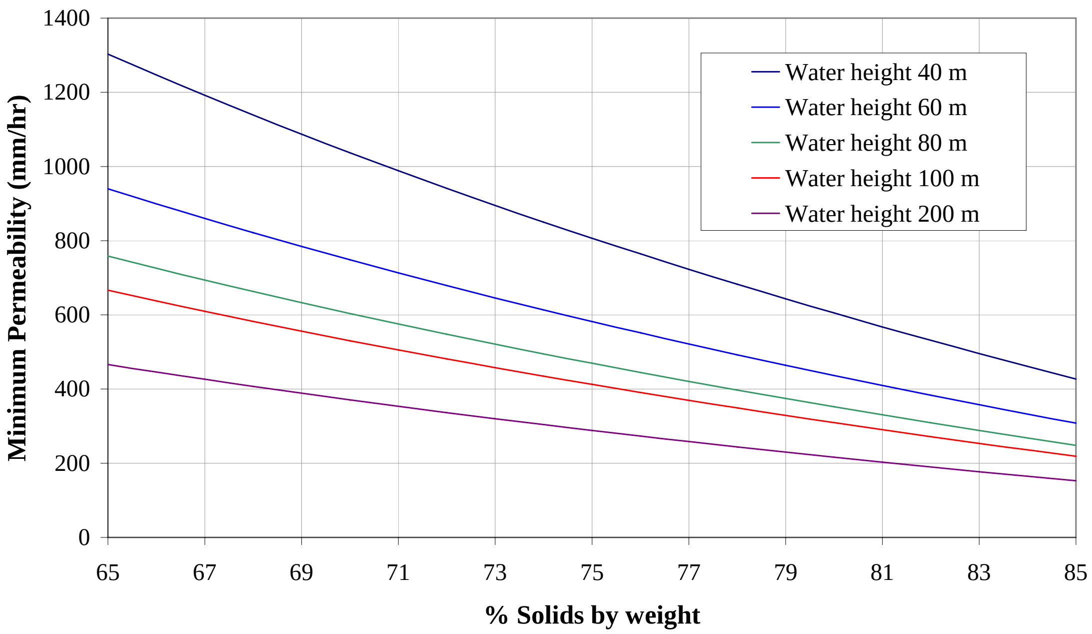


**FIG 6.15 - Minimum permeability requirements to prevent rise in water level in the stope**

The design chart shown in Fig. 6.15 is stope specific, and because it determines the minimum permeability to prevent any rise in water level for individual filling rates, it is excessively conservative. As described in Chapter 5, a small decant on the surface of the fill does not substantially effect the discharge rates or pore pressures, and it is expected that the water level will rise at least as rapidly as the fill level rises. These permeability values are the largest permeabilities required to prevent the water level from rising (i.e., all water that enters the stope exits the stope), and are therefore the upper bound.

**TABLE 6.4 - Three-dimensional hydraulic gradient variation with stope geometry**

| Run # | $B$ (m) | $D$ (m) | $X$ (m) | $H_w$ (m) | $i_{\text{(top of stope)}}$ | $i_{\text{(at drain exit)}}$ |
|---|---|---|---|---|---|---|
| 1 | 20 | 4 | 4 | 40 | 0.21 | 6.27 |
| 2 | 20 | 4 | 4 | 60 | 0.29 | 8.19 |
| 3 | 20 | 4 | 4 | 80 | 0.35 | 9.76 |
| 4 | 20 | 4 | 4 | 100 | 0.40 | 11.08 |
| 5 | 20 | 4 | 4 | 200 | 0.58 | 15.36 |
| 6 | 20 | 4 | 6 | 40 | 0.16 | 5.24 |
| 7 | 20 | 4 | 8 | 40 | 0.13 | 4.52 |
| 8 | 20 | 2 | 2 | 40 | 0.12 | 12.17 |
| 9 | 20 | 2 | 4 | 40 | 0.07 | 8.11 |
| 10 | 20 | 2 | 8 | 40 | 0.04 | 4.95 |
| 11 | 20 | 4 | 8 | 150 | 0.38 | 10.59 |

By calculating the variation in hydraulic gradient at the top of the stope, with increased water height for the 3-dimensional case (Table 6.4), we can see that for typical stope geometries where the $H_w/B$ ratio would be considerably less than 10, the hydraulic gradient is well below 1. As expected, when compared to the 2-dimensinoal calculations (Fig. 6.16) the variation of hydraulic gradient at the top of the stope is similar in trend (i.e., hydraulic gradient increasing with water height), but even lower in value in the case of 3-dimensional stopes of similar $H_w/B$ ratio.

Parametric studies undertaken in both 2 and 3-dimensions have shown that the hydraulic gradient throughout the stope is considerably sensitive to the stope and drain dimensions. Fig. 6.16 plots an example of this where the hydraulic gradient at the top of the stope is plotted against the stope height for a 20 m wide 2-dimensional stope and a 20 m x 20 m 3-dimensional stope. The 3-dimensional stope has a 4 m long 4 m x 4 m drain at the middle of the stope base. The 2-dimensional stope has a 4 m long and 1 m high drain. The difference in drain cross-sectional area of 4 m$^2$ (the 2-dimensional stope drain has a cross-sectional drain are of 20 m$^2$ and the 3-dimensional stope has a drain with 16 m$^2$) will have a small effect and the relative difference would be slightly larger had the simulations been done with identical drain cross-sectional areas.

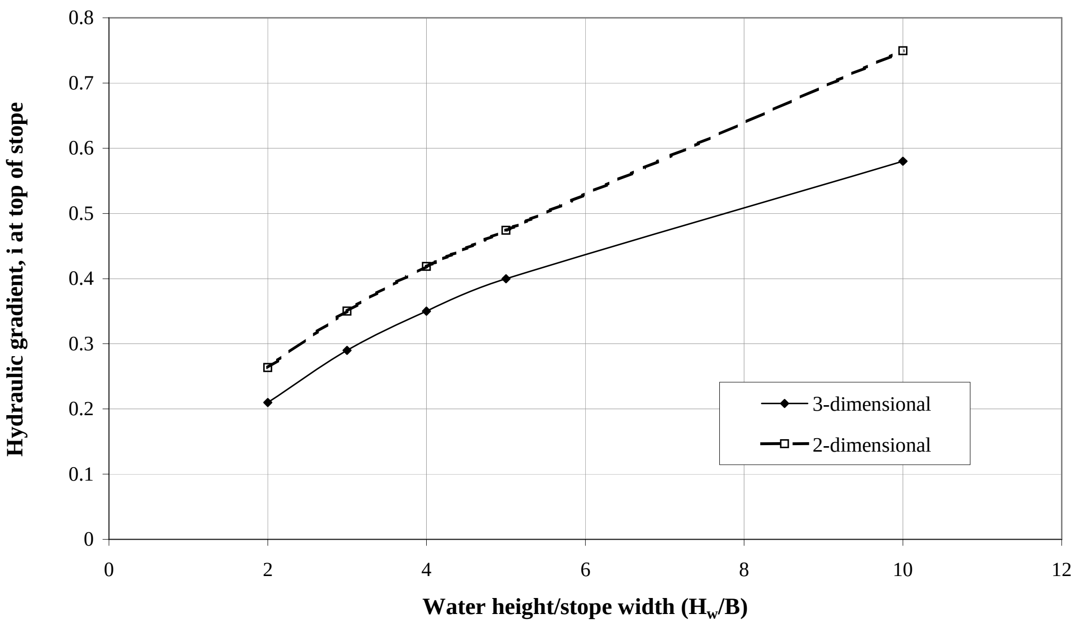


**FIG 6.16 - Variation of hydraulic gradient at the top of the stope height for 2-dimensional and 3-dimensional stopes**

## 6.4.2 Specific Gravity

Chapter 3 (section 3.5) details the linear relationship developed between the dry density of the settled fill and the specific gravity of the hydraulic fill soil grains. Having stopes filled at a particular solids content, and dry density directly proportional to specific gravity implies that the specific gravity will have a significant influence on fill and water heights during the filling of a stope, and in turn influence on discharge rates and maximum pore pressure values. As mentioned earlier, the specific gravity values of hydraulic fills range considerably and for over 15 Australian fills tested in Chapter 3, the average values fell between 2.77 and 4.35. To study the sensitivity of the stope filling process to variation in specific gravity, the verification stope filling problem described in section 6.3.2 was solved for three separate specific gravity values that cover the range within which Australian hydraulic fills typically fall. The simulations are based on continuous filling with no rest periods to speed solution time. Although this research found fill material C1 to have the maximum specific gravity value of 4.35 (Table 3.3) the value 4.33 was used as the upper limit because the mine from which this material was sourced commonly bases its calculations on this value. The properties of a specific fill are dependent on the parent ore of the tailings and so it is expected that the specific gravity of a particular fill will vary slightly over time. The lower limit of 2.77 (fill B2 from Table 3.3) and a central value of 3.5 were also used in simulations.

Fig. 6.17 shows the fill and water heights during the first 100 hours of filling for the verification problem described in section 6.3.2, solved with specific gravity values of 2.77, 3.50 and 4.33. The simulations take different lengths of time to fill due to the varying specific gravity values, and therefore all simulations were allowed to solve to 100 hours of filling so that trends in fill and water heights and discharge rates could be observed. There was decant water (i.e., the water level fell above the height of the fill material) throughout the filling for all three simulations. The rise in decant height relative to fill height with time increases with specific gravity (Fig. 6.17).

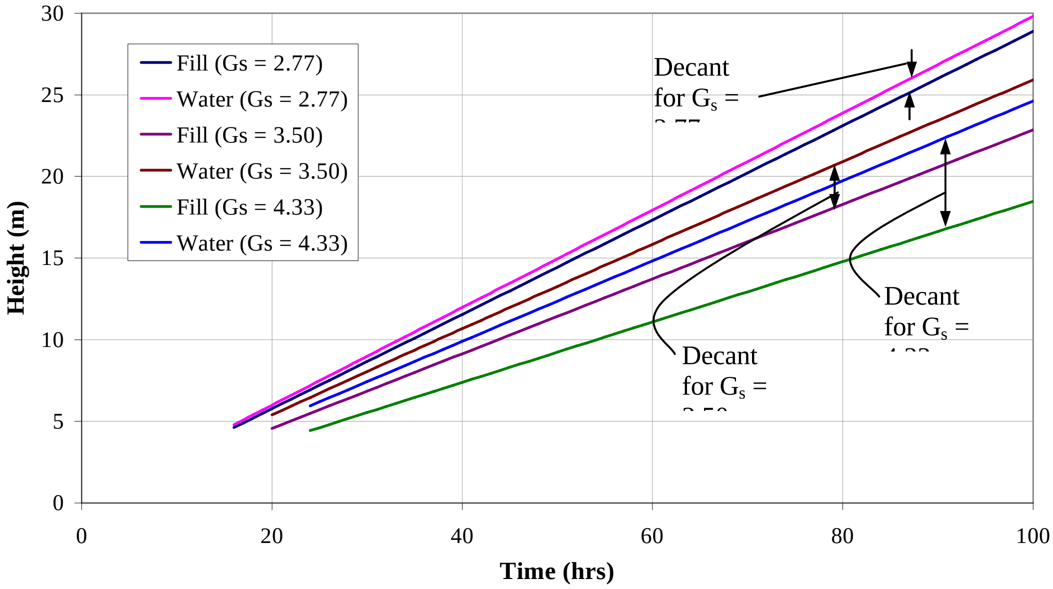


**FIG 6.17 - Fill and water height comparison between simulations filled with fills of various specific gravity values**

The discharge rates do not vary significantly between the three simulations (Fig 6.18). The exaggerated 'step-like' behaviour observed in Fig. 6.18 is a result of the program rounding water levels to the nearest zone and the mesh being relatively coarser than the 1 m grid due to the scaling. Had a finer mesh been used the curve would appear smoother.

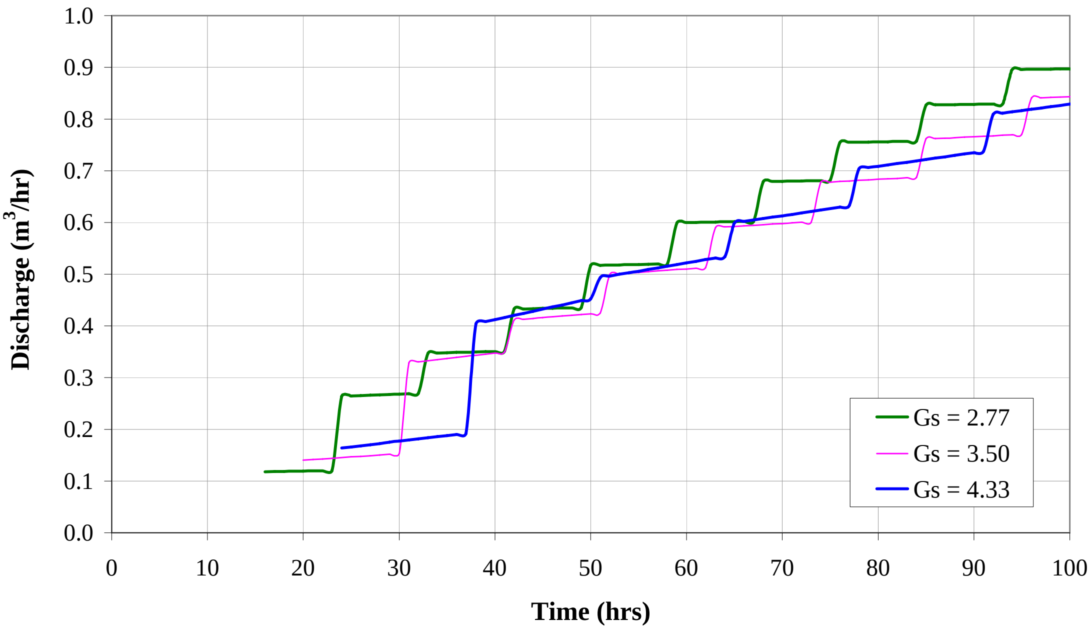


**FIG 6.18 - Discharge comparison between simulations filled with fills of various specific gravity values**

As expected, the fill height for the simulations using a specific gravity value of 4.33, increases the most slowly at 115.5 $m^3$/hr. At any given time, the decant height increases with increased specific gravity. There is significant difference between the rates at which the fill and water levels rise with the variation in specific gravity. By applying simple geomechanics the volumes of solids and water placed each hour may be calculated and for this example are shown in Table 6.5. By presenting the discharge rate at hour 100 as a percentage of the total water placed that hour (Table 6.5) it becomes very obvious that as was typically the case in Chapter 5, the discharge represents only a very small proportion of the total water accounted for during that hour. In this example, the discharge corresponds to less than 1% for each of the specific gravity simulations at this time.

**TABLE 6.5 - Water mass balance details for verification problem at hour 100 solved with specific gravities of 2.77, 3.50 and 4.33**

| Specific gravity ($G_s$) | Volume placed per hour ($m^3$/hr) | | Discharge rate ($m^3$/hr) | Discharge rate as a percentage of volume of water placed (%) | Decant water ($m^3$/hr) | Decant water disregarding discharge ($m^3$/hr) |
|---|---|---|---|---|---|---|
| | solids | water | | | | |
| 2.77 | 180.5 | 97.2 | 0.90 | 0.93 | 6.1 | 7.0 |
| 3.50 | 142.9 | 97.2 | 0.84 | 0.86 | 25.0 | 25.8 |
| 4.33 | 115.5 | 97.2 | 0.83 | 0.85 | 38.7 | 39.5 |

It is suggested that to obtain a rough (and conservative) estimate of fill and water heights operators may simply perform a specific gravity test and apply phase relations, disregarding discharge. Provided the discharge only represents a very small proportion of the water accounted for in a stope over an hour (which is particularly the case for fills with permeabilities down the lower end of the typical range) it would be acceptable to disregard the discharge volume when performing preliminary checks. This will provide the operators with a first glance appreciation for the relative build-up of decant expected for their material. Then through permeability testing, combined with the numerical modelling a more accurate prediction may be obtained.

### 6.4.3 Solids Content

For optimal economic advantage, stopes should be filled with a slurry at a solids (or water) content which maximises solid waste disposal, minimises the quantity of water requiring removal, while still being sufficiently moist to meet rheological requirements. If the fill is pumped at too high a solids content, the mine runs the risk of extreme costs and schedule delays associated with clogged pipes. If the slurry pumped has too low a solids content there will be time delays associated with draining the excess water so that the pore pressures don't exceed allowable limits. Each fill material has a specific optimum solids (or water) content for which the slurry best meets the balance between maximised solids disposal and minimised water added.

Using the continuously filled stope filling program discussed in section 6.3.2, and varying the solids content with which the slurry is placed, the effect on water heights, discharge rates and maximum pore pressures within the stope may be observed. Fig. 6.19 shows the water heights for the various solids content simulations relative to the fill height during the first 100 hours of filling. As mentioned in section 6.3.2, the simulations were based on a 25 m x 25 m square based stope with a 5 m x 5 m drain located centrally along the base of one of the walls. The permeability ($k$) of the fill was 5.4 x $10^{-3}$ m/hr, the dry density ($\rho_d$) of the fill was half the specific gravity, residual water content ($w_{res}$) was 25%, specific gravity ($G_s$) was 2.9, and the filling rate was scaled from a full sized stope filled at 250 t/hr.

As would be expected, increasing the solids content decreases the excess water requiring removal. For this example, the simulations filled at both 70% and 72% solids content had decant water throughout the entire filling of the stope, and the water level was below the fill height throughout filling for the simulation solved with 75% solids content.

Comparing Figs. 6.19, 6.20 and 6.21, we can see that for the 70% solids content simulation with the highest water level, the discharge rates and maximum pore pressures are also the highest at a specific time, simply because more water has entered the stope. The 72% solids content simulation with a slightly lower water level throughout, has a marginally lower discharge behaviour and marginally lower maximum pore pressures. The significantly lower water level for the 75% solids content simulation produced a lower discharge rates and significantly lower maximum pore pressures. At 100 hours, the water level difference between the stopes filled at 70% solids content and 75% solids content is over 7 m, which only produces a difference of 0.2 $m^3$/hr discharge (Fig. 6.20) and approximately 50 kPa difference in maximum pore pressures (Fig. 6.21). The pronounced ‘step-like’ pattern observed in Figs. 6.20 and 6.21 is due to the program rounding water levels to the nearest zone and the mesh being relatively coarser than the 1 m grid due to the scaling. As was the case for Fig. 6.18, had a finer modelling mesh been used the curve would appear smoother in both of these plots.

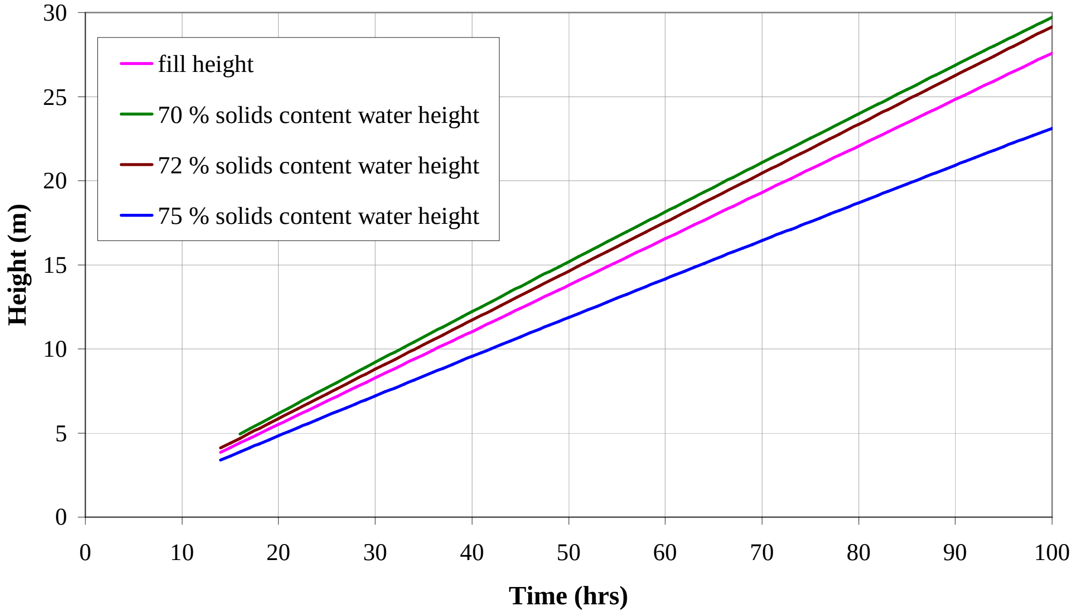


**FIG 6.19 - Fill and water height comparison between verification simulations filled at various solids contents**

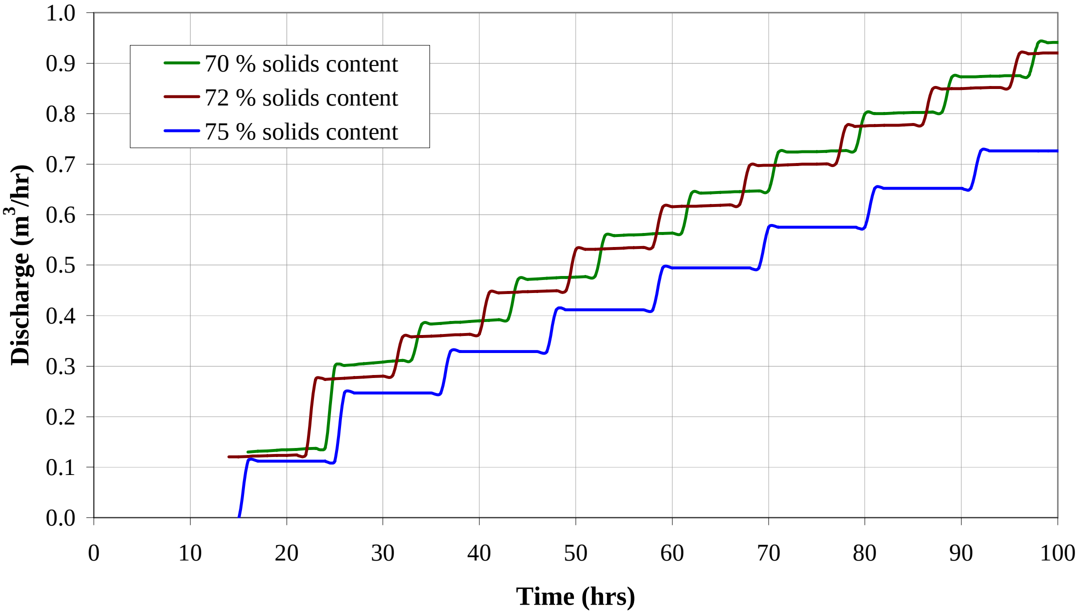


**FIG 6.20 - Discharge rate comparison between verification simulations filled at various solids contents**

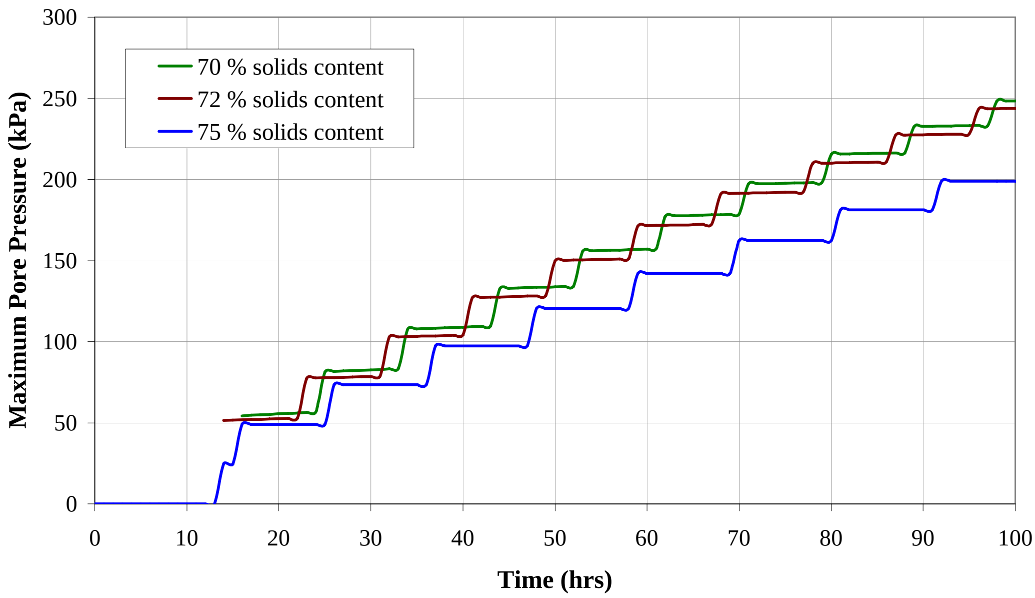


**FIG 6.21 - Maximum pore pressure comparison between verification simulations filled at various solids contents**

**TABLE 6.6 - Water balance details for verification problem at hours 100 and 545 solved with solids contents of 70%, 72% and 75%**

| Solids content (%) | Volume placed per hour ($m^3$/hr) | | Discharge rate ($m^3$/hr) | | Discharge rate as a percentage of volume of water placed (%) | |
|---|---|---|---|---|---|---|
| | solids | water | hour 100 | hour 545$_{\text{(stope full)}}$ max discharge | hour 100 | hour 545$_{\text{(stope full)}}$ max discharge |
| 70 | 178.6 | 107.1 | 0.94 | 2.33 | 0.88 | 2.17 |
| 72 | 178.6 | 97.2 | 0.92 | 2.21 | 0.95 | 2.27 |
| 75 | 178.6 | 83.3 | 0.73 | 1.99 | 0.88 | 2.39 |

Table 6.6 details the fill and water filling and discharge rates at hour 100, and at hour 545 (the point in which the stope was completely full and at maximum discharge rate and maximum pore pressure) for 70%, 72% and 75% solids content fill mixes placed in the verification stope (section 6.3.2). Like the verification problem these simulations were based on a 250 t/hr solids filling rate for a material with dry density of 1.4 t/m$^3$. By presenting the discharge rate as a percentage of the water placed that hour, it reiterates the point made in section 6.4.2, that often the discharge represents only a very small proportion of the water accounted for each hour. At 100 hours, this is less than 1% and even at maximum discharge rate when the stope was completely

filled the quantity of water that exits the drain is merely a little over 2% for each of the cases. Because the discharge water represents only a very small proportion of the water being accounted for the importance of determining the optimal solids (or water content) with which the fill is placed is further emphasised.

### 6.4.4 Residual Water Content

In minefills with clay fraction and in rocks, not all the voids are available to conduct water. When clays are present, some water is held on to the clay particles in the form of adsorbed water, forming a skin around the particle. In rocks, there can be dead ends where the voids are not interconnected and when filled with water, they will not be part of the flow path. Such water is known as immobile water and cannot be freely drained. The rest of the water can be drained and is thus called mobile water.

In hydraulic fill stopes also, partly due to the large dimensions, there is significant amount of immobile water that will not be drained in engineering times. Measurements from two different mines, shown in Table 6.7, clearly illustrate this point. Total water that entered the stope, the water that has drained till the drainage has completely stopped, and the remaining water for two different mines are given. Stope 1 is a cemented aggregate fill stope, and Stope 2 is a hydraulic fill stope. Residual water content is the water content of the fill when the drainage has stopped, and this accounts for 29% and 20% for the two mines in Table 6.7.

**TABLE 6.7 - Mass balance of water in two stopes**

| Stope | Total solids (t) | Total water in (t) | Water drained (t) | Remaining water (t) | Residual water content (%) |
|---|---|---|---|---|---|
| Stope 1 | 49200 | 20830 | 6554 | 14276 | 29 |
| Stope 2 | 201900 | 54000 | 12650 | 41350 | 20 |

The residual water content has a marked influence on the time required for the stope to fully drain. Using *FLAC*$^{3D}$ simulations, the difference in post filling water heights and with time are shown in Fig. 6.22 for five different assumed residual water contents. The post filling drainage starts at hour 1021 with both the fill and water heights at 150

m. The simulations were based on a 25 m x 25 m square based stope with a 5 m x 5 m drain located centrally along the base of one of the walls. The permeability ($k$) of the fill was 5.4 x $10^{-3}$ m/hr.

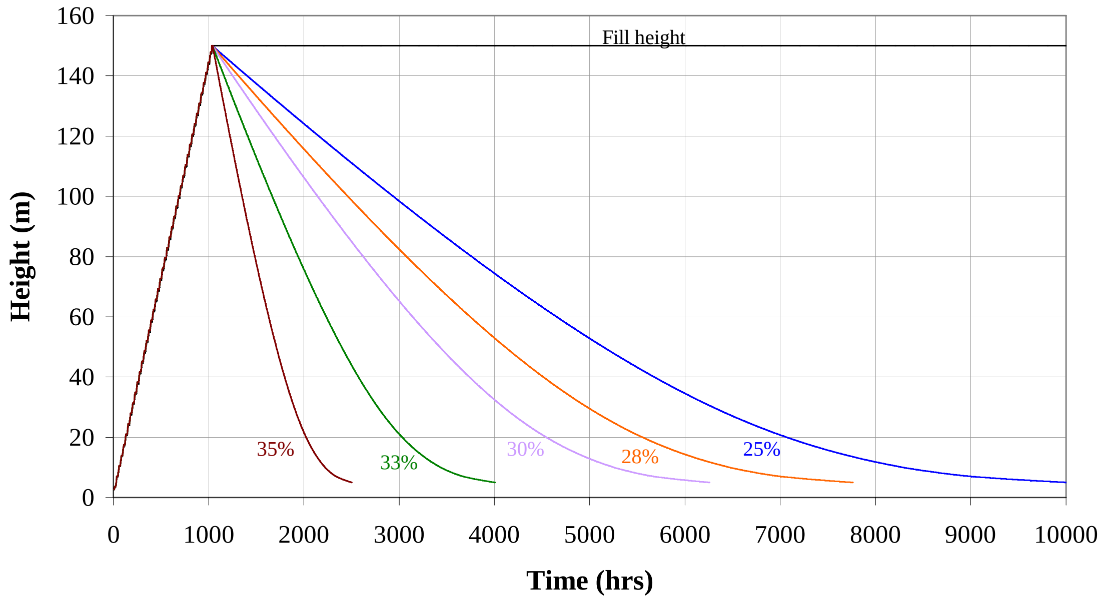


**FIG 6.22 - *FLAC*$^{3D}$ simulations of filling and draining a 25 m x 25 m x 150 m stope for various residual moisture content hydraulic fills**

In modelling hydraulic fill drainage, it is important to understand effective porosity ($n_{eff}$) that represents the void that are effectively available to conduct water. The effective porosity is defined in Chapter 5, by Eqn. 5.5 as:

$$n_{eff} = n - \frac{w_{res} G_s}{1+e}$$

Any modelling exercise should give due consideration to the residual water content and should attempt only to model the flow of drainable water and not the whole water that enters the stope. While draining, only the voids accounted for through effective porosity will be effective in conducting the water. The rest of the voids are occupied by the immobile residual water and do not form a part in the flow path. Therefore, it is necessary to assume a realistic value for the residual water content in such computations. Using a reasonable range for residual water content (based on fill history) these programs (Appendix 4, Program A4.1) may be used to provide a prediction for drainage time required to completely remove all free water from the stope so that adjacent works may commence. This will provide a very valuable tool to assist with mine operations.

### 6.4.5 Geometry

Due to the inherent individuality associated with a stope, size and geometry, as well as drive size, numbers, and location may vary considerably. Chapter 5 shows that the majority of discharge from a stope exits the base drains, and therefore only base drain arrangement is analysed in this work. Four typical drain positions are considered in this research, as inferences from data obtained from these arrangements may be made to determine the majority of typical base drain arrangements. The plan view of these four cases is given in Fig. 6.23. The lines of symmetry used in computational analysis, are shown as dashed lines.

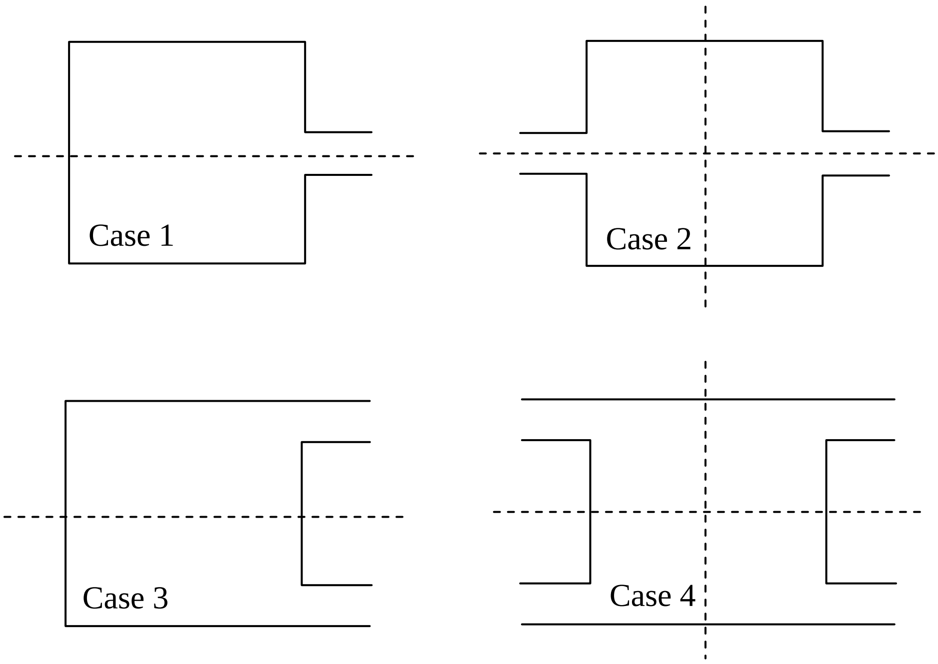


**FIG 6.23 - Plan view of four drain location cases analysed**

There are an infinite number of possible stope and drain geometry and size combinations, and therefore only a few typical arrangements and dimensions have been studied. This research investigates square based stopes. It should be noted, that because of the symmetry between some geometrical configurations, these results may be used to provide discharge and pore pressure predictions for other stope arrangements that have a ratio of width to depth of 2:1. Due to symmetry, Fig. 6.24 (a) would have half the total discharge of Fig. 6.24 (b), with each of the individual drains having identical discharge. The maximum pore water pressure values would be the same for both (a) and (b) in Fig. 6.24.

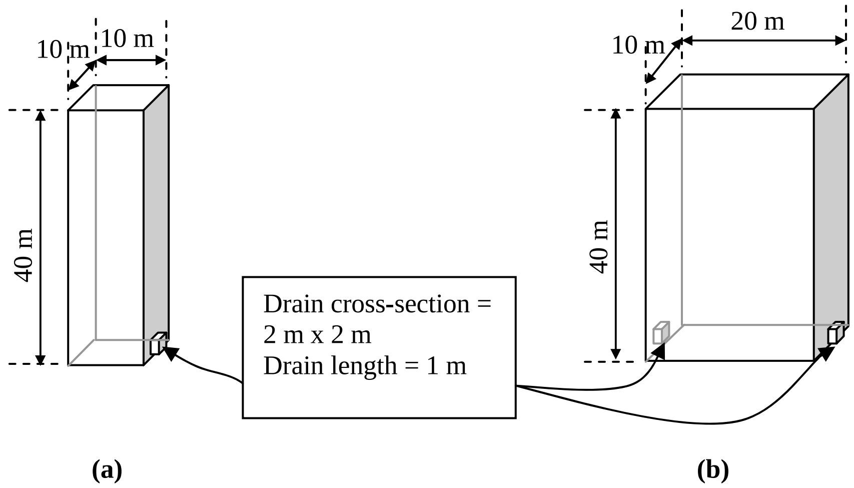


**FIG 6.24 - Example Case 1 and Case 2 simulations for stope width to depth ratios of 1:1 and 2:1 respectively**

To reduce the number of geometrical parameters studied, this research is based solely on square based stopes with square drains. The stope width and depth, drain length, drain width and height and height of water within the fill in Fig. 6.25 are denoted by $B$, $X$, $D$ and $H_w$, respectively. Several runs were made using $FLAC^{3D}$ for various combinations of typical values for $B$, $X$, $D$ and $H_w$, and for each run the flow rate ($Q$) and maximum pore water pressure within the fill ($u_{max}$) were computed. The values of $Q$ and $u_{max}$ computed were used to develop charts such that approximate solutions for these two parameters may be obtained for a range of typical geometries. Since the deslimed hydraulic fills are granular, they consolidate quickly and the excess pore water pressure is assumed to dissipate immediately upon placement. As was the case for the 2-dimensional model, the $FLAC^{3D}$ numerical model is solved as a flow-only problem, where the soil mass acts as an incompressible skeleton.

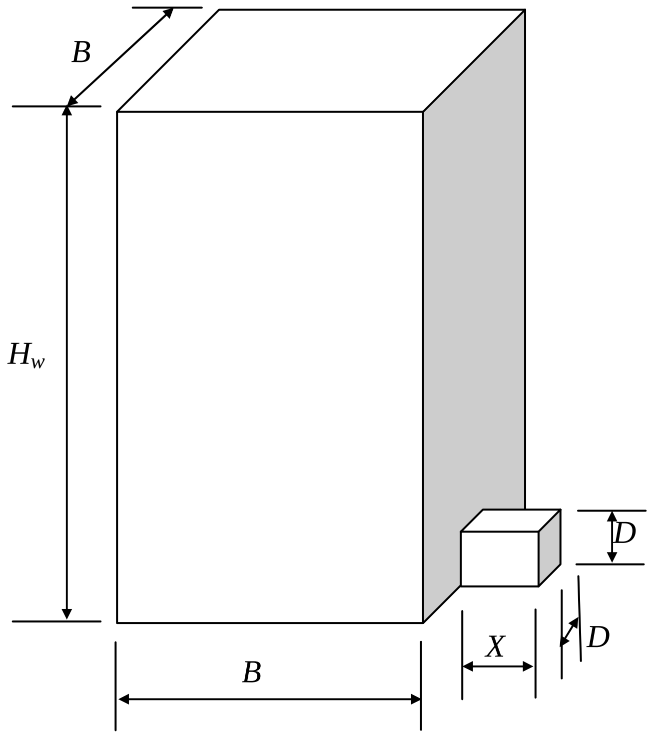


**FIG 6.25 – Geometrical variables for 3-dimensional Case 1 stope**

The effect of stope dimensions on discharge from the square based stopes studied in this research is best presented by non-dimensionalizing the results such that the data may be presented in the form of charts for each of the geometrical cases 1 through 4. From these charts, a user is able to determine the discharge rate and maximum pore pressure values for stopes scaled from the ones used to develop the charts. The charts are all based on filling cases in which the water height was equal to or less than the height of the fill (i.e., no decant). The effect of geometry on flow rate and pore pressure are described below using the design charts.

Flow Rate

Sivakugan et al. (2005) represented the discharge from a 2-dimensional stope using the dimensionless parameter $kh_L/Q$, where $k$, $h_L$ and $Q$ are the permeability, head loss across the hydraulic fill stope, and the flow rate. This parameter ($kh_L/Q$) is referred to (Harr 1962, 1977) as the form factor Φ, and is used in the development of the method of fragments. The dimensionless parameter $kh_L/Q$ is simply the ratio of the number of equipotential lines to the number of flow lines. It can be stated that:

$$\Phi = \frac{kh_L}{Q} = f\left(\frac{X}{D}, \frac{D}{B}, \frac{H_w}{B}\right) \qquad \text{Eqn. 6.15}$$

The relationship of $\Phi$ to $X/D$, $D/B$ and $H_w/B$ may be presented graphically using modelling results to give a broad overview of the effects of various dimensions on the form factor and discharge throughout the drain.

In 3-dimensions, flow rate will be represented by the dimensionless parameter $k(h_L)^2/Q$, where $k$, $h_L$ and $Q$ are the permeability, head loss across the hydraulic fill stope, and the flow rate ($m^3$/hr). As presented in section 6.2.2, when considering 3-dimensional scaling effects, scaling the stope dimensions by x will scale the discharge from the stope by $x^2$ (Eqn. 6.9).

The relationship between the parameter $k(h_L)^2/Q$, to $X/D$, $D/B$ and $H_w/B$ for each of the drain arrangement cases are presented in Figs. 6.26 through to 6.29, for $X/D$ = 0, 1, 2 and $D/B$ = 0.2 and 0.3. These plots give a broad overview of the effects of various dimensions on the total discharge from the stope. For cases 2 and 3, $Q$ is the sum of the discharge from the two drains, and in case 4 $Q$ is the sum of discharge from all four drains. To consider the individual discharge for a case relative to another, $Q$ must be divided by the corresponding number of drains for each of the cases.

These flow design charts allow mine operators to easily obtain a simple approximation of the discharge for a given geometry stope, provided the stope geometry, water level and permeability of the placed hydraulic fill are known. Alternatively, if the discharge from an underground stope is being monitored, and the approximate stope geometry and permeability of the placed hydraulic fill are known the current water level within the stope may be approximated using these charts. These charts provide a simple approximation to mine drainage performance for typical stope geometries.

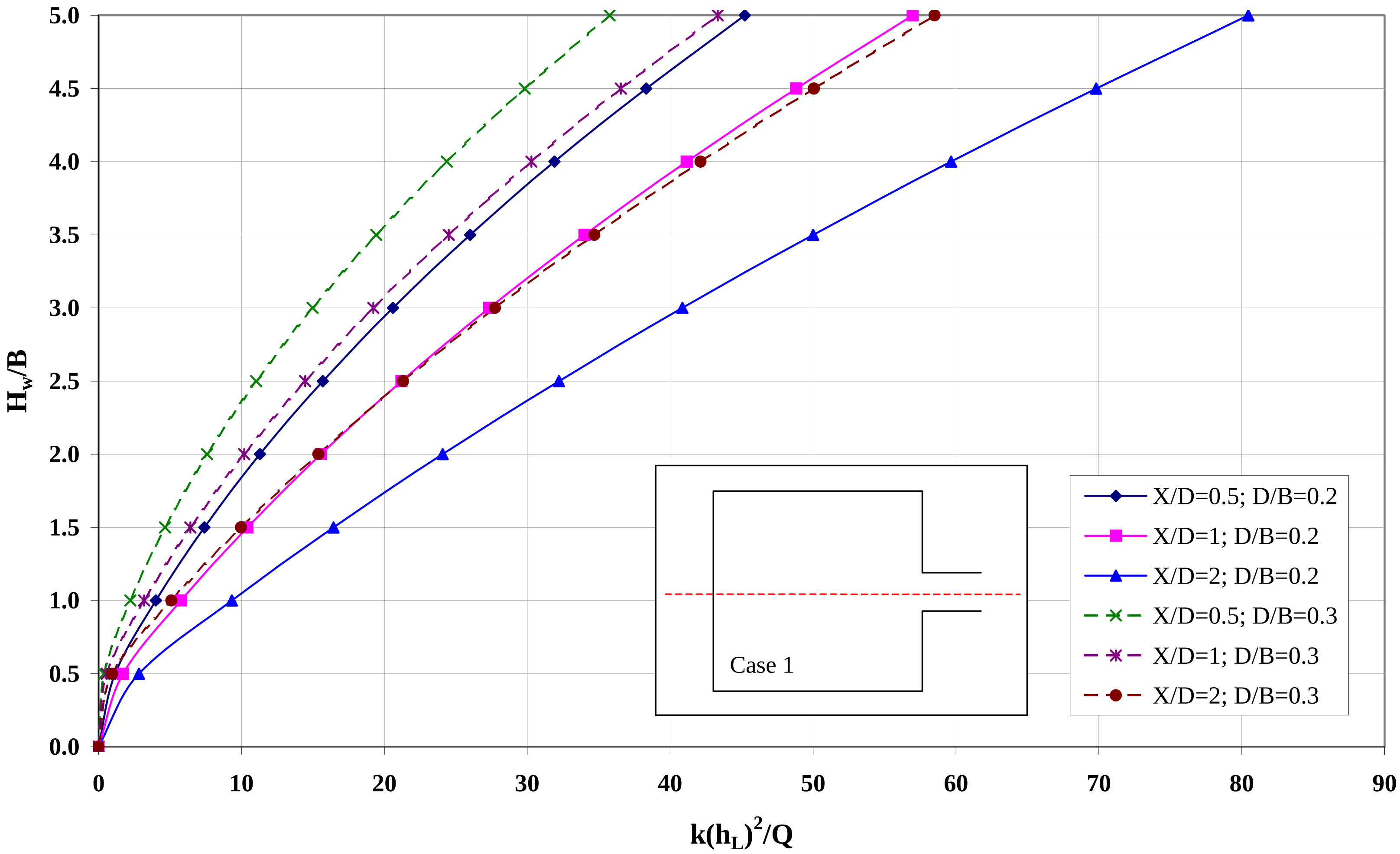


**FIG 6.26 - Three-dimensional total flow design chart for Case 1**

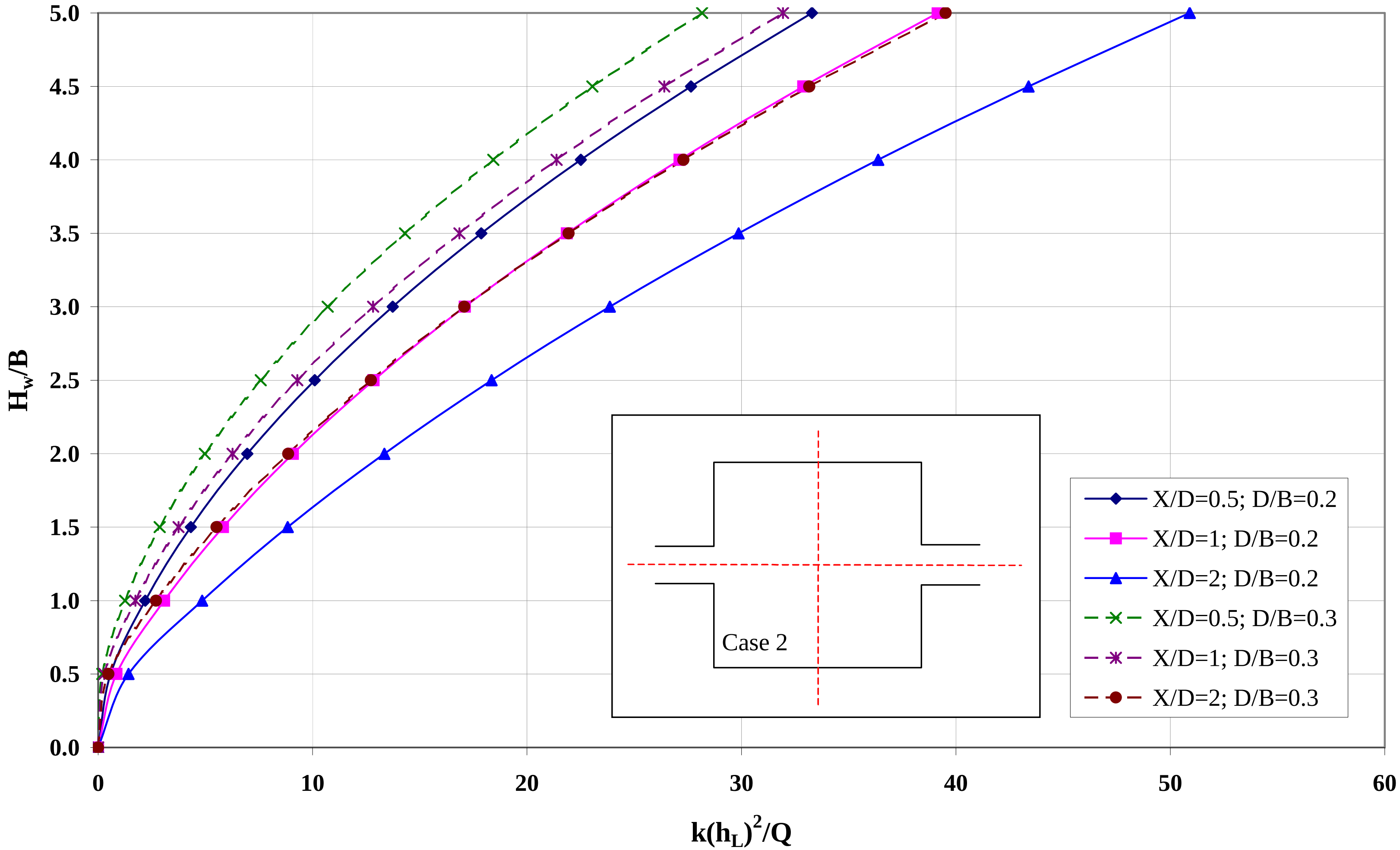


**FIG 6.27 - Three-dimensional total flow design chart for Case 2**

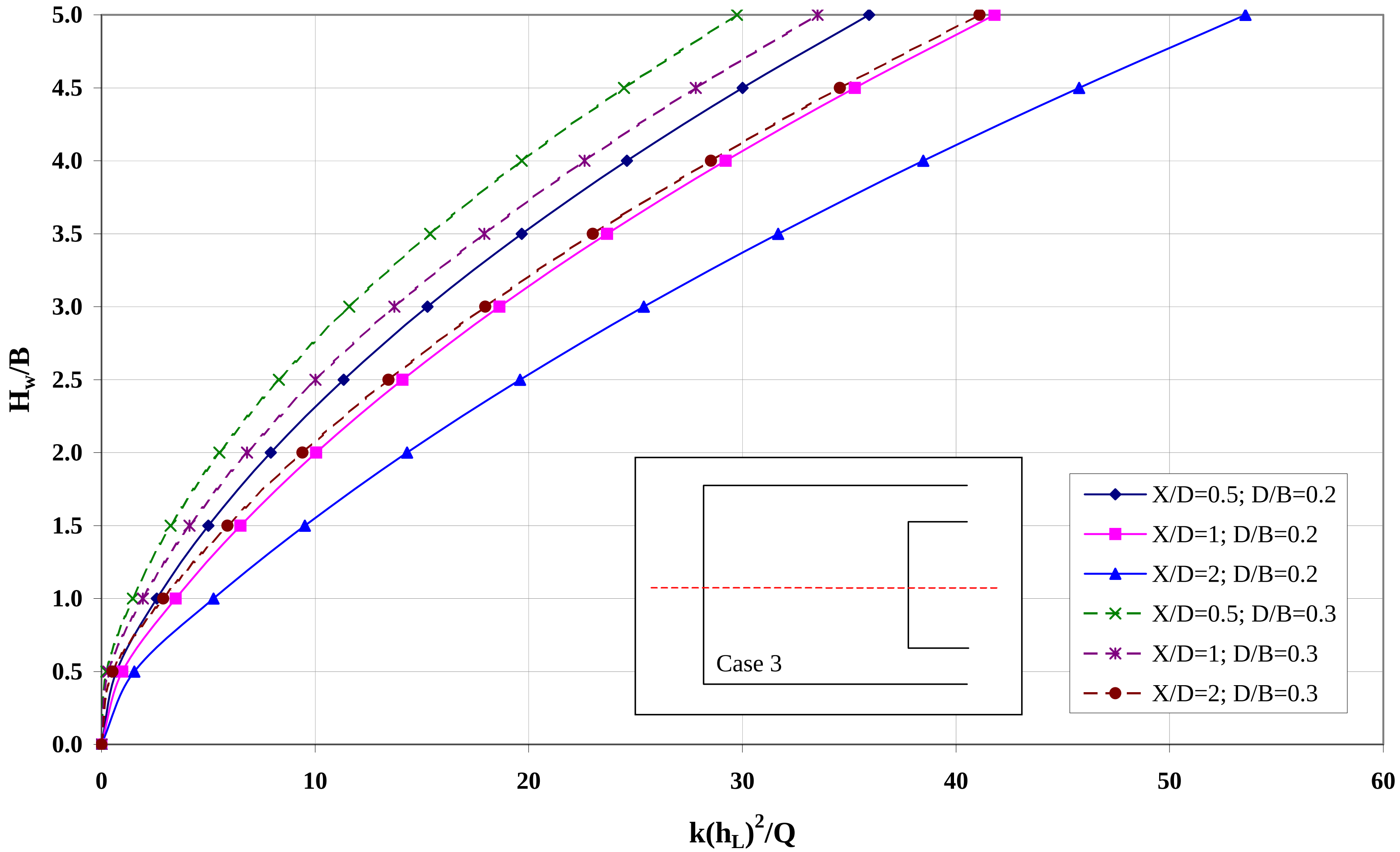


**FIG 6.28 - Three-dimensional total flow design chart for Case 3**

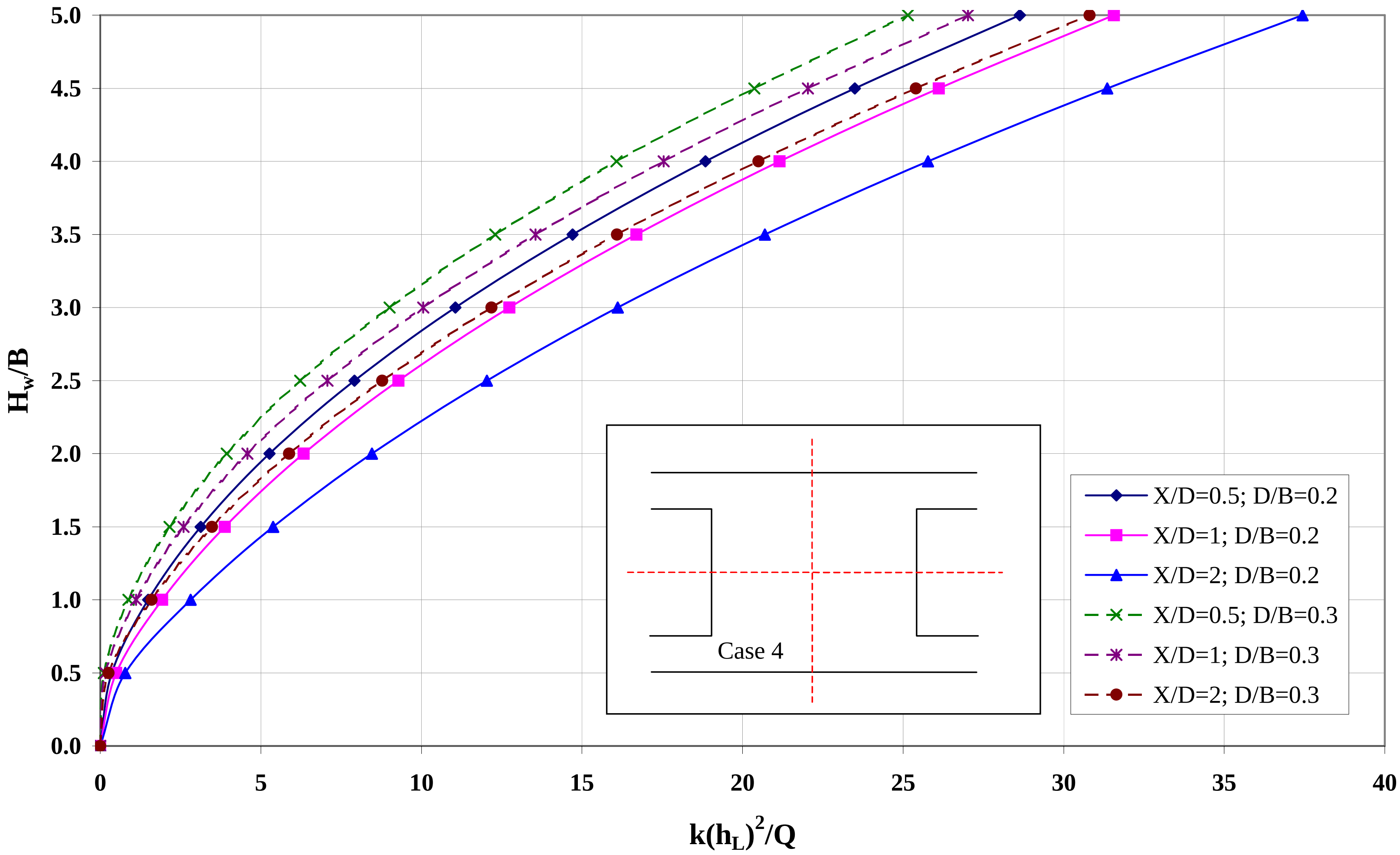


**FIG 6.29 - Three-dimensional total flow design chart for Case 4**

Maximum Pore Water Pressure

Development of pore water pressures, which results in liquefaction of the hydraulic fill, thus increasing the thrust on the barricade, is often attributed as the cause for barricade failures (Kuganathan, 2001). As a result, pore water pressure development within the hydraulic fill is of prime concern to the miners, and much attention has been directed to pore water pressure prediction within underground hydraulic fill stopes. For an intact, correctly functioning stope, the maximum pore water pressure occurs at the bottom of the stope at the point furthest from the barricades. The maximum pore water pressure locations for 2-dimensional and 3-dimensional stopes are indicated by stars in Figs. 6.30 and 6.31 respectively.

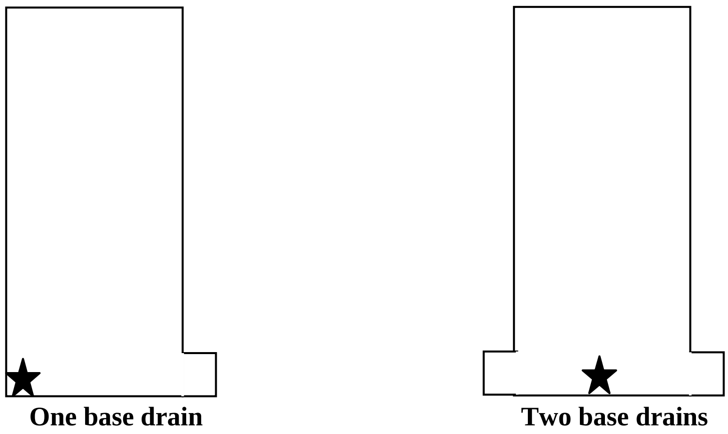


**FIG 6.30 - Maximum pore pressure locations shown on elevation view for 2-dimensional stopes**

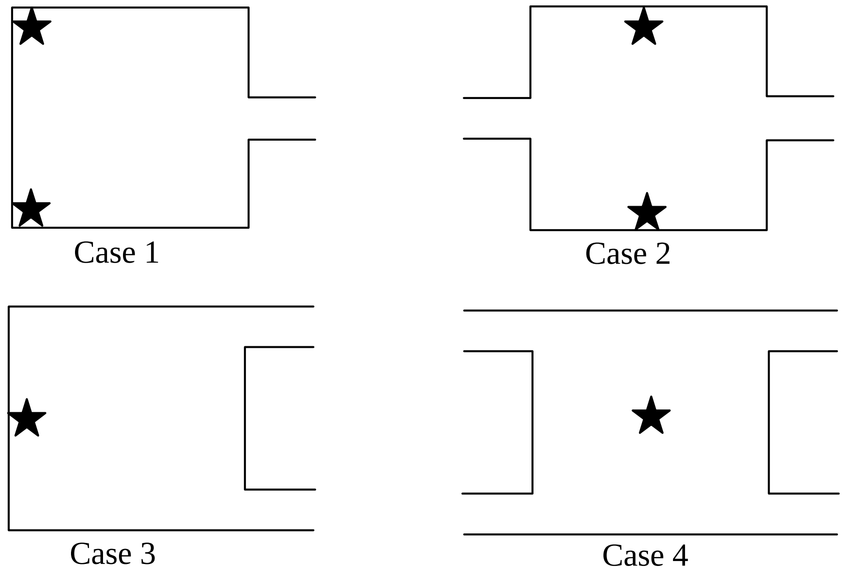


**FIG 6.31 - Maximum pore pressure locations shown on elevation view for 3-dimensional stopes**

A pore pressure coefficient β, can be introduced (Sivakugan et al. 2005) such that the maximum pore pressure for a given stope geometry is given by Eqn. 6.16.

$$u_{\max} = \beta \gamma_w H_w \qquad \text{Eqn. 6.16}$$

The pore pressure coefficient β must lie between 0 and 1. Several simulations were performed in both *FLAC* (Sivakugan et al. 2005) and *FLAC*$^{3D}$ for different values of $H_w/B$, $X/D$ and D/*B* and the corresponding maximum pore water pressures and β coefficients computed. The relationship between this parameter β, and X/D, D/B and $H_w$/B for each of the drain arrangement cases are presented in Figs. 6.32 through to 6.35, for X/D = 0, 1, 2 and D/B = 0.2 and 0.3. These plots give a broad overview of the effects of various dimensions on the maximum pore pressure throughout the stope. These pore pressures will be located in the positions indicated by stars in Fig. 6.31 and Figs. 6.32 through to 6.35).

The pore pressure design charts will be most valuable to mine operators in obtaining approximations for maximum pore pressure or water height within a stope, provided the parameter not being determined and the approximate stope geometry are known. For example, if in situ pore pressure monitoring has been placed within a stope at the point of maximum pore pressure (Figs. 6.30 and 6.31), then for typical stope geometries, the corresponding water level within the stope may be approximated using these charts.

These charts cover typical stope geometries, and it is suggested that for mining operations that do not have, or are not scheduled to have stopes of these typical dimensions and drain arrangements, then individual charts should be developed based on that mine's operation.

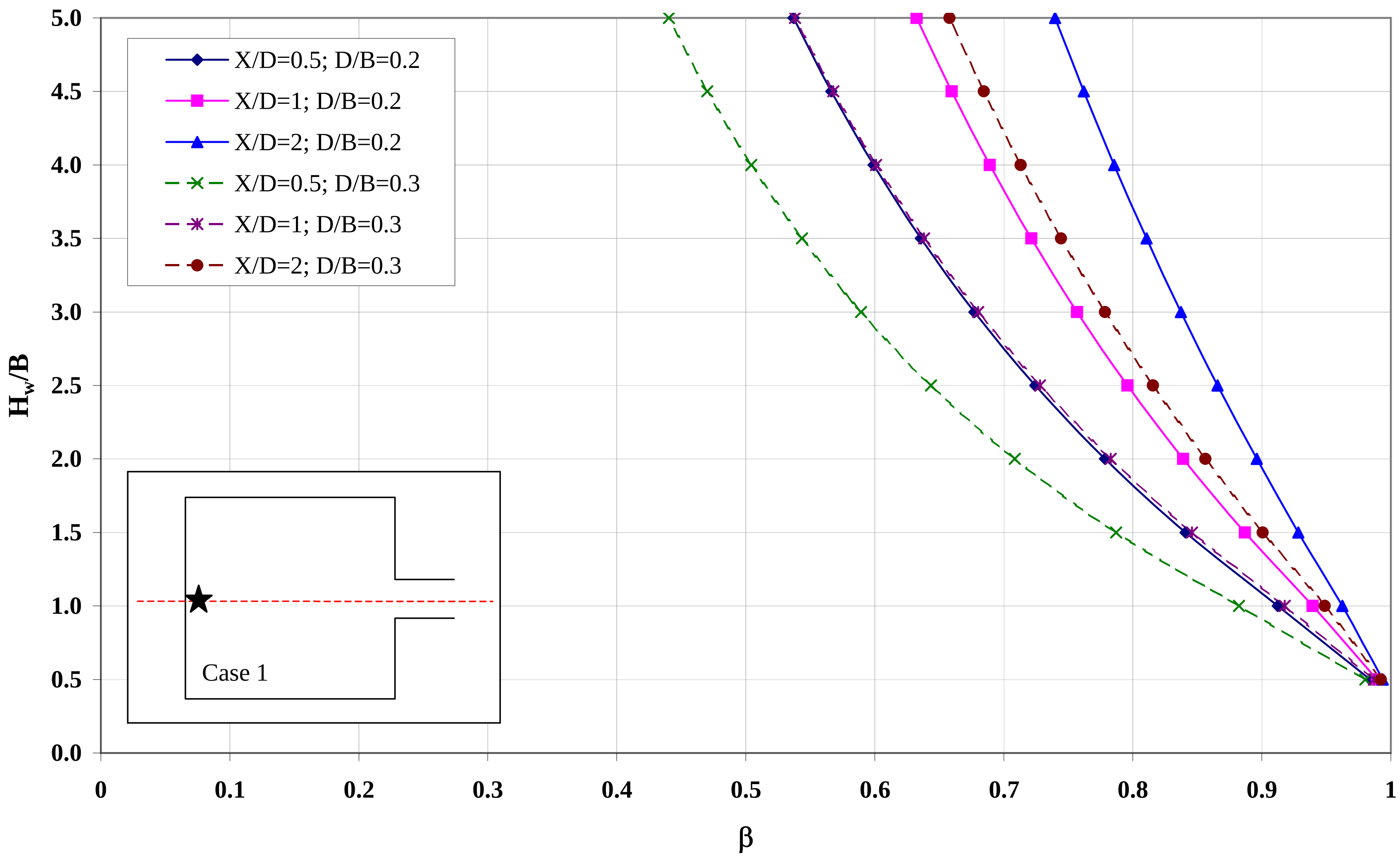


**FIG 6.32 - Three-dimensional maximum pore pressure design chart for Case 1**

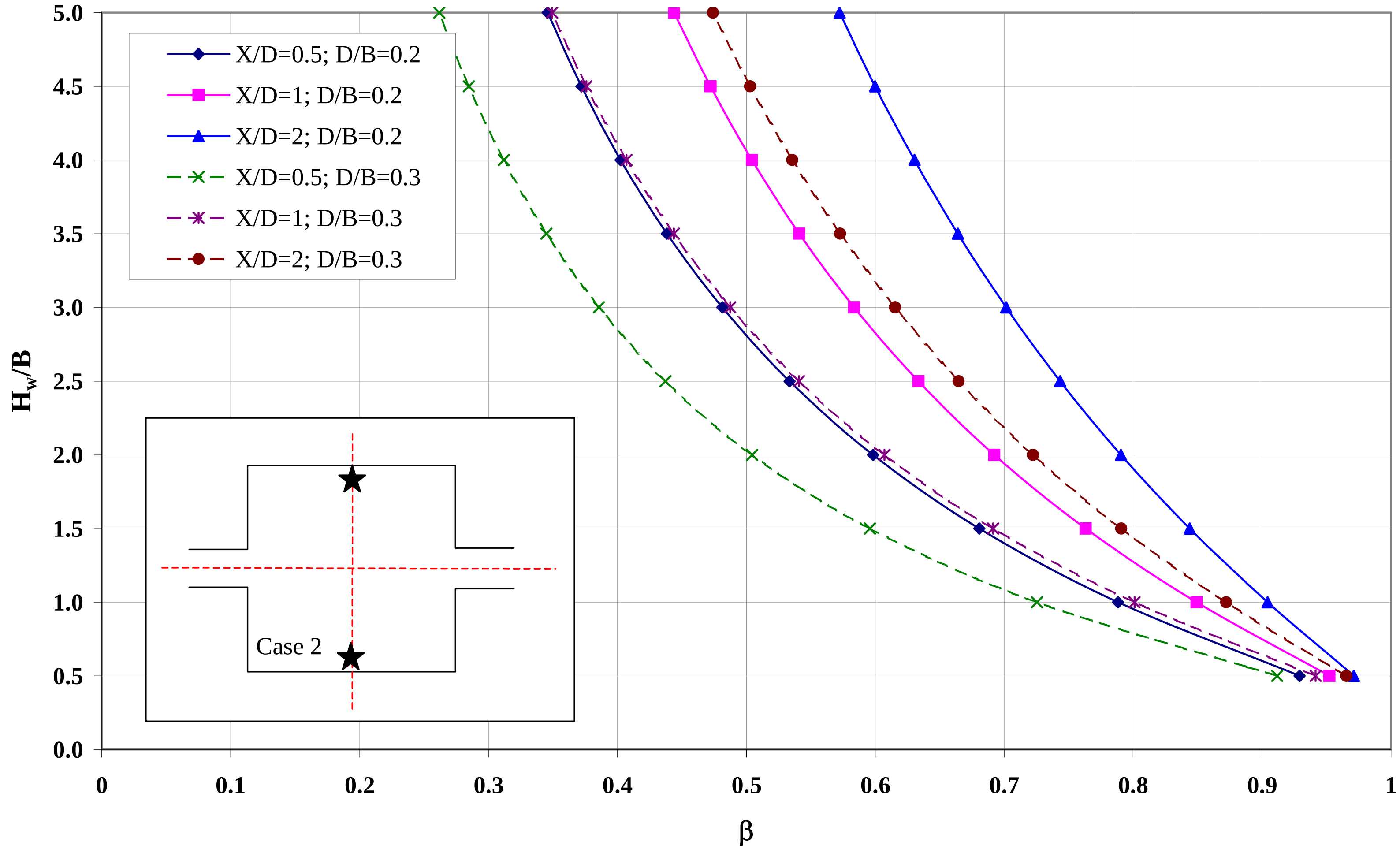


**FIG 6.33 - Three-dimensional maximum pore pressure design chart for Case 2**

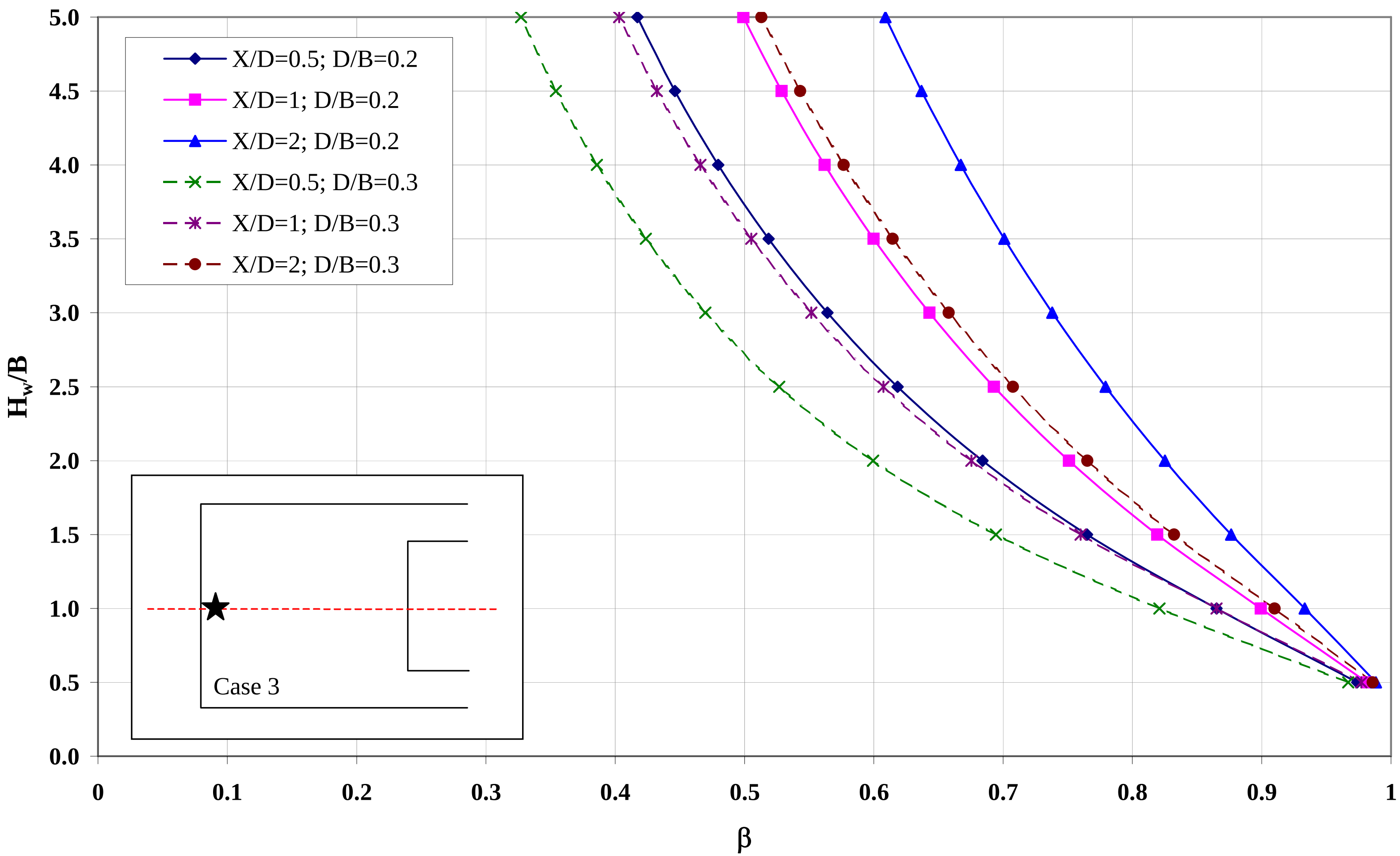


**FIG 6.34 - Three-dimensional maximum pore pressure design chart for Case 3**

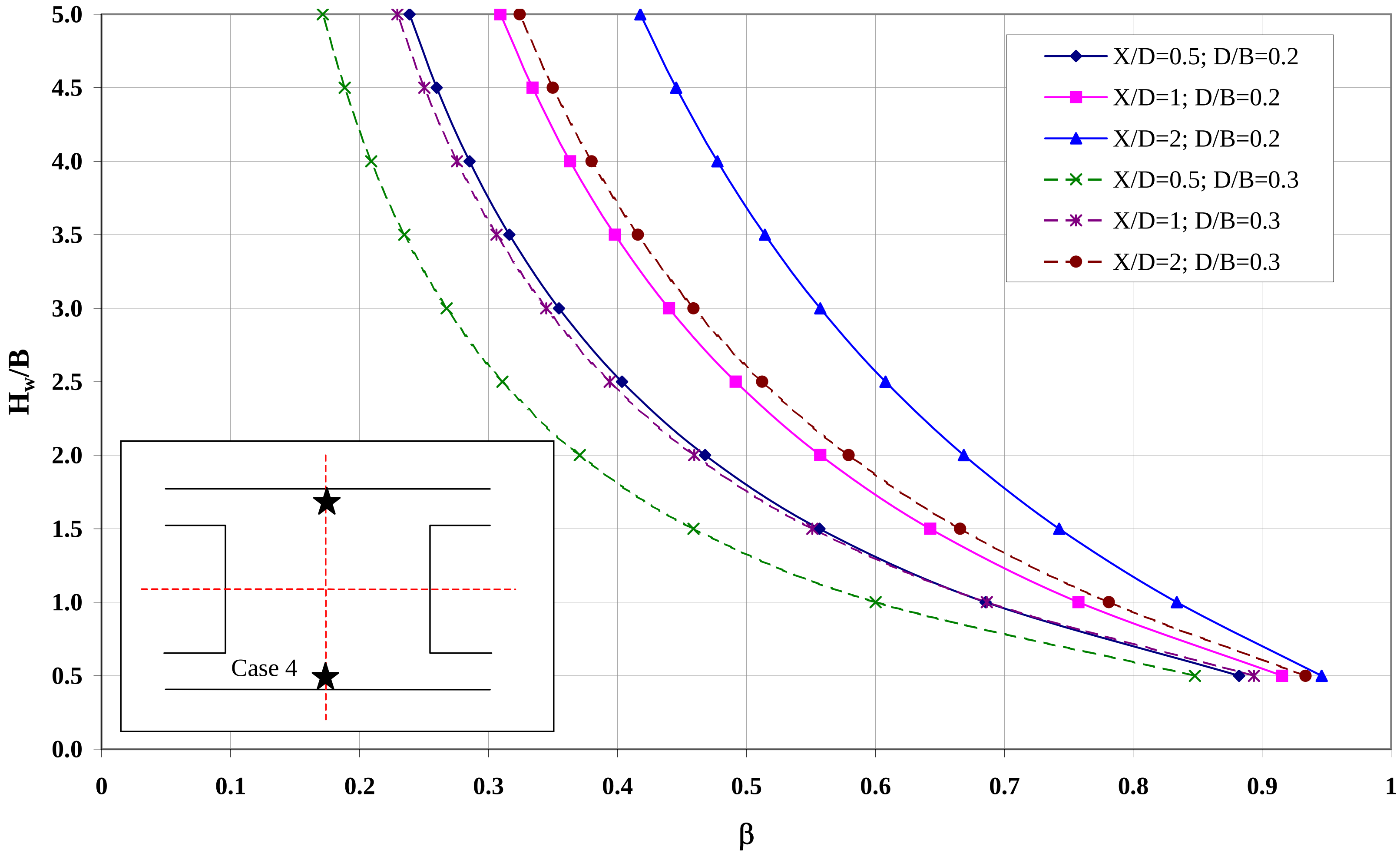


**FIG 6.35 - Three-dimensional maximum pore pressure design chart for Case 4**

Because of the geometrical nature of 2-dimensional modelling, the distance between the drain exit and the point of highest pore water pressure is larger for a 3-dimensional analysis than for an identical sized stope modelled in 2-dimensions. Therefore, it is expected that the maximum pore pressure measurements will be lower for 2-dimensional analysis than it is for 3-dimensional analysis, and hence the pore pressure coefficient β lower for the 2-dimensional simulations than for the 3-dimensional simulations. This is clearly shown in Fig. 6.36 which compares the pore pressure coefficient β computed using 2-dimensional and 3-dimensional modelling for identical *X/D* and *D/B* ratio stopes. At the $H_w/B$ ratio of 5, the 2-dimensional modelling the calculated β value is approximately 47% and 43% of the 3-dimensional calculation for *X/D* ratios of 1 and 2, respectively. This means that for this case, where the $H_w/B$ ratio is large, the 2-dimensional modelling predicts the maximum pore water pressure as almost half the 3-dimensional value. Therefore, for stopes with very large $H_w/B$ ratios the 2-dimensional design chart (Sivakugan et al. 2005) will provide a significantly lower prediction for the maximum pore pressure value, than the prediction provided by a 3-dimensional analysis which simulates the drain with a more realistic width and depth value. As the *X/D* ratio increases, the degree to which the 2-dimensional modelling under predicts the β coefficient and hence the maximum pore water pressure also decreases.

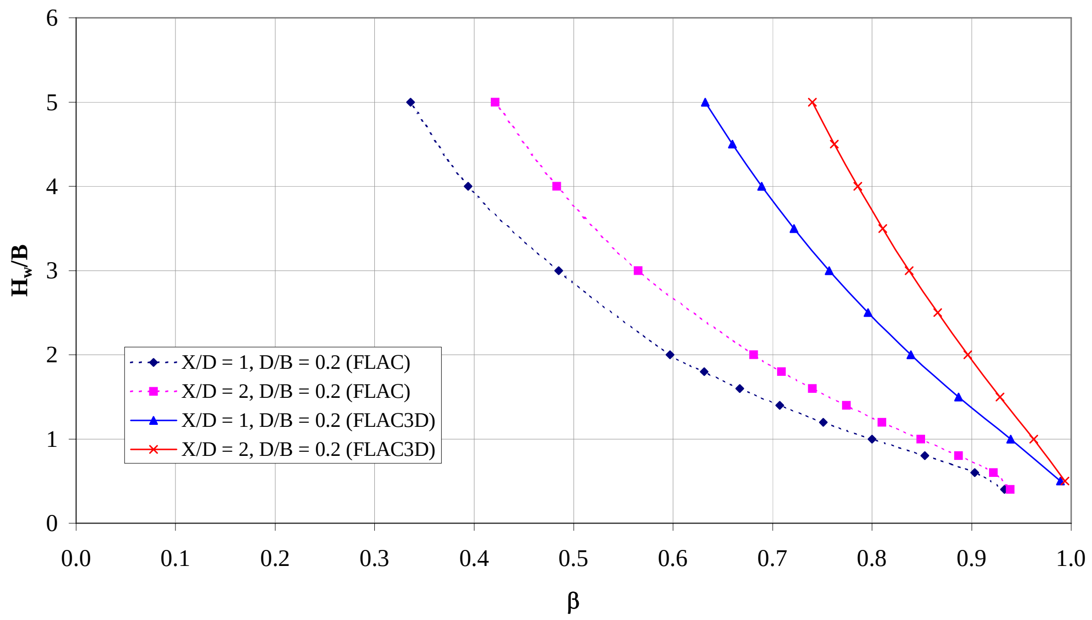


**FIG 6.36 - Pore pressure coefficient, β versus $H_w/B$ for 2-dimensional and 3-dimensional modelling**

The value in drain placement and numbers, relative to Case 1 may be studied by dividing the discharge and the maximum pore pressures for each of the other three cases by those measured for Case 1. These values for various $H_w/B$, D/B and X/D ratios are all recorded in Table A6.1 to A6.6 in Appendix 4. Figs 6.37 and 6.38 show the relative discharge efficiencies for the D/B ratios of 0.2, and 0.3 respectively, and Figs. 6.39 and 6.40 plot the maximum pore pressure values for the D/B ratios of 0.2 and 0.3 respectively relative to the standard Case 1 drain arrangement. These charts can be used to assist in determining the performance of subsequent drains.

Several trends are observed throughout these charts. Firstly, Case 4 with the most drains has the highest discharge rates and lowest maximum pore pressure values for all geometrical aspect ratios studied, and Case 1 with the fewest drains has the lowest discharge rates and highest maximum pore pressure values. Case 2 is marginally more effective in water removal and has consistently lower peak pore pressure values than Case 3, which also has 2 drains. The difference between the cases decreases with drain length and with increased drain width (the measurements were all recorded for drains with a square cross-section).

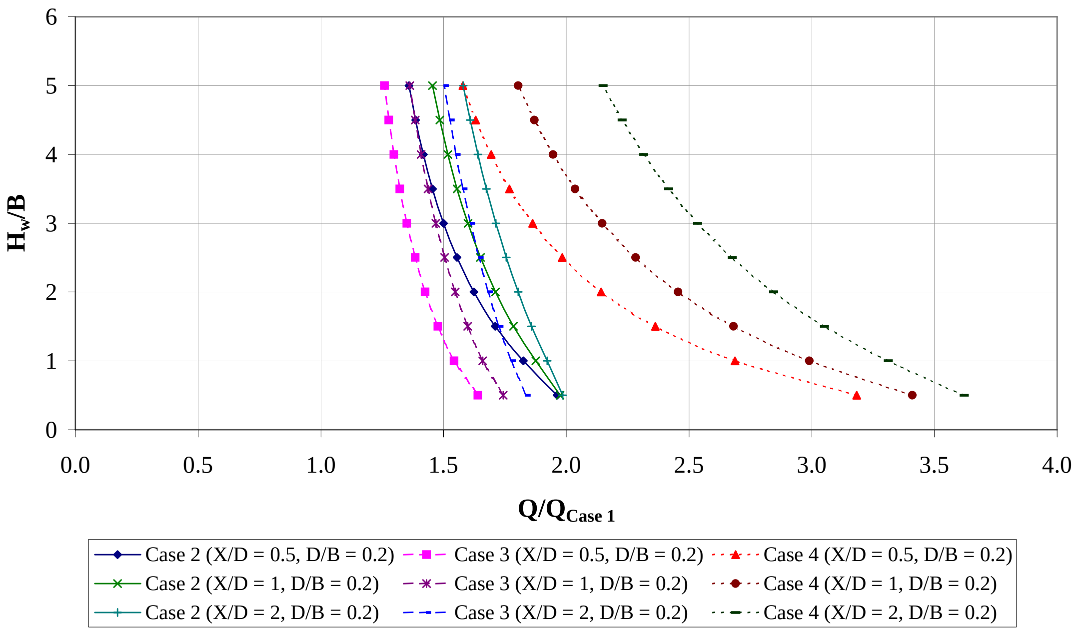


**FIG 6.37 - Case 2, 3 and 4 discharge rates /Case 1 discharge rates for D/B = 0.2**

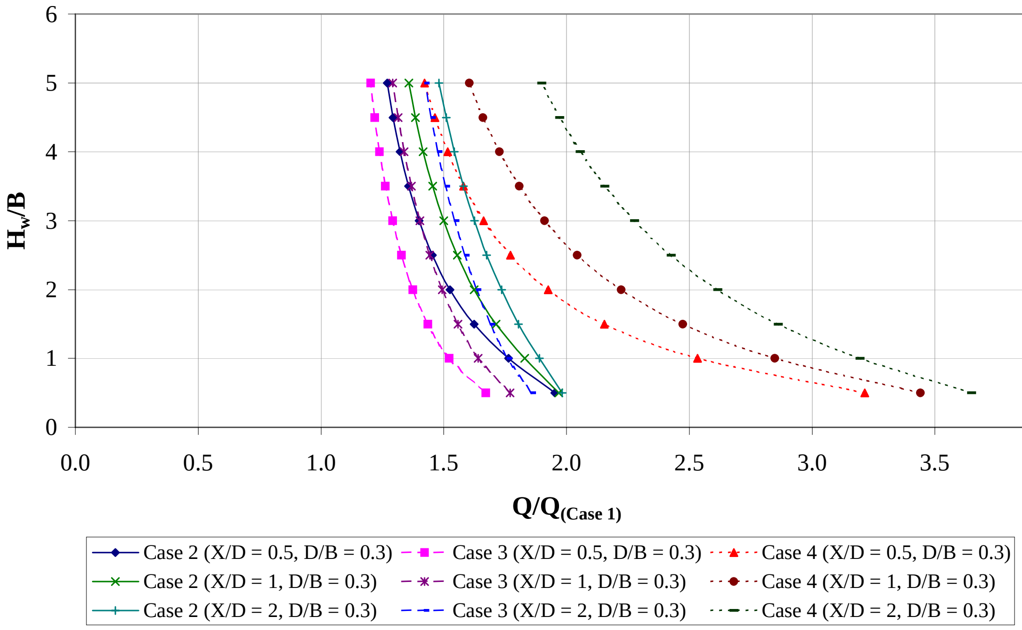


**FIG 6.38 - Case 2, 3 and 4 discharge rates/Case 1 discharge rates for D/B = 0.3**

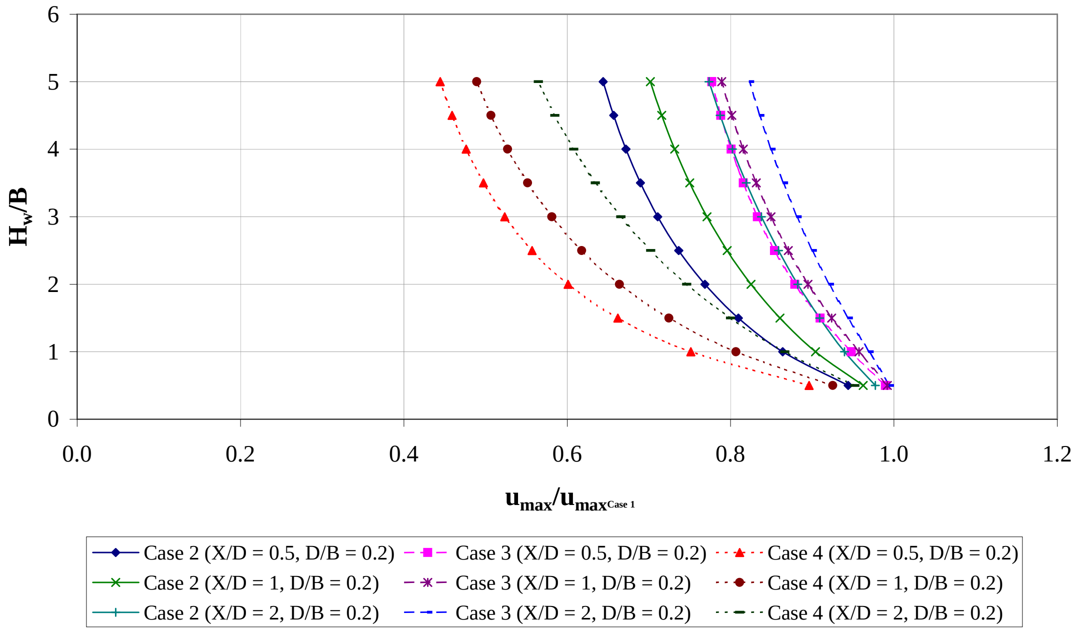


**FIG 6.39 - Case 2, 3 and 4 $u_{max}$/Case 1 $u_{max}$ for D/B = 0.2**

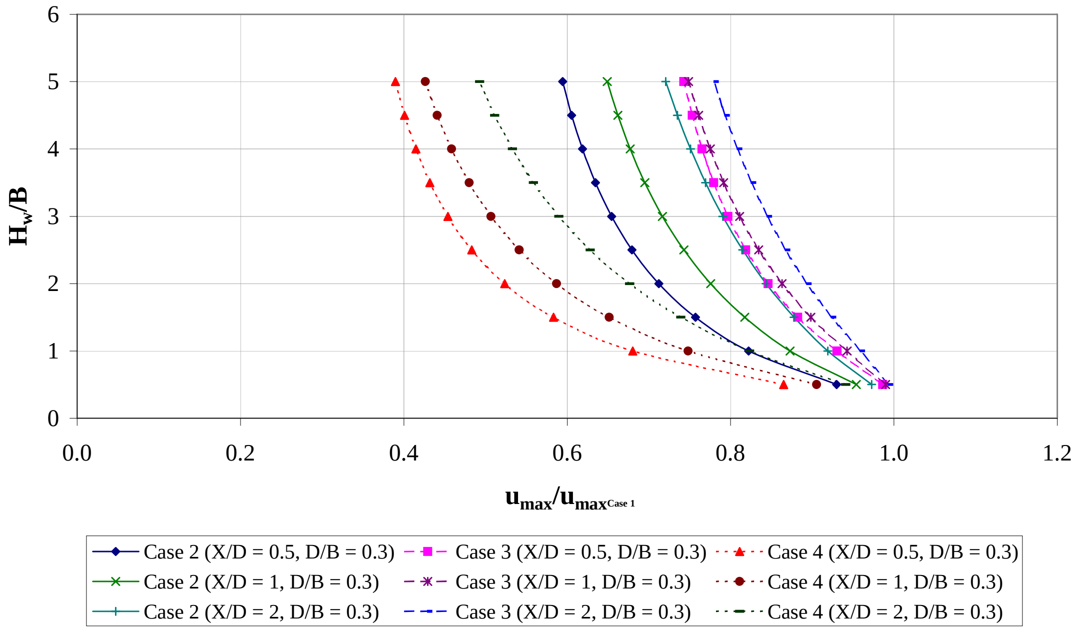


**FIG 6.40 - Case 2, 3 and 4 $u_{max}$/Case 1 $u_{max}$ for D/B = 0.3**

The efficiency of the drain performance relative to Case 1 plateaus to a maximum for pore pressure and a minimum for discharge at large $H_w/B$ values. This means that as the water level increases and the pore pressures increase, the benefit in extra base drains on reducing the pore water pressure increases despite the effectiveness in the extra drains on removing the water (relative to the Case 1 arrangement) decreasing. Discharge efficiency of subsequent drains increases with drain length.

## 6.5 Chapter Summary

This chapter has verified and implemented a 3-dimensional extension to the stope filling and drainage program presented in Chapter 5. The program uses the finite difference package FLAC$^{3D}$ to predict fill and water levels, discharge rates and pore pressures within 3-dimensional hydraulic fill stopes as they are being filled and drained. Steady-state FLAC$^{3D}$ analysis has also been used to develop dimensionless design charts for predicting the discharge and maximum pore water pressures within a 3-dimensional stope of typical geometrical configuration. Some of the major outcomes presented in this chapter include:

- A 3-dimensional flow net may be approached in the same manner as the 2-dimensional flow net with the equipotential lines now viewed as equipotential surfaces, and the flow channels incorporating the third dimension. Scaling up a stope by the factor of x will scale up the pore water pressure by x but the flow rate will be scaled by $x^2$ because of the third dimension. The velocity and hydraulic gradient remain unchanged as in the case of the 2-dimensional stopes.

- The geometrical simplification required when using either the Isaacs and Carter program or the *FLAC* program presented in Chapter 5, causes discharge to be over estimated and maximum pore water pressure to be under estimated.
- Simple 1-dimensional flow analysis previously used to determine the minimum permeability value required to prevent the rise of water within a stope is not applicable to real stope conditions because the assumption that the hydraulic gradient at the top of the stope is equal to one is incorrect. Through numerical modelling the 2 and 3-dimensional hydraulic gradients have been obtained using in both *FLAC* and *FLAC$^{3D}$* respectively, for typical stope geometries. Although the hydraulic gradient approaches one as the stope height approaches infinity, for stope dimensions practically used in a mine the value will be considerably lower than one. The hydraulic gradient values computed through numerical modelling for 2-dimensional stopes were higher than those for 3dimensional stopes.
- The solids content and specific gravity of the slurry placed will have a significant influence on the relative fill and water heights with time. A conservative estimate of fill and water heights may be obtained by disregarding discharge and using material properties in simple phase relations. This will provide the operators with a first glance appreciation for the relative build-up of decant expected for their material, then through permeability testing, combined with numerical modelling a more accurate prediction may be obtained.
- With all other parameters equal, the higher the specific gravity of the fill material, the higher the permeability required to maintain the water level at the same height as a stope filled using a fill with a lower specific gravity. This is because a larger volume of water is being added per volume of placed fill. Similarly, because of the larger quantity of water being added, the lower the

solids content the fill is placed, the higher the permeability required to keep the water level at the height resulting from fill pumped at a lower solids content.

- The 3-dimensional filling program presented in this chapter, which simulates the entire filling schedule, requires extremely lengthy solution times. It is suggested that by converting the program to an implicit solution the solution times would be reduced somewhat, and this should be included in future program development.
- The 3-dimensional numerical model presented in this chapter may be used to predict the time required for all free water to drain from a stope such that adjacent works may commence, which makes it a highly valuable tool for mine scheduling.
- As drain length increases, discharge decreases, and as drain cross-sectional area increases (for a square drain) discharge increases.
- As drain length increases and drain cross-sectional area decrease, the maximum pore water pressures increases.
- The 2-dimensional non-dimensionalized maximum pore water pressure design charts significantly underestimate the maximum pore water pressures of 3-dimensional stopes.
- Case 2 stope drain arrangement with drains on opposing walls (Fig. 6.23), is marginally more effective in water removal and produces lower maximum pore water pressures than Case 3 which also has 2 drains, but on the one stope wall. The degree of difference decreases with drain length and drain width (all measurements were for drains with square cross-sections).
- As the water level increases and the maximum pore water pressures increase, the benefit in extra base drains on reducing the pore water pressure increases despite the effectiveness in the extra drains on removing the water (relative to Case 1, Fig. 6.23) decreasing.

# Chapter 7

# Summary, Conclusions and Recommendations

## 7.1 Summary

A common method used for waste disposal in large scale underground metalliferous mining operations, involves the placement of a particular type of minerals processing by-product called *hydraulic fill*, into the massive voids created by the excavation of ore. A review was presented on previous research conducted into the current practices and published developments with regard to the placement of this material. This review showed that with the steady increase in pulp density over the past decade, current practices have hydraulic fills typically placed at solids densities exceeding 70% solids by weight, filling rates that range from approximately 150 to 300 t/hr, and fill/rest schedules that depend on processing abilities and other constraints.

To ensure good drainage, backfilling operations typically ensure that the by-product (usually deslimed by hydraulic cyclones) has an effective grain size ($D_{10}$), no smaller than 10 μm. The very wide range of geological conditions and mineralogical compositions from which the hydraulic fills may be sourced results in a very wide range of specific gravity values for hydraulic fills used across Australia as reported in literature. It has been found that as a result of the milling process, the grains are very sharp and angular and therefore friction angles are relatively high. Commonly accepted industry rule-of-thumb standard suggests that the permeability of the hydraulic fill should be no less than 100 mm/hr but many Australian and worldwide mines that have operated satisfactorily for years quote hydraulic fill permeability values substantially less than this value.

The review also briefly discusses some of the details with regard to the design and construction of the barricades used to contain the hydraulic fill within the stope as it is being placed, the in situ monitoring techniques that have been used on site to study pore pressure developments and barricade loading, as well as some of the numerical modelling techniques that have been used in the past to predict drainage behaviour within hydraulic fill stopes.

A thorough geotechnical characterisation of hydraulic fills used across Australia was conducted as part of this dissertation, and typical drainage and settlement properties of the hydraulic fills discussed, along with relationships developed from the laboratory work. This research also includes a comprehensive experimental study of the strength, stiffness and permeability of permeable barricade bricks commonly used in mines across Australia. The unique testing techniques and apparatus developed to study the brick properties are also described in detail.

A 2-dimensional numerical model was developed in the commercially available finite difference package *FLAC* to model the sequential filling and drainage of an idealised hydraulic fill stope. The 2-dimensional, finite difference model was validated against the model developed by L.T. Isaacs and J.P. Carter (Isaacs and Carter, 1983) for Mount Isa Mines Ltd. The *FLAC* stope filling program along with some steady-state runs using *FLAC*, was then used to prioritize the input parameters such that solution time was optimised when dealing with the 3-dimensional extension to the program.

The 3-dimensional extension to the stope filling program was undertaken in *FLAC*$^{3D}$ which is specifically designed for geotechnical and mining applications. This stope filling program was used to study the drainage behaviour of stopes in 3-dimensions during the entire filling and drainage schedule. Steady-state 3-dimensional numerical analysis using *FLAC*$^{3D}$, was also used to investigate geometrical effects on stope drainage behaviours, and design charts for typical stope drain arrangements were developed.

The increased knowledge into the drainage behaviours of underground hydraulic fill stopes and the improved tools for analysis presented in this dissertation reduce potential of failures such as that which occurred at Bronzewing Mine in 2000, killing three miners (Grice, 2002).

## 7.2 Conclusions

The conclusions drawn from this research are divided into the sections corresponding to the chapters of the thesis.

### 7.2.1 Hydraulic Fill Characterisation

A study of the drainage characteristics of hydraulic fills used across Australia was completed as part of this thesis. Some of the important conclusions from this laboratory work are:

- The grain size distribution for typical Australian hydraulic fills falls within a very narrow band. The particle shape is very angular which gives the fills relatively high friction angles. Unlike typical granular soils, hydraulic fills have a much wider range of specific gravity values that ranged from 2.8 to 4.4 for fills tested as part of this research.
- Regardless of whether a hydraulic fill is sedimented in a laboratory or in situ, when sedimented as a slurry with a typical solids content between 65% and 75%, all hydraulic fills were found to settle to a rather dense state (with relative densities of 55% - 80%), dry density (in $t/m^3$ or $g/cm^3$) of about 0.56 times the specific gravity, void ratio of 0.79 and porosity of 44%.
- The permeability of Australian hydraulic fills is typically between 10 mm/hr and 30 mm/hr which is significantly less than the 100 mm/hr often desired by the mining industry. A unique, light-weight, portable permeability testing apparatus was designed for on-site constant head and falling head hydraulic fill permeability testing.

### 7.2.2 Permeable Barricade Bricks

A series of laboratory studies were undertaken on typical Australian permeable barricade bricks used for the construction of underground hydraulic fill barricades with the main objective of determining the drainage and strength characteristics. The following outcomes were obtained from this work:

- A unique permeability cell was designed and fabricated to determine permeability of the permeable barricade bricks, under 1-dimensional flow similar to the situation in the mines. The apparatus enables determination of permeability using three different methods, namely, (a) constant head test (b) falling head test and (c) flow-under-pressure test. All three methods gave reproducible permeability measurements that were in agreement with each other. This is the first ever attempt to determine the permeability of barricade bricks, and has turned out to be rather successful.
- Although there was substantial deviation in permeability values between bricks, the average permeability of the permeable barricade bricks has been quantified as two to three orders of magnitude larger than that of hydraulic fill. Therefore, provided the barricades are constructed from the bricks in such a way that the construction or future migration of fines from the fill does not impede the drainage performance, it may be assumed that the barricade does not contribute to the pore pressure development within the fill, and hence the drainage of the system is not related to the permeability of these bricks.
- There is significant scatter in brick strength and stiffness values, and it has been shown that there is a distinct loss of strength (approximately 25%) as a result of wetting. Since the barricades remain wet during the filing and drainage, the dry brick strength should be reduced by 25% for barricade designs.

### 7.2.3 Two-Dimensional Modelling of Underground Hydraulic Fill Stopes

A replication of the 2-dimensional program written by L. Isaacs and J. Carter was coded in *FLAC*, and used in conjunction with some steady-state *FLAC* modelling to identify the critical parameters which would be used as the variables in the 3-dimensional extension of the program discussed in Chapter 6. The major outcomes from the 2-dimensional numerical modelling work include:

- The numerical model developed using *FLAC* has proven to be a very powerful tool in studying the filling and draining of a hydraulic fill stope. While matching the predictions from Isaacs and Carter, this *FLAC* model has several added features. It can include drain lengths and with some modifications, this can model non-vertical stopes.

- When there are drains located at several sublevels, the majority of the discharge from a stope exits the base drains. The further from the stope the barricades are located, the less effective they are at removing water from the stope.
- Discharge rates and the pore pressure distribution within a stope are significantly influenced by drain length. As the barricade gets further from the stope, the flow path increases and the hydraulic gradient across the entire model decreases, resulting in reduced flow velocity, hence discharge. Increasing the drain length increases the pore pressures within the stope.
- The critical parameters that affect the drainage performance of a stope were identified as:
    - Permeability
    - Specific gravity
    - Solids content of the slurry
    - Residual water content
    - Stope geometry
        - Drain length
        - Multiple drain position along the base of the stope

These were studied systematically using the 3-dimensional program developed in *FLAC*$^{3D}$.

### 7.2.4 Three-Dimensional Modelling of Underground Hydraulic Fill Stopes

A 3-dimensional extension to the stope filling program presented in Chapter 5 was designed and coded in *FLAC*$^{3D}$. This program is capable of simulating the filling and drainage of a 3-dimensional stopes with various input parameters such as material properties, filling rates, filling schedules, etc. Through the use of this numerical filling program as well as some steady-state *FLAC*$^{3D}$ numerical modelling work combined with scaling techniques, the following could be concluded:

- Often, under normal filling conditions, the discharge from a stope filled with a typical hydraulic fill represents only a very small proportion of the water being accounted for each hour (i.e., the water entering and exiting the stope during the hour). If this is the case, operators may disregard discharge and use equation Eqn. 6.11 to predict fill and water heights throughout the filling of a stope. The equation is not valid after the stope has been filled and the water is draining from the stope while no further fill is enters the stope. If the permeability values are very large, and the water level falls below the height of the fill these equations are slightly inaccurate in fill and water height predictions.

- Hydraulic fill specific gravity and the solids content with which the fill is placed have a significant influence on the quantity of water that enters the stope and subsequently needs to be drained from the stope.
- The filling program has been shown to be a highly valuable tool in mine scheduling provided reasonably accurate predictions of hydraulic fill residual water content can be made.
- Design charts presented in this dissertation may be used to assess the discharge rates and maximum pore water pressures from typical square based stope arrangements, and assess the effectiveness of additional drains on these parameters.

## 7.3 Recommendations for Future Research

Whilst there have been considerable advancements in understanding the drainage characteristics of both Australian hydraulic fills and the permeable barricade brick, the methods of testing these characteristics and the numerical modelling tools to predict the underground drainage behaviours, there are many areas that deserve further study. The recommendations outlined have been presented under the same titles as the chapters presented in this dissertation.

### 7.3.1 Hydraulic Fill Characterisation

- Direct shear tests can be carried out on hydraulic fills from different mines, placed at different relative densities, to confirm confidently that the $\phi'$-$D_r$ relationships seen in literature for granular soils underestimate $\phi'$ when used for hydraulic fills. Attempt should be made to develop a unique relation, (if different to Eqn. 3.11) between $D_r$ and $\phi'$ for hydraulic fills, which would be very valuable for static and dynamic analysis of hydraulic fills.
- Further permeability testing on cemented hydraulic fills to determine the degree with which the permeability is reduced with curing and percent cement.

- It is suggested that further research be carried out to better characterise typical values of in situ residual water content.
- The exact nature of the risk of liquefaction and methods of determining this risk are not fully understood within the industry, and it is suggested that research into liquefaction potential and assessment within hydraulic fill stopes would by highly valuable to the Australian mining industry.
- Any attempt to incorporate coupling into the numerical model would require a thorough understanding of the consolidation characteristics of the hydraulic fills. Limited oedometer tests on fills carried out by the author show that the primary consolidation is completed in less than two seconds, making it difficult to determine the coefficient of consolidation. It is suggested to carry out consolidation tests on much thicker samples (e.g., in a 150 mm diameter compaction mould) which would prolong the consolidation process, and enable determination of coefficient of consolidation $c_v$. The author has seen significant creep settlements in the oedometer samples. This needs further investigations and then may be related to creep behaviour of granular soils as observed by Schmertmann et al. (1978) and Burland and Burbidge (1985).
- Analysis into the liquefaction potential of hydraulic fills can be carried out through cyclic triaxial tests.

### 7.3.2 Permeable Barricade Bricks

- A thorough analysis can be carried out on the effective permeability of shotcrete or pumped concrete barricades and ancillary drainage.
- Further investigation is suggested into the potential of migration of fines and the influence on the barricade drainage performance

### 7.3.3 Two-Dimensional Modelling of Underground Hydraulic Fill Stopes

- Method of fragments has been identified as a potential tool for developing approximate solutions for discharge and pore water pressure developments within a 2-dimensional stope (Sivakugan et al., 2005). This is currently being implemented in an Excel based spreadsheet by another PhD student at JCU.

- To reduce solution time, the 2- dimensional program should be developed into a coupled 2-dimensional and 1-dimensional program. This is currently being implemented by a PhD student at JCU.
- Based on the availability of data, the 2-dimensional model presented in this dissertation can be modified to accommodate:
    - Inhomogeneity in the fill
    - Consolidation through a coupled analysis
    - Curing of cement, through temporal variation in fill properties

### 7.3.4 Three-Dimensional Modelling of Underground Hydraulic Fill Stopes

- The main drawback with the *FLAC*$^{3D}$ filling program developed in this dissertation is the lengthy solution time, which can be several days for a typical stope. This is the nature of *FLAC*$^{3D}$ explicit finite difference algorithm and similar solution times have been reported for other problems developed in *FLAC*$^{3D}$. One way to go around this is to simplify the model. Also, research should be directed into the adaptation of the program into using an implicit solution scheme. Also, to substantially reduce solution times, the 3-dimensional program should be developed into a coupled 3-dimensional and 1-dimensional program. This is currently being implemented by a PhD student at JCU.
- In 2-dimensions as well as 3-dimensions, the flow is perfectly 1-dimensional in the upper regions of the stope and within the drains. It may be possible to isolate the 1-dimensional flow regions and use *FLAC*$^{3D}$ only near the bottom stope where the flow is 3-dimensional.
- The 3-dimensional program may be adapted to model more complex geometries, including stopes that are not vertical and stopes having ancillary drains.
- The program should be validated directly against in situ data.
- *FLAC*$^{3D}$ that can be implemented on main frame computers can speed up the solution time significantly and makes *FLAC*$^{3D}$ very attractive as a research tool. This is expected from Itasca in the near future.

# *Appendix 1*

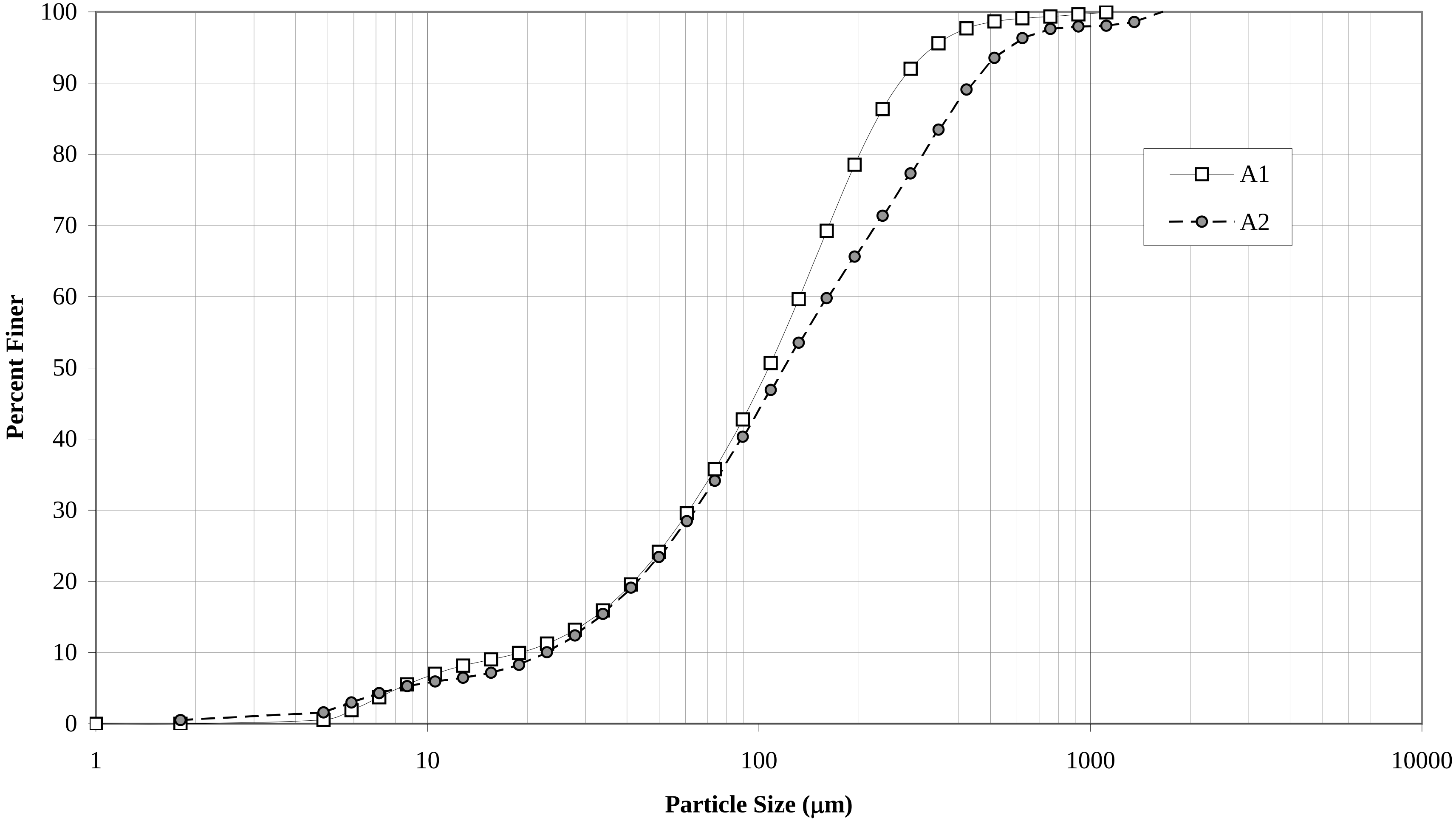


**FIG. A1.1 – Grain size distributions on hydraulic fill samples from mine A**

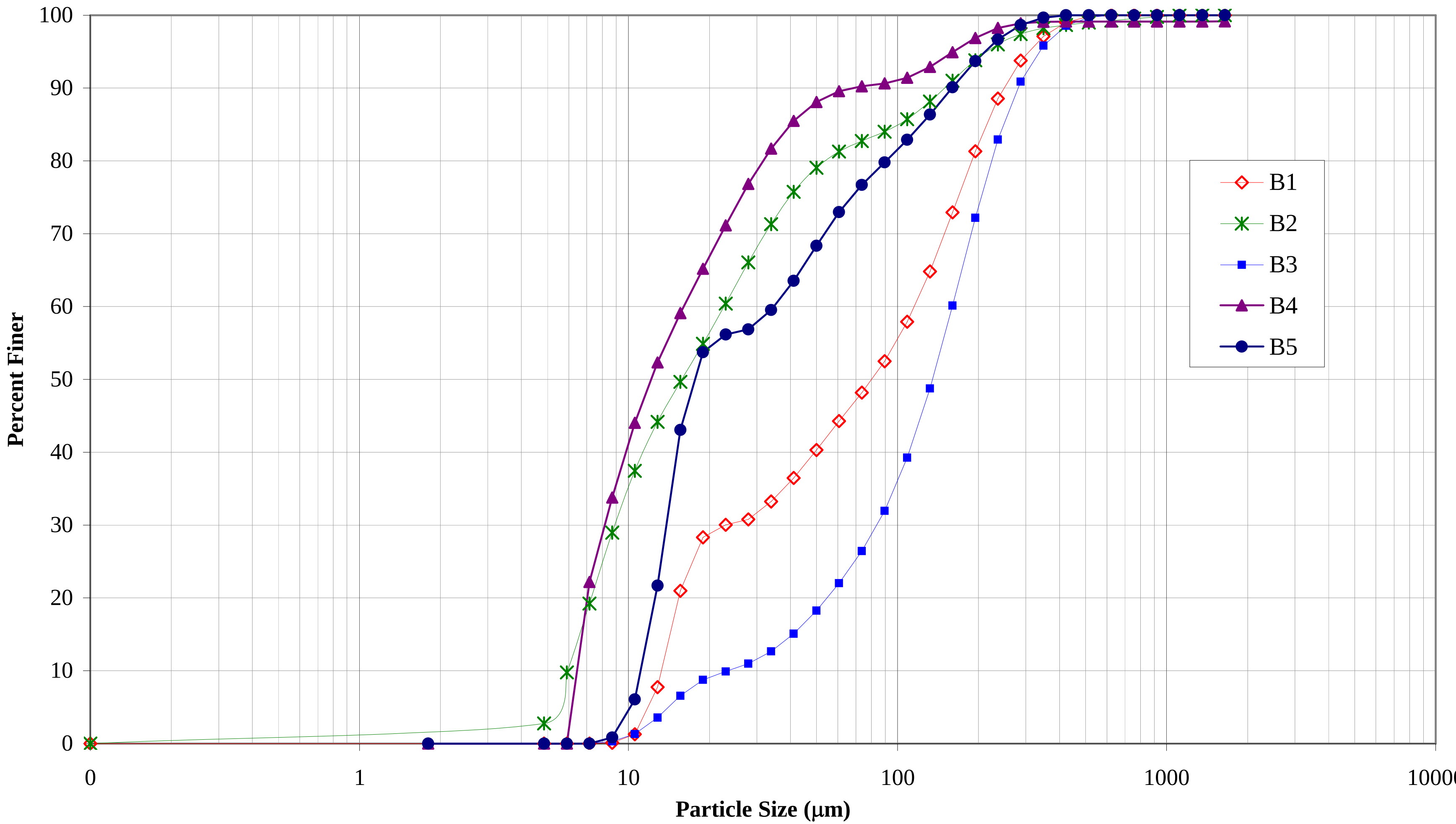


**FIG. A1.2 – Grain size distributions on hydraulic fill samples from mine B**

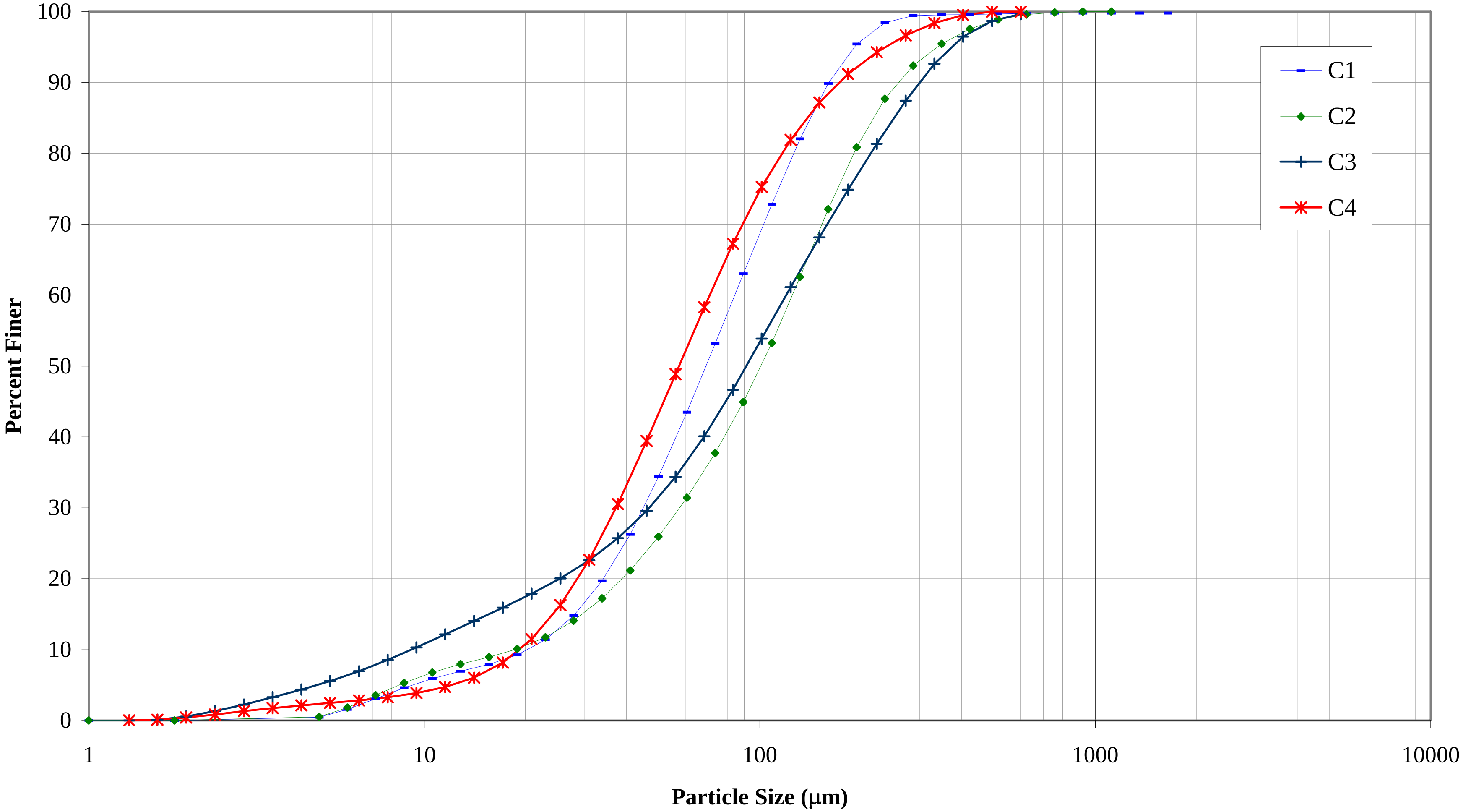


**FIG. A1.3 – Grain size distributions on hydraulic fill samples from mine C**

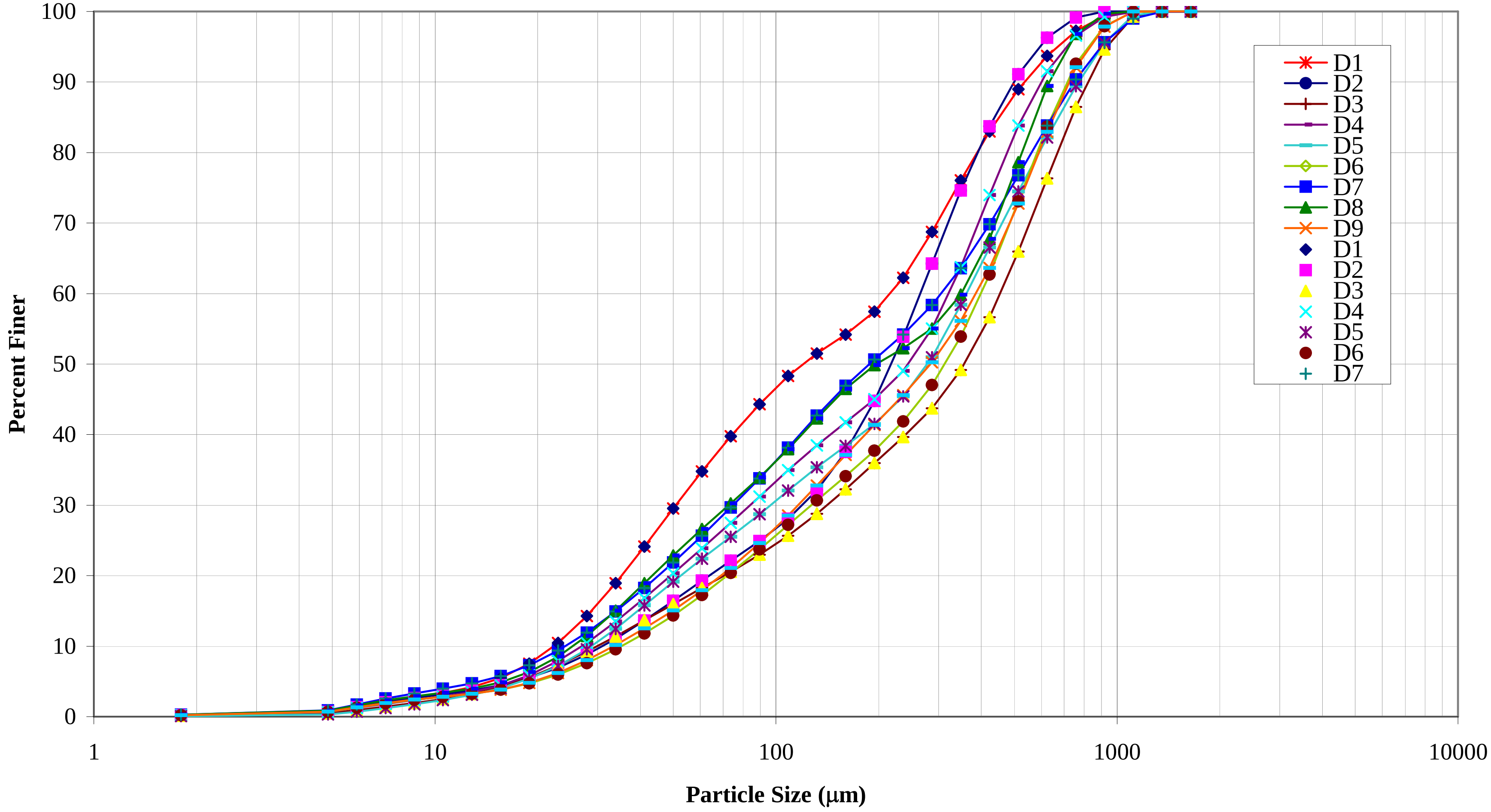


**FIG. A1.4 – Grain size distributions on hydraulic fill samples from mine D**

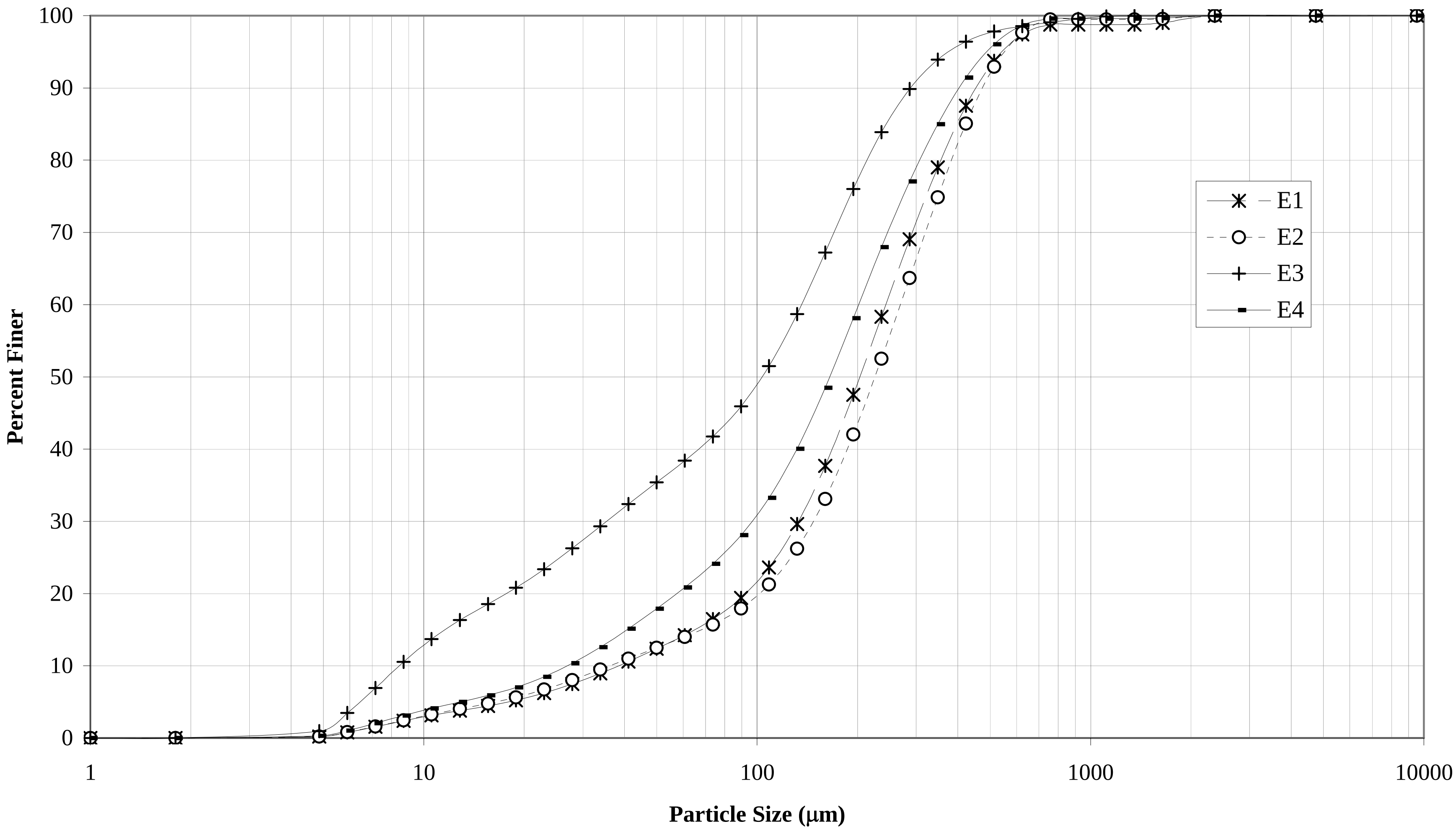


**FIG. A1.5 – Grain size distributions on hydraulic fill samples from mine E**

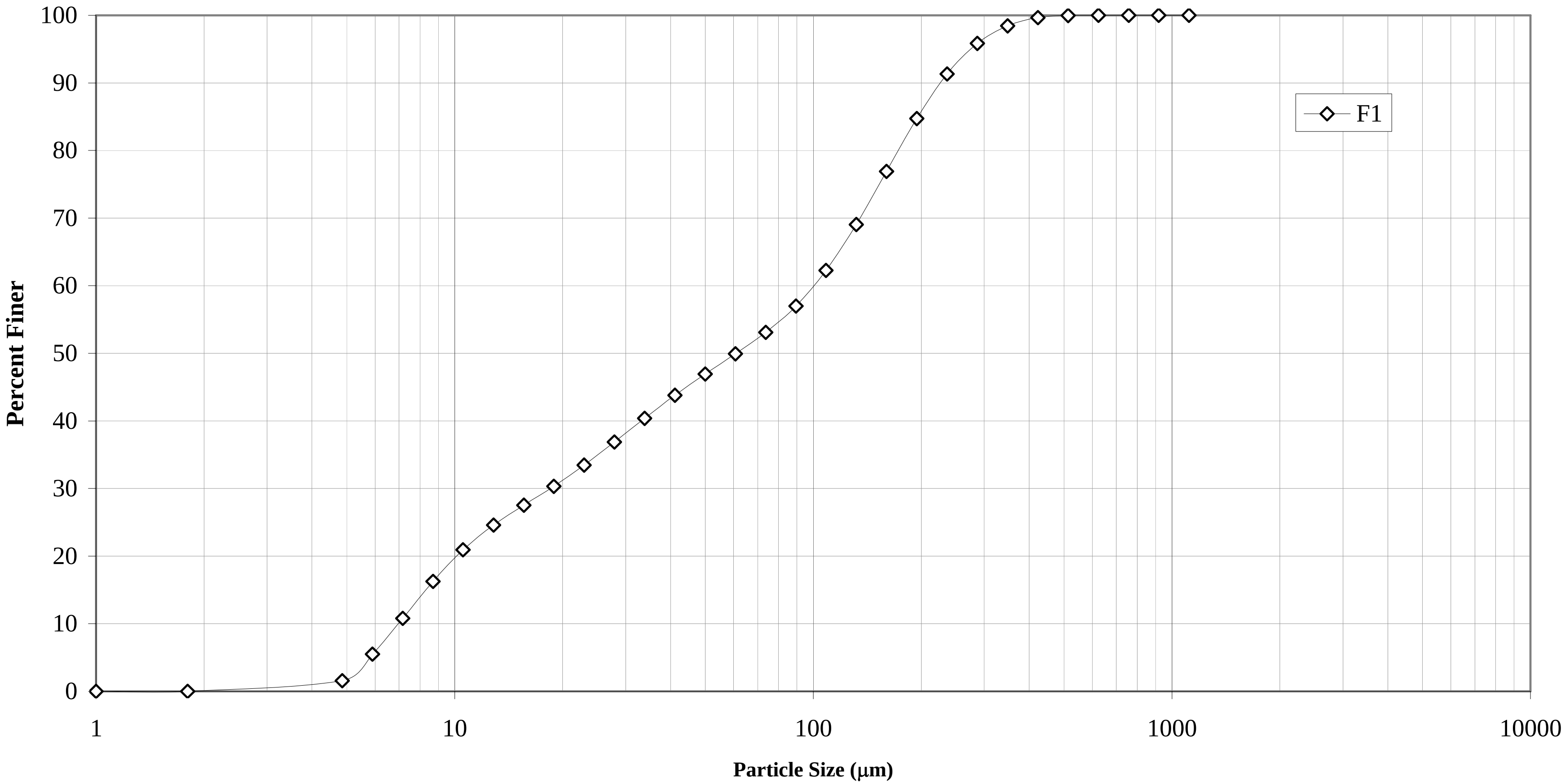


**FIG. A1.6 – Grain size distributions on hydraulic fill samples from mine F**

**TABLE A1.1 – Hydraulic fill permeability summary**

| | | | Permeability x$10^{-4}$ (cm/s) | | | | | |
|---|---|---|---|---|---|---|---|---|
| | | | Constant head | Falling head | Average | Water content (%) | Degree of saturation (%) | Dry density as multiple of $G_S$ |
| Mine A | A1 | a | 2.4 | 2.6 | 2.5 | 24.0 | 103 | 0.610 |
| | | b | 2.4 | 2.5 | 2.5 | 22.0 | 103 | 0.630 |
| | | c | 2.3 | 2.4 | 2.3 | 23.0 | 103 | 0.610 |
| | | d | 2.2 | 2.4 | 2.3 | 24.0 | 108 | 0.620 |
| | | e | 3.0 | 2.8 | 2.9 | 26.3 | 101 | 0.570 |
| | | f | 2.7 | 2.7 | 2.7 | 28.2 | 101 | 0.554 |
| | | g | 3.5 | 3.7 | 3.6 | 24.8 | 106 | 0.599 |
| | | h | 2.5 | 2.6 | 2.6 | 22.5 | 100 | 0.606 |
| | | i | 4.1 | 4.2 | 4.1 | 28.1 | 103 | 0.563 |
| | | j | 2.7 | 2.8 | 2.7 | 24.0 | 94 | 0.576 |
| | A2 | a | 4.8 | 5.1 | 5.0 | 24.8 | 98 | 0.584 |
| | | b | 5.6 | 5.7 | 5.7 | 24.0 | 100 | 0.600 |
| Mine B | B1 | a | 5.5 | 5.7 | 5.6 | 23.3 | 98 | 0.600 |
| | | b | 8.1 | --- | 8.1 | 23.0 | 98 | 0.600 |
| | | c | 4.9 | 4.9 | 4.9 | 23.3 | 97 | 0.590 |
| | B2 | a | 1.3 | 1.7 | 1.5 | 33.8 | 102 | 0.530 |
| | | b | 1.3 | 1.4 | 1.4 | 33.3 | 96 | 0.520 |
| | | c | 1.8 | 1.8 | 1.8 | 34.5 | 96 | 0.509 |
| Mine C | C1 | a | 5.5 | 5.3 | 5.4 | 17.2 | 102 | 0.582 |
| | | b | 6.5 | 5.4 | 6.0 | 17.6 | 92 | 0.546 |
| | | c | 6.4 | 7.0 | 6.7 | 19.1 | 104 | 0.554 |
| | | d | 5.4 | 4.3 | 4.8 | 18.2 | 98 | 0.551 |
| | | e | 5.3 | 7.7 | 6.5 | 18.8 | 105 | 0.564 |
| | | f | 6.0 | 6.8 | 6.4 | 18.3 | 107 | 0.576 |
| | C2 | a | 4.5 | 4.2 | 4.4 | 18.6 | 102 | 0.610 |
| | | b | 5.0 | 5.2 | 5.1 | 18.7 | 108 | 0.631 |
| | | c | 5.2 | 5.0 | 5.1 | 19.6 | 106 | 0.613 |
| | | d | 5.0 | 4.8 | 4.9 | 19.5 | 109 | 0.618 |
| | | e | 5.1 | 5.3 | 5.2 | 19.1 | 101 | 0.603 |
| | | f | 5.2 | 5.3 | 5.3 | 18.9 | 108 | 0.623 |
| | C3 | a | 4.9 | --- | 4.9 | 17.1 | 100 | 0.612 |
| | C4 | a | 6.3 | --- | 6.3 | 19.4 | 99 | 0.629 |
| Mine D | D1 | a | 5.7 | 6.0 | 5.9 | 17.6 | 100 | 0.646 |
| | | b | 5.1 | 5.2 | 5.2 | 17.6 | 100 | 0.642 |
| | | c | 5.7 | 6.1 | 5.9 | 18.5 | 100 | 0.632 |
| | | d | 5.9 | 6.1 | 6.0 | 19.8 | 100 | 0.617 |
| | | e | 5.7 | 5.9 | 5.8 | 18.7 | 100 | 0.622 |
| | D2 | a | 6.5 | 6.7 | 6.6 | 17.4 | 99 | 0.620 |
| | | b | 6.7 | 6.8 | 6.8 | 17.6 | 97 | 0.597 |
| | D3 | a | 13.5 | 14.3 | 13.9 | 19.9 | 100 | 0.591 |
| | | b | 15.9 | 16.0 | 16.0 | 20.3 | 100 | 0.585 |
| | D4 | a | 5.5 | 5.7 | 5.6 | 20.4 | 98 | 0.579 |
| | | b | 5.7 | 5.8 | 5.8 | 19.8 | 97 | 0.583 |
| | D5 | a | 6.9 | 7.1 | 7.0 | 20.0 | 100 | 0.590 |
| | | b | 6.9 | 7.2 | 7.1 | 20.0 | 99 | 0.586 |
| | D6 | a | 8.9 | 9.2 | 9.1 | 18.7 | 100 | 0.602 |
| | | b | 8.1 | 8.0 | 8.1 | 18.8 | 100 | 0.606 |
| | D7 | a | 5.4 | 5.3 | 5.4 | 20.1 | 99 | 0.597 |
| | | b | 6.0 | 6.1 | 6.1 | 20.1 | 98 | 0.595 |
| | D8 | a | 8.6 | 8.8 | 8.7 | 24.2 | 100 | 0.579 |
| | | b | 8.7 | 8.9 | 8.8 | 23.2 | 100 | 0.584 |
| | D9 | a | 7.7 | 8.0 | 7.9 | 21.4 | 100 | 0.577 |
| | | b | 6.9 | 7.2 | 7.1 | 20.2 | 97 | 0.583 |

# *Appendix 2*

**TABLE A2.1 – A1 brick dimensions and densities**

| Brick ID | Dimensions (mm) | | | | | | | | | | | | Volume ($cm^3$) | Dry Weight (g) | Bulk Density, $\rho_m$ ($g/cm^3$) |
|---|---|---|---|---|---|---|---|---|---|---|---|---|---|---|---|
| | Width | | | | Depth | | | | Length | | | | | | |
| | W1 | W2 | W3 | *Avg* | D1 | D2 | D3 | *Avg* | L1 | L2 | L3 | *Avg* | | | |
| A1_001 | 217 | 216 | 210 | *214* | 113 | 112 | 113 | *113* | 450 | 452 | 451 | *451* | 10875 | 19705 | 1.812 |
| A1_002 | 217 | 218 | 210 | *215* | 116 | 115 | 114 | *115* | 451 | 450 | 452 | *451* | 11126 | 21630 | 1.944 |
| A1_003 | 213 | 210 | 208 | *210* | 113 | 114 | 115 | *114* | 451 | 453 | 454 | *452* | 10822 | 20597 | 1.903 |
| A1_004 | 213 | 214 | 215 | *214* | 113 | 113 | 114 | *113* | 451 | 453 | 454 | *452* | 10913 | 19845 | 1.819 |

**TABLE A2.2 – A2 brick dimensions and densities**

| Brick ID | Dimensions (mm) | | | | | | | | | | | | Volume ($cm^3$) | Dry Weight (g) | Bulk Density, $\rho_m$ ($g/cm^3$) |
|---|---|---|---|---|---|---|---|---|---|---|---|---|---|---|---|
| | Width | | | | Depth | | | | Length | | | | | | |
| | W1 | W2 | W3 | *Avg* | D1 | D2 | D3 | *Avg* | L1 | L2 | L3 | *Avg* | | | |
| A2_001 | 206 | 206 | 207 | *206* | 115 | 114 | 113 | *114* | 453 | 451 | 452 | *452* | 10632 | 21622 | 2.034 |
| A2_002 | 207 | 210 | 211 | *209* | 114 | 112 | 114 | *113* | 453 | 453 | 452 | *453* | 10739 | 20550 | 1.914 |
| A2_003 | 207 | 210 | 212 | *210* | 113 | 114 | 113 | *113* | 453 | 452 | 458 | *454* | 10796 | 20266 | 1.877 |
| A2_004 | 206 | 211 | 215 | *211* | 112 | 112 | 113 | *112* | 452 | 452 | 450 | *451* | 10681 | 20823 | 1.950 |
| A2_005 | 208 | 210 | 212 | *210* | 111 | 114 | 114 | *113* | 450 | 455 | 453 | *453* | 10742 | 20855 | 1.941 |
| A2_006 | 219 | 216 | 210 | *215* | 115 | 114 | 112 | *114* | 456 | 452 | 450 | *453* | 11062 | 23278 | 2.104 |
| A2_007 | 217 | 216 | 210 | *214* | 115 | 114 | 113 | *114* | 455 | 452 | 450 | *452* | 11052 | 23308 | 2.109 |
| A2_008 | 210 | 210 | 212 | *211* | 114 | 112 | 111 | *112* | 453 | 452 | 450 | *452* | 10689 | 20577 | 1.925 |
| A2_009 | 213 | 211 | 210 | *211* | 114 | 114 | 112 | *113* | 453 | 452 | 449 | *451* | 10810 | 20346 | 1.882 |
| A2_010 | 211 | 213 | 212 | *212* | 114 | 114 | 113 | *114* | 450 | 450 | 448 | *449* | 10828 | 20591 | 1.902 |
| A2_012 | 215 | 215 | 215 | *215* | 114 | 114 | 114 | *114* | 454 | 454 | 454 | *454* | 11128 | 23432 | 2.106 |
| A2_013 | 211 | 211 | 211 | *211* | 113 | 113 | 113 | *113* | 452 | 452 | 452 | *452* | 10777 | 20451 | 1.898 |
| A2_014 | 211 | 212 | 211 | *211* | 114 | 113 | 113 | *113* | 451 | 451 | 453 | *452* | 10818 | 20943 | 1.936 |
| A2_016 | 211 | 211 | 211 | *211* | 113 | 113 | 113 | *113* | 452 | 452 | 452 | *452* | 10777 | 22645 | 2.101 |
| A2_017 | 214 | 214 | 214 | *214* | 113 | 113 | 113 | *113* | 450 | 450 | 450 | *450* | 10882 | 22297 | 2.049 |

**TABLE A2.3 – B brick dimensions and densities**

| Brick ID | Dimensions (mm) | | | | | | | | | | | | Volume ($cm^3$) | Dry Weight (g) | Bulk Density, $\rho_m$ ($g/cm^3$) |
|---|---|---|---|---|---|---|---|---|---|---|---|---|---|---|---|
| | Width | | | | Depth | | | | Length | | | | | | |
| | W1 | W2 | W3 | *Avg* | D1 | D2 | D3 | *Avg* | L1 | L2 | L3 | *Avg* | | | |
| B_001 | 189 | 190 | 191 | *190* | 92 | 91 | 92 | *91* | 390 | 393 | 394 | *392* | 6822 | 13736 | 2.013 |
| B_002 | 188 | 190 | 191 | *189* | 92 | 92 | 91 | *92* | 394 | 390 | 390 | *391* | 6774 | 13959 | 2.061 |
| B_003 | 191 | 190 | 188 | *189* | 92 | 90 | 91 | *91* | 392 | 394 | 395 | *394* | 6783 | 13694 | 2.019 |
| B_004 | 188 | 189 | 190 | *189* | 93 | 92 | 92 | *92* | 392 | 393 | 395 | *393* | 6842 | 14134 | 2.066 |
| B_005 | 191 | 189 | 186 | *189* | 92 | 92 | 91 | *91* | 390 | 396 | 400 | *395* | 6817 | 14105 | 2.069 |
| B_006 | 188 | 191 | 191 | *190* | 91 | 91 | 91 | *91* | 398 | 394 | 391 | *394* | 6803 | 14164 | 2.082 |
| B_007 | 190 | 190 | 187 | *189* | 91 | 91 | 91 | *91* | 395 | 396 | 389 | *393* | 6784 | 13854 | 2.042 |
| B_008 | 188 | 190 | 192 | *190* | 91 | 91 | 91 | *91* | 392 | 395 | 399 | *395* | 6825 | 13984 | 2.049 |
| B_009 | 188 | 190 | 191 | *190* | 92 | 91 | 91 | *92* | 399 | 397 | 391 | *396* | 6871 | 13921 | 2.026 |
| B_010 | 191 | 189 | 188 | *189* | 91 | 90 | 91 | *91* | 395 | 393 | 389 | *392* | 6757 | 13903 | 2.058 |

**TABLE A2.4 – Brick dimensions, porosity and specific gravity values**

| | **Brick ID** | **Dimensions (mm)** | | | | | | | | | | | | **Average volume ($cm^3$)** | **Dry weight (g)** | **Suspended wet weight (g)** | **Void volume $V_v$ ($cm^3$)** | **Porosity n** | **Average specific gravity $G_s$** |
|---|---|---|---|---|---|---|---|---|---|---|---|---|---|---|---|---|---|---|---|
| | | **Width** | | | | **Depth** | | | | **Length** | | | | | | | | | |
| | | *W 1* | *W 2* | *W 3* | *Avg* | *D 1* | *D 2* | *D 3* | *Avg* | *L 1* | *L 2* | *L 3* | *Avg* | | | | | | |
| **A1** | A1_ 001 | 217 | 216 | 210 | *214* | 113 | 112 | 113 | *113* | 450 | 452 | 451 | *451* | 10875 | 19705 | 11427 | 2597 | 0.24 | 2.38 |
| | A1_ 002 | 217 | 218 | 210 | *215* | 116 | 115 | 114 | *115* | 451 | 450 | 452 | *451* | 11126 | 21630 | 12503 | 1999 | 0.18 | 2.37 |
| | A1_ 003 | 213 | 210 | 208 | *210* | 113 | 114 | 115 | *114* | 451 | 453 | 454 | *452* | 10822 | 20597 | 12066 | 2291 | 0.21 | 2.41 |
| | A1_ 004 | 213 | 214 | 215 | *214* | 113 | 113 | 114 | *113* | 451 | 453 | 454 | *452* | 10913 | 19845 | 11542 | 2610 | 0.24 | 2.39 |
| | **Average** | | | | ***213*** | | | | ***114*** | | | | ***452*** | **10934** | **20444** | | **2374** | **0.22** | **2.39** |
| **A2** | A2_ 006 | 219 | 216 | 210 | *215* | 115 | 114 | 112 | *114* | 456 | 452 | 450 | *453* | 11062 | 23278 | 13190 | 974 | 0.09 | 2.31 |
| | A2_ 007 | 217 | 216 | 210 | *214* | 115 | 114 | 113 | *114* | 455 | 452 | 450 | *452* | 11052 | 23309 | 13254 | 997 | 0.09 | 2.32 |
| | A2_ 008 | 210 | 210 | 212 | *211* | 114 | 112 | 111 | *112* | 453 | 452 | 450 | *452* | 10689 | 20577 | 11759 | 1871 | 0.18 | 2.33 |
| | A2_ 009 | 213 | 211 | 210 | *211* | 114 | 114 | 112 | *113* | 453 | 452 | 449 | *451* | 10810 | 20346 | 11812 | 2276 | 0.21 | 2.38 |
| | A2_ 010 | 211 | 213 | 212 | *212* | 114 | 114 | 113 | *114* | 450 | 450 | 448 | *449* | 10828 | 20591 | 11935 | 2172 | 0.20 | 2.38 |
| | **Average** | | | | ***213*** | | | | ***113*** | | | | ***451*** | **10888** | **21620** | | **1658** | **0.15** | **2.34** |
| **B** | B_ 003 | 191 | 190 | 188 | *189* | 92 | 90 | 91 | *91* | 392 | 394 | 395 | *394* | 6783 | 13694 | 8343 | 1432 | 0.21 | 2.56 |
| | B_ 004 | 188 | 189 | 190 | *189* | 93 | 92 | 92 | *92* | 392 | 393 | 395 | *393* | 6842 | 14134 | 8549 | 1257 | 0.18 | 2.53 |
| | B_ 005 | 191 | 189 | 186 | *189* | 92 | 92 | 91 | *91* | 390 | 396 | 400 | *395* | 6817 | 14105 | 8566 | 1278 | 0.19 | 2.55 |
| | B_ 007 | 190 | 190 | 187 | *189* | 91 | 91 | 91 | *91* | 395 | 396 | 389 | *393* | 6784 | 13854 | 8447 | 1377 | 0.20 | 2.56 |
| | **Average** | | | | ***189*** | | | | ***91*** | | | | ***394*** | **6806** | **13947** | | **1336** | **0.20** | **2.55** |

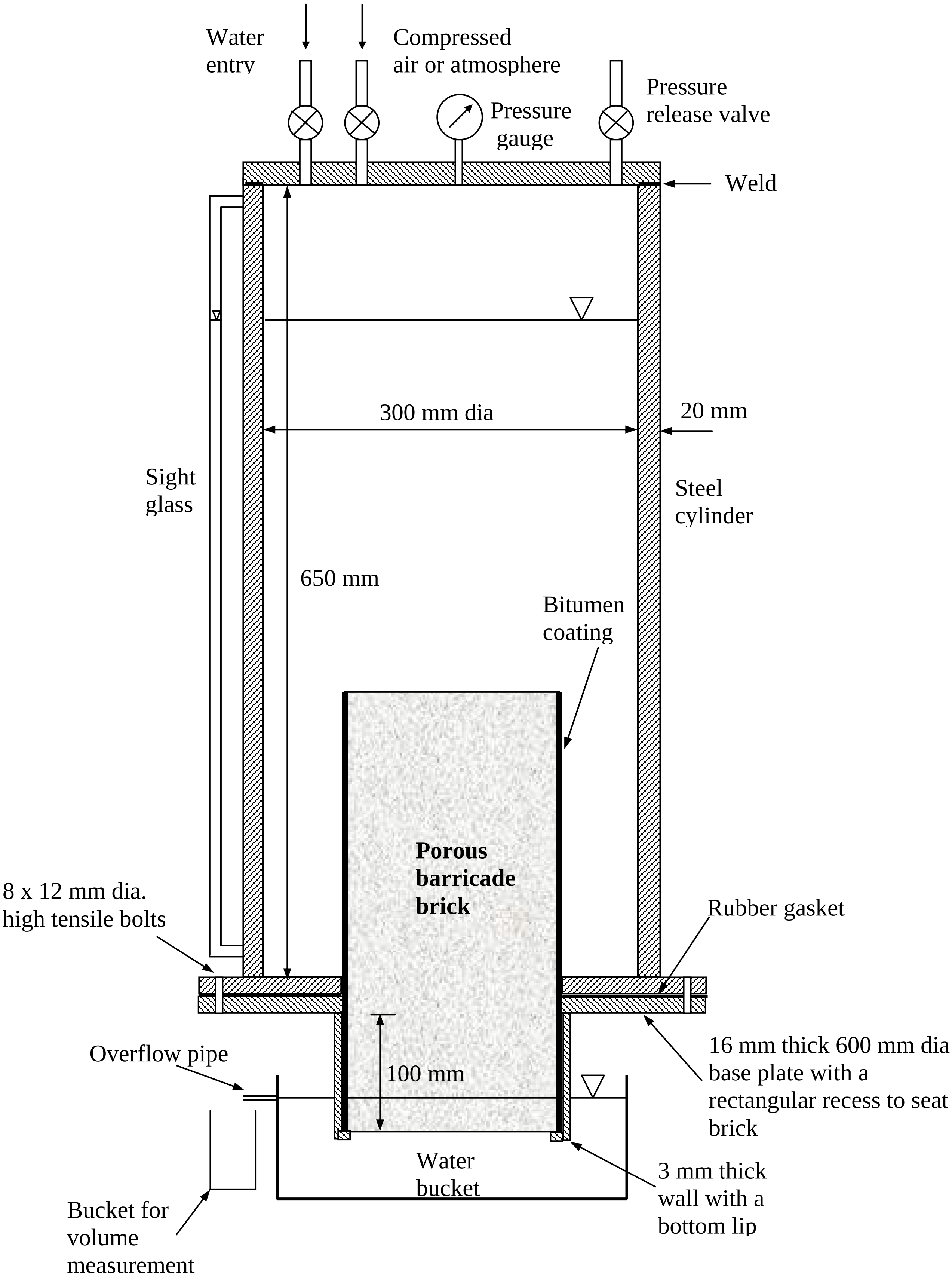


**FIG. A2.1 - Schematic diagram of the brick permeameter**

**TABLE A2.5 – Constant head permeability test data for A1 and A2 bricks**

| | | Permeability, k , @ x m of head (cm/sec) | | | |
|---|---|---|---|---|---|
| | **Head (m)** | **1.205** | **1.655** | **2.105** | **Average** |
| A1_001 | Test #1 | 0.274 | 0.332 | 0.384 | 0.303 |
| | Test #2 | 0.273 | 0.332 | 0.384 | |
| | Test #3 | 0.273 | 0.333 | 0.384 | |
| | ***Average*** | ***0.273*** | ***0.332*** | ***0.384*** | |
| A1_002 | Test #1 | 0.112 | 0.097 | 0.147 | 0.105 |
| | Test #2 | 0.109 | 0.097 | 0.147 | |
| | Test #3 | 0.111 | 0.100 | 0.147 | |
| | ***Average*** | ***0.111*** | ***0.098*** | ***0.147*** | |
| A1_003 | Test #1 | 0.077 | 0.074 | 0.066 | 0.075 |
| | Test #2 | 0.077 | 0.074 | 0.067 | |
| | Test #3 | 0.077 | 0.073 | 0.067 | |
| | ***Average*** | ***0.077*** | ***0.074*** | ***0.067*** | |
| A1_004 | Test #1 | 0.133 | 0.123 | 0.121 | 0.128 |
| | Test #2 | 0.133 | 0.121 | 0.121 | |
| | Test #3 | 0.134 | 0.122 | 0.121 | |
| | ***Average*** | ***0.133*** | ***0.122*** | ***0.121*** | |
| A2_004 | Test #1 | 0.109 | 0.107 | 0.109 | 0.108 |
| | Test #2 | 0.109 | 0.109 | 0.108 | |
| | Test #3 | 0.109 | 0.107 | 0.109 | |
| | ***Average*** | ***0.109*** | ***0.108*** | ***0.109*** | |
| A2_005 | Test #1 | 0.105 | 0.102 | 0.099 | 0.102 |
| | Test #2 | 0.105 | 0.100 | 0.098 | |
| | Test #3 | 0.104 | 0.100 | 0.098 | |
| | ***Average*** | ***0.104*** | ***0.100*** | ***0.098*** | |
| A2_012 | Test #1 | 0.096 | 0.085 | 0.078 | 0.090 |
| | Test #2 | 0.095 | 0.085 | 0.078 | |
| | Test #3 | 0.093 | 0.085 | 0.078 | |
| | ***Average*** | ***0.095*** | ***0.085*** | ***0.078*** | |
| A2_013 | Test #1 | 0.095 | 0.085 | 0.077 | 0.089 |
| | Test #2 | 0.094 | 0.084 | 0.077 | |
| | Test #3 | 0.094 | 0.084 | 0.077 | |
| | ***Average*** | ***0.094*** | ***0.085*** | ***0.077*** | |
| A2_014 | Test #1 | 0.051 | 0.052 | 0.052 | 0.051 |
| | Test #2 | 0.050 | 0.051 | 0.053 | |
| | Test #3 | 0.050 | 0.051 | 0.053 | |
| | ***Average*** | ***0.050*** | ***0.051*** | ***0.052*** | |
| A2_016 | Test #1 | 0.136 | 0.117 | 0.104 | 0.125 |
| | Test #2 | 0.133 | 0.116 | 0.104 | |
| | Test #3 | 0.133 | 0.116 | 0.104 | |
| | ***Average*** | ***0.134*** | ***0.116*** | ***0.104*** | |
| A2_017 | Test #1 | 0.013 | 0.011 | 0.011 | 0.012 |
| | Test #2 | 0.012 | 0.011 | 0.010 | |
| | Test #3 | 0.012 | 0.011 | 0.010 | |
| | ***Average*** | ***0.012*** | ***0.011*** | ***0.011*** | |

**TABLE A2.6 – Constant head permeability test data for B bricks**

| | Head (m) | 1.205 | 1.655 | 2.105 | Average |
|---|---|---|---|---|---|
| | | Permeability, k , @ x m of head (cm/sec) | | | |
| B_003 | Test #1 | 0.258 | 0.218 | 0.195 | 0.237 |
| | Test #2 | 0.254 | 0.218 | 0.195 | |
| | Test #3 | 0.254 | 0.218 | 0.195 | |
| | ***Average*** | ***0.255*** | ***0.218*** | ***0.195*** | |
| B_004 | Test #1 | 0.164 | 0.139 | 0.123 | 0.152 |
| | Test #2 | 0.164 | 0.140 | 0.123 | |
| | Test #3 | 0.164 | 0.140 | 0.123 | |
| | ***Average*** | ***0.164*** | ***0.140*** | ***0.123*** | |
| B_005 | Test #1 | 0.110 | 0.094 | 0.086 | 0.102 |
| | Test #2 | 0.109 | 0.095 | 0.084 | |
| | Test #3 | 0.109 | 0.095 | 0.086 | |
| | ***Average*** | ***0.110*** | ***0.095*** | ***0.085*** | |
| B_006 | Test #1 | 0.104 | 0.086 | 0.078 | 0.095 |
| | Test #2 | 0.104 | 0.086 | 0.078 | |
| | Test #3 | 0.103 | 0.086 | 0.078 | |
| | ***Average*** | ***0.104*** | ***0.086*** | ***0.078*** | |
| B_007 | Test #1 | 0.127 | 0.108 | 0.097 | 0.118 |
| | Test #2 | 0.129 | 0.110 | 0.096 | |
| | Test #3 | 0.127 | 0.108 | 0.097 | |
| | ***Average*** | ***0.127*** | ***0.109*** | ***0.097*** | |
| B_008 | Test #1 | 0.188 | 0.157 | 0.139 | 0.241 |
| | Test #2 | 0.186 | 0.156 | 0.138 | |
| | Test #3 | 0.184 | 0.156 | 0.139 | |
| | ***Average*** | ***0.233*** | ***0.248*** | ***0.139*** | |
| B Composite Brick #1 | Test #1 | 0.044 | 0.049 | 0.052 | 0.048 |
| | Test #2 | 0.044 | 0.050 | 0.053 | |
| | Test #3 | 0.051 | 0.051 | 0.052 | |
| | ***Average*** | ***0.046*** | ***0.050*** | ***0.052*** | |
| B Composite Brick #2 | Test #1 | 0.011 | 0.010 | 0.009 | 0.011 |
| | Test #2 | 0.011 | 0.010 | 0.009 | |
| | Test #3 | 0.011 | 0.010 | 0.009 | |
| | ***Average*** | ***0.011*** | ***0.010*** | ***0.009*** | |

**TABLE A2.7 – Falling head permeability test data for A1 and A2 bricks**

| Sample ID | Test No. | k1 (cm/s) | k2 (cm/s) | Average (cm/s) |
|---|---|---|---|---|
| A1_001 | Test #1 | 0.156 | 0.169 | 0.162 |
| | Test #2 | 0.145 | 0.158 | |
| | Test #3 | 0.216 | 0.234 | |
| | Test #4 | 0.099 | 0.107 | |
| | Test #5 | 0.210 | 0.216 | |
| | Test #6 | 0.116 | 0.114 | |
| | Test #7 | 0.109 | 0.107 | |
| | ***Average*** | ***0.157*** | ***0.166*** | |
| A1_002 | Test #1 | 0.025 | 0.026 | 0.026 |
| | Test #2 | 0.029 | 0.030 | |
| | Test #3 | 0.021 | 0.022 | |
| | ***Average*** | ***0.025*** | ***0.026*** | |
| A1_003 | Test #1 | 0.087 | 0.093 | 0.069 |
| | Test #2 | 0.061 | 0.065 | |
| | Test #3 | 0.051 | 0.056 | |
| | ***Average*** | ***0.066*** | ***0.071*** | |
| A1_004 | Test #1 | 0.136 | 0.149 | 0.144 |
| | Test #2 | 0.141 | 0.152 | |
| | Test #3 | 0.137 | 0.148 | |
| | ***Average*** | ***0.138*** | ***0.150*** | |
| A2_014 | Test #1 | 0.077 | 0.082 | 0.073 |
| | Test #2 | 0.069 | 0.074 | |
| | Test #3 | 0.064 | 0.068 | |
| | ***Average*** | ***0.093*** | ***0.098*** | |
| A2_016 | Test #1 | 0.101 | 0.106 | 0.095 |
| | Test #2 | 0.092 | 0.097 | |
| | Test #3 | 0.084 | 0.090 | |
| | ***Average*** | ***0.093*** | ***0.098*** | |

**TABLE A2.8 – Falling head permeability test data for B bricks**

| Sample ID | Test No. | k1 (cm/s) | k2 (cm/s) | Average (cm/s) |
|---|---|---|---|---|
| B_003 | Test #1 | 0.304 | 0.317 | 0.310 |
| | Test #2 | 0.301 | 0.317 | |
| | Test #3 | 0.302 | 0.317 | |
| | ***Average*** | ***0.302*** | ***0.317*** | |
| B_004 | Test #1 | 0.205 | 0.214 | 0.207 |
| | Test #2 | 0.202 | 0.212 | |
| | Test #3 | 0.197 | 0.208 | |
| | Test #4 | 0.202 | 0.212 | |
| | ***Average*** | ***0.202*** | ***0.212*** | |
| B_005 | Test #1 | 0.123 | 0.131 | 0.128 |
| | Test #2 | 0.123 | 0.133 | |
| | Test #3 | 0.123 | 0.132 | |
| | ***Average*** | ***0.123*** | ***0.132*** | |
| B_006 | Test #1 | 0.131 | 0.135 | 0.132 |
| | Test #2 | 0.129 | 0.134 | |
| | Test #3 | 0.129 | 0.134 | |
| | ***Average*** | ***0.130*** | ***0.135*** | |
| B_007 | Test #1 | 0.138 | 0.146 | 0.142 |
| | Test #2 | 0.139 | 0.146 | |
| | Test #3 | 0.139 | 0.146 | |
| | ***Average*** | ***0.138*** | ***0.146*** | |
| B_008 | Test #1 | 0.234 | 0.249 | 0.241 |
| | Test #2 | 0.234 | 0.248 | |
| | Test #3 | 0.233 | 0.247 | |
| | ***Average*** | ***0.233*** | ***0.248*** | |
| B Composite Brick #1 | Test #1 | 0.132 | 0.141 | 0.125 |
| | Test #2 | 0.121 | 0.134 | |
| | Test #3 | 0.102 | 0.121 | |
| | ***Average*** | ***0.118*** | ***0.132*** | |
| B Composite Brick #2 | Test #1 | 0.023 | 0.025 | 0.021 |
| | Test #2 | 0.020 | 0.021 | |
| | Test #3 | 0.018 | 0.019 | |
| | ***Average*** | ***0.020*** | ***0.022*** | |

**TABLE A2.9 – Flow-under-pressure permeability test data for A1 and A2 bricks**

| | | | | | **Pressure** | **25** | **50** | **100** | **100** | **137.9** | **206.85** | **275.8** | **344.75** | **kPa** |
|---|---|---|---|---|---|---|---|---|---|---|---|---|---|---|
| **A1** | A1_001 | width | 214 | mm | **Flow Rate** | 11.520 | 21.507 | 35.640 | 31.540 | 39.360 | 47.600 | 54.340 | 60.373 | **litres/min** |
| | | depth | 113 | mm | **Velocity** | 0.794 | 1.482 | 2.456 | 2.174 | 2.713 | 3.281 | 3.745 | 4.161 | **cm/s** |
| | | height | 451 | mm | **Hyd. Grad (i)** | 5.543 | 11.086 | 22.173 | 22.173 | 30.576 | 45.865 | 61.153 | 76.441 | |
| | | Area | 241.82 | $cm^2$ | **v/i** | 0.143 | 0.134 | 0.111 | 0.098 | 0.089 | 0.072 | 0.061 | 0.054 | **cm/s** |
| | A1_002 | width | 215 | mm | **Flow Rate** | 4.113 | 7.000 | 11.053 | 10.840 | 13.320 | 16.333 | 20.000 | 23.573 | **litres/min** |
| | | depth | 115 | mm | **Velocity** | 0.277 | 0.472 | 0.745 | 0.731 | 0.898 | 1.101 | 1.348 | 1.589 | **cm/s** |
| | | height | 451 | mm | **Hyd. Grad (i)** | 5.543 | 11.086 | 22.173 | 22.173 | 30.576 | 45.865 | 61.153 | 76.441 | |
| | | Area | 247.25 | $cm^2$ | **v/i** | 0.050 | 0.043 | 0.034 | 0.033 | 0.029 | 0.024 | 0.022 | 0.021 | **cm/s** |
| | A1_003 | width | 210 | mm | **Flow Rate** | 4.613 | 10.693 | 20.667 | 20.667 | 24.533 | 31.820 | 36.053 | 39.173 | **litres/min** |
| | | depth | 114 | mm | **Velocity** | 0.321 | 0.744 | 1.439 | 1.439 | 1.708 | 2.215 | 2.510 | 2.727 | **cm/s** |
| | | height | 452 | mm | **Hyd. Grad (i)** | 5.531 | 11.062 | 22.124 | 22.124 | 30.509 | 45.763 | 61.018 | 76.272 | |
| | | Area | 239.4 | $cm^2$ | **v/i** | 0.058 | 0.067 | 0.065 | 0.065 | 0.056 | 0.048 | 0.041 | 0.036 | **cm/s** |
| | A1_004 | width | 214 | mm | **Flow Rate** | 7.167 | 14.107 | 23.947 | 23.947 | 30.580 | 36.960 | 43.627 | 52.827 | **litres/min** |
| | | depth | 113 | mm | **Velocity** | 0.494 | 0.972 | 1.650 | 1.650 | 2.108 | 2.547 | 3.007 | 3.641 | **cm/s** |
| | | height | 452 | mm | **Hyd. Grad (i)** | 5.531 | 11.062 | 22.124 | 22.124 | 30.509 | 45.763 | 61.018 | 76.272 | |
| | | Area | 241.82 | $cm^2$ | **v/i** | 0.089 | 0.088 | 0.075 | 0.075 | 0.069 | 0.056 | 0.049 | 0.048 | **cm/s** |
| **A2** | A2_014 | width | 211 | mm | **Flow Rate** | 4.393 | 8.720 | 15.573 | 15.573 | 19.800 | 23.880 | 27.893 | 31.440 | **litres/min** |
| | | depth | 113 | mm | **Velocity** | 0.307 | 0.610 | 1.089 | 1.089 | 1.384 | 1.669 | 1.950 | 2.198 | **cm/s** |
| | | height | 451 | mm | **Hyd. Grad (i)** | 5.543 | 11.086 | 22.173 | 22.173 | 30.576 | 45.865 | 61.153 | 76.441 | |
| | | Area | 238.43 | $cm^2$ | **v/i** | 0.055 | 0.055 | 0.049 | 0.049 | 0.045 | 0.036 | 0.032 | 0.029 | **cm/s** |
| | A2_016 | width | 211 | mm | **Flow Rate** | 5.907 | 12.280 | 20.613 | 20.653 | 25.840 | 30.920 | 36.533 | 40.440 | **litres/min** |
| | | depth | 113 | mm | **Velocity** | 0.413 | 0.858 | 1.441 | 1.444 | 1.806 | 2.161 | 2.554 | 2.827 | **cm/s** |
| | | height | 452 | mm | **Hyd. Grad (i)** | 5.531 | 11.062 | 22.124 | 22.124 | 30.509 | 45.763 | 61.018 | 76.272 | |
| | | Area | 238.43 | $cm^2$ | **v/i** | 0.075 | 0.078 | 0.065 | 0.065 | 0.059 | 0.047 | 0.042 | 0.037 | **cm/s** |

**TABLE A2.10 – Flow-under-pressure permeability test data for B bricks**

| | | | | | Pressure | 25 | 50 | 100 | 100 | 137.9 | 206.85 | 275.8 | 344.75 | kPa |
|---|---|---|---|---|---|---|---|---|---|---|---|---|---|---|
| B | B_003 | width | 189 | mm | Flow Rate | 12.087 | 17.973 | 28.000 | 28.000 | 31.413 | 37.140 | 41.573 | 46.800 | litres/min |
| | | depth | 91 | mm | Velocity | 1.171 | 1.742 | 2.713 | 2.713 | 3.044 | 3.599 | 4.029 | 4.535 | cm/s |
| | | height | 394 | mm | Hyd. Grad (i) | 6.345 | 12.690 | 25.381 | 25.381 | 35.000 | 52.500 | 70.000 | 87.500 | |
| | | Area | 171.99 | $cm^2$ | v/i | 0.185 | 0.137 | 0.107 | 0.107 | 0.087 | 0.069 | 0.058 | 0.052 | cm/s |
| | B_004 | width | 189 | mm | Flow Rate | 7.800 | 12.107 | 17.493 | 17.507 | 20.493 | 25.573 | 29.920 | 34.880 | litres/min |
| | | depth | 92 | mm | Velocity | 0.748 | 1.160 | 1.677 | 1.678 | 1.964 | 2.451 | 2.868 | 3.343 | cm/s |
| | | height | 378 | mm | Hyd. Grad (i) | 6.614 | 13.228 | 26.455 | 26.455 | 36.481 | 54.722 | 72.963 | 91.204 | |
| | | Area | 173.88 | $cm^2$ | v/i | 0.113 | 0.088 | 0.063 | 0.063 | 0.054 | 0.045 | 0.039 | 0.037 | cm/s |
| | B_005 | width | 189 | mm | Flow Rate | 4.940 | 7.533 | 11.253 | 11.253 | 13.173 | 16.260 | 18.920 | 21.547 | litres/min |
| | | depth | 91 | mm | Velocity | 0.479 | 0.730 | 1.091 | 1.091 | 1.277 | 1.576 | 1.833 | 2.088 | cm/s |
| | | height | 395 | mm | Hyd. Grad (i) | 6.329 | 12.658 | 25.316 | 25.316 | 34.911 | 52.367 | 69.823 | 87.278 | |
| | | Area | 171.99 | $cm^2$ | v/i | 0.076 | 0.058 | 0.043 | 0.043 | 0.037 | 0.030 | 0.026 | 0.024 | cm/s |
| | B_006 | width | 190 | mm | Flow Rate | 5.513 | 8.160 | 11.613 | 12.213 | 14.067 | 16.880 | 20.320 | 20.667 | litres/min |
| | | depth | 91 | mm | Velocity | 0.531 | 0.787 | 1.119 | 1.177 | 1.356 | 1.627 | 1.959 | 1.992 | cm/s |
| | | height | 394 | mm | Hyd. Grad (i) | 6.345 | 12.690 | 25.381 | 25.381 | 35.000 | 52.500 | 70.000 | 87.500 | |
| | | Area | 172.9 | $cm^2$ | v/i | 0.084 | 0.062 | 0.044 | 0.046 | 0.039 | 0.031 | 0.028 | 0.023 | cm/s |
| | B_007 | width | 189 | mm | Flow Rate | 5.593 | 8.733 | 12.840 | 12.840 | 15.253 | 18.480 | 20.740 | 22.680 | litres/min |
| | | depth | 91 | mm | Velocity | 0.542 | 0.846 | 1.244 | 1.244 | 1.478 | 1.791 | 2.010 | 2.198 | cm/s |
| | | height | 393 | mm | Hyd. Grad (i) | 6.361 | 12.723 | 25.445 | 25.445 | 35.089 | 52.634 | 70.178 | 87.723 | |
| | | Area | 171.99 | $cm^2$ | v/i | 0.085 | 0.067 | 0.049 | 0.049 | 0.042 | 0.034 | 0.029 | 0.025 | cm/s |
| | B_008 | width | 190 | mm | Flow Rate | 8.340 | 12.467 | 18.040 | 18.040 | 21.947 | 24.940 | 29.307 | 31.840 | litres/min |
| | | depth | 91 | mm | Velocity | 0.804 | 1.202 | 1.739 | 1.739 | 2.116 | 2.404 | 2.825 | 3.069 | cm/s |
| | | height | 395 | mm | Hyd. Grad (i) | 6.329 | 12.658 | 25.316 | 25.316 | 34.911 | 52.367 | 69.823 | 87.278 | |
| | | Area | 172.9 | $cm^2$ | v/i | 0.127 | 0.095 | 0.069 | 0.069 | 0.061 | 0.046 | 0.040 | 0.035 | cm/s |
| | B Composite Brick #2 | width | 189 | mm | Flow Rate | 0.607 | 0.833 | 1.100 | 1.100 | 1.267 | 1.807 | 1.887 | 2.007 | litres/min |
| | | depth | 91 | mm | Velocity | 0.058 | 0.080 | 0.106 | 0.106 | 0.122 | 0.174 | 0.182 | 0.193 | cm/s |
| | | height | 408 | mm | Hyd. Grad (i) | 6.329 | 12.658 | 25.316 | 25.316 | 34.911 | 52.367 | 69.823 | 87.278 | |
| | | Area | 171.99 | $cm^2$ | v/i | 0.009 | 0.006 | 0.004 | 0.004 | 0.003 | 0.003 | 0.003 | 0.002 | cm/s |

**TABLE A2.11 – Unconfined compressive strength data for Mine D cores**

| Sample No. | def @ peak load (mm) | Peak load (N) | UCS (MPa) | E (Gpa) | $\varepsilon_f$ (%) |
|---|---|---|---|---|---|
| 1A | 0.560 | 30340 | 5.04 | 2.40 | 0.326 |
| 1B | 0.712 | 38500 | 6.43 | 1.95 | 0.413 |
| 2A | 0.606 | 24430 | 4.06 | 1.89 | 0.352 |
| 2B | 1.227 | 27790 | 4.59 | 0.79 | 0.715 |
| 3A | 0.580 | 38150 | 6.35 | 2.41 | 0.337 |
| 3Bwet | 0.539 | 33370 | 5.52 | 2.39 | 0.313 |
| 4A | 0.683 | 23430 | 3.89 | 1.20 | 0.397 |
| 4Bwet | 0.680 | 32817 | 5.42 | 2.62 | 0.395 |
| 5A | 0.663 | 22640 | 3.73 | 1.39 | 0.385 |
| 5B | 0.633 | 43310 | 7.14 | 2.78 | 0.368 |
| 6A | 0.582 | 32530 | 5.36 | 2.27 | 0.339 |
| 6B | 0.514 | 37990 | 6.26 | 2.26 | 0.298 |
| 7A | 0.608 | 30120 | 4.96 | 2.60 | 0.354 |
| 7B | 0.249 | 23390 | 3.86 | 2.30 | 0.145 |
| 8A | 1.132 | 49530 | 8.15 | 1.55 | 0.660 |
| 8Bwet | 1.065 | 34540 | 5.69 | 1.40 | 0.618 |
| 9A | 0.798 | 23680 | 3.91 | 0.94 | 0.464 |
| 9Bwet | 0.327 | 12790 | 2.11 | 1.36 | 0.190 |
| 10A | 0.658 | 36660 | 6.04 | 2.10 | 0.383 |
| 10Bwet | 0.846 | 16250 | 2.68 | 1.02 | 0.493 |
| 11A | 0.731 | 42220 | 6.97 | 2.32 | 0.426 |
| 11Bwet | 0.580 | 38124 | 6.30 | 2.83 | 0.338 |
| 12A | 0.968 | 23980 | 3.96 | 0.88 | 0.564 |
| 12Bwet | 0.764 | 16356 | 2.70 | 0.79 | 0.445 |
| 13A | 0.582 | 38910 | 6.44 | 2.39 | 0.338 |
| 13Bwet | 0.677 | 23340 | 3.88 | 1.46 | 0.393 |
| 14A | 1.519 | 33480 | 5.52 | 1.73 | 0.886 |
| 14Bwet | 0.969 | 21590 | 3.56 | 0.65 | 0.564 |
| 15A | 0.903 | 46120 | 7.61 | 1.70 | 0.525 |
| 15B | 0.827 | 39060 | 6.46 | 1.59 | 0.482 |
| 16A | 1.328 | 49920 | 8.25 | 1.43 | 0.774 |
| 16B | 0.546 | 37990 | 6.28 | 1.74 | 0.317 |
| 17A | 0.469 | 37780 | 6.25 | 2.95 | 0.274 |
| 17Bwet | 0.776 | 41128 | 6.81 | 3.08 | 0.451 |
| 18A | 0.489 | 39090 | 6.45 | 3.23 | 0.285 |
| 18Bwet | 0.896 | 24560 | 4.05 | 1.02 | 0.521 |
| 19A | 0.574 | 38660 | 6.38 | 2.10 | 0.334 |
| 19Bwet | 0.677 | 26735 | 4.42 | 2.04 | 0.394 |
| 20A | 0.488 | 34840 | 5.74 | 2.55 | 0.284 |
| 20Bwet | 1.207 | 15200 | 2.51 | 1.08 | 0.700 |
| 21A | 0.786 | 55920 | 9.22 | 3.05 | 0.458 |
| 21Bwet | 0.797 | 37270 | 6.15 | 1.41 | 0.465 |
| 22A | 0.633 | 63170 | 10.45 | 3.50 | 0.371 |
| 22Bwet | 0.787 | 48000 | 7.91 | 2.09 | 0.460 |
| 23A | 0.882 | 57890 | 9.55 | 2.10 | 0.513 |
| 23Bwet | 0.972 | 50230 | 8.28 | 2.32 | 0.566 |
| 24A | 1.020 | 56790 | 9.36 | 2.83 | 0.595 |
| 24Bwet | 0.921 | 63073 | 10.41 | 3.57 | 0.537 |
| 25A | 0.980 | 69560 | 11.44 | 3.61 | 0.572 |
| 25B | 0.438 | 60800 | 10.02 | 2.71 | 0.255 |
| 26A | 0.648 | 57650 | 9.49 | 3.29 | 0.376 |
| 26B | 1.023 | 54110 | 8.91 | 2.27 | 0.595 |
| 27A | 1.017 | 55240 | 9.10 | 2.03 | 0.596 |
| 27Bwet | 0.973 | 23580 | 3.88 | 0.88 | 0.566 |
| 28A | 1.507 | 40460 | 6.67 | 0.82 | 0.878 |
| 28B | 0.452 | 51770 | 8.55 | 2.71 | 0.263 |
| 29A | 0.843 | 41120 | 6.78 | 1.93 | 0.491 |
| 29Bwet | 0.930 | 35592 | 5.85 | 1.18 | 0.542 |
| 30A | 0.704 | 43040 | 7.08 | 2.31 | 0.411 |
| 30B | 0.526 | 39900 | 6.58 | 1.93 | 0.307 |
| 31A | 0.870 | 45180 | 7.43 | 2.22 | 0.509 |
| 31Bwet | 1.077 | 22710 | 3.74 | 0.96 | 0.632 |
| 32A | 1.559 | 54310 | 8.94 | 1.92 | 0.909 |
| 32Bwet | 0.845 | 39690 | 6.55 | 2.04 | 0.492 |
| 33A | 0.634 | 50100 | 8.25 | 3.05 | 0.370 |
| 33B | 0.594 | 39390 | 6.49 | 1.88 | 0.347 |
| 34A | 0.707 | 41980 | 6.90 | 2.03 | 0.412 |
| 34Bwet | 0.673 | 43500 | 7.16 | 3.05 | 0.392 |
| 35A | 0.689 | 50690 | 8.35 | 2.38 | 0.401 |
| 35B | 1.129 | 52790 | 8.69 | 2.15 | 0.658 |

| Sample No. | def @ peak load (mm) | Peak load (N) | UCS (MPa) | E (Gpa) | $\varepsilon_f$ (%) |
|---|---|---|---|---|---|
| 37A | 0.757 | 40390.0 | 6.65 | 2.53 | 0.443 |
| 37Bwet | 1.082 | 30726.0 | 5.06 | 2.20 | 0.631 |
| 38A | 1.093 | 66690.0 | 10.98 | 1.83 | 0.639 |
| 38B | 0.504 | 42720.0 | 7.05 | 2.14 | 0.293 |
| 39A | 0.808 | 58470.0 | 9.62 | 2.43 | 0.472 |
| 39B | | | | | 0.000 |
| 40A | 1.909 | 36820.0 | 6.06 | 0.63 | 1.111 |
| 40Bwet | 0.723 | 36760.0 | 6.05 | 2.04 | 0.420 |
| 41A | 0.895 | 60000.0 | 9.89 | 2.14 | 0.523 |
| 41B | | | | | 0.000 |
| 42A | 0.771 | 65480.0 | 10.79 | 2.99 | 0.451 |
| 42B | 0.357 | 39910.0 | 6.57 | 2.31 | 0.209 |
| 43A | 0.997 | 52620 | 8.68 | 1.98 | 0.581 |
| 43B | | | | | 0.000 |
| 44A | 1.099 | 76940 | 12.64 | 3.94 | 0.642 |
| 44Bwet | 0.885 | 57534 | 9.47 | 2.87 | 0.517 |
| 45A | 0.989 | 59500 | 9.77 | 2.59 | 0.578 |
| 45Bwet | 0.971 | 39420 | 6.50 | 1.87 | 0.565 |
| 46A | 0.794 | 53140 | 8.74 | 2.24 | 0.465 |
| 46B | 0.971 | 76460 | 12.61 | 3.74 | 0.565 |
| 47A | 0.841 | 47030 | 7.74 | 2.08 | 0.492 |
| 47Bwet | 0.960 | 37600 | 6.19 | 1.69 | 0.561 |
| 48A | 1.468 | 53650 | 8.84 | 1.72 | 0.858 |
| 48Bwet | 0.825 | 46770 | 7.69 | 1.81 | 0.481 |
| 49A | 0.934 | 72310 | 11.89 | 2.76 | 0.545 |
| 49B | 0.606 | 47200 | 7.77 | 1.66 | 0.354 |
| 50A | 1.374 | 44250 | 7.28 | 1.68 | 0.809 |
| 50Bwet | 1.252 | 41740 | 6.87 | 1.17 | 0.728 |

| |
|---|
| The additional JCU tests for research (JCU) - dry |
| The additional JCU tests for research (JCU) - soaked for a week |
| The additional JCU tests for research (JCU) - soaked for 90 days |
| 90 days soaked (lost while crushing) |
| Cores tested at Uni of Qld by Keith Clark |
| Cores tested for Mine D (all A and 5B) |
| One missing brick |

**TABLE A2.12 – Harr’s gamma function table**

| N | Γ(N) | N | Γ(N) | N | Γ(N) | N | Γ(N) |
|---|---|---|---|---|---|---|---|
| 1.00 | 1.00000 | 1.25 | 0.90640 | 1.50 | 0.88623 | 1.75 | 0.91906 |
| 1.01 | 0.99433 | 1.26 | 0.90440 | 1.51 | 0.88659 | 1.76 | 0.92137 |
| 1.02 | 0.98884 | 1.27 | 0.90250 | 1.52 | 0.88704 | 1.77 | 0.92376 |
| 1.03 | 0.98355 | 1.28 | 0.90072 | 1.53 | 0.88757 | 1.78 | 0.92623 |
| 1.04 | 0.97844 | 1.29 | 0.89904 | 1.54 | 0.88818 | 1.79 | 0.92877 |
| 1.05 | 0.97350 | 1.30 | 0.89747 | 1.55 | 0.88887 | 1.80 | 0.93038 |
| 1.06 | 0.96874 | 1.31 | 0.89600 | 1.56 | 0.88964 | 1.81 | 0.93408 |
| 1.07 | 0.96415 | 1.32 | 0.89464 | 1.57 | 0.89049 | 1.82 | 0.93685 |
| 1.08 | 0.95973 | 1.33 | 0.89338 | 1.58 | 0.89142 | 1.83 | 0.93969 |
| 1.09 | 0.95546 | 1.34 | 0.89222 | 1.59 | 0.89243 | 1.84 | 0.94261 |
| 1.10 | 0.95135 | 1.35 | 0.89115 | 1.60 | 0.89352 | 1.85 | 0.94561 |
| 1.11 | 0.94740 | 1.36 | 0.89018 | 1.61 | 0.89468 | 1.86 | 0.94869 |
| 1.12 | 0.94359 | 1.37 | 0.88931 | 1.62 | 0.89592 | 1.87 | 0.95184 |
| 1.13 | 0.93993 | 1.38 | 0.88854 | 1.63 | 0.89724 | 1.88 | 0.95507 |
| 1.14 | 0.93642 | 1.39 | 0.88785 | 1.64 | 0.89864 | 1.89 | 0.95838 |
| 1.15 | 0.93304 | 1.40 | 0.88726 | 1.65 | 0.90012 | 1.90 | 0.96177 |
| 1.16 | 0.92980 | 1.41 | 0.88676 | 1.66 | 0.90167 | 1.91 | 0.96523 |
| 1.17 | 0.92670 | 1.42 | 0.88636 | 1.67 | 0.90330 | 1.92 | 0.96877 |
| 1.18 | 0.92373 | 1.43 | 0.88604 | 1.68 | 0.90500 | 1.93 | 0.97240 |
| 1.19 | 0.92089 | 1.44 | 0.88581 | 1.69 | 0.90678 | 1.94 | 0.97610 |
| 1.20 | 0.91817 | 1.45 | 0.88566 | 1.70 | 0.90864 | 1.95 | 0.97988 |
| 1.21 | 0.91558 | 1.46 | 0.88560 | 1.71 | 0.91057 | 1.96 | 0.98374 |
| 1.22 | 0.91311 | 1.47 | 0.88563 | 1.72 | 0.91258 | 1.97 | 0.98767 |
| 1.23 | 0.91075 | 1.48 | 0.88575 | 1.73 | 0.91467 | 1.98 | 0.99171 |
| 1.24 | 0.90852 | 1.49 | 0.88595 | 1.74 | 0.91683 | 1.99 | 0.99581 |
| | | | | | | 2.00 | 1.00000 |

THIS IMAGE HAS BEEN REMOVED DUE TO
COPYRIGHT RESTRICTIONS

**FIG. A2.2 - Pearson's system (Harr, 1977)**

**FIG. A2.3 – Unconfined compressive strength frequency data for A2 barricade brick dry cores, with approximation by beta distribution**

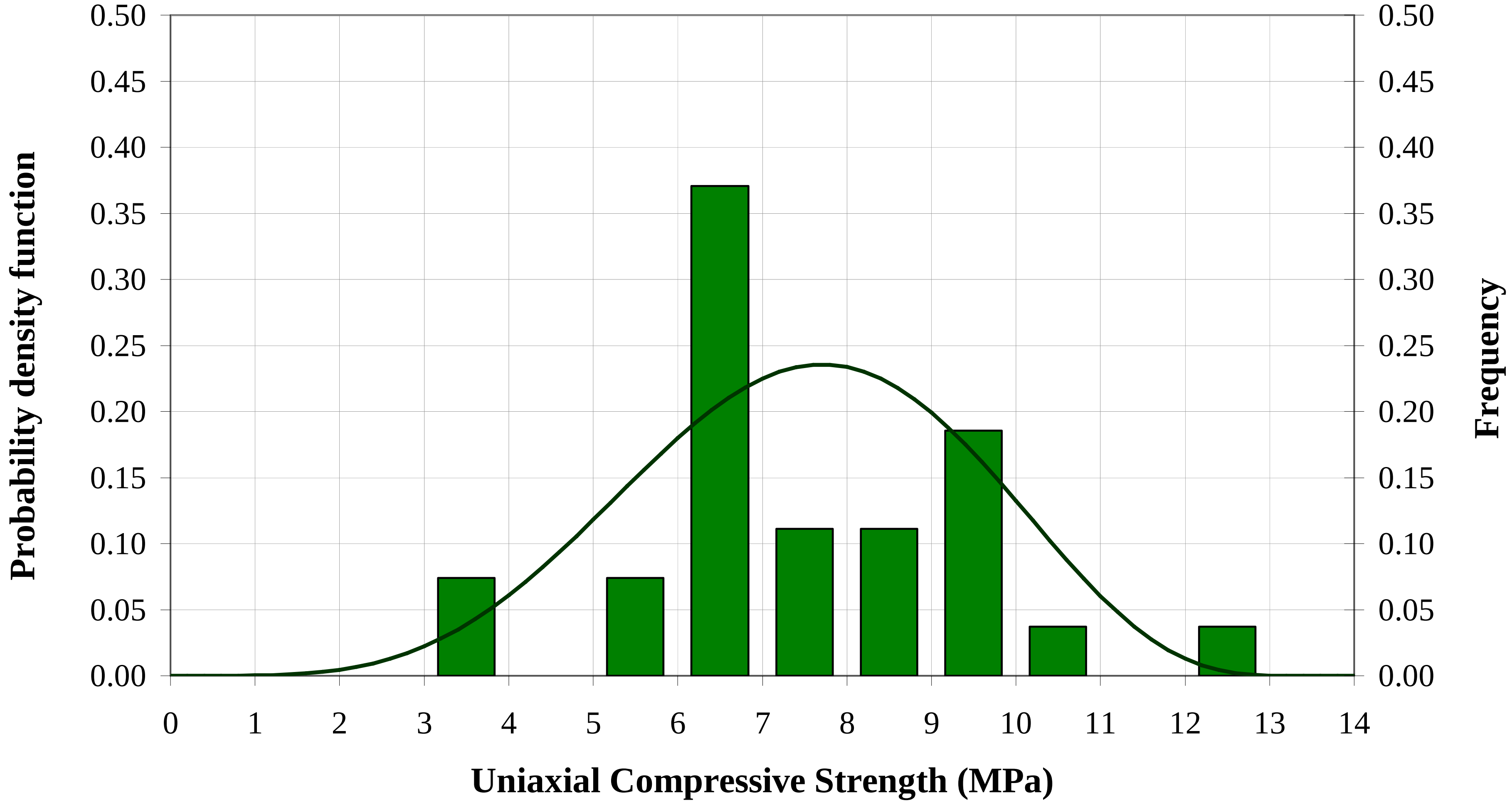

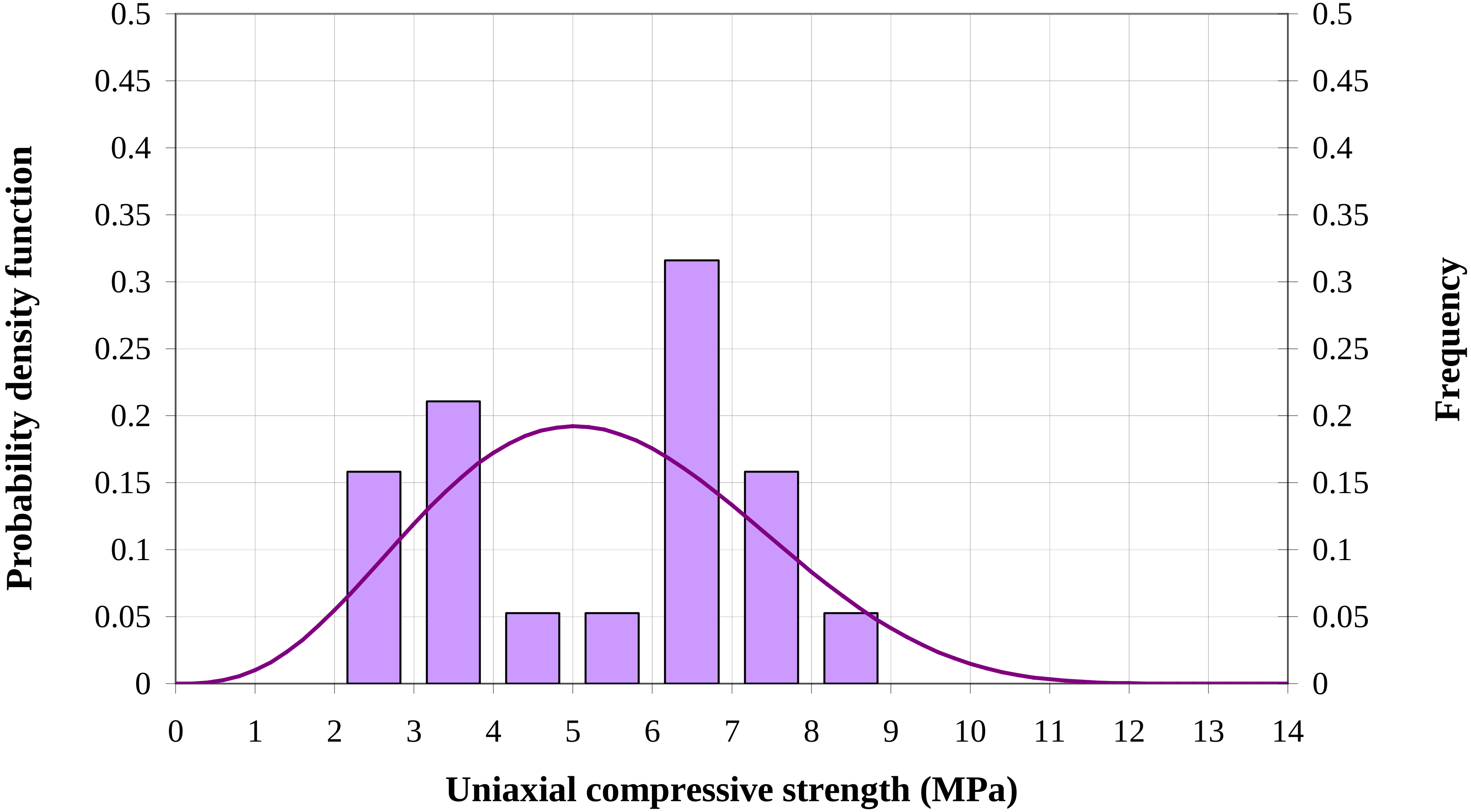


**FIG. A2.4 – Unconfined compressive strength frequency data for A2 barricade brick 7 day wetted cores, with approximation by beta distribution**

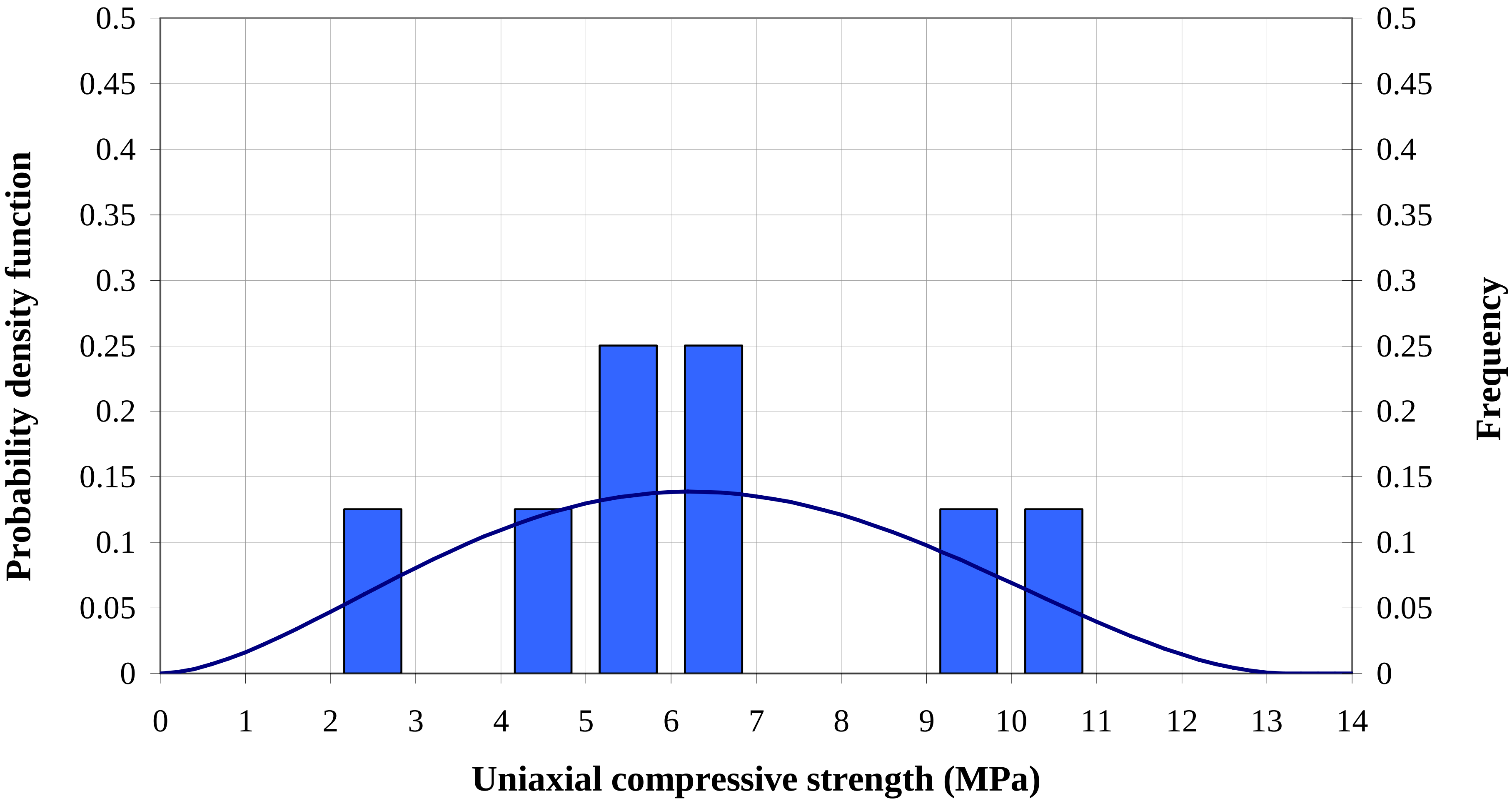


**FIG. A2.5 – Unconfined compressive strength frequency data for A2 barricade brick 90 day wetted cores, with approximation by beta distribution**

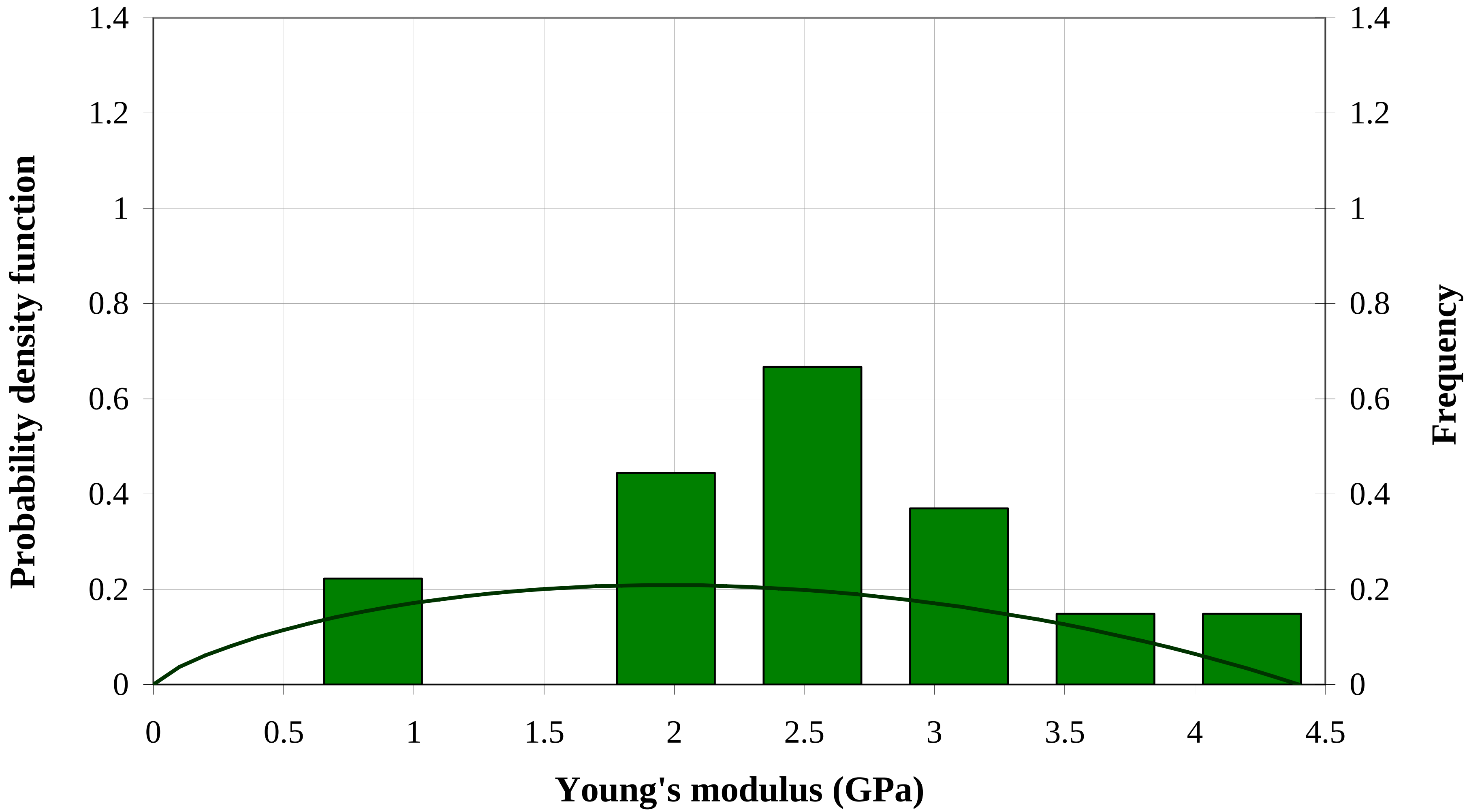


**FIG. A2.6 – Young's modulus frequency data for A2 barricade brick dry cores, with approximation by beta distribution**

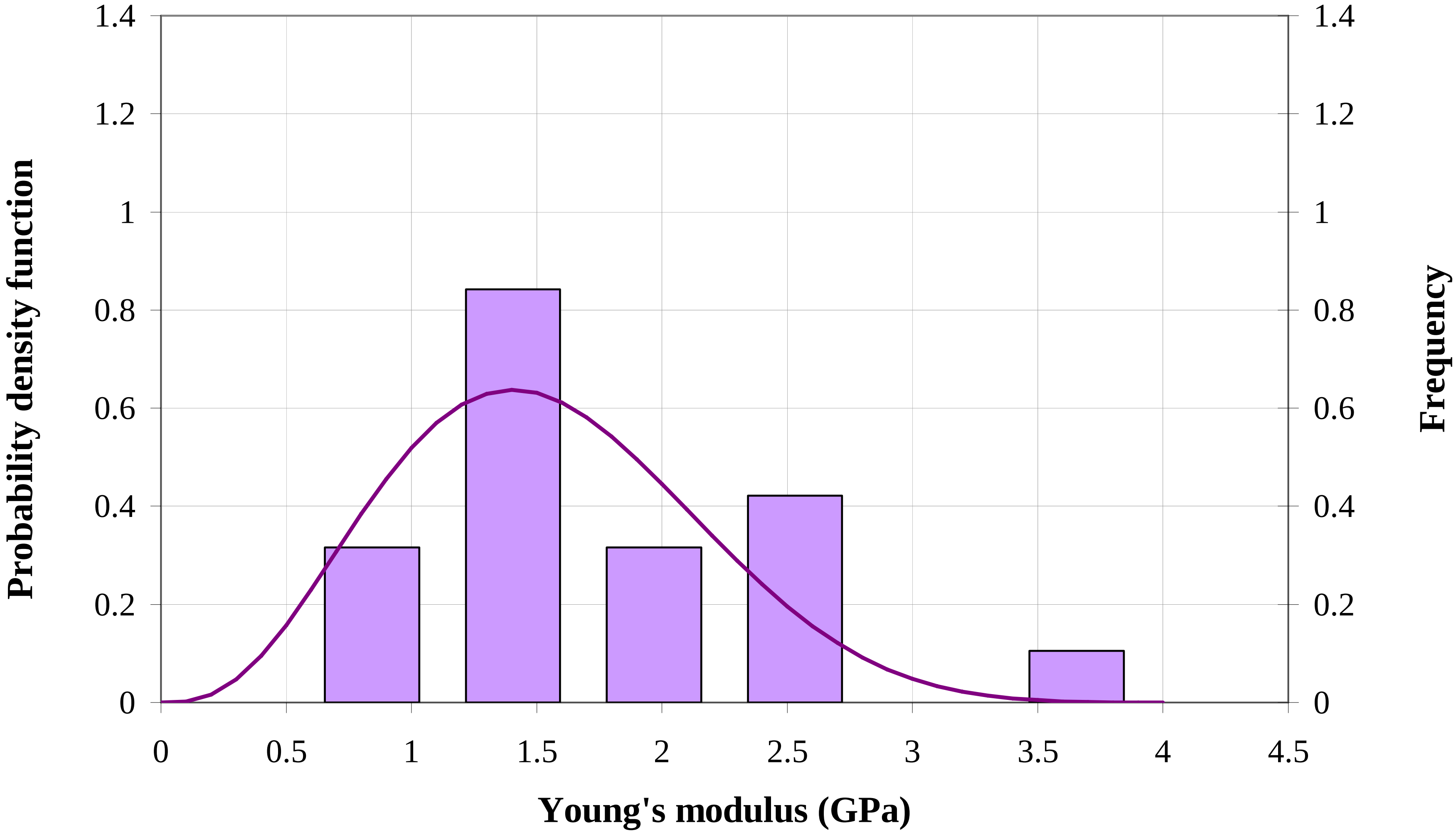


**FIG. A2.7 – Young’s modulus frequency data for A2 barricade brick 7 day wetted cores, with approximation by beta distribution**

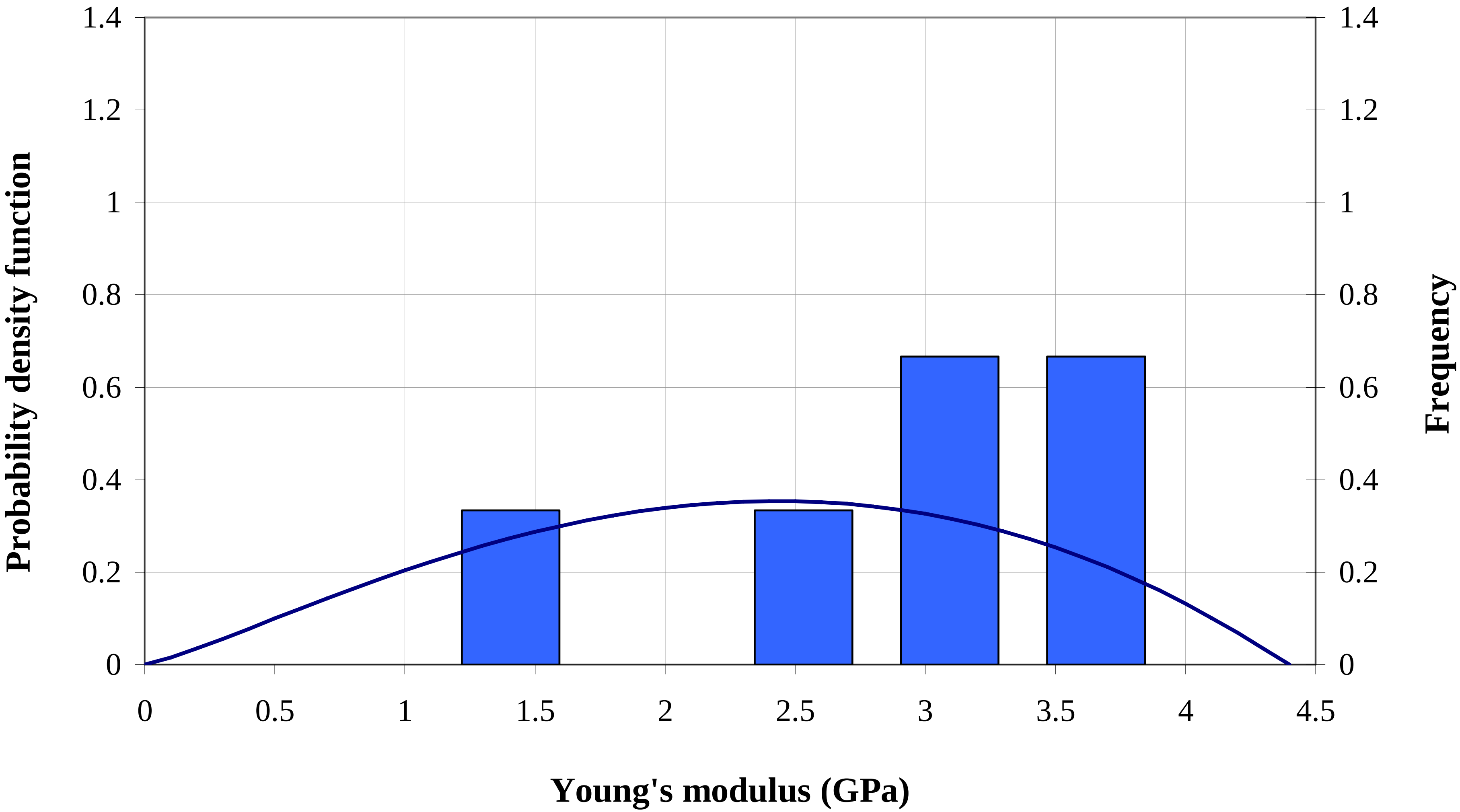


**FIG. A2.8 – Young’s modulus frequency data for A2 barricade brick 90 day wetted cores, with approximation by beta distribution**

# *Appendix 3*

**TABLE A3.1 – Filling and drainage records from R454 stope at Mount Isa Mines Ltd. (Traves, 1988)**

THIS TABLE HAS BEEN REMOVED DUE TO COPYRIGHT RESTRICTIONS

**TABLE A3.1 (cont.) – Filling and drainage records from R454 stope at Mount Isa Mines Ltd. (Traves, 1988)**

THIS TABLE HAS BEEN REMOVED DUE TO COPYRIGHT RESTRICTIONS

THESE IMAGES HAVE BEEN REMOVED DUE TO
COPYRIGHT RESTRICTIONS

**FIG. A3.1 – Plan view of R454 stope at Mount Isa Mines Ltd. (Traves, 1988)**

THESE IMAGES HAVE BEEN REMOVED DUE TO
COPYRIGHT RESTRICTIONS

**FIG. A3.2 – Sections of R454 stope at Mount Isa Mines Ltd. (Traves, 1988)**

**Program A3.1 – Source listing *FISH* code for program used to monitor the real time taken to solve the 2-dimensional *FLAC* steady-state model to a convergence of sratio = 0.001**

```
; Two Dimensional Machine Computation Analysis
; Timed solving for 2D Steady State Stope Drainage Problem
; Worst Case = 25m x 150m stope with water & fill at full height
;
; Kirralee Rankine
; James Cook University
;
;
; *** Initial Input Parameters ***
; Specify Input Parameters
Define inputparameters
realfillperm=0.0054 ; m/hr
fillperm=(realfillperm/(60*60))/9810      ; FLAC units for permeability
fillspecgrav=2.9                    ; Specific Gravity
filldrydens=fillspecgrav/2          ; Fill dry density (t/m3)
fillpor=1-(filldrydens/fillspecgrav)      ; fill porosity
stopewidth=25      ; stope width (m)
stopeheight=150      ; stope height (m)
currentwaterht=150
currentfillht=150
ppatbase=9.81*1000*currentwaterht
nodeswide=26
nodeshigh=151
numnodes=(nodeswide*nodeshigh)
;
end
inputparameters      ; run inputparamters
;
define calculatedischarge
    cumflow=0
    cumdischarge=0
    loop j(1,2)
        thenodeflow=gflow(nodeswide,j)
        cumflow=cumflow+(-1*(thenodeflow))
        hrdischarge=cumflow*3600
    end_loop
;
;
; *** Find Position and Value for Maximum Pore Pressure ***
  maxpp = 0
  loop ipos (1,nodeswide)
    loop jpos (1,nodeshigh)
    thepp=gpp(ipos,jpos)
        if thepp > maxpp then
        maxpp = thepp
    xxx=ipos
    yyy=jpos
        end_if
    end_loop
  end_loop
;
    table(1,1)=hrdischarge
    table(1,2)=maxpp
    table(1,3)=xxx
    table(1,4)=yyy

;
```

```
end
;
;
def timediff
  timediff=(t1-t0)/numnodes
end
def time0
  t0=clock/100.0
end
def time1
  t1=clock/100.0
end
;
; *** Model geometry ***
; Geomety for 25m x 25m x 150m stope
; 1m grid spacing
config gw
grid 25,150
gen 0,0 0,150 25,150 25,0 i=1,nodeswide j=1,nodeshigh        ; square stope
set gravity=9.81
set flow=on
set mech=off
;
title
25 m x 150 m stope with 1 m high drain flush with stope wall
;
; *** Identify Monitor Points ***
 hist gpp i=1 j=1
;
model mohr i=1,26 j=1,nodeshigh
prop den=1500 shear=3e8 bulk=5e8 coh=5e5 fric=0 tens=0
set gravity=9.81
set flow=on
set mech=off
water dens=1000 bulk=1e3
prop perm fillperm por fillpor
ini pp ppatbase var 0 -9.81e3 i=1,nodeswide j=1,nodeshigh
apply pp=0 i=1,26 j=nodeshigh
apply pp=0 i=nodeswide j=1,2
fix sat j=nodeshigh i=1,nodeswide
fix sat i=nodeswide j=1,2
time0
solve sratio 1e-3
time1
;
calculatedischarge
Save sratio1e-3.sav
;
set log on
print table 1
print hrdischarge
print maxpp
print timediff
set log off
```

**Program A3.2 - Source listing *FISH* and *FLAC* code for 2-dimensional stope filling program**

```
; Two-Dimensional Simulation of Stope Filling
;
; Kirralee Rankine
; James Cook University
;
; Cycle Based on 12 hrs filling followed by 12 hrs draining continuously until stope is filled
;
; *** Initial Input Parameters ***
; Specify Input Parameters
Define inputparameters
realfillperm=0.0054 ; m/hr
fillperm=(realfillperm/(60*60))/9810      ; FLAC units for permeability
fillspecgrav=2.9      ; Specific Gravity
filldrydens=fillspecgrav/2      ; Dry Density of Fill (t/m3)
fillmoistcont=0.25      ; moisture content
fillpor=1-(filldrydens/fillspecgrav)      ; fill porosity
fillvoidratio=fillpor/(1-fillpor)      ; fill void ratio
satmoistcont=fillvoidratio/fillspecgrav      ; saturated moisture content of fill
percentsolids=0.72      ; slurry percent solids
filleffpor=fillpor-(fillmoistcont*fillspecgrav/(1+fillvoidratio))      ; effective porosity
stopewidth=25      ; stope width (m)
stopedepth=25      ; stope depth (m)
stopeheight=150      ; stope height (m)
fillingrate1=250      ; solids filling rate t/hr
fillingrate=(fillingrate1/filldrydens)/(stopedepth*stopewidth)      ; filling rate for 2D geometry (m/hr)
waterfillingrate1=fillingrate1*(1-percentsolids)/percentsolids
waterfillingrate2=waterfillingrate1 - (fillingrate1*satmoistcont)      ; decant water
waterfillingrate=waterfillingrate2/(stopewidth*stopedepth)      ; water filling rate for 2D geometry
(m/hr)
;
hrsfilling=12
hrsdraining=12
currentfillht=0
currentwaterht=0
count=0
totaldischarge=0
totvolwaterin=0
totvolwaterout=0
numperiods=int(stopeheight/((hrsfilling)*fillingrate))
;
end
inputparameters      ; run inputparamters
;
; FISH program to calculate discharge and store results in a table
; TABLE 1 => x=Hour number, y=Hourly discharge from the stope computed at exit
; TABLE 2 => x=Hour number, y=Hourly inflow from water table to the fill computed at water level
; TABLE 3 => x=Hour number, y=Fill height
; TABLE 4 => x=Hour number, y=Water height
; TABLE 5 => x=Hour number, y=Maximum pore pressure
; TABLE 6 => x=Hour number, y=x-coordinate of max pore pressure
; TABLE 7 => x=Hour number, y=y-coordinat of max pore pressure
;
define calculatedischarge
    cumflow=0
    cumdischarge=0
    loop j(1,2)
        thenodeflow=gflow(26,j)
        cumflow=cumflow+(-1*(thenodeflow))
```

```
               hrdischarge=cumflow*stopedepth*3600
       end_loop
;
               pnt1pp=pp(25,1)
               pnt2pp=pp(24,1)
               hydgrad=(pnt2pp-pnt1pp)/9810
               velocity=realfillperm*hydgrad
               hrhyddischarge=velocity*stopedepth*3600
;
; Check flow is in equilibrium
       cuminflow=0
       loop i(1,26)
               thenodeinflow=gflow(i,nodeatwaterht)
               cuminflow=cuminflow+(thenodeinflow)
               hrinflow=cuminflow*stopedepth*3600
       end_loop
;
; Find Position and Value for Maximum Pore Pressure
  maxpp = 0
  loop ipos (1,26)
       loop jpos (1,151)
       thepp=gpp(ipos,jpos)
             if thepp > maxpp then
             maxpp = thepp
       xxx=ipos
       yyy=jpos
             end_if
       end_loop
  end_loop
;
       table(1,realhr)=hrdischarge
       table(2,realhr)=hrinflow
       table(3,realhr)=currentfillht
       table(4,realhr)=currentwaterht
       table(5,realhr)=maxpp
       table(6,realhr)=xxx
       table(7,realhr)=yyy
       table(8,realhr)=hrhyddischarge
;;;
end
;
;
; *** Model geometry ***
; Geomety for 25m x 25m x 150m stope
; 1m grid spacing
config gw
grid 25,150
gen 0,0 0,150 25,150 25,0 i=1,26 j=1,151        ; square stope
set gravity=9.81
set flow=on
set mech=off

;
title
25 m x 150 m stope with 1 m high drain flush with stope wall
;
; *** Identify Monitor Points ***
 hist gpp i=1 j=1
;
;
```

```
call KRstage1.dat
call KRstage2.dat
;call kirristage3.dat
save cfDCExample.sav
;
set log on
print table 1
print table 3
print table 4
print table 5
set log off
```

---

```
; *** Full cycles of 12 hr filling and 12 hr resting ***
;
; FISH to simulate the filling cycle
;
Define fullcycles
;
loop theperiod (1,numperiods)
;
; *** Fill ***
    loop fillhrcount (1,hrsfilling)
        realhr=(theperiod-1)*(hrsfilling+hrsdraining)+fillhrcount
        timefilling=(theperiod-1)*hrsfilling+fillhrcount
        currentfillht=currentfillht+fillingrate
        twin=currentfillht*stopewidth*stopedepth*filldrydens
                    totvolwaterin=twin*(1-percentsolids)/percentsolids
        volwaterinstope=totvolwaterin-totvolwaterout
        volsolids=currentfillht*stopewidth*stopedepth
        volvoids=volsolids*fillpor
        ;
        if volvoids>volwaterinstope
                    totvolresmoist=currentfillht*stopewidth*stopedepth*filldrydens*fillmoistcont
                    volfreewater=volwaterinstope-totvolresmoist
        currentwaterht=(volfreewater/filleffpor)/(stopewidth*stopedepth)
      else
      voldecant=volwaterinstope-volvoids
      currentwaterht=currentfillht+(voldecant/(stopewidth*stopedepth))
      end_if
        if currentwaterht>stopeheight
        excess=(currentwaterht-stopeheight)*stopewidth*stopedepth
        totalexcess=totalexcess+excess
        currentwaterht=stopeheight
        end_if
        roundfillht=int(currentfillht+0.5)
        roundwaterht=int(currentwaterht+0.5)
        nodeatwaterht=roundwaterht+1
        nodeatfillht=roundfillht+1
        waterbound1=nodeatwaterht+0.1
        waterbound2=nodeatwaterht-0.1
        ;
            if currentwaterht<1
            hrdischarge=0
            hrinflow=0
            else
    ; *** CASE 1 *** (Water level above height of Fill)
        if currentwaterht>currentfillht
        ppattop=9.81*1000*(currentwaterht-currentfillht)
```

```
        ppatbase=1000*9.81*currentwaterht
        change=-1(ppatbase-ppattop)
        command
        model mohr i=1,26 j=1,nodeatfillht
        prop den=1500 shear=3e8 bulk=5e8 coh=5e5 fric=0 tens=0
        set gravity=9.81
        set flow=on
        set mech=off
        water dens=1000 bulk=1e3
        prop perm fillperm por fillpor
        ini pp ppatbase var 0 change i=1,26 j=1,nodeatfillht
        apply pp=ppattop i=1,26 j=nodeatfillht
        apply pp=0 i=26 j=1,2
        fix sat j=nodeatfillht i=1,26
        fix sat i=26 j=1,2
        solve sratio 1e-2
        calculatedischarge
        save cfillingnodrain.sav
        print hrdischarge
        apply remove gw i=1,26 j=nodeatfillht
        end_command
        ;
    ; *** CASE 2 *** (Water level below height of Fill)
        else
        ppatbase=9.81*1000*currentwaterht
        change=-1*ppatbase
        command
        model mohr i=1,26 j=1,nodeatwaterht
        model null i=1,26 j=nodeatwaterht,151
        prop den=1500 shear=3e8 bulk=5e8 coh=5e5 fric=0 tens=0
        set gravity=9.81
        set flow=on
        set mech=off
        water dens=1000 bulk=1e3
        prop perm fillperm por fillpor
        ini pp ppatbase var 0 change i=1,26 j=1,nodeatwaterht
        apply pp=0 i=1,26 j=nodeatwaterht
        apply pp=0 i=26 j=1,2
        fix sat i=1,26 j=nodeatwaterht
        fix sat i=26 j=1,2
        solve sratio 1e-2
        save cfillingnodrain.sav
        calculatedischarge
        print hrdischarge
        apply remove gw i=1,26 j=nodeatwaterht
        end_command
        end_if
        ;
        totdischarge=totdischarge+hrdischarge
        totvolwaterout=totdischarge
            end_if
        ;
    end_loop
;
; *** Rest ***
    loop resthrcount (1,hrsdraining)
        realhr=realhr+1
        timefilling=(theperiod)*hrsfilling
        twin=currentfillht*stopewidth*stopedepth*filldrydens
                  totvolwaterin=twin*(1-percentsolids)/percentsolids
```

```
    volwaterinstope=totvolwaterin-totvolwaterout
    volsolids=currentfillht*stopewidth*stopedepth
    volvoids=volsolids*fillpor
    ;
    if volvoids>volwaterinstope
              totvolresmoist=currentfillht*stopewidth*stopedepth*filldrydens*fillmoistcont
              volfreewater=volwaterinstope-totvolresmoist
    currentwaterht=(volfreewater/filleffpor)/(stopewidth*stopedepth)
  else
  voldecant=volwaterinstope-volvoids
  currentwaterht=currentfillht+(voldecant/(stopewidth*stopedepth))
  end_if
        if currentwaterht>stopeheight
        excess=(currentwaterht-stopeheight)*stopewidth*stopedepth
        totalexcess=totalexcess+excess
        currentwaterht=stopeheight
        end_if
    roundfillht=int(currentfillht+0.5)
    roundwaterht=int(currentwaterht+0.5)
    nodeatwaterht=roundwaterht+1
    nodeatfillht=roundfillht+1
    waterbound1=nodeatwaterht+0.1
    waterbound2=nodeatwaterht-0.1
    ;
        if currentwaterht<1
        hrdischarge=0
        hrinflow=0
        else
; *** CASE 1 *** (Water level above height of Fill)
    if currentwaterht>currentfillht
    ppattop=9.81*1000*(currentwaterht-currentfillht)
    ppatbase=1000*9.81*currentwaterht
    change=-1(ppatbase-ppattop)
    command
    model mohr i=1,26 j=1,nodeatfillht
    prop den=1500 shear=3e8 bulk=5e8 coh=5e5 fric=0 tens=0
    set gravity=9.81
    set flow=on
    set mech=off
    water dens=1000 bulk=1e3
    prop perm fillperm por fillpor
    ini pp ppatbase var 0 change i=1,26 j=1,nodeatfillht
    apply pp=ppattop i=1,26 j=nodeatfillht
    apply pp=0 i=26 j=1,2
    fix sat j=nodeatfillht i=1,26
    fix sat i=26 j=1,2
    solve sratio 1e-2
    calculatedischarge
    save fillingnodrain.sav
    print hrdischarge
    apply remove gw i=1,26 j=nodeatfillht
    end_command
    ;
; *** CASE 2 *** (Water level below height of Fill)
    else
    ppatbase=9.81*1000*currentwaterht
    change=-1*ppatbase
    command
    model mohr i=1,26 j=1,nodeatwaterht
    model null i=1,26 j=nodeatwaterht,151
```

```
        prop den=1500 shear=3e8 bulk=5e8 coh=5e5 fric=0 tens=0
        set gravity=9.81
        set flow=on
        set mech=off
        water dens=1000 bulk=1e3
        prop perm fillperm por fillpor
        ini pp ppatbase var 0 change i=1,26 j=1,nodeatwaterht
        apply pp=0 i=1,26 j=nodeatwaterht
        apply pp=0 i=26 j=1,2
        fix sat i=1,26 j=nodeatwaterht
        fix sat i=26 j=1,2
        solve sratio 1e-2
        save fillingnodrain.sav
        calculatedischarge
        print hrdischarge
        apply remove gw i=1,26 j=nodeatwaterht
        end_command
        end_if
        ;
        totdischarge=totdischarge+hrdischarge
        totvolwaterout=totdischarge
            end_if
        ;
    end_loop
;
end_loop
;
end
;
fullcycles
```

---

```
Define topup
count=0
; *** Fill till stope is full ***
loop while currentfillht<stopeheight
        realhr=realhr+1
        count=count+1
        timefilling=(theperiod)*hrsfilling+count
        currentfillht=currentfillht+fillingrate
        twin=currentfillht*stopewidth*stopedepth*filldrydens
                totvolwaterin=twin*(1-percentsolids)/percentsolids
        volwaterinstope=totvolwaterin-totvolwaterout
        volsolids=currentfillht*stopewidth*stopedepth
        volvoids=volsolids*fillpor
        ;
        if volvoids>volwaterinstope
                totvolresmoist=currentfillht*stopewidth*stopedepth*filldrydens*fillmoistcont
                volfreewater=volwaterinstope-totvolresmoist
        currentwaterht=(volfreewater/filleffpor)/(stopewidth*stopedepth)
      else
      voldecant=volwaterinstope-volvoids
      currentwaterht=currentfillht+(voldecant/(stopewidth*stopedepth))
      end_if
            if currentwaterht>stopeheight
            excess=(currentwaterht-stopeheight)*stopewidth*stopedepth
            totalexcess=totalexcess+excess
            currentwaterht=stopeheight
            end_if
```

```
          if currentfillht>stopeheight
          currentfillht=stopeheight
          end_if
      roundfillht=int(currentfillht+0.5)
      roundwaterht=int(currentwaterht+0.5)
      nodeatwaterht=roundwaterht+1
      nodeatfillht=roundfillht+1
      waterbound1=nodeatwaterht+0.1
      waterbound2=nodeatwaterht-0.1
      ;
          if currentwaterht<1
          hrdischarge=0
          hrinflow=0
          else
; *** CASE 1 *** (Water level above height of Fill)
      if currentwaterht>currentfillht
      ppattop=9.81*1000*(currentwaterht-currentfillht)
      ppatbase=1000*9.81*currentwaterht
      change=-1(ppatbase-ppattop)
      command
      model mohr i=1,26 j=1,nodeatfillht
      prop den=1500 shear=3e8 bulk=5e8 coh=5e5 fric=0 tens=0
      set gravity=9.81
      set flow=on
      set mech=off
      water dens=1000 bulk=1e3
      prop perm fillperm por fillpor
      ini pp ppatbase var 0 change i=1,26 j=1,nodeatfillht
      apply pp=ppattop i=1,26 j=nodeatfillht
      apply pp=0 i=26 j=1,2
      fix sat j=nodeatfillht i=1,26
      fix sat i=26 j=1,2
      solve sratio 1e-2
      calculatedischarge
      save cfillingnodrain.sav
      print hrdischarge
      apply remove gw i=1,26 j=nodeatfillht
      end_command
      ;
; *** CASE 2 *** (Water level below height of Fill)
      else
      ppatbase=9.81*1000*currentwaterht
      change=-1*ppatbase
      command
      model mohr i=1,26 j=1,nodeatwaterht
      model null i=1,26 j=nodeatwaterht,151
      prop den=1500 shear=3e8 bulk=5e8 coh=5e5 fric=0 tens=0
      set gravity=9.81
      set flow=on
      set mech=off
      water dens=1000 bulk=1e3
      prop perm fillperm por fillpor
      ini pp ppatbase var 0 change i=1,26 j=1,nodeatwaterht
      apply pp=0 i=1,26 j=nodeatwaterht
      apply pp=0 i=26 j=1,2
      fix sat i=1,26 j=nodeatwaterht
      fix sat i=26 j=1,2
      solve sratio 1e-2
      save cfillingnodrain.sav
      calculatedischarge
```

```
            print hrdischarge
            apply remove gw i=1,26 j=nodeatwaterht
            end_command
            end_if
            ;
            totdischarge=totdischarge+hrdischarge
            totvolwaterout=totdischarge
                  end_if
            ;
      end_loop
;
command
save stopefull.sav
plot grid pp fill flow
end_command
end
topup
```

# *Appendix 4*

**PROGRAM A4.1 - Source listing *FISH* and *FLAC$^{3D}$* code 3-dimensional stope filling program**

```
; Three-Dimensional Simulation of Stope Filling - 0 m Drain
;
; Kirralee Rankine
; James Cook University
;
; Cycle Based on continuous filling until fill reaches stope height
; 70 % Solids Content
;
; *** Initial Input Parameters ***
; Specify Input Parameters
Define inputparameters
realfillperm=0.0054 ; m/hr
fillperm=(realfillperm/(60*60))/9810      ; FLAC units for permeability
fillspecgrav=2.9      ; Specific Gravity
filldrydens=0.5*fillspecgrav      ; Dry Density of Fill (t/m3)
fillmoistcont=0.25      ; moisture content
fillpor=1-(filldrydens/fillspecgrav)      ; fill porosity
fillvoidratio=fillpor/(1-fillpor)      ; fill void ratio
satmoistcont=fillvoidratio/fillspecgrav      ; saturated moisture content of fill
percentsolids=0.70      ; slurry percent solids
filleffpor=fillpor-(fillmoistcont*fillspecgrav/(1+fillvoidratio))  ; effective porosity
zs=1      ; zone size
;
width=10      ; stope width (m)
depth=10      ; stope depth (m)
hb=depth/zs                  ; half depth (m)
zonesw=width/zs ; zones in width
zonesb=depth/zs  ; zones in depth
zoneshb=hb/zs    ; zones in half depth direction
stopeheight=60      ; stope height (m)
zoneshigh=stopeheight/zs  ; zones in height
dr=2              ; drain depth (m)
hd=dr/zs                     ; half drain depth (m)
h=2               ; drain height (m)
x=0               ; length of drain (m)
zonesdr=dr/zs                ; drain zones
zoneshd=1                    ; half drain zones
zonesh=h/zs                  ; drain height zones
zonesx=x/zs                  ; drain length zones
stdpos=0                     ; start position for drain in y-direction (m)
;
drnodes=zonesdr+1
hdnodes=zoneshd+1
hnodes=zonesh+1
wnodes=zonesw+1
bnodes=zonesb+1
hbnodes=zoneshb+1
bbound1=depth+0.1
bbound2=depth-0.1
hbbound1=hb+0.1
hbbound2=hb-0.1
wbound1=width+0.1
wbound2=width-0.1
xbound1=width+x+0.1
xbound2=width+x-0.1
xbound=width+x
;
inputfillingrate=16          ; solids filling rate t/hr
```

```
symm=2
;
fillingrate1=inputfillingrate
fillingrate=(fillingrate1/filldrydens)/(width*depth)        ; vertical fill lift (m/hr)
waterfillingrate1=fillingrate1*(1-percentsolids)/percentsolids
;
hrsfilling=24
hrsdraining=0
currentfillht=0
currentwaterht=0
realhr=0
totaldischarge=0
totvolwaterin=0
totvolwaterout=0
numperiods=int(stopeheight/((hrsfilling)*fillingrate))
scalefac=2.5
;
end
inputparameters   ; run inputparamters
;
; FISH program to calculate discharge and store results in a table
; TABLE 1 => x=Hour number, y=Hourly discharge from the stope computed at exit
; TABLE 2 => x=Hour number, y=Fill height
; TABLE 3 => x=Hour number, y=Water height
; TABLE 4 => x=Hour number, y=Maximum pore pressure
; TABLE 5 => x=Hour number, y=x-coordinate of max pore pressure
; TABLE 6 => x=Hour number, y=y-coordinat of max pore pressure
; TABLE 7 => x=Hour number, y=z-coordinat of max pore pressure
;
define calculatedischarge
        cumflow=0
        cumdischarge=0
        xcord=xbound     ; x co-ordinate for drain node
        loop ynode (1,hdnodes)
                ycord=stdpos+(ynode-1)*zs            ; y co-ordinate for drain node
                loop znode (1,hnodes)
                        zcord=(znode-1)*zs           ; z co-ordinate for drain node
                        thenode=gp_near(xcord,ycord,zcord)
                        thenodeflow=gp_flow(thenode)
                        cumflow=cumflow+(-1*(thenodeflow))
                end_loop
        end_loop
hrdischarge=cumflow*3600*symm
scaledQ=hrdischarge*scalefac*scalefac
scaledfillht=currentfillht*scalefac
scaledwaterht=currentwaterht*scalefac
;
; Find Position and Value for Maximum Pore Pressure
  maxpp = 0
loop zpos(1,nodeatfillht)
        zz=(zpos-1)*zs
        loop xpos (1,wnodes)
        xx=(xpos-1)*zs
                loop ypos (1,hbnodes)
                yy=(ypos-1)*zs
                pppoint=gp_near(xx,yy,zz)
                ppatpoint=gp_pp(pppoint)
                        if ppatpoint > maxpp then
                        maxpp = ppatpoint
                        end_if
```

```
                end_loop
        end_loop
scaledpp=maxpp*scalefac
end_loop
;
        table(1,realhr)=scaledQ
        table(2,realhr)=scaledfillht
        table(3,realhr)=scaledwaterht
        table(4,realhr)=scaledpp
        table(5,realhr)=xx
        table(6,realhr)=yy
        table(7,realhr)=zz
;;;
end
;
;
; *** Model geometry ***
; Geomety for 20m x 20m x 60m stope
config fl
gen zone brick size zonesw,zoneshb,zoneshigh p0 (0,0,0) p1 add (width,0,0) p2 add (0,hb,0) p3 add
(0,0,stopeheight)
gen zone brick size zonesx,zoneshd,zonesh p0 (width,0,0) p1 add (x,0,0) p2 add (0,hd,0) p3 add (0,0,h)
;
;
title
Solids Content 70 %
;
;
call stage1.dat
save SC70perstage1.sav
call stage2.dat
save SC70perstage2.sav
call stage3.dat
save SC70perstage3.sav
set logfile SC70percent
set log on
print table 1
print table 2
print table 3
print table 4
set log off
```

```
; *** Full cycles of continuous filling ***
;
; FISH to simulate the filling cycle
;
Define fullcycles
;
loop theperiod(1,numperiods)
;
; *** Fill ***
    loop fillhrcount (1,hrsfilling)
        realhr=(theperiod-1)*(hrsfilling+hrsdraining)+fillhrcount
        timefilling=(theperiod-1)*hrsfilling+fillhrcount
        currentfillht=currentfillht+fillingrate
         twin=currentfillht*width*depth*filldrydens
        totvolwaterin=twin*(1-percentsolids)/percentsolids
        volwaterinstope=totvolwaterin-totvolwaterout
        volsolids=currentfillht*width*depth
```

```
        volvoids=volsolids*fillpor
        ;
        if volvoids>volwaterinstope
         totvwres=currentfillht*width*depth*filldrydens*fillmoistcont
        volfreewater=volwaterinstope-totvwres
        currentwaterht=(volfreewater/filleffpor)/(width*depth)
      else
      voldecant=volwaterinstope-volvoids
      currentwaterht=currentfillht+(voldecant/(width*depth))
      end_if
        if currentwaterht>stopeheight
        excess=(currentwaterht-stopeheight)*width*depth
        totalexcess=totalexcess+excess
        currentwaterht=stopeheight
        end_if
              roundfillht=int(currentfillht+0.5)
              roundwaterht=int(currentwaterht+0.5)
              nodeatwaterht=roundwaterht/zs+1
              nodeatfillht=roundfillht/zs+1
              waterbound1=roundwaterht+0.1
              waterbound2=roundwaterht-0.1
              fillbound1=roundfillht+0.1
              fillbound2=roundfillht-0.1
              ;
                     if roundfillht<h
                     hrdischarge=0
                     hrinflow=0
                     else
       ; *** CASE 1 *** (Water level above height of Fill)
              if currentwaterht>currentfillht
              ppattop=9.81*1000*(currentwaterht-currentfillht)
              ppatbase=1000*9.81*currentwaterht
              command
              group satfill range x -0.1 xbound1 z -0.1 fillbound1
              range name satfill group satfill
              model mohr range group satfill
              prop dens=1500 shear=3e8 bulk=5e8 coh=5e5 fric=0 tens=0 range group satfill
              model null range group satfill not
              model fl_iso range group satfill
              prop perm fillperm por fillpor
              set fl biot off
              ;
              ; --- Initial Conditions ---
              ini fmod 1e3
              ini sat 0.0
              ini sat 1 range group satfill
              ini pp ppatbase grad 0 0 -9.81e3 range group satfill
              apply pp=0 range x xbound2 xbound1 y 0 hd z 0 h
              fix pp range x xbound2 xbound1 y 0 hd z 0 h
              apply pp=ppattop range z fillbound1 fillbound2
              fix pp range z fillbound1 fillbound2
              ;
              ; --- settings ---
              set grav 0 0 -9.81
              ini fdensity 1e3
              ini ftens 0.0
              set mech off
              set fl on
              ;
;             set fluid ratio 1e-3
```

```
                solve
                calculatedischarge
                save filling.sav
                print scaledQ
                print realhr
                apply remove gp range z fillbound1 fillbound2
                end_command
                ;
        ; *** CASE 2 *** (Water level below height of Fill)
                else
                ppatbase=1000*9.81*currentwaterht
                command
                group satfill range x -0.1 xbound1 z -0.1 waterbound1
                range name satfill group satfill
                model mohr range group satfill
                prop dens=1500 shear=3e8 bulk=5e8 coh=5e5 fric=0 tens=0 range group satfill
                model null range group satfill not
                model fl_iso range group satfill
                prop perm fillperm por fillpor
                set fl biot off
                ;
                ; --- Initial Conditions ---
                ini fmod 1e3
                ini sat 0.0
                ini sat 1 range group satfill
                ini pp ppatbase grad 0 0 -9.81e3 range group satfill
                apply pp=0 range x xbound2 xbound1 y 0 hd z 0 h
                fix pp range x xbound2 xbound1 y 0 hd z 0 h
                apply pp=0.001 range z waterbound1 waterbound2
                fix pp range z waterbound1 waterbound2
                ;
                ; --- settings ---
                set grav 0 0 -9.81
                ini fdensity 1e3
                ini ftens 0.0
                set mech off
                set fl on
                ;
;               set fluid ratio 1e-3
                solve
                calculatedischarge
                save filling.sav
                print scaledQ
                print realhr
                apply remove gp range z waterbound1 waterbound2
                end_command
                end_if
                ;
                totdischarge=totdischarge+hrdischarge
                totvolwaterout=totdischarge
                end_if
                ;
    end_loop
;
; *** Rest ***
    loop resthrcount (1,hrsdraining)
        realhr=realhr+1
        timefilling=(theperiod)*hrsfilling
         twin=currentfillht*width*depth*filldrydens
        totvolwaterin=twin*(1-percentsolids)/percentsolids
```

```
    volwaterinstope=totvolwaterin-totvolwaterout
    volsolids=currentfillht*width*depth
    volvoids=volsolids*fillpor
    ;
    if volvoids>volwaterinstope
            totvwres=currentfillht*width*depth*filldrydens*fillmoistcont
    volfreewater=volwaterinstope-totvwres
    currentwaterht=(volfreewater/filleffpor)/(width*depth)
else
voldecant=volwaterinstope-volvoids
currentwaterht=currentfillht+(voldecant/(width*depth))
end_if
        if currentwaterht>stopeheight
        excess=(currentwaterht-stopeheight)*width*depth
        totalexcess=totalexcess+excess
        currentwaterht=stopeheight
        end_if
            roundfillht=int(currentfillht+0.5)
            roundwaterht=int(currentwaterht+0.5)
            nodeatwaterht=roundwaterht/zs+1
            nodeatfillht=roundfillht/zs+1
            waterbound1=roundwaterht+0.1
            waterbound2=roundwaterht-0.1
            fillbound1=roundfillht+0.1
            fillbound2=roundfillht-0.1
            ;
                    if roundfillht<h
                    hrdischarge=0
                    hrinflow=0
                    else
            ;
  ; *** CASE 1 *** (Water level above height of Fill)
            if currentwaterht>currentfillht
            ppattop=9.81*1000*(currentwaterht-currentfillht)
            ppatbase=1000*9.81*currentwaterht
            command
            group satfill range x -0.1 xbound1 z -0.1 fillbound1
            range name satfill group satfill
            model mohr range group satfill
            prop dens=1500 shear=3e8 bulk=5e8 coh=5e5 fric=0 tens=0 range group satfill
            model null range group satfill not
            model fl_iso range group satfill
            prop perm fillperm por fillpor
            set fl biot off
            ;
            ; --- Initial Conditions ---
            ini fmod 1e3
            ini sat 0.0
            ini sat 1 range group satfill
            ini pp ppatbase grad 0 0 -9.81e3 range group satfill
            apply pp=0 range x xbound2 xbound1 y 0 hd z 0 h
            fix pp range x xbound2 xbound1 y 0 hd z 0 h
            apply pp=ppattop range z fillbound1 fillbound2
            fix pp range z fillbound1 fillbound2
            ;
            ; --- settings ---
            set grav 0 0 -9.81
            ini fdensity 1e3
            ini ftens 0.0
            set mech off
```

```
                set fl on
                ;
                set fluid ratio 1e-3
                solve
                calculatedischarge
                save filling.sav
                print scaledQ
                print realhr
                apply remove gp range z fillbound1 fillbound2
                end_command
                ;
        ; *** CASE 2 *** (Water level below height of fill)
                else
                ppatbase=1000*9.81*currentwaterht
                command
                group satfill range x -0.1 xbound1 z -0.1 waterbound1
                range name satfill group satfill
                model mohr range group satfill
                prop dens=1500 shear=3e8 bulk=5e8 coh=5e5 fric=0 tens=0 range group satfill
                model null range group satfill not
                model fl_iso range group satfill
                prop perm fillperm por fillpor
                set fl biot off
                ;
                ; --- Initial Conditions ---
                ini fmod 1e3
                ini sat 0.0
                ini sat 1 range group satfill
                ini pp ppatbase grad 0 0 -9.81e3 range group satfill
                apply pp=0 range x xbound2 xbound1 y 0 hd z 0 h
                fix pp range x xbound2 xbound1 y 0 hd z 0 h
                apply pp=0.001 range z waterbound1 waterbound2
                fix pp range z waterbound1 waterbound2
                ;
                ; --- settings ---
                set grav 0 0 -9.81
                ini fdensity 1e3
                ini ftens 0.0
                set mech off
                set fl on
                ;
;               set fluid ratio 1e-3
                solve
                calculatedischarge
                save filling.sav
                print scaledQ
                print realhr
                apply remove gp range z waterbound1 waterbound2
                end_command
                end_if
                end_if
                ;
                totdischarge=totdischarge+hrdischarge
                totvolwaterout=totdischarge
    end_loop
end_loop
;
end
;
fullcycles
```

```
Define topup
count=0
; *** Fill till stope is full ***
loop while currentfillht<stopeheight
        realhr=realhr+1
        count=count+1
        timefilling=(theperiod)*hrsfilling+count
        currentfillht=currentfillht+fillingrate
              twin=currentfillht*width*depth*filldrydens
        totvolwaterin=twin*(1-percentsolids)/percentsolids
        volwaterinstope=totvolwaterin-totvolwaterout
        volsolids=currentfillht*width*depth
        volvoids=volsolids*fillpor
        ;
        if volvoids>volwaterinstope
              totvwres=currentfillht*width*depth*filldrydens*fillmoistcont
        volfreewater=volwaterinstope-totvwres
        currentwaterht=(volfreewater/filleffpor)/(width*depth)
      else
      voldecant=volwaterinstope-volvoids
      currentwaterht=currentfillht+(voldecant/(width*depth))
      end_if
            if currentwaterht>stopeheight
            excess=(currentwaterht-stopeheight)*width*depth*symm
            totalexcess=totalexcess+excess
            currentwaterht=stopeheight
            end_if
            if currentfillht>stopeheight
            currentfillht=stopeheight
            end_if
              roundfillht=int(currentfillht+0.5)
              roundwaterht=int(currentwaterht+0.5)
              nodeatwaterht=roundwaterht/zs+1
              nodeatfillht=roundfillht/zs+1
              waterbound1=roundwaterht+0.1
              waterbound2=roundwaterht-0.1
              fillbound1=roundfillht+0.1
              fillbound2=roundfillht-0.1
              ;
                     if roundfillht<h
                     hrdischarge=0
                     hrinflow=0
                     else
       ; *** CASE 1 *** (Water level above height of Fill)
              if currentwaterht>currentfillht
              ppattop=9.81*1000*(currentwaterht-currentfillht)
              ppatbase=1000*9.81*currentwaterht
              command
              group satfill range x -0.1 xbound1 z -0.1 fillbound1
              range name satfill group satfill
              model mohr range group satfill
              prop dens=1500 shear=3e8 bulk=5e8 coh=5e5 fric=0 tens=0 range group satfill
              model null range group satfill not
              model fl_iso range group satfill
              prop perm fillperm por fillpor
              set fl biot off
              ;
              ; --- Initial Conditions ---
```

```
                ini fmod 1e3
                ini sat 0.0
                ini sat 1 range group satfill
                ini pp ppatbase grad 0 0 -9.81e3 range group satfill
                apply pp=0 range x xbound2 xbound1 y 0 hd z 0 h
                fix pp range x xbound2 xbound1 y 0 hd z 0 h
                apply pp=ppattop range z fillbound1 fillbound2
                fix pp range z fillbound1 fillbound2
                ;
                ; --- settings ---
                set grav 0 0 -9.81
                ini fdensity 1e3
                ini ftens 0.0
                set mech off
                set fl on
                ;
;               set fluid ratio 1e-3
                solve
                calculatedischarge
                save filling.sav
                print scaledQ
                print realhr
                apply remove gp range z fillbound1 fillbound2
                end_command
                ;
        ; *** CASE 2 *** (Water level below height of Fill)
                else
                ppatbase=1000*9.81*currentwaterht
                command
                group satfill range x -0.1 xbound1 z -0.1 waterbound1
                range name satfill group satfill
                model mohr range group satfill
                prop dens=1500 shear=3e8 bulk=5e8 coh=5e5 fric=0 tens=0 range group satfill
                model null range group satfill not
                model fl_iso range group satfill
                prop perm fillperm por fillpor
                set fl biot off
                ;
                ; --- Initial Conditions ---
                ini fmod 1e3
                ini sat 0.0
                ini sat 1 range group satfill
                ini pp ppatbase grad 0 0 -9.81e3 range group satfill
                apply pp=0 range x xbound2 xbound1 y 0 hd z 0 h
                fix pp range x xbound2 xbound1 y 0 hd z 0 h
                apply pp=0.001 range z waterbound1 waterbound2
                fix pp range z waterbound1 waterbound2
                ;
                ; --- settings ---
                set grav 0 0 -9.81
                ini fdensity 1e3
                ini ftens 0.0
                set mech off
                set fl on
                ;
;               set fluid ratio 1e-3
                solve
                calculatedischarge
                save filling.sav
                print hrdischarge
```

```
                print realhr
                apply remove gp range z waterbound1 waterbound2
                end_command
                end_if
                ;
                totdischarge=totdischarge+hrdischarge
                totvolwaterout=totdischarge
                end_if
                ;
    end_loop
;
command
save stopefull.sav
end_command
end
topup
;
```

---

```
define draintillempty
currentfillht=stopeheight
currentwatersht=stopeheight
fillmoistcont=0.25        ; moisture content
filleffpor=fillpor-(fillmoistcont*fillspecgrav/(1+fillvoidratio))
; *** Drain till empty ***
    loop while currentwaterht>5
   loop resthrcount (1,hrsdraining)
        realhr=realhr+1
        timefilling=(theperiod)*hrsfilling
         twin=currentfillht*width*depth*filldrydens
        totvolwaterin=twin*(1-percentsolids)/percentsolids
        volwaterinstope=totvolwaterin-totvolwaterout
        volsolids=currentfillht*width*depth
        volvoids=volsolids*fillpor
        ;
        if volvoids>volwaterinstope
                totvwres=currentfillht*width*depth*filldrydens*fillmoistcont
        volfreewater=volwaterinstope-totvwres
        currentwaterht=(volfreewater/filleffpor)/(width*depth)
      else
      voldecant=volwaterinstope-volvoids
      currentwaterht=currentfillht+(voldecant/(width*depth))
      end_if
            if currentwaterht>stopeheight
            excess=(currentwaterht-stopeheight)*width*depth
            totalexcess=totalexcess+excess
            currentwaterht=stopeheight
            end_if
                roundfillht=int(currentfillht+0.5)
                roundwaterht=int(currentwaterht+0.5)
                nodeatwaterht=roundwaterht/zs+1
                nodeatfillht=roundfillht/zs+1
                waterbound1=roundwaterht+0.1
                waterbound2=roundwaterht-0.1
                fillbound1=roundfillht+0.1
                fillbound2=roundfillht-0.1
                ;
                        if roundfillht<h
                        hrdischarge=0
                        hrinflow=0
                        else
```

```
        ;
; *** CASE 1 *** (Water level above height of Fill)
        if currentwaterht>currentfillht
        ppattop=9.81*1000*(currentwaterht-currentfillht)
        ppatbase=1000*9.81*currentwaterht
        command
        group satfill range x -0.1 xbound1 z -0.1 fillbound1
        range name satfill group satfill
        model mohr range group satfill
        prop dens=1500 shear=3e8 bulk=5e8 coh=5e5 fric=0 tens=0 range group satfill
        model null range group satfill not
        model fl_iso range group satfill
        prop perm fillperm por fillpor
        set fl biot off
        ;
        ; --- Initial Conditions ---
        ini fmod 1e3
        ini sat 0.0
        ini sat 1 range group satfill
        ini pp ppatbase grad 0 0 -9.81e3 range group satfill
        apply pp=0 range x xbound2 xbound1 y 0 hd z 0 h
        fix pp range x xbound2 xbound1 y 0 hd z 0 h
        apply pp=ppattop range z fillbound1 fillbound2
        fix pp range z fillbound1 fillbound2
        ;
        ; --- settings ---
        set grav 0 0 -9.81
        ini fdensity 1e3
        ini ftens 0.0
        set mech off
        set fl on
        ;
        set fluid ratio 1e-3
        solve
        calculatedischarge
        save filling.sav
        print scaledQ
        print realhr
        apply remove gp range z fillbound1 fillbound2
        end_command
        ;
; *** CASE 2 *** (Water level below height of fill)
        else
        ppatbase=1000*9.81*currentwaterht
        command
        group satfill range x -0.1 xbound1 z -0.1 waterbound1
        range name satfill group satfill
        model mohr range group satfill
        prop dens=1500 shear=3e8 bulk=5e8 coh=5e5 fric=0 tens=0 range group satfill
        model null range group satfill not
        model fl_iso range group satfill
        prop perm fillperm por fillpor
        set fl biot off
        ;
        ; --- Initial Conditions ---
        ini fmod 1e3
        ini sat 0.0
        ini sat 1 range group satfill
        ini pp ppatbase grad 0 0 -9.81e3 range group satfill
        apply pp=0 range x xbound2 xbound1 y 0 hd z 0 h
```

```
                fix pp range x xbound2 xbound1 y 0 hd z 0 h
        apply pp=0.001 range z waterbound1 waterbound2
                fix pp range z waterbound1 waterbound2
                ;
                ; --- settings ---
                set grav 0 0 -9.81
                ini fdensity 1e3
                ini ftens 0.0
                set mech off
                set fl on
                ;
;               set fluid ratio 1e-3
                solve
                calculatedischarge
                save draining.sav
                print scaledQ
                print realhr
                apply remove gp range z waterbound1 waterbound2
                end_command
                end_if
                end_if
                ;
                totdischarge=totdischarge+hrdischarge
                totvolwaterout=totdischarge
    end_loop
end
draintillempty
```

**PROGRAM A4.2 - Source listing *FISH* and *FLAC$^{3D}$* code 3-dimensional steady-state Case 1 program**

```
; Steady State Stope
;
; CASE 1 - Single drain, modelled in half symmetry
; Steady state simulations to develop design charts
;
; Kirralee Rankine
; James Cook University
;
; *** Initial Input Parameters ***
; Specify Input Parameters
Define inputparameters
realfillperm=0.0054 ; m/hr
fillperm=(realfillperm/(60*60))/9810     ; FLAC3D units for permeability
fillspecgrav=2.9     ; Specific Gravity
filldrydens=0.5*fillspecgrav     ; Dry Density of Fill (t/m3)
fillmoistcont=0.25     ; moisture content
fillpor=1-(filldrydens/fillspecgrav)     ; fill porosity
fillvoidratio=fillpor/(1-fillpor)     ; fill void ratio
satmoistcont=fillvoidratio/fillspecgrav     ; saturated moisture content of fill
percentsolids=0.72     ; slurry percent solids
filleffpor=fillpor-(fillmoistcont*fillspecgrav/(1+fillvoidratio))  ; effective porosity
;
B=10    ; stope width (m)
hb=B/2  ; half stope width for half symmetry
x=4             ; drain length (m)
dw=2            ; square drain width (m)
hdw=dw/2
fullheight=300
;
; use 0.5 m grid spacing throughout
zonespace=0.5
xzones=x/zonespace
dwzones=dw/zonespace
hdwzones=hdw/zonespace
bzones=b/zonespace
hbzones=hb/zonespace
fullzones=fullheight/zonespace
;
; number of nodes
dwnodes=dwzones+1
hdwnodes=hdwzones+1
hbnodes=hbzones+1
bnodes=bzones+1
fullnodes=fullzones+1
;
; boundaries
xbound1=B+x+0.1
xbound2=B+x-0.1
xbound=B+x
stpoint=(B-dw)/2
endpoint=stpoint+dw
ppatbase=height*9.81*1000
;
end
inputparameters   ; run inputparamters
;
```

```
; FISH program to calculate discharge and store results in a table
; TABLE 1 => x=row number, y=water height
; TABLE 2 => x=row number, y=Discharge rate
; TABLE 3 => x=Hour number, y=Maximum Pore pressure
;
define calculatedischarge
	cumflow=0
	cumdischarge=0
	xcord=xbound	; x co-ordinate for drain node
	loop ynode (1,hdwnodes)
		ycord=((ynode-1)*zonespace)	; y co-ordinate for drain node
		loop znode (1,dwnodes)
			zcord=(znode-1)*zonespace	; z co-ordinate for drain node
			thenode=gp_near(xcord,ycord,zcord)
			thenodeflow=gp_flow(thenode)
			cumflow=cumflow+(-1*(thenodeflow))
		end_loop
	end_loop
hrdischarge=cumflow*3600*2	; half symmetry
;
; Find Position and Value for Maximum Pore Pressure
  maxpp = 0
xcount=Bzones+1
ycount=hbzones+1
heightcount=heightzones+1
loop zpos(1,heightcount)
	zz=((zpos-1)*zonespace)
	loop xpos (1,xcount)
	xx=(xpos-1)*zonespace
		loop ypos (1,ycount)
		yy=(ypos-1)*zonespace
		pppoint=gp_near(xx,yy,zz)
		ppatpoint=gp_pp(pppoint)
			if ppatpoint > maxpp then
			maxpp = ppatpoint
			end_if
		end_loop
	end_loop
end_loop
;
	table(1,heightfac)=Height
	table(2,heightfac)=hrdischarge
	table(3,heightfac)=maxpp
;
end
;
; *** Model geometry ***
; Geomety
config fl
gen zone brick size Bzones,hBzones,fullzones p0 (0,0,0) p1 add (B,0,0) p2 add (0,hB,0) p3 add
(0,0,fullheight)
gen zone brick size xzones,hdwzones,dwzones p0 (B,0,0) p1 add (x,0,0) p2 add (0,hdw,0) p3 add
(0,0,dw)
;
;
define solveit
;
loop heightfac (1,10)
height=heightfac*B/2
Heightbound1=height+0.1
```

```
Heightbound2=height-0.1
ppatbase=1000*9.81*height
Heightzones=height/zonespace
Heightnodes=Heightzones+1
;
command
title
Case 1 - Single Drain with Half Symmetry
;
group fill range z -0.1 heightbound1
model mohr range group fill
model null range group fill not
prop dens=1500 shear=3e8 bulk=5e8 coh=5e5 fric=0 tens=0 range group fill
model fl_iso range group fill
prop perm fillperm por fillpor range group fill
set fl biot off
;
; --- Initial Conditions ---
ini fmod 1e3
ini sat 1 range group fill
ini pp ppatbase grad 0 0 -9.81e3 range group fill
apply pp=0 range x xbound1 xbound2 y 0 hdw z 0 dw
fix pp range x xbound1 xbound2 y 0 hdw z 0 dw
apply pp=0.001 range z heightbound2 heightbound1
fix pp range z heightbound1 heightbound2
;
; --- settings ---
set grav 0 0 -9.81
ini fdensity 1e3
ini ftens 0.0
set mech off
set fl on
;
set fluid ratio 1e-5
solve
calculatedischarge
print hrdischarge maxpp height
;
apply remove gp range x xbound2 xbound1 y 0 hdw z 0 dw
apply remove gp range z heightbound1 heightbound2
save 10x10drain2x2x4.sav
end_command
end_loop
end
solveit
;
set logfile case1d2x4b10halfzone
set log on
print table 1
print table 2
print table 3
set log off
;
```

**TABLE A4.1 – Three-dimensional discharge and maximum pore pressure efficiencies for Cases 2, 3 and 4 relative to Case 1, at *X/D* = 0.5 and *D/B* = 0.2**

| | | X/D = 0.5, D/B = 0.2 | | | | | |
|---|---|---|---|---|---|---|---|
| | | Case 2 / Case 1 | | Case 3 / Case 1 | | Case 4 / Case 1 | |
| Water Height (m) | $H_w/B$ | Discharge | Maximum Pore Pressure | Discharge | Maximum Pore Pressure | Discharge | Maximum Pore Pressure |
| 0 | 0.0 | --- | --- | --- | --- | --- | --- |
| 5 | 0.5 | 1.963 | 0.944 | 1.640 | 0.990 | 3.183 | 0.896 |
| 10 | 1.0 | 1.825 | 0.864 | 1.542 | 0.948 | 2.687 | 0.751 |
| 15 | 1.5 | 1.710 | 0.810 | 1.477 | 0.910 | 2.363 | 0.662 |
| 20 | 2.0 | 1.623 | 0.769 | 1.426 | 0.879 | 2.142 | 0.601 |
| 25 | 2.5 | 1.555 | 0.737 | 1.384 | 0.854 | 1.983 | 0.557 |
| 30 | 3.0 | 1.500 | 0.711 | 1.350 | 0.833 | 1.863 | 0.524 |
| 35 | 3.5 | 1.455 | 0.690 | 1.322 | 0.816 | 1.769 | 0.497 |
| 40 | 4.0 | 1.418 | 0.672 | 1.298 | 0.801 | 1.693 | 0.476 |
| 45 | 4.5 | 1.386 | 0.657 | 1.277 | 0.788 | 1.631 | 0.459 |
| 50 | 5.0 | 1.359 | 0.644 | 1.259 | 0.777 | 1.579 | 0.445 |

**TABLE A4.2 – Three-dimensional discharge and maximum pore pressure efficiencies for Cases 2, 3 and 4 relative to Case 1, at *X/D* = 1 and *D/B* = 0.2**

| | | X/D = 1, D/B = 0.2 | | | | | |
|---|---|---|---|---|---|---|---|
| | | Case 2 / Case 1 | | Case 3 / Case 1 | | Case 4 / Case 1 | |
| Water Height (m) | $H_w/B$ | Discharge | Maximum Pore Pressure | Discharge | Maximum Pore Pressure | Discharge | Maximum Pore Pressure |
| 0 | 0.0 | --- | --- | --- | --- | --- | --- |
| 5 | 0.5 | 1.975 | 0.962 | 1.743 | 0.992 | 3.410 | 0.925 |
| 10 | 1.0 | 1.875 | 0.904 | 1.660 | 0.957 | 2.991 | 0.807 |
| 15 | 1.5 | 1.785 | 0.861 | 1.598 | 0.924 | 2.682 | 0.725 |
| 20 | 2.0 | 1.711 | 0.825 | 1.547 | 0.895 | 2.455 | 0.664 |
| 25 | 2.5 | 1.650 | 0.796 | 1.505 | 0.871 | 2.283 | 0.618 |
| 30 | 3.0 | 1.599 | 0.771 | 1.468 | 0.850 | 2.147 | 0.581 |
| 35 | 3.5 | 1.555 | 0.750 | 1.436 | 0.831 | 2.036 | 0.552 |
| 40 | 4.0 | 1.517 | 0.732 | 1.409 | 0.816 | 1.946 | 0.527 |
| 45 | 4.5 | 1.484 | 0.716 | 1.384 | 0.802 | 1.870 | 0.507 |
| 50 | 5.0 | 1.455 | 0.702 | 1.363 | 0.789 | 1.805 | 0.489 |

**TABLE A4.3 – Three-dimensional stope discharge and maximum pore pressure efficiencies for Cases 2, 3 and 4 relative to Case 1, at *X/D* = 2 and *D/B* = 0.2**

| | | X/D = 2, D/B = 0.2 | | | | | |
|---|---|---|---|---|---|---|---|
| | | Case 2 / Case 1 | | Case 3 / Case 1 | | Case 4 / Case 1 | |
| Water Height (m) | $H_w/B$ | Discharge | Maximum Pore Pressure | Discharge | Maximum Pore Pressure | Discharge | Maximum Pore Pressure |
| 0 | 0.0 | --- | --- | --- | --- | --- | --- |
| 5 | 0.5 | 1.985 | 0.977 | 1.836 | 0.995 | 3.620 | 0.952 |
| 10 | 1.0 | 1.922 | 0.940 | 1.777 | 0.970 | 3.312 | 0.866 |
| 15 | 1.5 | 1.858 | 0.909 | 1.726 | 0.944 | 3.051 | 0.800 |
| 20 | 2.0 | 1.804 | 0.882 | 1.682 | 0.921 | 2.845 | 0.746 |
| 25 | 2.5 | 1.755 | 0.859 | 1.644 | 0.900 | 2.676 | 0.702 |
| 30 | 3.0 | 1.713 | 0.838 | 1.610 | 0.881 | 2.535 | 0.666 |
| 35 | 3.5 | 1.674 | 0.819 | 1.579 | 0.865 | 2.416 | 0.635 |
| 40 | 4.0 | 1.640 | 0.802 | 1.551 | 0.850 | 2.315 | 0.608 |
| 45 | 4.5 | 1.609 | 0.787 | 1.526 | 0.836 | 2.227 | 0.585 |
| 50 | 5.0 | 1.581 | 0.774 | 1.503 | 0.823 | 2.150 | 0.565 |

**TABLE A4.4 – Three-dimensional stope discharge and maximum pore pressure efficiencies for Cases 2, 3 and 4 relative to Case 1, at *X/D* = 0.5 and *D/B* = 0.3**

| | | X/D = 0.5, D/B = 0.3 | | | | | |
|---|---|---|---|---|---|---|---|
| | | Case 2 / Case 1 | | Case 3 / Case 1 | | Case 4 / Case 1 | |
| Water Height (m) | $H_w/B$ | Discharge | Maximum Pore Pressure | Discharge | Maximum Pore Pressure | Discharge | Maximum Pore Pressure |
| 0 | 0.0 | --- | --- | --- | --- | --- | --- |
| 5 | 0.5 | 1.952 | 0.930 | 1.672 | 0.986 | 3.214 | 0.865 |
| 10 | 1.0 | 1.764 | 0.822 | 1.522 | 0.930 | 2.533 | 0.680 |
| 15 | 1.5 | 1.623 | 0.757 | 1.436 | 0.882 | 2.154 | 0.583 |
| 20 | 2.0 | 1.525 | 0.712 | 1.374 | 0.846 | 1.925 | 0.523 |
| 25 | 2.5 | 1.454 | 0.679 | 1.328 | 0.818 | 1.772 | 0.483 |
| 30 | 3.0 | 1.399 | 0.654 | 1.291 | 0.797 | 1.662 | 0.454 |
| 35 | 3.5 | 1.357 | 0.635 | 1.263 | 0.779 | 1.580 | 0.432 |
| 40 | 4.0 | 1.322 | 0.619 | 1.239 | 0.765 | 1.516 | 0.415 |
| 45 | 4.5 | 1.294 | 0.606 | 1.219 | 0.753 | 1.464 | 0.401 |
| 50 | 5.0 | 1.270 | 0.594 | 1.202 | 0.743 | 1.422 | 0.390 |

**TABLE A4.5 – Three-dimensional stope discharge and maximum pore pressure efficiencies for Cases 2, 3 and 4 relative to Case 1, at *X/D* = 1 and *D/B* = 0.3**

| | | X/D = 1, D/B = 0.3 | | | | | |
|---|---|---|---|---|---|---|---|
| | | Case 2 / Case 1 | | Case 3 / Case 1 | | Case 4 / Case 1 | |
| Water Height (m) | $H_w/B$ | Discharge | Maximum Pore Pressure | Discharge | Maximum Pore Pressure | Discharge | Maximum Pore Pressure |
| 0 | 0.0 | --- | --- | --- | --- | --- | --- |
| 5 | 0.5 | 1.969 | 0.954 | 1.769 | 0.990 | 3.442 | 0.905 |
| 10 | 1.0 | 1.830 | 0.873 | 1.641 | 0.943 | 2.848 | 0.748 |
| 15 | 1.5 | 1.713 | 0.817 | 1.558 | 0.898 | 2.473 | 0.652 |
| 20 | 2.0 | 1.624 | 0.776 | 1.494 | 0.863 | 2.222 | 0.587 |
| 25 | 2.5 | 1.555 | 0.743 | 1.443 | 0.834 | 2.044 | 0.541 |
| 30 | 3.0 | 1.499 | 0.717 | 1.402 | 0.811 | 1.911 | 0.507 |
| 35 | 3.5 | 1.454 | 0.695 | 1.368 | 0.792 | 1.808 | 0.480 |
| 40 | 4.0 | 1.416 | 0.677 | 1.339 | 0.775 | 1.726 | 0.458 |
| 45 | 4.5 | 1.384 | 0.662 | 1.314 | 0.761 | 1.659 | 0.441 |
| 50 | 5.0 | 1.357 | 0.649 | 1.293 | 0.749 | 1.604 | 0.426 |

**TABLE A4.6 – Three-dimensional stope discharge and maximum pore pressure efficiencies for Cases 2, 3 and 4 relative to Case 1, at *X/D* = 2 and *D/B* = 0.3**

| | | X/D = 2, D/B = 0.3 | | | | | |
|---|---|---|---|---|---|---|---|
| | | Case 2 / Case 1 | | Case 3 / Case 1 | | Case 4 / Case 1 | |
| Water Height (m) | $H_w/B$ | Discharge | Maximum Pore Pressure | Discharge | Maximum Pore Pressure | Discharge | Maximum Pore Pressure |
| 0 | 0.0 | --- | --- | --- | --- | --- | --- |
| 5 | 0.5 | 1.982 | 0.973 | 1.857 | 0.993 | 3.649 | 0.941 |
| 10 | 1.0 | 1.890 | 0.919 | 1.759 | 0.959 | 3.195 | 0.823 |
| 15 | 1.5 | 1.805 | 0.878 | 1.691 | 0.924 | 2.862 | 0.739 |
| 20 | 2.0 | 1.735 | 0.844 | 1.635 | 0.894 | 2.615 | 0.676 |
| 25 | 2.5 | 1.675 | 0.815 | 1.586 | 0.868 | 2.426 | 0.628 |
| 30 | 3.0 | 1.624 | 0.790 | 1.544 | 0.845 | 2.277 | 0.590 |
| 35 | 3.5 | 1.581 | 0.769 | 1.508 | 0.826 | 2.156 | 0.559 |
| 40 | 4.0 | 1.543 | 0.751 | 1.476 | 0.809 | 2.055 | 0.533 |
| 45 | 4.5 | 1.510 | 0.735 | 1.448 | 0.793 | 1.971 | 0.511 |
| 50 | 5.0 | 1.481 | 0.721 | 1.423 | 0.780 | 1.899 | 0.493 |

# References

Aubertin, M., Li, L., Arnoldi, S., Simon, R., Belem, T., Bussiere, B. and Benzaazoua, M. (2003). "Interaction between backfill and rockmass in narrow stopes." *Soil & Rock America 2003*, Cambridge, Massachusetts, AA Balkema, Roterdam, 1157-1164.

Australian Standards AS 1289.2.1.1 (1992) – Methods of testing soils for engineering purposes –Determination of the moisture content of a soil – Oven drying method (Standard method)

Australian Standards AS 1289.3.5.1 (1995) – Methods of testing soils for engineering purposes –Soil classification tests

Australian Standards AS 1289.3.5.2 (1995) – Methods of testing soils for engineering purposes – Determination of the soil particle density of a soil – Standard method

Australian Standards AS 1289.6.7.2 (2001) – Methods of testing soils for engineering purposes – Soil strength and consolidation tests – Determination of permeability of a soil - Falling head method for a remoulded specimen.

Australian Standards AS 1289.6.7.3 (2001) – Methods of testing soils for engineering purposes – Soil strength and consolidation tests – Determination of permeability of a soil – Constant head method for a remoulded specimen.

Australian Standards AS 1289.6.2.2 (1998) – Methods of testing soils for engineering purposes – Soil strength and consolidation tests – Determination of shear strength of a soil – Direct shear test using a shear box.

Australian Standards AS 1289.6.4.1 (1998) – Methods of testing soils for engineering purposes - Soil strength and consolidation tests – Determination of compressive strength of a soil – Compressive strength of a specimen tested in undrained triaxial compression without measurement of pore water pressure.

American Society for Testing and Materials ASTM D4253, (1993) - Standard Test Methods for Maximum Index Density and Unit Weight of Soils Using a Vibratory Table

Barnes, G.E. (2000). *Soil Mechanics – Principles and Practice,* 2nd Edition, MacMillan Press Ltd., London, 476 pp.

Barrett, J.R. and Cowling, R. (1980). "Investigation of cemented fill stability in 1100 orebody, Mount Isa Mines, Ltd., Queensland, Australia", *Transactions, Institute of Mining and Metallurgy*, Section A, 89, A118-A128.

Barrett, J.R., Coulthard, M.A. and Dight, P.M. (1978). "Determination of fill stability", *Mining with Backfill, Proceedings of 12th Canadian Rock Mechanics Symposium*, CIM, 19, Sudbury, Ontario.

Belem, T., Harvey, A., Simon, R., and Aubertin, M. (2004). "Measurement and prediction of internal internal stresses in an underground opening during its filling with cemented fill", *Proceedings of the 5th International Symposium on Ground Support, Ground Support in Mining and Underground Construction*, Perth, Western Australia, 619-130.

Black, A.B. (1944). "The application of hydraulic stopingpartially deslimed mill residue in stopes at Broken Hill South Limited", *The AusIMM Proceedings*, 135.

Bloss, M.L. (1992). "Prediction of cemented rock fill stability design procedures and modelling techniques". PhD Thesis, Department of Mining and Metallurgical Engineering, University of Queensland, Brisbane, Australia.

Bloss, M.L. and Chen, J. (1998). Drainage research at Mount Isa Mines Limited 1992 – 1997, *Proceedings of the 6th International Symposium on Mining with Backfill: Minefill '98*, Ed. M. Bloss, Brisbane, Australia, 111-116.

Boger, D.V. (1998). “Environmental rheology and the mining industry”. *Proceedings of the 6$^{th}$ International Symposium on Mining with Backfill: Minefill ’98*, Ed. M. Bloss, Brisbane, Australia, 15-17.

Brady, B.H.G. and Brown, E.T. (1985). *Rock Mechanics for Underground Mining*, George Allen and Unwin (Publishers) Ltd., London; 2nd Edition: 1993.

Brady, A.C. and Brown, J.A. (2002). “Hydraulic fill at Osborne mine,” *Proceedings of the 7$^{th}$ Underground Operators’ Conference*, Townsville, Australia, 161-165.

Bridges, M.C. (2003). “A New Era of Fill-Retaining Barricades,” *Digging Deeper*, AMC Consultants, October, www.amcconsultants.com.au 2-5.

British Standards BS1377: Part 2: 1990:7.3 – Bulk and dry density immersion in water

Budavari, S. (1983). “Response of the Rockmass to Excavations Underground,” *Rock Mechanics in Mining Practice,* Monographs Series Vol 5, (Ed: Budavari), South African Institute of Mining and Metallurgy: Johannesburg, 55–76.

Budhu, M. (2000). *Soil Mechanics and Foundations*, John Wiley and sons Inc., New York. 557 pp.

Burland, J.B. and Burbidge, M.C. (1985). “Settlements of foundations on sand and gravel.” *Proc. Inst. Civ. Eng.* Part 1, 78, 1325-1381.

Carman, P.C. (1956). *Flow of Gases Through Porous Media*, Academic Press Inc., New York.

Carrier III, D.W., Bromwell, L.G. and Somogyi, F. (1983). “Design capacity of slurried mineral waste ponds.” *Journal of Geotechnical Engineering*, 109(5), 699-716.

Cedergren, H.R. (1967). *Seepage, Drainage and Flow Nets*, John Wiley & Sons Inc., New York.

Clarke, I.H. (1988). “The properties of hydraulically placed backfill.” *Proceedings of Backfill South African Mines*, Johannesburg, SAIMM, 15-33.

Clough, GW, Iwabuchi, J, Rad, NS and Kuppusamy, T. (1989). “Influence of Cementation on liquefaction of sands.” *Journal of Geotechnical Engineering*, 115(8), 1107-1117.

Corson, D.R., Dorman, R.K. and Sprute, R.H. (1981). “Improving the support characteristics of hydraulic fill.” *Application of Rock Mechanics to Cut and Fill Mining, The Institute of Mining and Metallurgy*, Eds. O. Stephansson and M.J. Jones, 93-99.

Cowling, R., Grice, A.G. and Isaacs, L.T. (1988), “Simulation of hydraulic filling of large underground mining excavations.” *Proceedings of 6th International Conference on Numerical Methods in Geomechanics*, Innsbruck, Austria, pp 1869-1876.

Cowling, R., Voboril, A., Isaacs, L.T., Meek, J.L., and Beer, G. (1989). “Computer models for improved fill performance.” *Innovations in Mining Backfill Technology*, Eds. Hassani et al., Balkema, Rotterdam, 165-174.

Cowling, R. (1998). “Twenty-five years of mine filling: Developments and directions.” *Proceedings of the 6th International Symposium on Mining with Backfill: Minefill ’98*, Ed. M. Bloss, Brisbane, Australia, 3-10.

Cowling, R. (2002). Personal communication.

Cowling, R. (2003). Personal communication.

Cubrinovski, M. and Ishihara, K. (2001). “Correlation between penetration resistance and relative density of sandy soils”, *Proceedings of the 15th International Conference on Soil Mechanics and Geotechnical Engineering*, Istanbul, Turkey, 393-396.

Das, B.M., (1985). *Advanced Soil Mechanics*, Hemisphere Publishing Corporation, Singapore. 503 pp.

Das, B.M., (2002). *Principles of Geotechnical Engineering*, 5th Edition, Brooks/Cole – Thomsom Learning, USA. 578 pp.

Duffield, C., Gad, E. and Bamford, W. (2003). "Investigation into the Structural Behaviour of Mine Brick Barricades." *Australian Institute of Mining and Metallurgy*, March/April, (2), 45-50.

Duncan, J.M., and Buchingnani, A.L. (1976). *An Engineering Manual for Settlement Studies*, Geotechnical Engineering Report, University of California at Berkeley, 94 pp.

Fourie, A.B., Hofmann, B.A., Mikula, R.J., Lord, E.R.F. and Robertson, P.K. (2001). "Partially saturated tailings sand below the phreatic surface", *Géotechnique* 51(7), 577-585.

Grice, A.G. (1989). "Fill Research at Mount Isa Mines Limited." *Innovations in Mining Backfill Technology*, Balkema, Rotterdam, pp 15-22.

Grice, A.G. (1998 a). "Stability of hydraulic backfill barricades." *Proceedings of the 6th International Symposium on Mining with Backfill*, AusIMM, Brisbane.

Grice, A.G. (1998 b). "Underground mining with backfill." *Proceedings of the 2nd Annual Summit – Mine Tailings Disposal Systems*, Brisbane.

Grice, A.G. and Fountain, L.J. (1991). "The fill information system." *Second Australian Conference on Computer Applications in the Mineral Industry*, University of Wollonggong, NSW.

Grice, A.G., Wilwain, A, and Urquhart, K. (1993). "Backfilling operations at Mount Isa Mines 1998-1992." *Proceedings of the 5th International Symposium on Mining with Backfill: Minefill '93*, Johannesburg, South Africa.

Grice, T. (2001). “Recent minefill developments in Australia.” *Proceedings of the 7th International Symposium on Mining with Backfill: Minefill ’01*, Seattle, USA, 351-357.

Grice, T. (2004). Personal communication.

Hatanaka, M., Uchida, A., Taya, Y., Takehara, N, Hagisawa, T., Sakou, N. and Ogawa, S. (2001). “Permeability characteristics of high-quality undisturbed gravely soils measured in laboratory tests.” *Soils and Foundations*, 41(3), 45–55.

Hamrin, H. (1982). “Choosing an Underground Mining Method.” *In: Underground Mining Methods Handbook*, ed. by W.A. Hustrulid. New York: Soc. Mng. Engr. - AIME, Sec. 1.6, 88-112.

Harr, M.E. (1962). *Groundwater and Seepage*, McGraw-Hill International Book Company, New York.

Harr, M.E. (1977). *Mechanics of Particulate Media – A Probabilistic Approach*, McGraw-Hill International Book Company, USA.

Hazen, A. (1930). *Water supply. American Civil Engineers Handbook*, Wiley, New York.

Hazen, A. (1892). *Physical properties of sands and gravels with reference to their use in filtration*, Report Mass, State Board of Health.

Herget, G. and De Korompay, V. (1987). “In situ drainage properties of hydraulic backfills,” *Proceedings of Mining with Backfill, Research and Innovations*, CIM, 19, 117-123.

Holtz, R.D. and Kovacs, W.D. (1981). *An Introduction to Geotechnical Engineering*, Prentice Hall.

Isaacs, L.T. and Carter, J.P. (1983). "Theoretical study of pore water pressures developed in hydraulic fill in mine stopes." *Transactions of Institution of Mining and Metallurgy* (Section A: Mining Industry), 92, A93-A102.

Itasca, (2002). *FLAC version 4.0 Users Manuals*. Itasca Consulting Group, Thresher Square East, 708 South Third Street, Suite 310, Minneapolis, Minnesota, 55415 USA.

Itasca, (2002). *FLAC$^{3D}$ version 2.1 Users Manuals*. Itasca Consulting Group, Thresher Square East, 708 South Third Street, Suite 310, Minneapolis, Minnesota, 55415 USA.

Keren, L. and Kainain, S. (1983). "Influence of tailings particles on physical and mechanical properties of fill." *Proceedings of the International Symposium on Mining with Backfill*, Eds. S Granholm, A.A. Balkema, Sweden, 21-29

Kozeny, J. (1927). Ueber kapillare Leitung des Wassers in Boden, *Wien Akad*. Wiss., 136, 1271 pp.

Kozeny, J. (1933). Theorie und Berechnung der Brunnen, *Wasserkr. Wasserwritch.*, 28, 104 pp.

Kuganathan, K. (2001). "Mine backfilling, backfill drainage and bulkhead construction – A safety first approach." *Australia's Mining Monthly*, February, 58-64.

Kuganathan, K. (2001). "Design and Construction of Shotcrete Bulkheads with Engineered Drainage System for Mine Backfilling." *International Seminar on Surface Support Liners, Australian Centre for Geomechanics*, Section 8, 1-15.

Kuganathan, K. (2002). "A method to design efficient mine backfill drainage systems to improve safety and stability of backfill bulkheads and fills." *Proceedings of the 7th Underground Operators' Conference*, Townsville, Australia, 181-188.

Lambe, T.W. and Whitman R.V. (1979). *Soil Mechanics, SI Version, Series in Soil Engineering*, John Wiley and Sons, New York.

Lambe, T.W. (1951). *Soil Testing for Engineers*, John Wiley and Sons, New York.

Lamos, A.W. (1993). "An assessment of the effects of ultrafine aggregate components on the properties of mine backfills." *Proceedings of the 5th International Symposium on Mining with Backfill: Minefill '01*, Johannesburg, South Africa, 173-179.

Liston, D. (2003). "Placement properties, geotechnical characterisation and drainage analysis of hydraulic backfill in mines." B.E. Thesis, School of Engineering, James Cook University, Townsville, Australia.

Leonards, G.A. (1962). *Foundation Engineering*, McGraw-Hill Book Company, New York. 1107 pp.

Meyerhof, G.G. (1957). "Discussion on research on determining the density of sands by penetration testing." *Proceedings of the 4th International Conference on Soil Mechanics and Foundation Engineering*, London, UK, 3, 110 pp.

Mitchell, R.J. (1998). "The Eleventh Annual R.M. Hardy Keynote Address, 1997: Centrifugation in Geoenvironmental Practice and Education." *Canadian Geotechnical Journal*, 35(4), 630-640.

Mitchell, R.J., Smith, J.D. and Libby, D.J. (1975). "Bulkhead Pressures Due to Cemented Hydraulic Mine Backfills." *Canadian Geotechnical Journal*, 12(3), 362-371.

Mitchell, R.J. and Wong, B.C. (1982). "Behaviour of Cemented Tailings Sands." *Canadian Geotechnical Journal*, 19(3), 289 – 295.

Nantel, J. (1998). "Recent Developments and Trends in Backfill Practices in Canada." *Proceedings of the 6th International Symposium on Mining with Backfill: Minefill '98*, Ed. M. Bloss, Brisbane, Australia, 11-14.

Neindorf, L.B. (1983). "Fill operating practices at Mount Isa Mines." *Proceedings, Symposium Mining with Backfill*, University of Lulea. 179-187.

Nicholson, D.E. and Wayment, W.R. (1964). "Properties of hydraulic backfills and preliminary vibratory compaction tests." *United States Department of the Interior, Bureau of Mines*. 31 pp.

Nnadi, G.N. and Mitchell, R.J. (1991). "Use of centrifuge models to study simulated blast loadings on backfills." *Canadian Institute of Mining and Metallurgy, Rock Mechnaics Bulletin*, 84(951), 58-63.

Ouellet, J. and Servant, S. (1998). "Numerical simulation of the drainage in a mining stope filled with hydraulic backfill." *Proceedings of the 6th International Symposium on Mining with Backfill: Minefill '98*, Ed. M. Bloss, Brisbane, Australia, 105-110.

Peck, R.B., Hanson, W.E. and Thornburn, T.H. (1974). *Foundation Engineering*, 2nd Ed., John Wiley and Sons, New York, 514 pp.

Pettibone, H.C. and Kealy, C.D. (1971). "Engineering properties of mine tailings," *Journal of Soil Mechanics and Foundations Division*, ASCE, 97(SM9), 1207-1225.

Rankine, K.J. (2000). "Geotechnical Characterisation and Stability Analysis of BHP Cannington Paste Backfill." B.E. Hons. Thesis, James Cook University, Townsville, Queensland, Australia.

Rankine, K.J., Rankine, K.S. and Sivakugan, N. (2003). "Three-dimensional drainage modeling of hydraulic fill mines." *Proceedings from the 12th Asian and Regional Conference on Soil Mechanics and Geotechnical Engineering*, Singapore, 937-940.

Rankine, K.J., Sivakugan, N. and Rankine, K.S. (2004). "Laboratory tests for mine fills and barricade bricks." *Proceedings from the 9th Australian and New Zealand Conference on Geomechanics*, Auckland, New Zealand, 1, 218-224.

Rankine, K.J., Sivakugan, N. and Cowling, R. (2005). "Emplaced Characteristics of Hydraulic Fills In a Number of Australian Mines." *Geotechnical and Geological Engineering*, Springer. (In press).

Rankine, R.M., Rankine, K.J., Sivakugan, N., Karunasena, W., Bloss, M.L. (2001). “Geotechnical Characterization and Stability Analysis of BHP Cannington Paste Backfill.” *XV$^{th}$ International Conference on Soil Mechanics and Geological Engineering*, August, 2001, Istanbul Turkey, 1241-1244.

Reddi, L.N. (2004), *Seepage in Soils – Principles and applications*, John Wiley and Sons, Inc., Hoboken, New Jersey. 383 pp.

Samarasinghe, A.M., Huang, Y.H. and Drnevich, V.P. (1982). “Permeability and consolidation of normally consolidated soils.” *Journal of the Geotechnical Engineering Division*, ASCE, 108(GT1), 55-60.

Sivakugan, N., Rankine, K.J. and Rankine, K.S. (2005). “Study of drainage through hydraulic fill stopes using method of fragments.” *Geotechnical and Geological Engineering*, Springer, In Press.

Skempton, A.W. (1986). “Standard penetration test procedures and the effects in sands of overburden pressure, relative density, particle size, aging and overconsolidation.” *Géotechnique*, 36(3), 425-447.

Sridharan, A, and Prakash, K. (2002). “Permeability of Two-Layer Soils.” *Geotechnical Testing Journal*, ASTM, Vol. 25, No. 4, December, pp 443-448.

Taylor, D.W. (1948). *Fundamentals of Soil Mechanics*, John Wiley & Sons Inc., New York, 700 pp.

Terzaghi, K, and Peck, R.B. (1967). *Soil Mechanics in Engineering Practice*, 2$^{nd}$ Edition, John Wiley & Sons Inc., New York, 729 pp.

Terzaghi, K., Peck, R.B., and Mesri, G. (1996). *Soil Mechanics in Engineering Practice*, 3$^{rd}$ Edition, John Wiley & Sons Inc., New York, 549-549.

Thomas, E.G. (1978). "Fill permeability and its significance in mine fill practice." *Mining with Backfill*, 12th Canadian Rock Mechanics Symposium, Montreal, CIMM.

Thomas, E.G. and Holtham, P.N. (1989). "The basics of preparation of deslimed mill tailing hydraulic fill." Innovations in Mining Backfill Technology, Ed. Hassani et al., Rotterdam, Balkerna, 425-431.

Tomlinson, S.S. and Vaid, Y.P. (2000). "Seepage forces and confining pressure effects on piping erosion", *Canandian Geotechnical Journal*, 37(1), 1–13.

Traves, W.H. (1988). "A three dimensional model of the drainage of back-filled open stopes." Masters Thesis, Department of Civil Engineering, University of Queensland, Brisbane, Queensland.

Traves, W.H. and Isaacs, L.T. (1991). "Three-dimensional modelling of fill drainage in mine stopes." *Transactions of the Institution of Mining and Metallugy, Section A (Mining Industry)*, The Institution of Mining and Metallurgy, A66-A71.

Wallace, K. (1975). "A procedure for numerical analysis of transient moisture in saturated and unsaturated earth structures." Report, James Cook University, Townsville, Qld.

Wen, B., Aydin, A. and Duzgoren-Aydin, N.S. (2002). "A comparative study of particle size analysis by sieve-hydrometer and laser diffraction methods." *Geotechnical Testing Journal*, ASTM, Dec, 25(4), 434-442.

Wilson, J.C., (1979). Forward, Fill technology in underground metalliferous mines, International Academic Services Limited, Kingston, Ontario, Canada.

www.ce.washington.edu/~liquefaction/html/main.html

www.mountisabrickworks.com.au

www.wsws.org/articles/2000/jul2000/mine-j01_prn.shtml

Yamaguchi, U. and Yamatomi, J. (1983). “A consideration on the effect of backfill for the ground stability.” Proceedings of the International Symposium on Mining with Backfill, Sweden, 443-451.